3-15-2017

Optimizing Design Parameters for Thin Film Composite Hollow Fiber Membranes and Modules for Osmotic Processes

Jian Ren
jian.ren@uconn.edu

Optimizing Design Parameters for Thin Film Composite Hollow Fiber Membranes and Modules for Osmotic Processes

Jian Ren, PhD

University of Connecticut, 2017

Osmotic processes have been considered sustainable solutions for extracting clean water and concentrating impaired water by forward osmosis (FO) and harvesting the osmotic pressure gradient for power generation via pressure retarded osmosis (PRO). Thin film composite (TFC) membranes are considered a preferred platform for osmotic processes wherein the selective and support layers can be tailored independently for preferred chemistry and structure. Hollow fiber TFC membranes in particular have garnered interests because of their high packing density. In this dissertation study, high performance TFC membranes were designed for applications in osmotic processes. Departing from previous hollow fiber membrane developments that focused on utilizing novel materials and fabrication methods, this dissertation focused on elucidating the fundamental structure-property-performance relationships of TFC hollow fiber membranes for osmotic processes. The impact of support layer structure was studied using lab-made hollow fiber supports. The impact of support surface pore size was systematically investigated using commercial ultrafiltration (UF) platforms. The results demonstrate that TFC hollow fiber FO membranes with excellent performance can be made with intrinsically hydrophilic materials, and can be produced at both lab-scale and module-scale with relative ease using off-the-shelf UF membranes. Finally, to optimize design and operation parameters in the hollow fiber FO process at various scales, a computational fluid dynamics model was developed to elucidate the inextricable link between various parameters and to optimize the design parameters for TFC hollow fiber membranes and modules for osmotic processes.

Optimizing Design Parameters for Thin Film Composite Hollow Fiber Membranes and Modules for Osmotic Processes

Jian Ren

B.S., Sichuan University, 2011

A Dissertation

Submitted in Partial Fulfillment of the

Requirements for the Degree of

Doctor of Philosophy

at the

University of Connecticut

2017

APPROVAL PAGE

Doctor of Philosophy Dissertation

Optimizing Design Parameters for Thin Film Composite Hollow Fiber Membranes and Modules for Osmotic Processes

Presented by

Jian Ren, B.S.

Major Advisor_____

Dr. Jeffrey R. McCutcheon

Associate Advisor_____

Dr. Leslie M. Shor

Associate Advisor_____

Dr. Richard S. Parnas

Associate Advisor_____

Dr. Luyi Sun

Associate Advisor_____

Dr. Douglas H. Adamson

University of Connecticut

2017

ACKNOWLEDGMENTS

First and foremost, I would like to express my sincere gratitude to my major advisor, Dr. Jeffrey McCutcheon. I thank him for taking me on as his student and for shaping my research work. The work in this dissertation would not have been possible without his guidance and support. I also greatly acknowledge the opportunities that he gave me by sending me to various conferences and nominating me for various fellowships and awards – he was extremely supportive and encouraging in the past five years. I am grateful to his continuous guidance and patience as he also honed my professional writing and presentation skills. To me, he is far beyond an academic advisor but an advisor of lifetime!

I must express my gratitude to my advisory committee members, Dr. Leslie Shor, Dr. Richard Parnas, Dr. Douglas Adamson and especially, Dr. Luyi Sun, for their time, encouragement and valuable guidance, especially during my proposal defense. I also wish to thank Dr. George Bollas for his support and encouragement during the development of the model in this dissertation. I greatly thank Ms. Leah Winterberger, Ms. Susan Soucy and Ms. Marita Decozio-Wiley for all their timely support and guidance during my time here at UConn. I greatly acknowledge the help and favors that I have received from Mr. Mark Drobney and Mr. Joe Csiki at the machine shop, the hollow fiber spinning system would not have been built without their help. I would also like to thank Mr. Lichun Zhang, Mr. Roger Ristau, Ms. Laura Pinatti, Mr. Adam Wentworth at IMS, and Mr. Mark Biron at C2E2 who have been very helpful for my projects. I also gratefully acknowledge the collaborators in all my research projects.

I wish to thank all of my lab colleagues (in alphabetical order): Dr. Mustafa Al-Furaiji, Dr. Dan Anastasio, Dr. Jason Arena, Ms. Nicole Beauregard, Dr. Ngoc Bui, Mr. Maqsud Chowdhury, Dr. Hui Gong, Dr. Wenming Hao, Dr. Liwei Huang, Dr. Cong Ma, Dr. Seetha Manickam, Mr. Brendan O'Grady, Mr. Kevin Reimund, Dr. Basma Waisi, Ms. Yichen Wang,

and Ms. Lingling Xia. I acknowledge Dr. Ngoc Bui, Dr. Liwei Huang, Dr. Jason Arena, Dr. Seetha Manickam, and Dr. Dan Anastasio for being the perfect examples and mentors to me. I greatly thank the coauthors of my publications: Mr. Maqsud Chowdhury, Ms. Lingling Xia, Mr. Brendan O'Grady, Dr. Cong Ma, and Ms. Jie Qi for their great contributions to my work. Along with my lab colleagues, I gratefully thank all of my friends, both at UConn and elsewhere, for being great friends with me and helping me maintain my sanity.

Finally, I thank my wonderful parents, Ruixia Chen and Liancheng Ren, who have raised me to be the person I am today. Thank you for all the unconditional love and continuous support throughout my years of study in China and US. I also dedicate this thesis to my parents, whose affection, love, encouragement and prays of day and night make me able to get such success and honor of graduation with a Doctor of Philosophy degree.

Table of Contents

List of Tables

List of Figures

Chapter 1. Introduction

1.1 Motivation

Water is needed in every aspect of our life. Whether it is growing food, producing energy, manufacturing goods, maintaining personal hygiene, or drinking, it is a core responsibility of the public sector to provide clean, safe and inexpensive water to everyone [1]. However, this responsibility is becoming difficult to meet with widespread water scarcity being exacerbated by overuse and climate change [2, 3]. With shortages of water come stunted economic growth and possible health hazards as lower quality waters are brought to bear to fill gaps in water availability in China [4, 5]. Growing up in Northern China, I knew exactly how the water scarcity impacted my life. These challenges are not only being felt in Northern China, the water crises has become a global concern. In its 12th edition, The Global Risks Report 2017 once again listed "Water Crises" as the most impactful societal risk that would occur and with massive and devastating impacts [6].

Expansion of the water supply can solve this problem through the tapping of non-traditional water sources such as seawater, domestic wastewater, mining wastewater (i.e. produced water), and industrial wastewater [3]. Membrane technology may offer a means of treating these difficult waters and converting them into safe water for a variety of uses [7-9]. One promising membrane technology is Forward osmosis (FO). The FO platform technology has garnered explosive interests amongst the membrane technologies within the past decade [10-13]. Unlike hydraulically driven membrane processes, FO utilizes osmotic pressure difference to drive water across a semipermeable membrane from a dilute feed solution to a concentrated draw

solution while rejecting most solutes. FO requires no applied hydraulic pressure and has been considered for applications involving the treatment of waters with high salinity and fouling propensity [12-14]. The promise of FO has been demonstrated in various applications such as wastewater treatment [15, 16], seawater desalination [17, 18], brine/product concentration [19, 20] and combined with other membrane processes (such as reverse osmosis and membrane distillation) for better system performance [21-24].

As the field of FO experienced development during the past decade, high performance FO membranes have been developed in both academia and industry [25-33]. Among them, hollow fiber FO membranes showed great promise due to the high performance, high packing density, as well as the self-supported structure [29, 30]. Hollow fiber membranes have long been considered a valuable platform for membrane separations because their higher packing densities relative to flat sheet configurations (i.e. plate-and-frame and spiral wound) [34]. Such benefit allows for large membrane area in small footprint systems. Hollow fiber membranes have shown immense promise for ultrafiltration, dialysis, gas separation and reverse osmosis for many years [35-38]. Recently, hollow fiber membranes also been developed by the forward osmosis community [12, 39].

These membranes were largely based on a thin film composite (TFC) membrane design platform, where an ultra-thin selective layer could be supported on a chemically different porous support layer. The two layers could be tailored independently to specifically address membrane structure and chemical needs for good FO performance [40-42]. For making good FO membranes, previous studies have shown that the selective layer needs to have high water permeance and solute selectivity while the support layer needs to be thin, highly porous, and minimally tortuous (*i.e.* a low structural parameter [25, 43, 44]) to minimize the internal concentration polarization (ICP) [45, 46]. To design a high performance hollow fiber membrane for FO process, understanding the fundamental structure-performance would be

especially important. As the selective layer chemistry and structure-performance relationship has been well documented in the literature [42, 47-51], this dissertation work focused on studying the support layer structure-performance relationship as well as the interfacial property-performance relationship.

As high performance membranes being developed for FO at laboratory scale by exploiting those relationships, much of them were focused on novel materials or structures [25, 26, 29, 52-57]. These membranes, while performing well in the lab, have not translated well to the commercial applications. Barriers to commercialization are rooted in the fact that "academic" membranes are often made using unconventional methods or with new materials. Risk averse companies are less likely to bring an unconventional membrane to market as they may be difficult to fabricate or place into modules.

In this work, commercial hollow fiber ultrafiltration platforms were utilized as the supporting structure to develop TFC hollow fiber FO membranes at both lab scale and industrial scale. Such effort may have ramifications across FO research groups since now they have the ability to fabricate TFC hollow fiber membranes via a simple and facile process. The ability to fabricate membranes, especially those that can exhibit high packing density at module scale, is essential to applied research in osmotic processes given the challenges in finding stable and consistent supplies of commercial FO membranes.

To further bridge the gap between academic laboratories and the commercial sector, a comprehensive understanding of how new membranes can impact performance at the module/element level is needed. Since the experimental would be costly and time-consuming, a good way to do this is via computational modeling. In this work, a *comprehensive* and *experimentally verified* computational fluid dynamics model was developed to establish the relationships between both membrane properties and module design and overall performance (water flux and draw solute flux). With such a tool, academics and industry alike would be able

to design an element around their specific membrane technology, design a membrane around their required element specifications, or design both a membrane and element for a specific osmotic process.

1.2 Objective and scope of dissertation

The objective of this dissertation work include:

i. To evaluate the osmotic flux performance metrics in the forward osmosis process.

ii. To develop high performance thin film composite membranes for forward osmosis using intrinsic hydrophilic supporting materials.

iii. To study the effect of support layer properties (including cross-section structure and surface pore size) on overall osmotic flux performance of thin film composite membranes.

iv. To develop thin film composite hollow fiber membranes using existing commercial platform at both lab scale and industrial scale.

v. To understand the mass transfer limitation in hollow fiber module during forward osmosis operation at scale.

vi. To build a computational fluid dynamics model to simulate and predict hollow fiber module performance in FO processes.

1.3 Thesis organization

In **Chapter 2**, an overview of the background, theory, and development of hollow fiber membranes for osmotically driven membrane processes were provided. Two major osmotically driven membrane processes, forward osmosis and pressure retarded osmosis (PRO), were discussed. The developments of hollow fiber membranes for FO and PRO were discussed in

detail.

Chapter 3 identified the performance metrics of osmotic performance tests by evaluating a commercial thin film composite flat sheet membrane. This was the first commercially thin film composite membrane for forward osmosis developed by Hydration Technology Innovation (HTI). The TFC membrane tested exhibited high water permeance and good mechanical strength relative to other membranes therefore was used as a commercial benchmark in the field of FO. This work has been published in *Desalination*, 343 (2014), 187-193.

In **Chapter 4**, high performance membranes were developed with intrinsically hydrophilic sulfonated polysulfone (SPSU) in the flat sheet configuration. The reasoning behind their use lies in their intrinsic hydrophilicity which promotes wetting and mass transfer in this support layer. The use of this supporting material with different polyester (PET) nonwoven backings were combined in order to better understand how backing choice and membrane midlayer material choice interrelate. By varying the degree of sulfonation in the support midlayer along with selecting backing nonwovens with appropriate characteristics, the best membranes exhibited water flux of about 70 $L\,m^{-2}h^{-1}$ using 1 M sodium chloride draw solution against deionized water in PRO mode. The use of the PET in these membrane imparted impressive mechanical properties while still keeping the structural parameter low (as low as 277 μm). This was the lowest structural parameter of the fabric backed TFC membranes reported in the open literature. This work has been published in *Polymer*, 103 (2016), 486-497.

Chapter 5 to 8 focused on thin film composite hollow fiber membranes for FO. In **Chapter 5**, an intrinsically hydrophilic polyacrylonitrile (PAN) hollow fiber supported TFC membrane was developed. A selective polyamide thin film was synthesized on the membrane shell side via interfacial polymerization. The impact of fiber pore structure was investigated during the study with some of the membranes exhibiting water flux of 36.6 $L\,m^{-2}h^{-1}$ using 1 M sodium

chloride draw solution against deionized water in PRO mode. These results suggest the potential of utilizing intrinsically hydrophilic polymeric hollow fibers with finely tuned pore structures as support for TFC membranes for osmotic processes. This work has been published in *Desalination*, 372 (2015) 67-74.

In **Chapter 6**, a systematic investigation on the influence of support layer pore size on the osmotic performance of TFC hollow fiber FO membranes was conducted. A series of commercially available ultrafiltration membranes with similar physical and chemical properties but different pore sizes were employed as the support layer. The resulting roughness of the selective layer was found to be dependent on support layer pore size. Osmotic flux tests revealed that the membrane performance is dependent on this roughness with rougher membranes exhibiting higher fluxes in many cases. Aside from elucidating the impact of support layer pore size on osmotic performance, the potential of making high performance membranes on existing commercial hollow fiber platforms was also demonstrated for the first time. This work is currently under review.

Chapter 7 described the development of thin film composite hollow fiber membranes at module scale. In this work, commercial ultrafiltration hollow fiber membranes (Koch Membrane Systems) were used as supports for polyamide TFC membranes. These membranes were already potted into 18-inch modules before the in-situ formation of the polyamide on the lumen of the fibers. Two fiber sizes were selected for comparison, and all membranes tested exhibited remarkably good FO performance (both water and solute flux) given that the supporting materials had undergone no tailoring or adjustment. The use of commercial modules also allow for volume-normalized performance metrics to be considered as a new way to define FO performance. This work has been accepted by *Industrial & Engineering Chemistry Research* and is in press.

In **Chapter 8**, a comprehensive and experimentally verified computational fluid dynamics

model that established relationships between both membrane properties and module design and overall performance (water flux and draw solute flux) was developed. With such a tool, academics and industry alike would be able to design an element around their specific membrane technology, design a membrane around their required element specifications, or design both a membrane and element for a specific osmotic process. This work is currently in preparation for submission.

Finally, **Chapter 9** details the concluding remarks and provides an outlook on the potential, challenges, and recommendations in hollow fiber membrane and module design for forward osmosis for use in a wide range of applications.

An evaluation of the osmotic performance of a next generation biomimetic hollow fiber membrane for FO was conducted and demonstrated in **Appendix 1**. It was a newly launched hollow fiber FO membrane from Aquaporin A/S, Denmark. These membranes were tested in miniature module form at bench scale. Under various osmotic testing conditions, these membranes exhibited excellent performance that is more than adequate to provide necessary flow for a high surface area hollow fiber modules at pilot scale.

1.4 Key contributions

In this dissertation, high performance thin film composite membranes were designed for applications in forward osmosis process. Departing from previous hollow fiber membrane development studies that focused on utilizing novel materials and fabrication methods, this dissertation focused on elucidating the fundamental structure-performance relationship of thin film composite hollow fiber membranes for forward osmosis. To optimize design and operation parameters in the hollow fiber FO process at various scales, a computational fluid dynamics model was developed to elucidate the inextricable link between various parameters in the

membrane and module design.

Specifically, major contributions are summarized as below:

i. Developed high performance thin film composite membranes using an intrinsically hydrophilic sulfonated polysulfone (SPSU) with fabric integral structure. This membrane has the lowest structural parameter of the fabric backed TFC membranes reported in the open literature.

ii. Demonstrated successful in-situ interfacial polymerization of polyamide on the shell surface of an intrinsically hydrophilic hollow fiber support for the first time. A batch coating method was developed for interfacial polymerization with the membrane exhibiting good performance. This finding provides new options for TFC hollow fiber membrane design and fabrication.

iii. Provided new insights into membrane design based on the systematically study of how hollow fiber support layer surface pore size as a singular independent variable influenced the selective layer formation and osmotic performance of TFC FO membranes.

iv. Demonstrated the capability of making TFC hollow fiber FO membranes on commercial ultrafiltration membrane platform. Such efforts have ramifications across FO research groups since now they have the ability to fabricate TFC hollow fiber membranes via a simple and facile process.

v. Developed an experimentally verifiable modeling tool for predicting hollow fiber element performance which would enable prediction of element performance for a variety of osmotic processes. This model would help identify which independent parameters are most important when considering *both* membrane *and* element design.

Chapter 2. Hollow fiber membranes for osmotic processes: Literature review

To be submitted as

Ren, J., Xia, L., McCutcheon, J.R., "Hollow fiber membranes for osmotic processes: A review".

2.1 Introduction

Water, energy and food are essential for human well-being, poverty reduction and sustainable development [58]. Under the pressure of population growth and mobility, economic development and climate change, the global demand for freshwater, energy and food will increase significantly over the next decades [58, 59]. To supplement the global supply of fresh water and clean energy, osmotically driven membrane processes have emerged as a sustainable solution [10, 60]. Unlike pressure driven membrane processes, in the osmotically driven membrane processes, osmotic pressure difference is utilized to drive water across a semipermeable membrane from a dilute feed solution to a concentrated draw solution while rejecting most solutes [10]. The osmotic processes could provide sustainable solutions for extracting clean water and concentrating impaired water by the means of forward osmosis (FO). On the other hand, the osmotic pressure gradient could be harvested for power generation via the means of pressure retarded osmosis (PRO).

2.1.1 Osmotically driven membrane processes

Osmosis is the spontaneous transport of solvent (mostly water) through a semi-permeable barrier/membrane from a feed stream of high solvent concentration/activity (i.e., low solute concentration) to a draw stream of low solvent concentration/activity (i.e., high solute concentration [10, 60]. Unlike pressure driven membrane processes (e.g. reverse osmosis, nanofiltration, ultrafiltration, microfiltration, etc.), osmotically driven membrane processes are driven by the osmotic pressure generated by a draw solution or osmotic agent.

Osmotic pressure is defined as the hydrostatic pressure required for stopping the diffusion of the solvent through the membrane [10]. A number of relationships have been developed to relate solute concentrations to osmotic pressure. Often, Van't Hoff equation is used to describe osmotic pressure as a function of concentration of dissolved solute molecules or ions in ideal solutions at low concentration:

$$\pi = icRT \quad (2.1)$$

Where i is the solute dissociation constant, c is the concentration of the solute, R is the gas constant, and T is the temperature.

Osmotic processes consists of three main categories: forward osmosis (FO), pressure retarded osmosis (PRO) and reverse osmosis (RO). The driving force and regime type are described using a figure modified from a review by Cath et al. [10]. The top nature occurring process is forward osmosis (FO) during which water spontaneously transports across the membrane driven by the osmotic pressure gradient ($\Delta\pi$) between the two solutions. When a hydrostatic pressure (ΔP) is applied to the salty water side, the permeate water is retarded and even ceased when ΔP is equal to $\Delta\pi$. At any stage when ΔP is between 0 and $\Delta\pi$, water still flows into the salty water because $\Delta\pi$ remains larger than ΔP. This phenomenon is termed as pressure retarded osmosis (PRO) where the driving force for water transport is reduced to $\Delta\pi - \Delta P$. When the

transmembrane pressure ΔP is greater than $\Delta\pi$, the direction of water permeation is reversed because water is forced to permeate through the membrane from the salty water into the fresh water. This incident is referred to as reverse osmosis (RO) which has been extensively used for seawater desalination. In principle, no extra energy is required for FO; energy could be produced by PRO, while energy must be provided for RO. Therefore, FO and PRO are considered as osmotically driven membrane processes, and are commonly practiced as potential processes for water treatment and power generation, respectively.

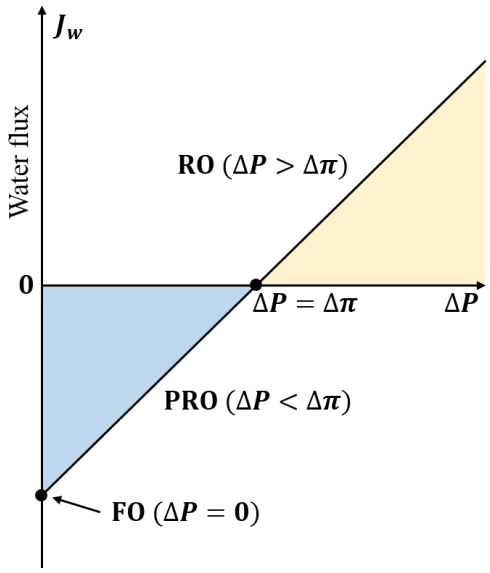

Figure 2.1 Illustration of flux vs. driving force in osmotic processes. Adapted from Journal of Membrane Science, 281, Tzahi Y. Cath et al., Forward osmosis: Principles, applications, and recent developments, 70-87, Copyright (2006), with permission from Elsevier [10].

2.1.1.1 Forward osmosis

Forward osmosis (FO) processes are a pool of technologies seeking to harness the osmotic pressure difference between two aqueous systems separated by a semi-permeable membrane [10, 12]. The general governing equation for water flux in an FO process can be expressed by:

$$J_w = A \cdot \Delta\pi \quad (2.2)$$

Where J_w is the water flux, A is the water permeability coefficient of the selective layer,

$\Delta\pi$ is the osmotic pressure difference.

FO processes can emerge in various forms:

1. Forward osmosis water treatment/desalination (FO): also simply as forward osmosis, this is the most commonly used term to describe any salinity driven process. FO refers to the osmotic separations where drinking water is the primary product, which requires the separation of water from draw solute. In FO, a membrane is place between saline feed solution and osmotic agent draw solution. Water is driven from the relatively dilute saline solution into the draw solution while rejecting the solutes. Diluted draw solution would be separated as water product and recovered draw solutes. The FO process can be applied in seawater desalination [17, 61, 62], wastewater treatment [63, 64], and produced water treatment [15, 65, 66].
2. Direct osmotic concentration (DOC): also known as dewatering process. The concentrated feed solution is the product. This process can be applied in the concentration of products like liquid food [67, 68], landfill leachate [69], produced water [15, 16] and pharmaceuticals [70].
3. Direct osmotic dilution (DOD): the diluted draw solution is the product. The direct osmotic dilution has been applied to develop personal hydration bags or community hydration can/well by Hydration Technology Innovations (HTI) [71]. This process was also applied in fertilizer driven FO desalination for direct fertigation [72, 73].

2.1.1.2 Pressure retarded osmosis

Pressure retarded osmosis (PRO) process harnesses the chemical potential difference caused by naturally occurring and engineered salinity gradients and converts it into electricity using a hydraulic pressure intermediate. To work, saline water is hydraulically pressurized to a level below its osmotic pressure, thus retarding the osmotic flow but creating a resistance to

generate work. The subsequent expansion of the diluted saline water through a hydroturbine generates electricity. The membrane performance for PRO applications is usually evaluated in terms of power density (W). *W* is defined as the power output per unit membrane area (W/m^2). Numerically, W is determined by the product of the transmembrane hydrostatic pressure ΔP and the water flux J_w across the membrane [74]:

$$W = J_w \times \Delta P \quad (2.3)$$

Without considering the concentration polarization effects, the ideal J_w can be calculated as:

$$J_w = A(\Delta\pi - \Delta P) \quad (2.4)$$

Where A is the water permeability coefficient of the selective layer, $\Delta\pi$ is the osmotic pressure difference.

However, the effective osmotic pressure gradient across the membrane is less than the osmotic pressure difference between the bulk salty water and fresh water (i.e., $\Delta\pi < \pi_s - \pi_f$) in real osmotically driven membrane processes. This is due to the mass transfer limitation in the osmotic processes.

2.1.2 Mass transfer limitation in osmotic processes

The membrane for osmotic processes is typically asymmetric structure, which consists of a dense selective layer, which mediates solute and water transport, and a porous support, which provides the mechanical strength. Concentration polarization (CP) is a boundary layer phenomenon that usually occurs at a membrane's selective interface [75-78]. This phenomenon, illustrated in Figure 2.2, has been considered the most significant obstacle to adequate membrane performance for osmotic processes.

As shown in Figure 2.2, osmotic flux tests can be carried out with the membrane oriented in both FO mode (the membrane selective layer faces the feed solution) and PRO mode (the membrane selective layer faces the draw solution). For example in FO mode, when solutes are

rejected from the selective layer, their concentration increases at the selective interface and a gradient is formed within the mass transfer boundary layer [79]. For a highly selective membrane with a low permeate solute concentration, the interfacial concentration on the feed side of a membrane can be defined by the equation:

$$c_{F,m} = c_{F,b}\exp\left(\frac{J_w}{k}\right) \quad (2.5)$$

Where J_w is the water flux through the membrane, k is the mass transfer coefficient, and $C_{F,m}$ and $C_{F,b}$ are the concentrations at the membrane interface and in the bulk feed solution, respectively. Equation 2.5 can be written in terms of osmotic pressures (π) when the osmotic pressure is assumed to be linearly proportional to concentration:

$$\frac{\pi_{F,m}}{\pi_{F,b}} = \exp\left(\frac{J_w}{k}\right) \quad (2.6)$$

This boundary layer is also present during osmosis. However, an additional dilutive CP phenomenon also occurs on the draw side of the membrane.

$$\frac{\pi_{D,m}}{\pi_{D,b}} = \exp(-J_w K) \quad (2.7)$$

Where $\pi_{D,m}$ and $\pi_{D,b}$ are now indicative of the membrane interface and bulk draw solution osmotic pressures. The negative exponential term indicates dilution at the membrane interface.

K is the resistance to solute diffusion within the membrane support. K is defined as

$$K = \frac{t\tau}{\varepsilon D_s} = \frac{S}{D_s} \quad (2.8)$$

Where D_s is the solute diffusion coefficient, and ε, τ, and t, are the porosity, tortuosity and thickness of the support layer, respectively. S is the structure parameter [80],

$$S = \frac{t\tau}{\varepsilon} \quad (2.9)$$

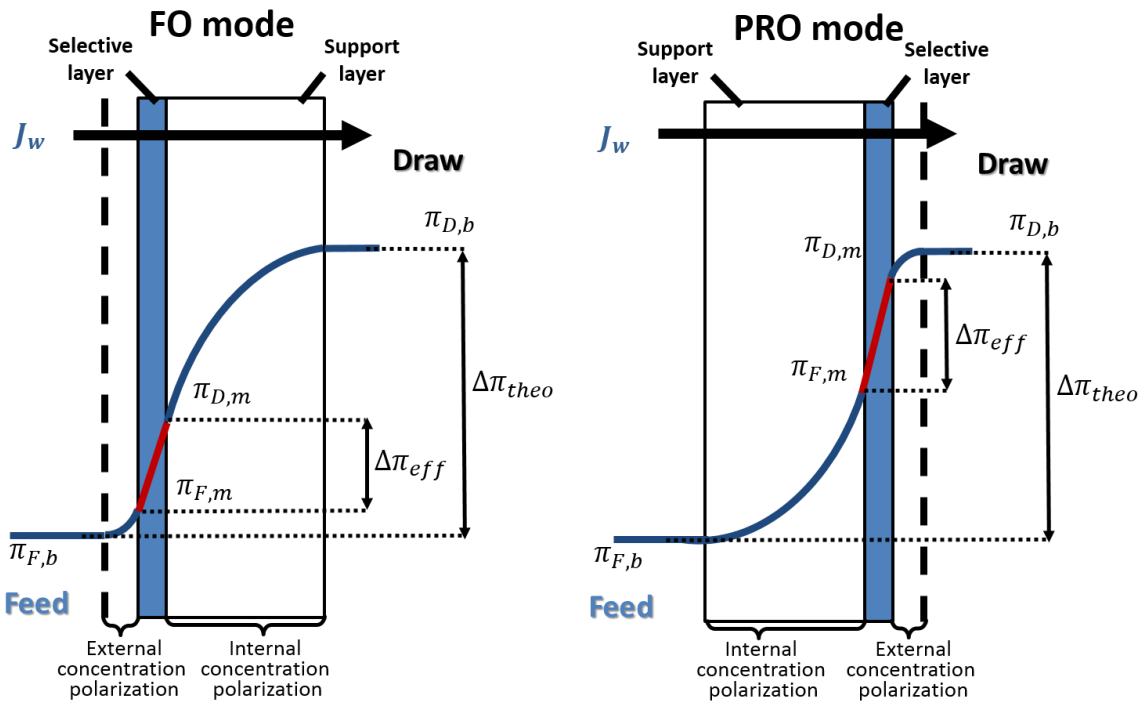

Figure 2.2 Illustration of internal and external concentration polarization in FO mode and PRO mode.

With these CP moduli taken into account, the water flux governing equation would be:

FO mode: $$J_w = A\left[\pi_{D,b}\, exp\left(-\frac{J_w S}{D_s}\right) - \pi_{F,b}\, exp\left(\frac{J_w}{k_F}\right)\right] \quad (2.10)$$

PRO mode: $$J_w = A\left[\pi_{D,b}\, exp\left(-\frac{J_w}{k_D}\right) - \pi_{F,b}\, exp\left(\frac{J_w S}{D_s}\right)\right] \quad (2.11)$$

Relationship between ICP and structure parameter implies that an ideal FO membrane may be an interfacial composite built on a thin, highly porous and minimally tortuous support. What's more, hydrophilic support is also favored for FO membranes. The water and solute transport can only occur through "wetted pores". The unsaturated pores of hydrophobic support reduce solute diffusivity and available pathways for water transport [81].

2.1.3 Membrane design

As with any membrane processes, performance metrics for membranes in osmotic processes are largely centered on high water flux and high selectivity. Based on the theoretical

treatment above, we can compose a series of criteria that membranes need to exhibit to achieve these metrics for osmotically driven processes [82].

High reverse solute flux selectivity. This is a criteria for the selective layer. The loss of draw solute needs to be minimized during osmotic process via reverse solute flux, which refers to the back permeation of draw solutes from the draw solution through the membrane selective layer into the feed [39].

Low structural parameter. This is a criteria for the support layer. The ideal supporting structure is thin, highly porous, minimally tortuous and hydrophilic to exhibit a low structural parameter to minimize the diffusion path and enhance back diffusion of draw solute.

Chemical and thermal stability. The membrane needs to maintain stable in the presence of various draw and feed solutes. Most notably, the membrane should be chlorine-tolerant in the desalination applications.

Mechanical strength and pressure tolerance. Good mechanical strength is required to handle and operate the membranes in osmotic processes. Minimal pressure tolerance is required for FO processes due to no/low hydraulic pressure uses. Excellent pressure tolerance is required for PRO process.

Easy to manufacture, economically favorable. The materials used in membranes should be inexpensive and easy to produce in large quantities. The membranes should be easy to manufacture on a continuous production line at reasonable speeds. The module operation should allow small footprint systems and be economically favorable.

With these membrane design criteria, membranes would be developed for osmotic processes based on available platforms and configurations as discussed below.

2.1.3.1 Flat sheet membrane configuration

Flat sheet configuration is the basic and conventional membrane manufacture platform.

Namely, flat sheet membrane is the membrane in a sheet form that performs as a barrier for separations. As industrial membrane plants, such as today's seawater RO plants, often require large membrane areas to perform the separation, today's flat sheet membranes are required to be economically and efficiently packaged into membrane modules. Generally, flat sheet membranes allow for two types of membrane modules: plate-and-frame and spiral-wound.

Plate-and-frame modules. The earliest designs of membrane modules were based on basic filtration and consisted of flat sheet membranes held in a type of filter press, as known as plate-and-frame module [34, 83]. These modules included membrane, feed spacers, and product spacers layered together between two end plates. Feed is forced across the membrane surface, passes through the membrane, enters the permeate channel, and is collected by a manifold. Plate-and-frame units have been developed for some small-scale applications, but these units are expensive to scale up. Plate-and-frame modules are now only used in electrodialysis and pervaporation systems and in a limited number of reverse osmosis and ultrafiltration applications with highly fouling feeds [34].

Spiral-wound modules. The early design of spiral-wound modules were used in artificial kidney designs [34]. The spiral-wound module is consisting of membrane envelopes of spacers and membranes wound around a perforated central collection tube and placed inside a tubular pressure vessel [34]. Feed passes axially down the module across the membrane envelope and permeates into the membrane envelope, where it spirals towards the center and exits through the collection tube. Spiral-wound modules allow for higher packing density as larger area of membranes are packed in a limited volume module. The standard industrial spiral-wound module has an 8-in. diameter and 40 in. length, and is commonly used in reverse osmosis and ultrafiltration applications.

2.1.3.2 Hollow fiber membrane configuration

The techniques for making flat sheet membranes can be adapted to produce membranes in the form of thin tubes or fibers. Hollow fiber membranes are the membranes with capillary geometrical shape. An important advantage of hollow fiber membranes is that compact modules with very high membrane surface areas can be formed [34]. Therefore, hollow fiber membranes are desired in many membrane applications because of their high packing densities relative to flat sheet configuration.

Hollow fiber modules. Hollow fiber membrane modules are normally formed in two basic geometries: shell-side (outer space of fiber) feed and lumen-side (inner space of fiber) feed designs. In hollow fiber modules, a bundle of fibers is contained in a pressure vessel. The system is either pressurized from the shell side while permeate passes through fiber wall and exits through open fiber ends, or the feed circulates through the lumen of the fibers and the permeate exits through the shell channel. The high packing density allows for small footprint systems and makes low flux performance more tolerable. The morphology and self-supporting shape of the hollow fibers also allow for a spacer-free module preparation, and a low cost module fabrication.

Hollow fiber modules are used for high-pressure gas separation applications with fine fibers (fibers of 50 to 200 μm diameter) providing lowest cost design and high pressure tolerance [34]. In liquid separation applications, such as ultrafiltration, the diameters are typically larger to lessen the impact of pressure drop in the fiber lumens. However, as the diameter of the fibers in the module increases, the membrane area decreases. Therefore, optimizing the design parameters for hollow fiber membrane/module for a specific process is important.

In the commercial sector of osmotic processes, membrane modules have been developed using all three module types above. In academia, numerous high performance membranes were

developed for osmotic processes in the past decade in both flat sheet and hollow fiber configurations.

2.2 Membrane development for osmotic processes

Although the concept of harvesting osmotic gradient energy was proposed back in 1954 [84], the development of membranes for it was not launched until forty years later. The historical *membrane developments* in osmotic processes are summarized in Figure 2.3. Before 1990s, early work on osmotic processes focused on proving PRO concept using mathematic models and predicting performance from RO and NF experiments using commercially available RO or NF membranes [74]. Since Hydration Technology Innovation (HTI) (formerly Osmotek and Hydration Technology Inc.) (Albany, Oregon) founded in 1986, the commercial sector started to manufacture and apply forward osmosis membrane technology to filtration, concentration, removal and recycling of water [85]. The first commercially available FO membrane was developed by HTI based on cellulose triacetate (CTA) integral asymmetric platform. With the CTA membranes, the proof-of-concept activities included the first FO dewatering system for producing blue green algae, the first FO water treatment plant for landfill leachate, the first personal emergency hydration device, etc. However, the membrane development activities in the osmotic processes field were still limited in the commercial space.

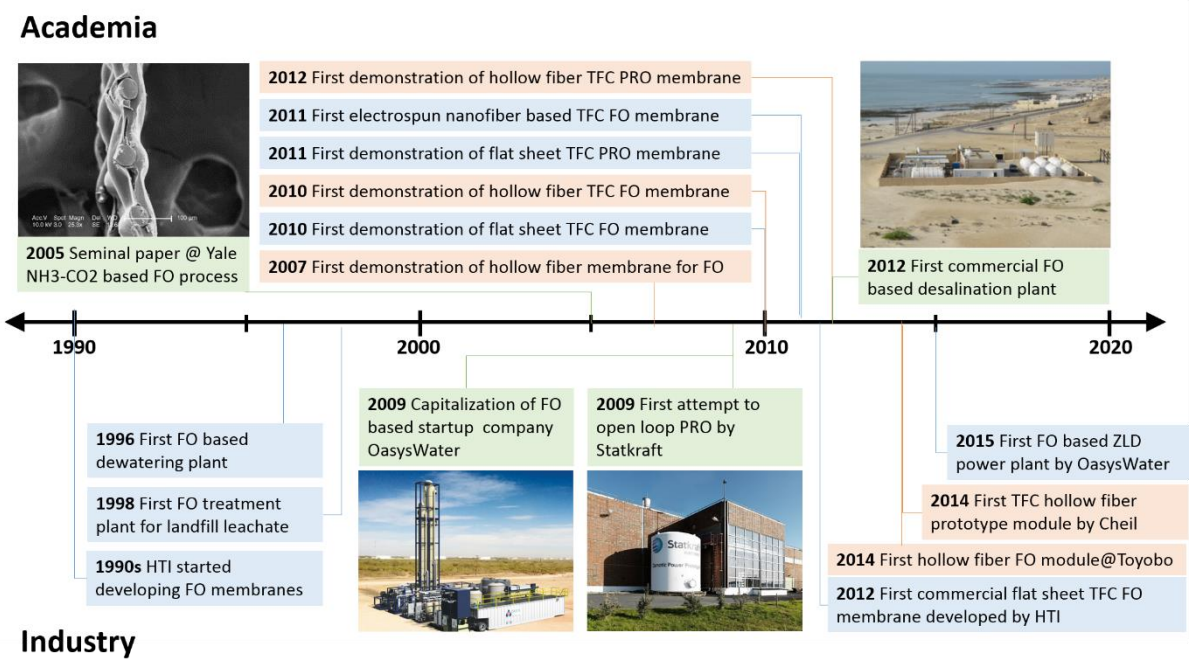

Figure 2.3. Historical membrane developments in osmotic membrane processes. In this figure, the half above the axis shows the activities in academia while the bottom half shows activities in industry. Events related to **flat sheet membrane** are labeled in blue, **hollow fiber membrane** in orange, and **key milestones** in the field are in green.

Until 2005, a seminal paper by McCutcheon et al. introduced the ammonia-carbon dioxide FO process as a potential desalination process that utilizes low-grade thermal energy has stimulated academic interest in FO [17]. Subsequently, a dramatic increase in the number of research articles and patents were documented [10, 12, 13]. Motivated by applications in water reuse, desalination and power production, a bevy of research on transport modeling [28–31][86], thermodynamics [32–34], designer draw solutions [24–27], and most notably, new membrane developments [1–3,5,14,23] have emerged.

New membranes developed for the osmotic processes are based on the two membrane configurations, flat sheet membrane and hollow fiber membrane. As discussed in previous section, the higher packing density of hollow fiber membrane allows for small footprint

systems and makes low flux performance more tolerable. The morphology and self-supporting shape of the hollow fibers also allow for a spacer-free module preparation. These benefits have translated well for osmotic processes, making them a preferred platform for FO. Therefore, the focus of this literature review is based on the hollow fiber membrane development for osmotic processes, though both configurations are discussed in the historical membrane developments (as shown in Figure 2.3).

Amongst the first academic membranes developed for FO were integral asymmetric hollow fiber membranes developed in 2007. Polybenzimidazole (PBI) and cellulose acetate (CA) were chosen because of their excellent nanofiltration (NF) characteristics [53, 87, 88]. Thermal and chemical treatments were used to enhance their selectivity and the resultant membranes showed good rejection to divalent ions. However, the relatively low selectivity to monovalent ions limited their capabilities in desalination applications.

A leap forward in osmotic process membrane development occurred when reverse osmosis (RO)-like thin film composite (TFC) membranes emerged in 2010. Laboratory scale TFC flat sheet and hollow fiber membranes emerged using typical membrane materials (polysulfone, PSU and polyethersulfone, PES, respectively) with properties and structures tailored for FO and thus exhibited superior flux and selectivity performance, especially to the monovalent ions, which allows for the potential application in desalination [25, 29].

The follow up academic interests in developing high performance membranes for osmotic processes were boosted by the commercial market back in time. Both FO and PRO received significant attention, and capital, for marketing osmotic process on a large commercial scale. In 2009, Oasys Water (Boston, MA), as a spin-off from Yale, constructed the first pilot scale system for FO desalination while Statkraft (Norway) started the construction of the first PRO power plant. Since PRO operations require adequate membrane strength and pressure-tolerance, membranes specifically designed for PRO process were developed in the following years in

academia, in both flat sheet and hollow fiber configurations [89, 90].

Since then, numerous research studies emerged from academia focusing on improving the membrane performance by employing novel materials and structures [25, 26, 29, 52, 91-93]. In industry, the first commercial TFC flat sheet membrane was developed for applications in both FO and PRO processes [32]. Details about this membrane is discussed in Chapter 3. Following up companies Oasys Water [33, 94], Toray [95] and Porifera [96] developed their own proprietary TFC flat sheet membranes. In the hollow fiber counterpart, Toyobo (Japan) offers a full scale hollow fiber module based on asymmetric cellulose acetate platform [97]. Samsung Cheil Industries (Korea) claims to have a semi-pilot TFC hollow fiber module [73, 98]. Aquaporin A/S (Denmark) is advertising a TFC hollow fiber FO membrane that incorporates biological proteins into its structure, details about this membrane is discussed in Appendix 1.

Looking at the historical events in the field of osmotic processes, we see that the membranes developed in academia have then been mimicked in industry shortly thereafter. Looking at recent FO progresses in industry, we note that a number of companies have been pursuing the hollow fiber membrane platform (Toyobo, Cheil, Aquaporin etc.). This recent emergence of commercial interest in hollow fibers has compelled us to summarize this particular aspect of the FO field and include its beginnings in academia where fundamental structure-property-performance relationships were first defined.

2.3 Progresses in hollow fiber membranes for osmotic processes

2.3.1 Hollow fiber membrane design options

The high packing density of hollow fiber membrane allows for small footprint systems and makes low flux performance more tolerable. The morphology and self-supporting shape of the hollow fibers also allow for a spacer-free module preparation. These benefits have translated well for osmotic processes, making them a preferred platform.

2.3.1.1 Asymmetric membrane vs. thin film composite membrane

Two types of membranes have been generally used for osmotic processes, asymmetric membrane and thin film composite membrane. The former one is well-known, conventional route which is typically prepared via the phase separation method [99]. For hollow fiber fabrication, the asymmetric membrane allows for one-step membrane formation as both selective (skin) and support layer are formed simultaneously during spinning, resulting in the integral structure with same polymer material.

On the other hand, thin film composite (TFC) membrane is prepared via a process known as interfacial polymerization (IP) [42, 100]. Generally, the IP process is conducted on a porous membrane support, typically prepared via phase separation. Two monomers from two phases crosslink at support surface to form ultrathin selective layer (typically aromatic polyamide, PA). The advantages of fabricating TFC membranes via interfacial polymerization are that the structure and properties of the substrate and the selective layer can be individually tailored and optimized to achieve desired permeability and salt rejection.

2.3.1.2 Shell-selective vs. lumen-selective

As discussed in Section 2.1.3.2, hollow fiber membrane modules are normally formed in two basic geometries: shell-side (outer space of fiber) feed and lumen-side (inner space of fiber) feed designs. For asymmetric membranes, skin layers would be formed on both shell and lumen surfaces is the bore fluid and coagulation bath are same non-solvent. However, this provides options for TFC membrane fabrications since the selective layer can be synthesized in-situ on either the shell (outer) surface or the lumen (inner) surface of hollow fiber. The benefits and drawbacks of shell-selective and lumen-selective hollow fiber membranes for osmotic processes are summarized in Table 2.1.

As Table 2.1 presented, both shell-selective and lumen-selective hollow fiber membranes have their own benefits and drawbacks. The development of shell-selective membranes was largely hampered by the difficulties during the interfacial polymerization process (IP) [101, 102]. Only a few membranes were developed as shell-selective. A batch coating method has been developed by Ren et al. based on typical dip-coating IP process on shell surface of hydrophilic hollow fiber supports [101]. However, this process requires careful distribution of fibers in coating process, thus is not very efficient. Sun et al. developed a vacuum-assisted IP process which allows selective layer formation in a bundle [102], thus showed more promise on large scale. Other studies are mainly focused on lumen-selective membranes, and are discussed in the following sections. Due to the difference in membrane design criteria of FO and PRO membranes, the currently developed hollow fiber membranes are discussed separately for these two applications.

	Shell-selective	Lumen-selective
Illustration	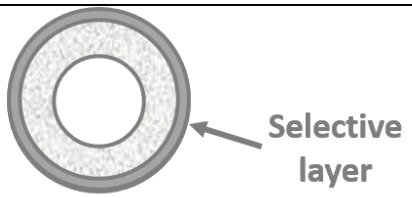	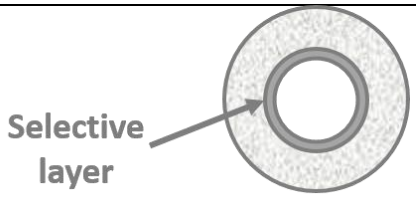
Benefits	• More effective surface area • Less fouling/clogging propensity • Less feed pressure drop	• Easy to conduct IP in bundle • Higher burst pressure-tolerance of capillary fiber
Drawbacks	Difficult to conduct IP: • Fiber overlap induces defects when conduct IP in bundle • Roller contact induces defects when conduct IP in continuous process	• Less effective surface area per module • Fouling and clogging propensity when treating challenging water

Table 2.1. Summary of benefits and drawbacks of shell-selective and lumen-selective hollow fiber membranes for osmotic processes.

2.3.2 Hollow fiber membranes for FO

2.3.2.1 Asymmetric hollow fiber membranes for FO

Amongst the first hollow fiber membranes developed for FO were integral asymmetric membranes. Polybenzimidazole (PBI, chemical structure shown in Figure 2.4) and cellulose acetate (CA) were chosen because of their excellent nanofiltration (NF) characteristics [53, 87, 88]. Thermal and chemical treatments were used to enhance their selectivity and the resultant membranes showed good rejection to divalent ions. However, the relatively low selectivity to monovalent ions limited their capabilities in desalination applications.

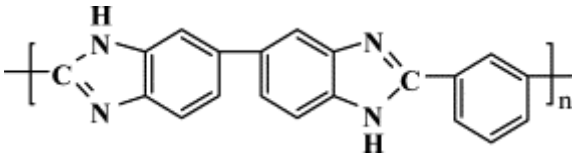

Figure 2.4. Chemical structure of polybenzimidazole (PBI).

Follow-up work was focused on enhancing the water flux for FO applications by reducing the mass transfer resistance within membrane structure. Yang et al. used dual-layer composite membranes via co-extrusion spinning method where the schematic diagram of spinneret is shown in Figure 2.4. In this design, PBI was used as the selective layer that provided NF level shell-selectivity while the support layer was comprised of polyethersulfone/ polyvinylpyrrolidone (PES/PVP) for a reduced mass transfer resistance in membrane [54]. However, one drawback that exists for the dual-layer co-extrusion spinning is the delamination between selective and support layers.

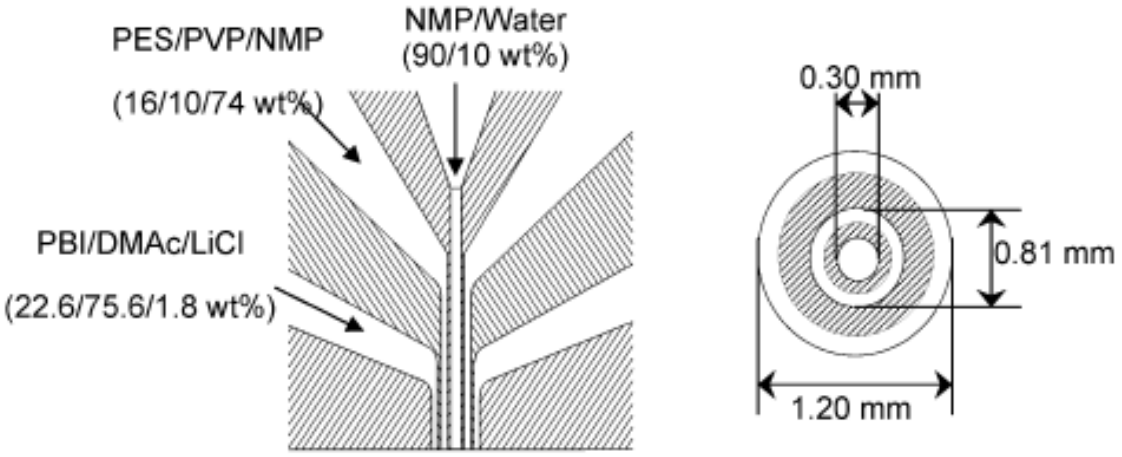

Figure 2.5. Schematic diagram of spinneret for dual-layer hollow fiber spinning. Reprinted with permission from Environmental Science & Technology, 43, Qian Yang et al., Dual-Layer Hollow Fibers with Enhanced Flux As Novel Forward Osmosis Membranes for Water Production, 2800-2805 [54]. Copyright 2009 American Chemical Society.

To avoid delamination between selective and support layers, Fu et al. developed a dual-layer hollow fiber membrane with a mixed matrix PBI/polyhedral oligomeric silsesquioxane

(POSS) shell-selective layer and a polyacrylonitrile/PVP support layer to provide the required strength for both FO and PRO [57]. POSS influenced on morphology and performance of the developed membranes while POSS and PVP both assisted macrovoid-free and delamination-free dual-layer membrane as shown in Figure 2.6 [57].

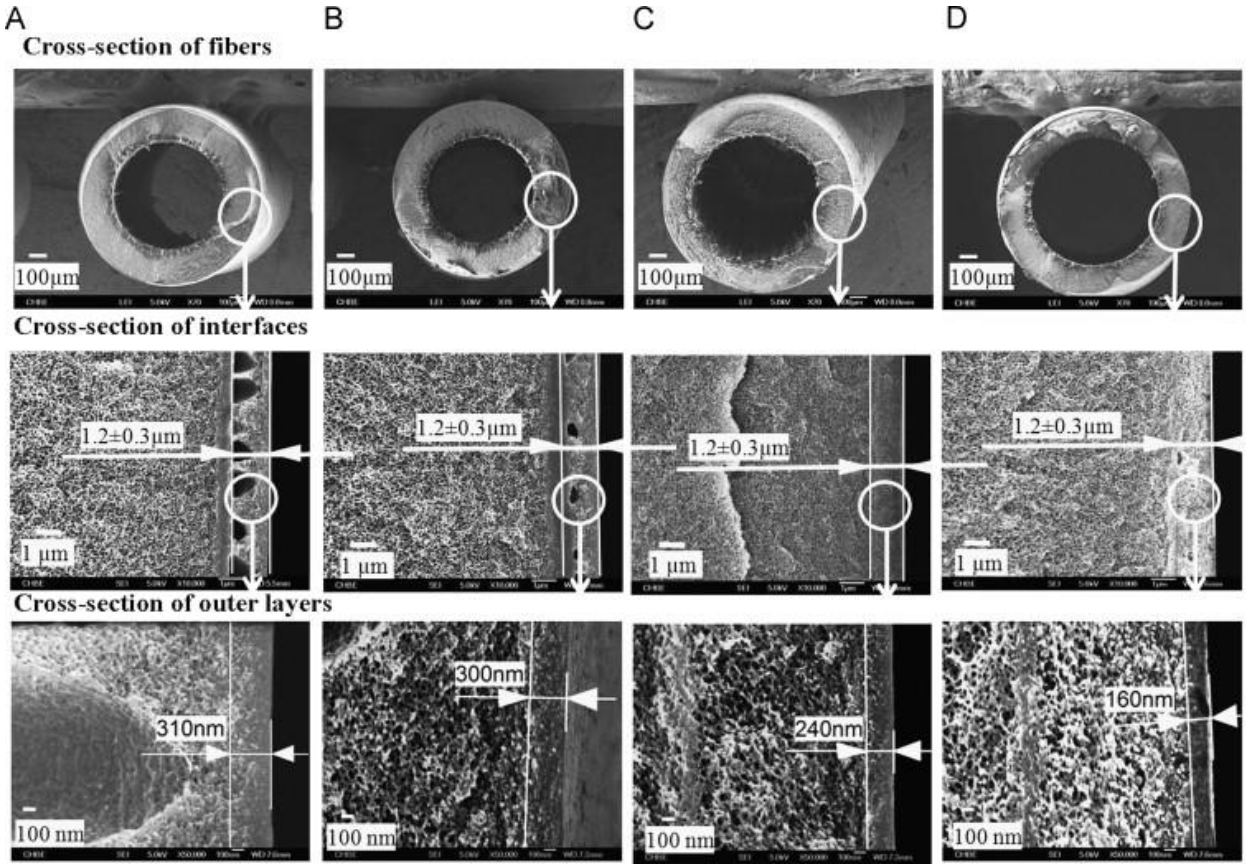

Figure 2.6. Cross-section morphology of PBI/POSS–PAN/PVP hollow fiber membranes as a function of POSS wt%. (A) PBI-PAN-P0 (no POSS), (B) PBI-PAN-P0.5 (C) PBI-PAN-P1.0 and (D) PBI-PAN-P1.5. Reprinted from Journal of Membrane Science, 443, Feng-Jiang Fu et al., POSS-containing delamination-free dual-layer hollow fiber membranes for forward osmosis and osmotic power generation, 144-155, Copyright (2013), with permission from Elsevier [57].

Instead of using PBI as the selective layer, another set of studies utilized polyamide-imide (PAI, Torlon) as the substrate material to develop hollow fiber membranes and followed by

polyelectrolyte post-treatment with ployethyleneimine (PEI) to achieve a NF-like selective layer [103, 104]. The reaction scheme is shown in Figure 2.7. Similarly, to enhance the water flux, Setiawan et al. developed dual-layer hollow fiber membrane with PAI for the shell-selective layer and PES for the porous support layer using the previously described co-extrusion method, followed up with PEI polyelectrolyte modification to produce a NF-like thin layer [105, 106]. To further improve FO performance, Goh et al. immobilized multi-walled carbon nanotube (MWCNT) in PAI-PEI structure and the resulting membrane showed almost 30% enhancement of water flux in FO process [107]. These membranes all exhibited good flux performance, but were still limited to nanofiltration selectivity.

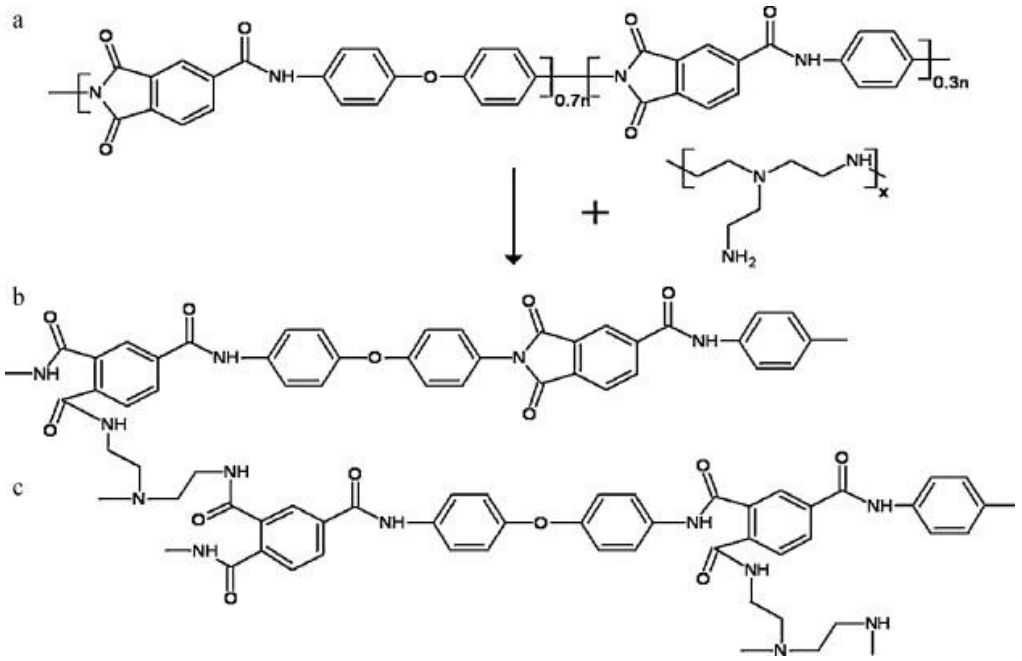

Figure 2.7. Reaction scheme between (a) poly(amide–imide) (PAI) and (b) polyethyleneimine (PEI); (c) cross-link PAI. Reprinted from Journal of Membrane Science, 369, Laurentia Setiawan et al., Fabrication of novel poly(amide–imide) forward osmosis hollow fiber membranes with a positively charged nanofiltration-like selective layer, 196-205, Copyright (2011), with permission from Elsevier [103].

2.3.2.2 Thin film composite hollow fiber membranes for FO

A leap forward in composite hollow fiber membrane occurred when Wang et al. first synthesized a reverse osmosis (RO)-like thin film composite (TFC) hollow fiber membrane in 2010 [29]. The polyamide (PA) selective layer was formed via *in-situ* interfacial polymerization (IP) on the lumen surface of a porous polyethersulfone (PES) hollow fiber substrate. This IP procedure was adopted from the conventional RO membrane developments [42], represents the most commonly used recipe using monomers of m-phenylenediamine (MPD) and trimesoyl chloride (TMC). The illustration of IP process is shown in Figure 2.8. The cross-sectional SEM images of this hollow fiber membrane is shown in Figure 2.9. This membrane, for the first time, demonstrated the potential of making TFC membranes on hollow fiber platform while showing great performance. Since then, a number of novel membranes were developed for FO with the focuses on both the selective and support layer design toward an enhanced water flux.

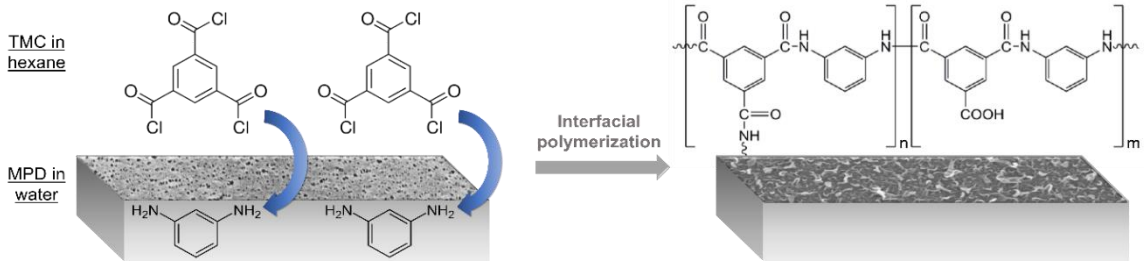

Figure 2.8. Illustration of interfacial polymerization for making thin film composite membranes.

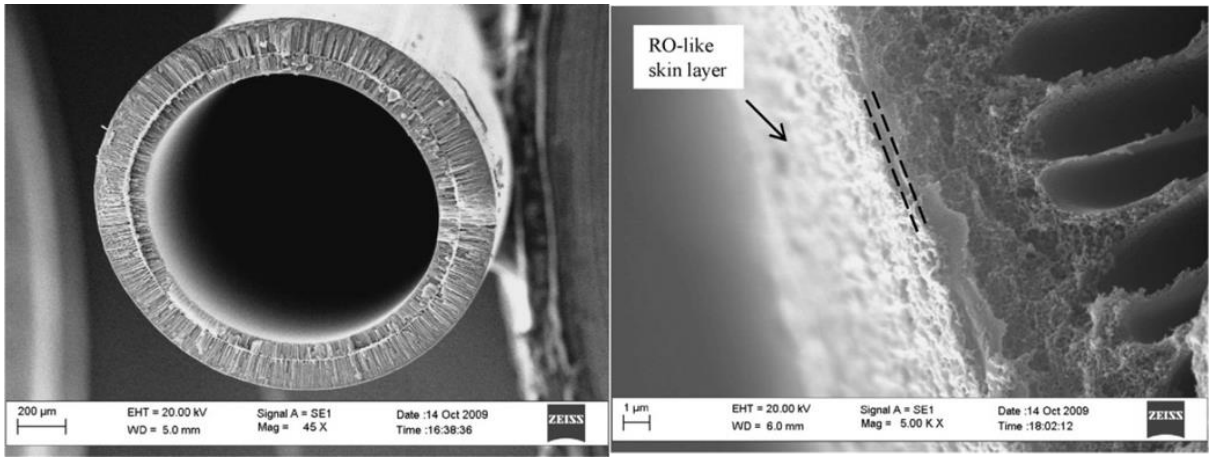

Figure 2.9. Cross-sectional SEM image of TFC hollow fiber membrane at 45×(left) and 5000 × (right). Adapted from Journal of Membrane Science, 355, Rong Wang et al., Characterization of novel forward osmosis hollow fiber membranes, 158-167, Copyright (2010), with permission from Elsevier [29].

2.3.2.1.1 Selective layer design

Most of the selective layer design for hollow fiber membranes for FO is based on the conventional RO-like selective layer due to the high permselectivity of the formed aromatic polyamide and the maturity of this technique. Though there are a handful of worthwhile efforts in the selective layer design.

Liu et al. developed a semi-dynamic layer-by-layer polyelectrolyte deposition to form a NF-like lumen-selective layer on PES porous hollow fiber support [108]. The layer-by-layer (LBL) polyelectrolyte deposited membranes have benefits due to the ease of selective layer formation and their stability and versatility. The illustration of LBL deposition on hollow fiber membrane lumen surface is shown in Figure 2.10. The resulting LBL membranes performed well in the FO process, with only two layer deposition, the LBL membranes demonstrated high water flux (up to 70 L/m^2 h using 0.5 M $MgCl_2$ as draw solution in PRO mode) and reduced salt leakage (around 0.5 g/m^2 h using 1 M $MgCl_2$ draw solution in FO mode). However, it is

worth noting that the draw solution provided a higher osmotic driving force with $MgCl_2$ draw solute. Moreover, Mg^{2+} ions are more easily retained which results in lower reverse salt flux. Meanwhile, to reach adequate permselectivity of the selective layer, multiple cycles of LBL deposition is needed, which would induces concerns in the scaling up of this technique.

Figure 2.10. Schematic illustration of LBL deposition on hollow fiber membrane lumen surface. Polyelectrolytes used are poly(styrene sulfonate) (PSS) and poly(allylamine hydrochloride) (PAH). Reprinted from Reactive and Functional Polymers, 86, Chang Liu et al., Enhanced hollow fiber membrane performance via semi-dynamic layer-by-layer polyelectrolyte inner surface deposition for nanofiltration and forward osmosis applications, 154-160, Copyright (2015), with permission from Elsevier [108].

The selective layer design was also demonstrated in Fang et al.'s work on developing double-selective layers hollow fiber membranes for FO [109, 110]. Composite hollow fiber membranes with two selective skin layers on both shell and lumen surfaces were developed for FO. A polyamide RO-like selective layer was formed on the lumen surface as the major selective layer. The secondary NF-like shell-selective layer, aiming to reduce the ICP [109] or organic fouling [110], was prepared using the PAI/PEI polyelectrolyte post-treatment or LBL polyelectrolyte deposition, respectively. The surface morphology of the RO-like lumen-selective layer and NF-like shell-selective layer prepared via LBL assembly is shown in Figure 2.11. This was a worthwhile trial to develop FO membranes for high salinity and fouling propensity water treatment, though the significant mass transfer resistance was induced due to

the secondary selective layer.

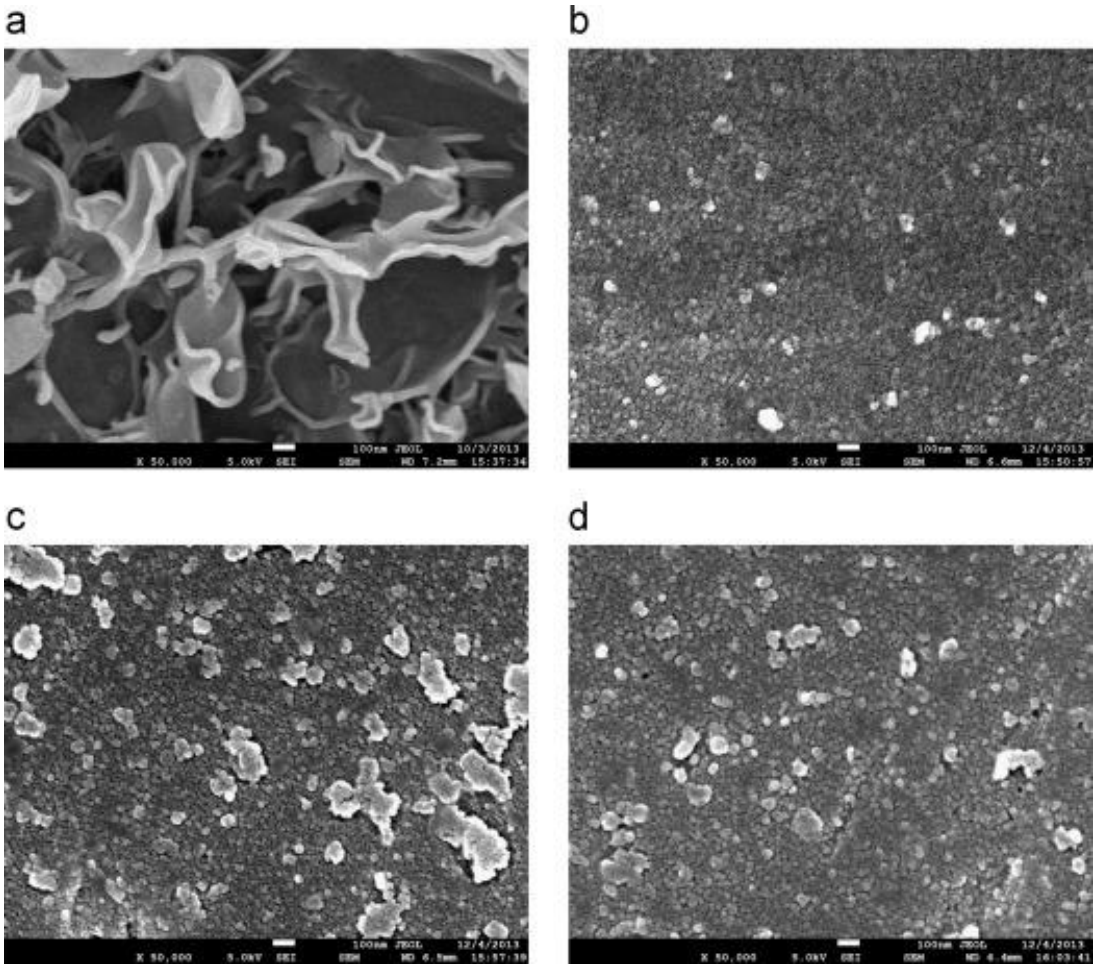

Figure 2.11. Surface morphology of RO-like IP inner skin layer: (a) at 50,000×; surface morphology of NF-like LBL assembled outer skin layer: (b) 1.5 bilayers at 50,000×; (c) 2.0 bilayers at 50,000×; (d) 2.5 bilayers at 50,000×. Reprinted from Journal of Membrane Science, 492, Wangxi Fang et al., Composite forward osmosis hollow fiber membranes: Integration of RO- and NF-like selective layers for enhanced organic fouling resistance, 147-155, Copyright (2015), with permission from Elsevier [110].

2.3.2.1.2 Support layer design

As suggested by the FO membrane design criteria, the support layer needs to be thin, highly porous, and minimally tortuous (*i.e.* a low structural parameter [25, 43, 44]) to minimize the internal concentration polarization (ICP) [45, 46]. Therefore, a majority of the effort to make

TFC hollow fiber FO membranes has focused on the design of the support layer. These efforts include the innovations in both the membrane materials and structures.

2.3.2.1.2.1 Support layer material design

Novel substrate materials were studied and aimed for a lower structural parameter and greater hydrophilicity [111]. So far, three hollow fiber FO membranes were developed with hydrophilic materials. The materials are summarized in Table 2.2. Zhong et al. used direct sulfonated polyphenylenesulfone (sPPSU) as substrate material for TFC hollow fiber membrane. With increased degree of sulfonation, the hydrophilicity of substrate was increased and resulted in higher FO performance [112, 113]. Ren et al. developed a shell-selective TFC hollow fiber membrane using intrinsic hydrophilic polyacrylonitrile (PAN) as supporting material. Different pore structures of fibers were considered by altering the fabrication technique while the best membrane exhibited a low structural parameter of ~ 300 μm [101]. Han et al. used a hydrophilic cellulose acetate butyrate (CAB) as supporting material. The CAB hollow fiber membrane was further modified with polydopamine (PDA) to improve hydrophilicity. The resulting membrane exhibited high water flux, water recovery and salt/oil rejection but low fouling propensity in water reclamation from emulsified oily wastewater [64].

ID	Materials	Chemical structure	Cross-section morphology
Zhong [112]	Sulfonated polyphenylene-sulfone (sPPSU)	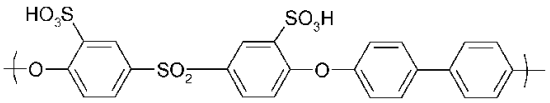	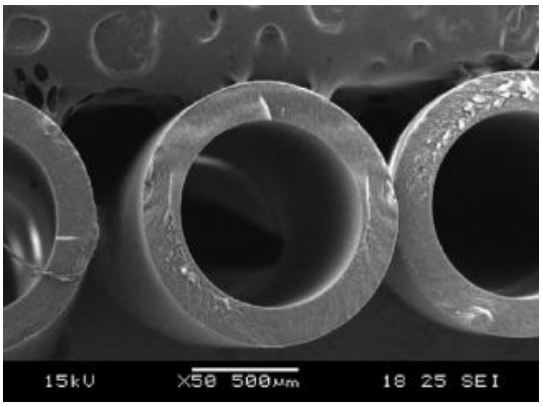
Ren [101]	Polyacrylonitrile (PAN)	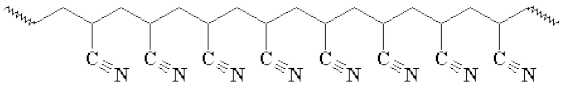	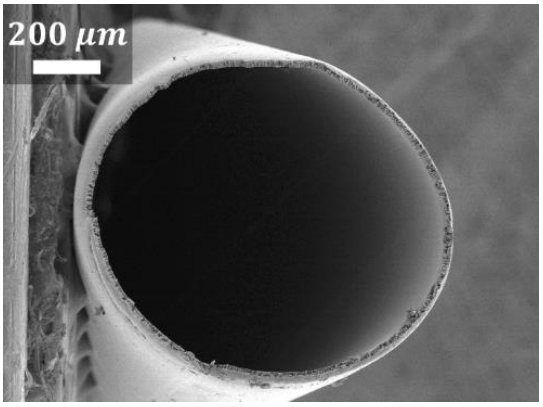
Han [64]	Cellulose acetate butyrate (CAB)	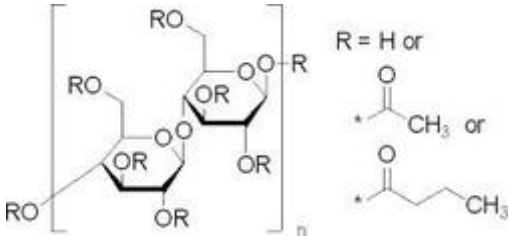	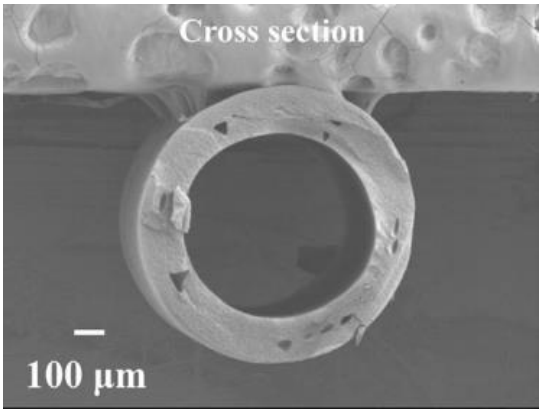

Table 2.2. Summary of hydrophilic support materials used for TFC hollow fiber FO membrane developments. SEM images adapted from Environmental Science & Technology, 47, P. Zhong et al., Development of Thin-Film Composite forward osmosis hollow fiber membranes using direct sulfonated polyphenylenesulfone (sPPSU) as membrane substrates, 7430-7436 [112], copyright 2013 American Chemical Society; J. Ren et al., Desalination, 372,

Polyacrylonitrile supported thin film composite hollow fiber membranes for forward osmosis, 67-74, Copyright (2015), with permission from Elsevier [101]; and Water Research, 81, G. Han et al., Water reclamation from emulsified oily wastewater via effective forward osmosis hollow fiber membranes under the PRO mode, 54-63, Copyright (2015), with permission from Elsevier [64].

2.3.2.1.2.2 Support layer structure design

Another route to making high performance TFC hollow fiber membranes for FO is via the design of the support layer structure. With the focus on tailoring the support layer structure, the membrane materials selection was based on the commonly used membrane materials such as polysulfone (PSU), polyethersulfone (PES), and polyimide (PI). Among them, PES is the most commonly used polymeric material for fabrication of support layer for TFC hollow fiber FO membranes.

Initially, Wang et al. developed the first TFC hollow fiber membrane for FO using PES porous support [29]. The characterization reveals that the FO hollow fiber membranes possess a large lumen. The substrates are highly porous with a narrow pore size distribution. The selective layers present excellent intrinsic separation properties with a hydrophilic rejection layer and good mechanical strength. Based on this initial work, Chou et al. further tailored the support layer structure by eliminating the shell skin layer by increasing the air gap in the spinning process to prolong the phase separation and result in a loose shell skin [30]. The resulting membrane outperformed their first generation PES-based TFC hollow fiber membrane and is still served as one of the most representative hollow fiber FO membrane in this field. The morphology of this membrane is shown in Figure 2.12. Subsequently, Shi et al. further investigated the effect of substrate structure on the FO performance of PES hollow fiber membranes. Cross-section structures with different proportions of needle-like pores, sponge-

like pores and large macrovoids were investigated, but no significant difference were found in their FO performances [114]. Developed in the same research group at Nanyang Technological University (NTU), all these PES-based hollow fiber membranes have similar cross section structure consisted of proportions of needle-like pores, sponge-like pores and large macrovoids. However, it was believed that the existence of large macrovoids would induce mechanical weak points in the membrane operations, though the mechanical requirement less concerned in FO processes.

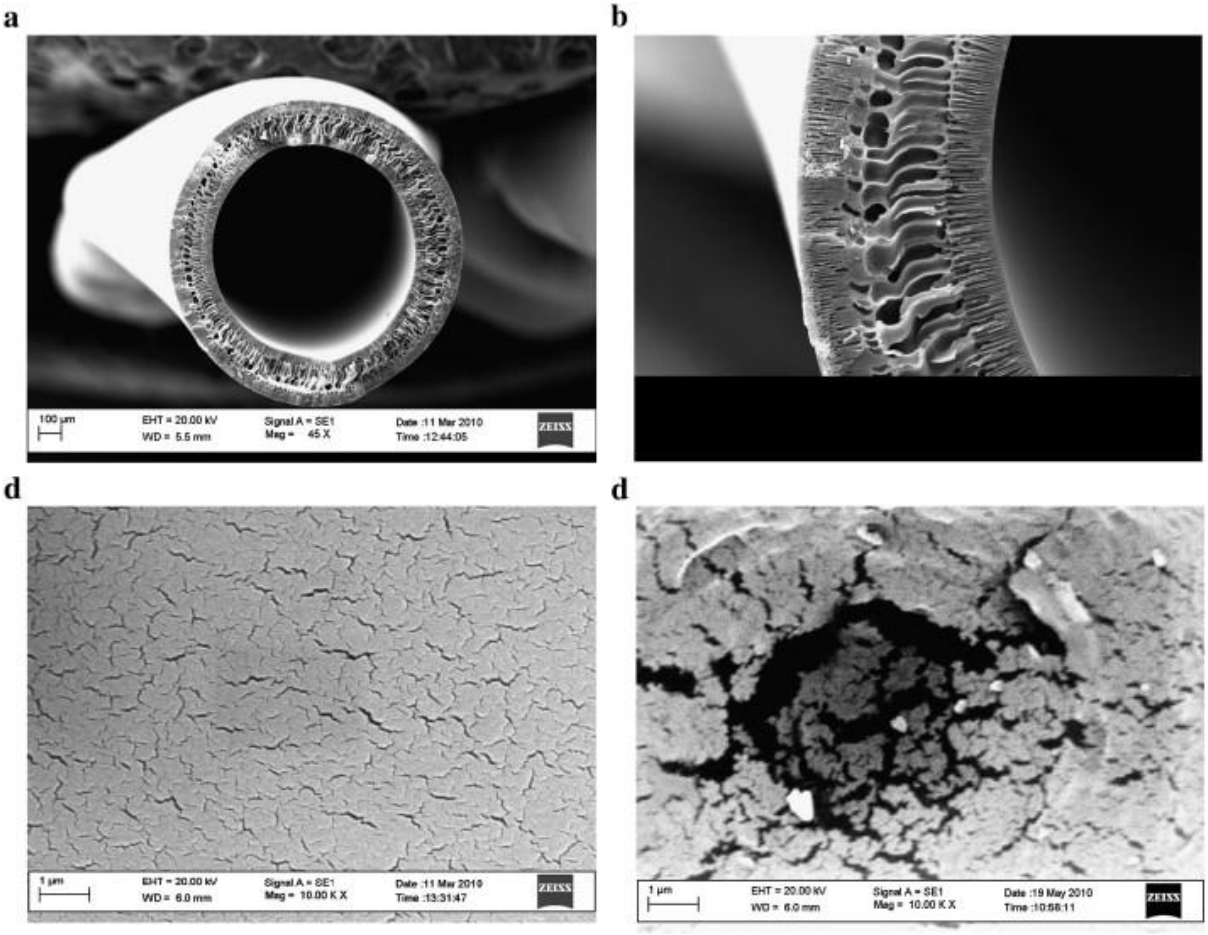

Figure. 2.12. Morphology of #C-PES hollow fiber substrates (a) cross-section at 45×, (b) enlarged at 200×; (c) inner surface layer enlarged at 10,000×; and (d) outer surface layer enlarged at 10,000×. Reprinted from Desalination, 261, Shuren Chou et al., Characteristics and potential applications of a novel forward osmosis hollow fiber membrane, 365-372, Copyright (2010), with permission from Elsevier [30].

Departing from the conventional structure consists of needle-like pores, sponge-like pores and large macrovoids, Sukitpaneenit et al. from National University of Singapore (NUS) developed the first macrovoid-free hollow fiber FO support using the same material, PES [31]. To achieve the formation of macrovoid-free and fully sponge-like structure, a finely tuned polymer dope solution with the composition of PES/PEG/NMP/water was used. PEG-400 and water were carefully added into polymer dope solution to induce gradual phase separation to avoid macrovoids that caused by abrupt solvent/non-solvent exchange during spinning. Furthermore, to eliminate a shell skin layer, the PES hollow fiber support was spun through a dual-layer co-extrusion spinneret with pure solvent in the outer channel to delay the phase separation. The strategies to control the phase separation process with the aid of co-extrusion technology is demonstrated in Figure 2.13. The cross section and surface morphology of this finely tailored macrovoid-free membrane is shown in Figure 2.14. As a result, this macrovoid-free TFC hollow fiber membrane showed slightly inferior FO performance than the membrane developed by Chou et al. but demonstrated significantly enhanced strength, which resulted in a more stable operation process [115].

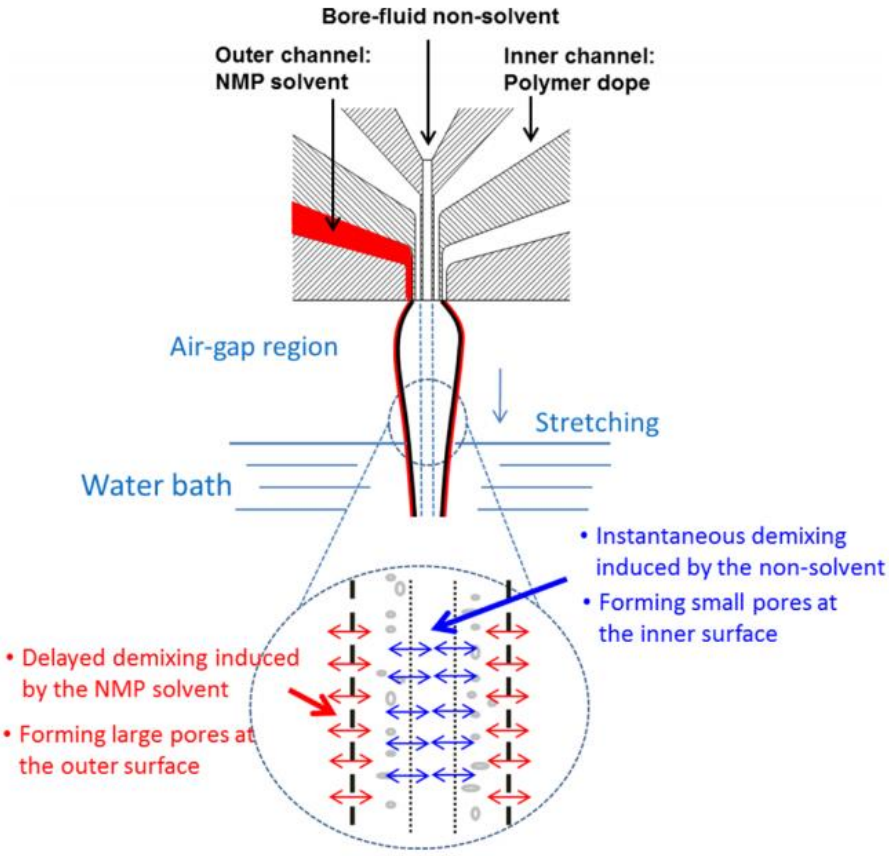

Figure 2.13. Strategies used by Sukitpaneenit et al. to control the phase separation process with the aid of co-extrusion technology employing a dual-layer spinneret. Reprinted with permission from Environmental Science & Technology, 46, P. Sukitpaneenit et al., High Performance Thin-Film Composite Forward Osmosis Hollow Fiber Membranes with Macrovoid-Free and Highly Porous Structure for Sustainable Water Production, 7358-7365 [31]. Copyright 2012 American Chemical Society.

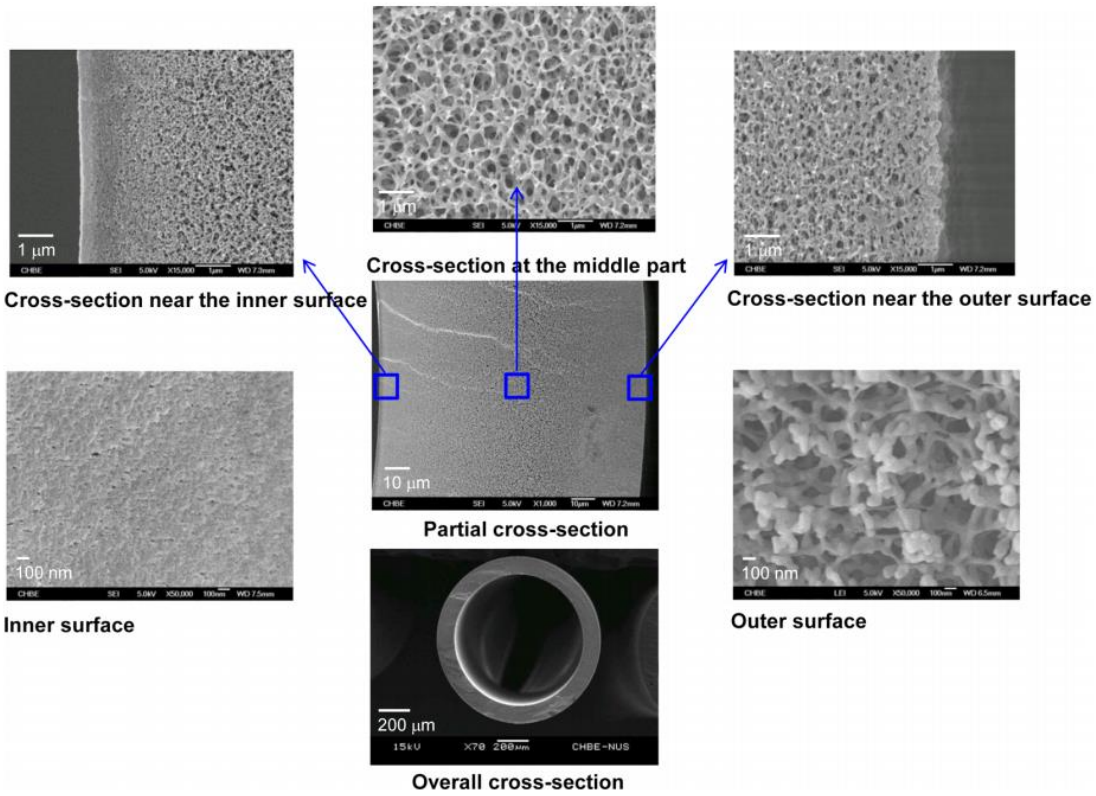

Figure 2.14. Cross section and surface morphologies of macrovoid-free hollow fiber membrane supports developed by Sukitpaneenit et al. Reprinted with permission from Environmental Science & Technology, 46, P. Sukitpaneenit et al., High Performance Thin-Film Composite Forward Osmosis Hollow Fiber Membranes with Macrovoid-Free and Highly Porous Structure for Sustainable Water Production, 7358-7365 [31]. Copyright 2012 American Chemical Society.

As these discussed hollow fiber membranes are all based on single-bore configuration. They often encounter issues such as long-term stability and potting durability. Fine fibers break easily and entangle one another during backwash, shaking, aeration, or mechanical cleaning. To improve the long-term reliability, multi-bore hollow fiber membranes were developed for FO [116, 117]. A schematic diagram of a triangle shape tri-bore spinneret is shown in Figure 2.15.

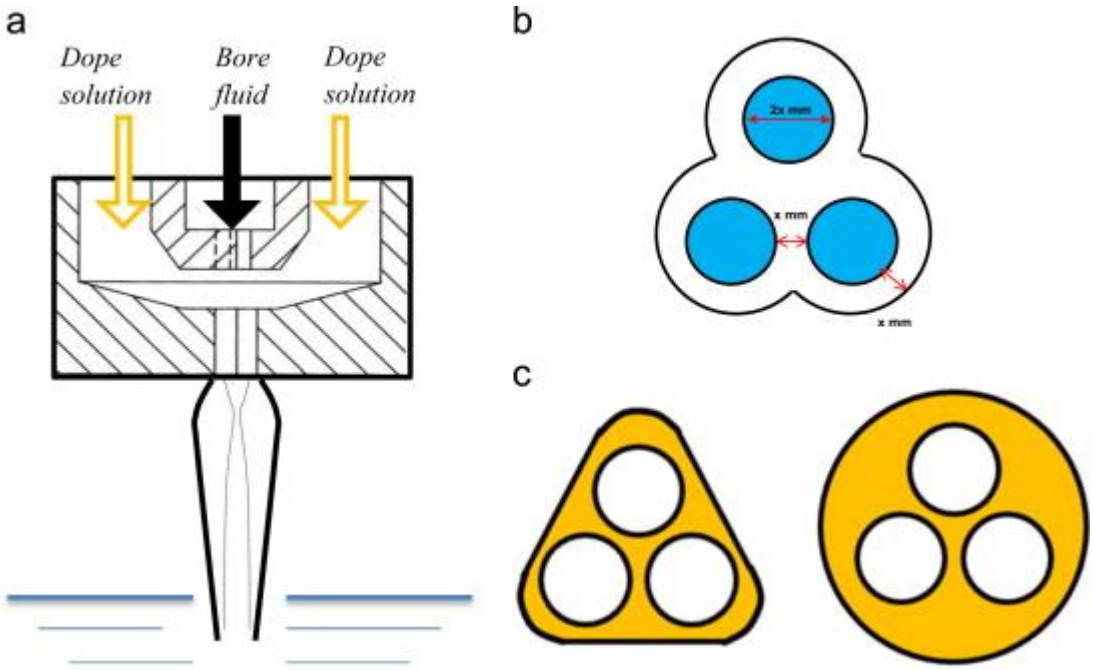

Figure. 2.15. (A) Single layer tri-needle spinneret; (B) bottom view of the tri-needle spinneret; (C) cross sections of as-spun tri-bore HFs. Reprinted from Journal of Membrane Science, 461, Lin Luo et al., Novel thin-film composite tri-bore hollow fiber membrane fabrication for forward osmosis, 28-38, Copyright (2014), with permission from Elsevier [116].

Due to the requirement of mechanical property, polyimide (Matrimide) and copolyimide (P84, BTDA-TDI/MDI, copolyimide of 3,3’,4,4’-benzophenone tetra-carboxylic dianhydride) were used as the support materials. The morphology of a represented tri-bore hollow fiber FO membrane is shown in Figure 2.16. These newly developed triangle tri-bore hollow fibers have impressive mechanical strength with enhanced permeation properties. Though the osmotic performance was slightly inhibited by introducing extra mass transfer resistance zones in the structure. Theoretically, the module consisting of triangle and tri-bore hollow fiber membranes would significantly increase the packing density and result in enhanced water output per module.

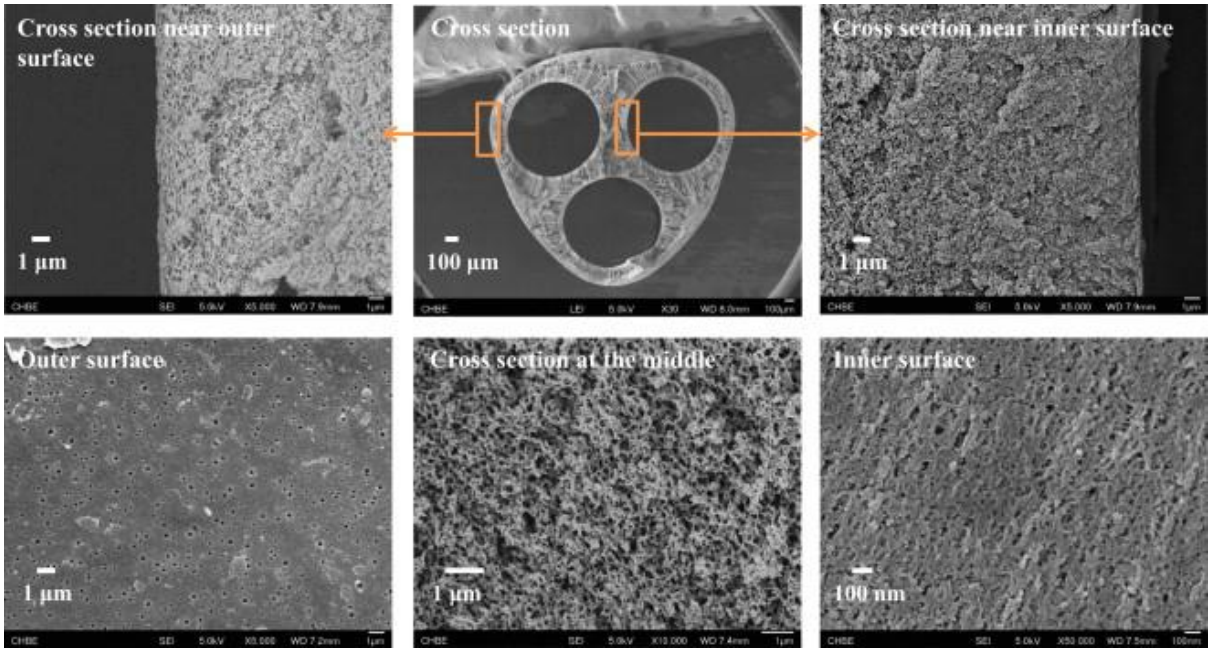

Figure. 2.16. Cross section and surface morphologies of a representative tri-bore hollow fiber membrane, TB3. Reprinted from Journal of Membrane Science, 461, Lin Luo et al., Novel thin-film composite tri-bore hollow fiber membrane fabrication for forward osmosis, 28-38, Copyright (2014), with permission from Elsevier [116].

2.3.3 Hollow fiber membranes for PRO

2.3.3.1 Asymmetric hollow fiber membranes for PRO

The first dual layer asymmetric hollow fiber membrane was fabricated by Fu et al. [57] consisting polybenzimidazole (PBI)/ polyhedral oligomeric silsesquioxane (POSS) outer-selective layer and a sponge-like polyacrylonitrile (PAN)/ polyvinylpyrrolidone (PVP) inner support layer. It was found that the addition of small amount of POSS into the PBI selective layer could help to achieve a higher permeate flux and a stronger PBI layer, while polyvinylpyrrolidone (PVP) could eliminate delamination at the sacrifice of water flux. Later, the performance of the dual layer membrane had been further improved by a post-treatment

step that involves flowing ammonium persulfate (APS) solution and DI water counter-currently, which was believed to remove the PVP molecules entrapped in the substrate and enhance water permeability significantly from 0.42 to 1.28 LMH/bar [118]. As the APS concentration increases, the water flux in the PRO process was increased while the salt leakage was slightly decreased. With the optimal APS concentration of 5 wt.%, the post-treated membrane showed a maximum power density of 5.10 W/m^2 at a hydraulic pressure of 15.0 bar when using 1 M NaCl as the draw solution and 10 mM NaCl as the feed. To our best knowledge, this is the best dual-layer PRO hollow fiber membrane directly fabricated from the non-solvent induced phase inversion for osmotic power generation. However, there is room to further improve the PRO performance of these integrally skinned hollow fiber membranes via (1) employing hydrophilic and robust materials, and (2) well controlling the phase inversion process to further improve the membrane mechanical strength, increase the membrane permeability and selectivity, but reduce the membrane structural parameter.

2.3.3.2 Thin film composite hollow fiber membranes for PRO

The first reported PRO hollow fiber membrane had been developed by Chou et al. using polyethersulfone (PES) substrate [90]. The membrane offered a decent power density of 10.6 W/m^2 at a pressure of 7 bar when using 1 M NaCl as the draw solution and 40 mM NaCl as the feed. However, the burst pressure was less than 10 bar. Later, to improve the fiber strength and PRO performance, a more robust material polyether-imide (PEI) was chosen as substrate material due to its higher tensile strength (3.65 GPa) than that (2.7 GPa) of polyethersulfone (PES) [119]. In addition, the mechanical strength had been further improved by controlling the structure of the substrate to have a sponge-like rather than the finger–like morphology used previously. The resultant TFC-PRO hollow fiber membrane could operate at hydraulic pressure as high as 15 bar and achieve a power density of 20.9 W/m^2 using 1 M NaCl as the draw

solution and 1 mM NaCl as the feed.

Zhang et al. also successfully developed PES-based TFC PRO hollow fiber membrane with high PRO performance as well as high mechanical strength where PES hollow fiber support had been carefully designed with diversified structure from macrovoid to sponge-like structure [120]. The morphology of a representative PES hollow fiber support is shown in Figure 2.17. The hollow fiber membrane produced a maximum power density of 24.3 W/m^2 at 20.0 bar by using 1 M NaCl as the concentrated brine and deionized (DI) water as the feed. In their study, it also found that, not only the mechanical stability of the TFC membranes is largely determined by the supporting substrate, the water permeability A and salt permeability B of the resultant TFC membrane at both low and high hydraulic pressure are also highly affected by the pore size and pore size distribution of the support. The desired PRO HF substrate should be: 1) a high porosity in the porous layer needed to reduce internal concentration polarization, 2) a thick and relatively dense skin layer underneath the TFC layer required to maintain good mechanical stability and stress dissipation, 3) a small with a narrow pore size distribution of the supporting layer underneath the TFC layer preferred to form a less-defective, mechanically stable TFC layer with high A as well as low B. The importance of low reverse salt permeance B has also been emphasized [121]. It showed that a large B value not only causes an instant drop in the initial water flux but also accelerates the flux decline at high hydraulic pressures, leading to reduced optimal operating pressure and maximal power density. Furthermore, it was found that a high B could cause significant salts accumulation in the feed along the large membrane module, leading to large reductions in both water flux and power density.

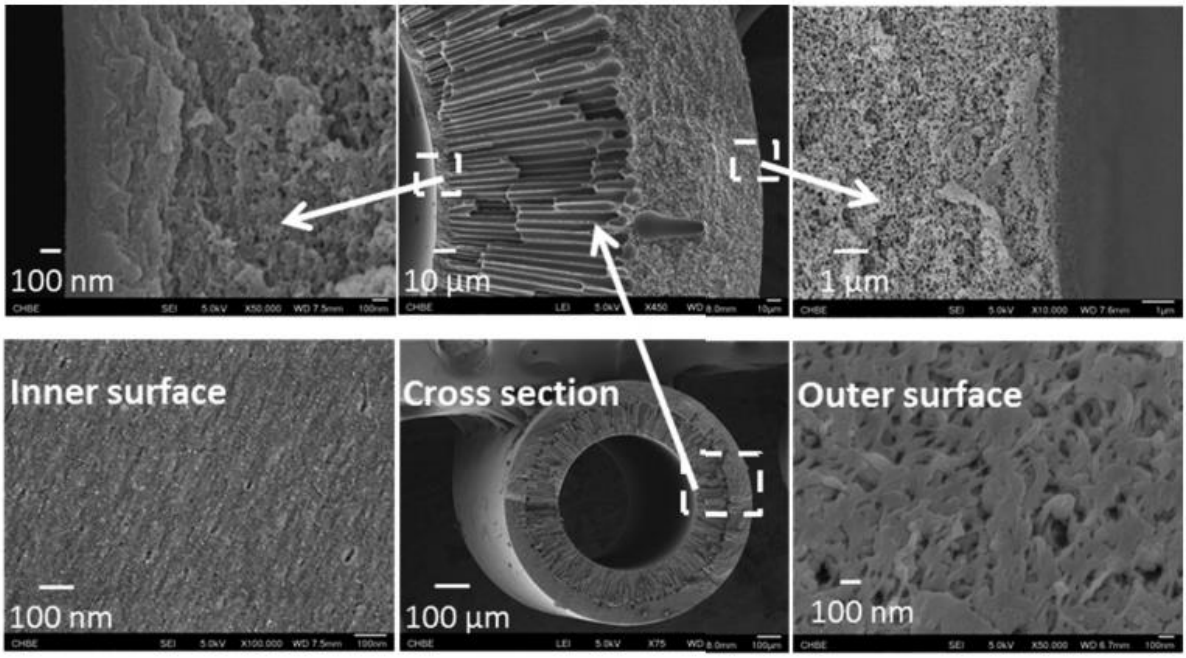

Figure 2.17. The cross section and surface morphologies of the PES hollow fiber support developed by Zhang et al. Reprinted with permission from Environmental Science & Technology, 47, S. Zhang et al., Minimizing the instant and accumulative effects of salt permeability to sustain ultrahigh osmotic power density, 10085-10092 [121]. Copyright 2013 American Chemical Society.

Han et al. fabricated a series of novel TFC membrane based on well-constructed Matrimid® hollow fiber substrates [122-124]. By manipulating the chemistry of polymer solutions and the kinetics of phase inversion processes, laboratory PRO tests showed that the newly developed TFC hollow fiber membranes exhibited a power density as high as 16.5 W/m^2 with a very low specific reverse salt flux ($\frac{J_s}{J_w}$) of 0.015 mol L^{-1} at a hydraulic pressure of 15 bar when using synthetic seawater brine (1.0 M NaCl) as the draw solution and deionized water as feed [124]. Also, the polyamide selective layer could be chemically modified using novel post-fabrication procedures to achieve desired power density, as shown in Figure 2.18. The impressive

mechanical stability and attractive power density suggest the great practicability of the newly developed composite membranes for harvesting osmotic energy via PRO process [123].

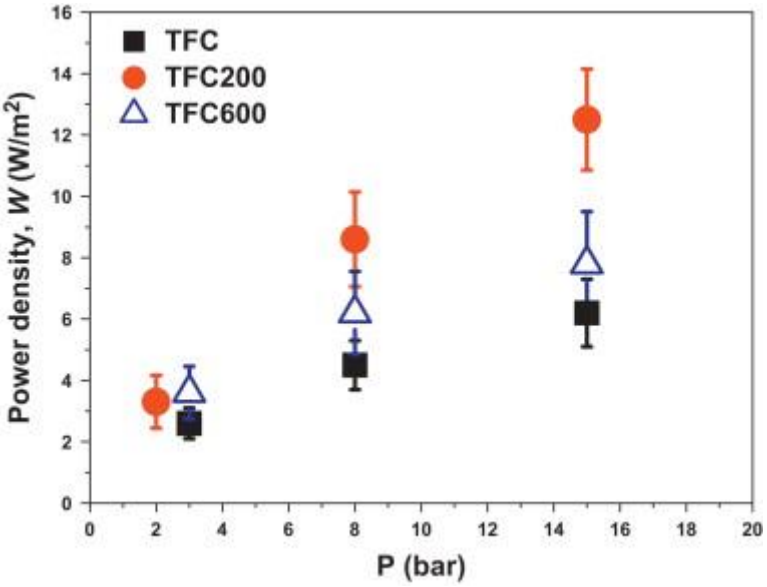

Figure 2.18. Power density of TFC, TFC200 and TFC600 membranes vs. trans-membrane pressure. (Draw solution: seawater brine (1 M NaCl), feed solution: deionized water, and temperature: 25 °C). Reprinted from Journal of Membrane Science, 440, G. Han et al., High performance thin film composite pressure retarded osmosis (PRO) membranes for renewable salinity-gradient energy generation, 108-121, Copyright (2013), with permission from Elsevier [123].

Li et al. prepared a series of P84 co-polyimide hollow fiber membrane supports with various structures, dimensions, pore characteristics, and mechanical properties for inner-selective TFC-PRO membranes by controlling the phase inversion process during spinning [125]. In another work, they had successfully designed antifouling PRO TFC membranes by synthesizing a dendritic hydrophilic polymer with well-controlled grafting sites, hyperbranched polyglycerol (HPG), and then grafting it on PES hollow fiber membrane supports. The illustration of the grafting process is demonstrated in Figure 2.19. Compared to

the pristine PES membranes, and conventional poly(ethylene glycol) (PEG)-grafted membranes, the HPG grafted membranes show much superior fouling resistance [126].

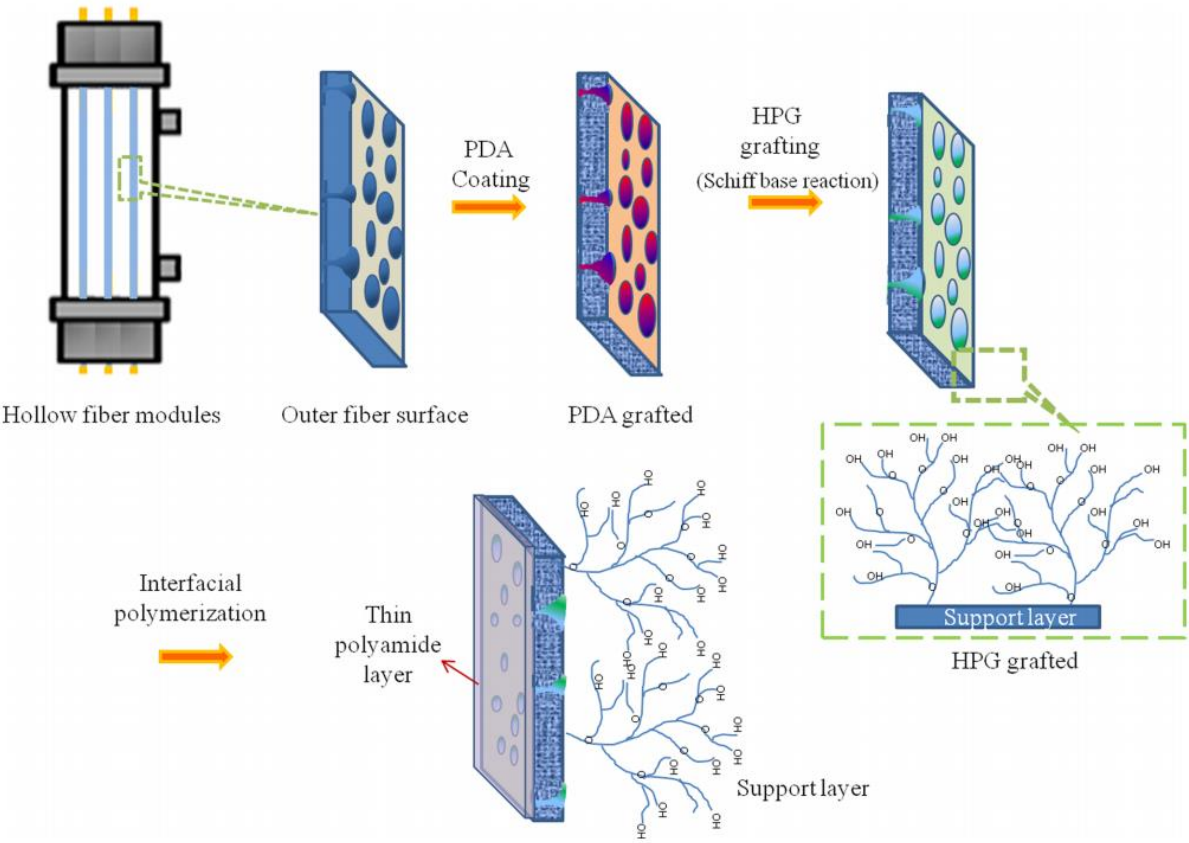

Figure 2.19. Schematic procedure for the fabrication of HPG-graft-TFC membranes. Reprinted with permission from Environmental Science & Technology, 48, X. Li et al., Anti-fouling behavior of hyperbranched polyglycerol-grafted poly (ether sulfone) hollow fiber membranes for osmotic power generation, 9898-9907 [126]. Copyright 2014 American Chemical Society.

As reviewed above, all the membrane were lumen-selective configuration due to the challenges to fabricate shell-selective hollow fiber membrane discussed above. There are limited study for shell-selective hollow fiber membrane fabrication. In Sun's work, a defect-free thin-film composite membrane module was achieved by vacuum-assisted interfacial polymerization to effectively drawn the excess water into the fiber lumen while the MPD stays

in the pores of the hollow fibers indicated in Figure 2.20. The morphology of the formed selective layer shown in Figure 2.20 offered a salt rejection of 74.53%, which was significantly improved compared to 0 % rejection of control membrane without vacuum assisted IP [102]. To enhance the PRO performance, the structure of the TFC layer was improved by coating a cushion layer of PDA prior to the interfacial polymerization step. PDA as a bio-inspired material has recently been proven to benefit PRO membranes in terms of mechanical strength and surface hydrophilicity because of its strong adhesive nature and covalent bonding between the polyimide support and TFC layer through free amine and hydroxyl groups [127]. The water permeance had been enhance from 1.5 LMH/bar to 5 LMH/bar. The newly developed membranes can stand over 20 bar with a peak power density of 7.63 W/m^2, which is equivalent to 13.72 W/m^2 of its inner-selective hollow fiber counterpart with the same module size, packing density, and fiber dimensions. Another work conducted by Ingole et al. also used PDA to modify PES hollow fiber substrate to form outer-selective TFC HF membrane, enhanced water flux and power density were observed [128].

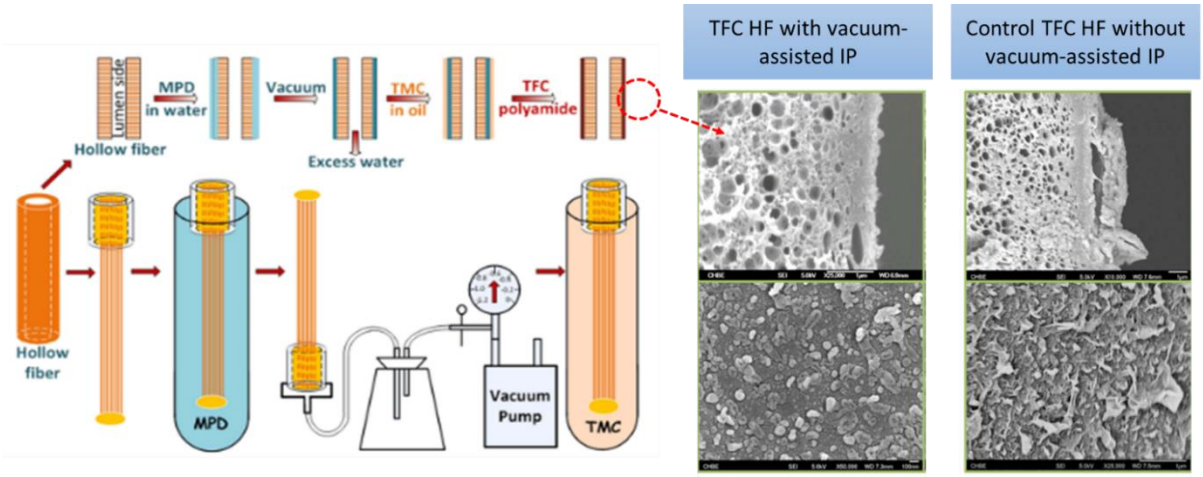

Figure 2.20. Left: Simplified process for preparing the shell-selective TFC hollow fiber membrane bundles for PRO power generation. Right: Top-row images are the cross-sectional morphology of the outer edge, while the bottom-row images are the outer surface of the shell-selective hollow fiber membranes developed by Sun et al. Reprinted with permission from

Environmental Science & Technology, 47, S.-P. Sun et al., Outer-Selective Pressure-Retarded Osmosis Hollow Fiber Membranes from Vacuum-Assisted Interfacial Polymerization for Osmotic Power Generation, 13167-13174 [102]. Copyright 2013 American Chemical Society.

2.4 Summary

This literature review provides a summary of current progress in osmotic processes, with a main focus on recent membrane developments. The understanding of transport behavior and mass transfer limitation is of importance to guide rational membrane design. The thorough reviewing of the progresses in membrane development for osmotic processes would provide immense insights in the future membrane design.

Innovative efforts have been made in all aspects such as the platform selection, selective layer synthesis method, support layer material selection, fabrication process, and structure design etc. With that, the thin film composite platform attracted most attentions with adopting novel hydrophilic materials, delicate modification methods and intensive fabrication processes (dual layer co-extrusion and tri-bore spinning etc.). All of the above-mentioned membranes showed good performance and great promise as the next generation hollow fiber membrane for osmotic processes. Meanwhile, fundamental understanding that elucidates the structure-performance relationship and guides the optimization of membrane and module design is also of great value.

Chapter 3. Evaluating Commercial Thin Film Composite Membrane for Forward Osmosis

Published as

Ren, J., McCutcheon, J.R., "A new commercial thin film composite membrane for forward osmosis", *Desalination*, 343 (2014), 187-193. DOI: 10.1016/j.desal.2013.11.026.

3.1. Introduction

Seawater desalination and wastewater reuse have received worldwide attention to alleviate the water stress caused by population growth and increasing resource consumption [7, 129]. Forward osmosis (FO) has been touted as a high water recovery and low energy consuming desalination option [12, 13, 129]. FO utilizes osmotic pressure difference to drive water across a semipermeable membrane from a dilute feed solution to a concentrated draw solution while rejecting most solutes [10]. Over the past decade, FO has attracted considerable attention in a number of fields in both industrial application and academic research [12, 13].

However, the development of FO has been hampered by the lack of effective membranes. Early studies were limited to existing commercial membranes, most of which were designed for reverse osmosis (RO) [10]. There have been a number of studies focusing on the development of high performance membranes specifically for FO [25, 29, 91], but they are all limited to lab scale fabrication techniques.

Since FO saw its resurgence in the middle of the last decade, the only commercially

available FO membrane has been the cellulose acetate (CA) asymmetric membrane from Hydration Technology Inc. (HTI, Albany, OR). The HTI CA membrane has an optimized structure for FO consisting of a thin selective layer followed by a relatively loose and thin support layer embedded with a mesh for strength [13, 111]. The hydrophilic nature of cellulose acetate as the matrix material favors proper wetting compared with hydrophobic membranes, but is susceptible to hydrolysis [130, 131]. Moreover, concerns about low water flux and high salt flux due to the relatively poor water permeability and selectivity, respectively, of CA membranes has limited the use of FO to niche applications [132].

In this study, a newly designed TFC membrane from HTI is introduced as a commercially available FO membrane which is made in a continuous process on a 40-inch production line. This TFC membrane inherits the mesh-embedded structure from the CA membrane but surpasses it by tailoring a porous support layer that promotes high water flux, low salt crossover, and hydrolytic resistance.

3.2. Experimental

3.2.1. Materials

Thin film composite (TFC) membranes and asymmetric cellulose triacetate (CA) membranes were provided by HTI. The TFC membrane is considered by HTI to be their early generation membrane. Both the CA and TFC membranes are fabricated on a 40-inch continuous production line. 2-propanol (isopropyl alcohol, IPA, anhydrous, 99%) was purchased from J.T.Baker (Center Valley, PA). Red food coloring from McCormick & Company Inc. (Sparks, MD) was used to ensure integrity of the membrane. For the osmotic flux tests, sodium chloride (NaCl, crystalline, certified ACS, Fisher Scientific) and deionized (DI) water from a Millipore Integral 10 water system (Millipore, USA) were used.

3.2.2 Membrane Preparation

Some of the TFC membranes were wetted using a 50 wt % solution of isopropyl alcohol (IPA) for 5 minutes at room temperature [111, 133]. The IPA was then thoroughly rinsed out of the membranes using DI water and stored at 5℃ in DI water. These are referred to as prewetted TFC in this study. CA membranes were not prewetted since they easily saturate when exposed to water.

3.2.3 Membrane characterization

3.2.3.1 Scanning Electron Microscopy

The surface morphology and cross-sectional structure of the TFC membranes were imaged with scanning electron microscopy (SEM). A cold cathode field emission scanning electron microscope JSM- 6335F (FESEM, JEOL Ltd., Japan) and a FEI Phenom desktop SEM (FEI Company, OR) were used for surface and cross-sectional morphology imaging, respectively. To view the cross sections of the membranes, the samples were submerged in liquid nitrogen to preserve the pore structure and cut with a razor blade. Prior to imaging, the samples were sputter coated with a thin layer of gold.

3.2.3.2 Contact Angle

The contact angles of the selective and support layers of the TFC membrane were measured using the sessile drop method on a CAM 101 series contact angle goniometer (KSV Company Linthicum Heights, MD). The values were taken as an average of six points with a droplet volume of 10±1μL. All measurements were taken at room temperature.

3.2.3.3 Attenuated Total Reflection Fourier-transform Infrared Spectroscopy

Attenuated total reflection Fourier-transform infrared (ATR-FTIR) spectroscopy was used to study the materials of the selective and support layers of the TFC membrane. ATR-FTIR spectra were obtained using a Jasco 670 plus FTIR spectrometer equipped with an ATR element (45° multi-reflection germanium crystal).

3.2.4 Water Permeance and Salt Permeability

Pure water permeance, salt permeability and salt rejection - of the CA and TFC membranes were evaluated in a laboratory-scale cross-flow RO test unit described elsewhere [91, 127]. McCormick^{TM} red food grade dye (1 mL) was added into feed water (10 mL) to detect pin-holes. Pure water permeance was measured at $20\pm0.5℃$ and averaged over four pressures ranging from 100 to 250 psi. Pure water flux (J_w) was calculated by dividing the volumetric permeate rate by the membrane area and measured from at least four samples. Salt rejection (R) tests were conducted using a feed solution of 2000 mg/L NaCl and a feed pressure of 125 psi. Intrinsic water permeance and salt permeability were derived by Yip et al. [25] and assumed to be constant and independent of pressure and salt concentration. The salt permeability (B) was determined from [25, 130, 134]

$$\mathrm{B} = J_w \left(\frac{1-R}{R}\right) \exp\left(-\frac{J_w}{k}\right) \quad (3.1)$$

where k is the mass transfer coefficient for the cross-flow channel of the RO membrane cell [132].

3.2.5 Osmotic Flux Testing

Osmotic water flux and reverse salt flux through CA and TFC membranes were characterized using a custom lab-scale cross-flow forward osmosis system. The experimental

setup was described in earlier investigations [111, 132]. Osmotic flux tests were carried out with the membrane oriented in both FO mode (the membrane selective layer faces the feed solution) and PRO mode (the membrane selective layer faces the draw solution). Two testing conditions - a recently published standard methodology [133] and one suggested by HTI - were used.

3.2.5.1 Standard Method

As new membranes are developed, especially commercial membranes, it is necessary to test performance under a standard protocol to make reasonable comparisons with other membranes. Recently, Cath et al. developed a method that was intended to standardize FO membrane testing [133]. In this method, water and salt fluxes were measured at 20 ± 0.5 ℃ using DI feed and 1 M NaCl draw solution. The cross flow velocities were maintained at 0.25 m/s on both sides of the membrane and the Reynolds number in both channels was set to 1125. No hydraulic transmembrane pressure or channel spacers were used. As in previously described methods for testing performance of FO membranes, the mass of draw solution reservoir was constantly monitored on a scale which outputs data to a computer. The osmotic water flux (J_w) was calculated by normalizing the volumetric flow rate by the effective membrane area [111]. Similarly, the salt flux (J_s) was calculated by dividing the NaCl mass flow rate by the membrane area and was accomplished by measuring the conductivity of the feed solutions at certain time points during the tests.

3.2.5.2 HTI Method

For full scale FO operations, the HTI TFC membrane is most likely to be used in a spiral wound element. An 8-inch diameter spiral wound TFC membrane element was developed by

HTI and has been commercially available since August, 2012. To date only a handful investigations have been done on spiral wound FO membrane modules. The effect of draw solution concentration and operating conditions on water flux was discussed by Xu et al in 2009 [135] while the effects of structural features were investigated by Kim and Park in 2011 [136]. As new membranes are developed, testing in elements is expensive and impractical. Also, for comparison to other membranes developed in the academic space, flat sheet studies are more appropriate. However, when conducting flat sheet studies, we can try to mimic the operating conditions in a spiral wound element. HTI provided such a method.

For the HTI method, the temperature and draw solution concentration were kept same as those in standard method at $20\pm0.5℃$ and 1 M NaCl, respectively. To simulate the mass transfer near the membrane surface in spiral wound FO elements, turbulence enhancing spacers (diamond pattern, ~0.8mm in thickness and ~2.5mm spacing) were used to fill the flow channel on both feed and draw sides of the membrane [18]. Furthermore, a cross flow velocity of 0.30 m/s (Reynolds number 1350) and a small transmembrane hydraulic pressure of 4 psi was used as well to better simulate the conditions in a typical HTI element. Such a low pressure differential is not anticipated to cause substantial water flux. McCormick™ red food grade dye was added to the high pressure side to detect the pin-holes.

3.2.6 Membrane Structural Parameter

As asymmetric membrane, the HTI TFC membrane comprises a thin selective layer supported by a porous support layer. Both experimental and modeling studies have shown that this support layer imparts a resistance to solute diffusion and causes internal concentration polarization (ICP) [25, 43, 44, 111, 137]. The membrane structural contributions to this phenomenon are defined using what is known as the structural parameter, S. It is defined as the product of the thickness (t) and tortuosity (τ), divided by the porosity (ε) (i.e., $S = t\tau/\varepsilon$) of

the membrane support layer.

In the experimental tests, the membrane effective structural parameter can be determined using the empirical equation previously described [45],

$$S = \left(\frac{D}{J_w}\right) \ln \frac{B + A\pi_{D,b}}{B + J_w + A\pi_{F,m}} \quad (3.2)$$

where D is the diffusion coefficient of the draw solute, J_w is the measured water flux in FO mode, $\pi_{D,b}$ is the bulk osmotic pressure of the draw solution, and $\pi_{F,m}$ is the osmotic pressure at the membrane surface on the feed side (0 for DI feed).

3.3. Results and Discussion

3.3.1 Characterization of Membrane

3.3.1.1 Scanning Electron Microscopy

The FESEM images of the top (selective) and bottom (support) surfaces of the TFC membrane are shown in Figure 3.1. The selective layer has a ridge and valley morphology which is a typical characteristic of a polyamide layer formed via interfacial polymerization [25, 137]. The selective layer shows uniform and continuous morphology, without defects or pin-holes. The FESEM images of the bottom surface of the support layer as shown in Figure. 3.1d, 3.1e, and 1f show a porous structure with pore size ranging from 100 to 600 nm.

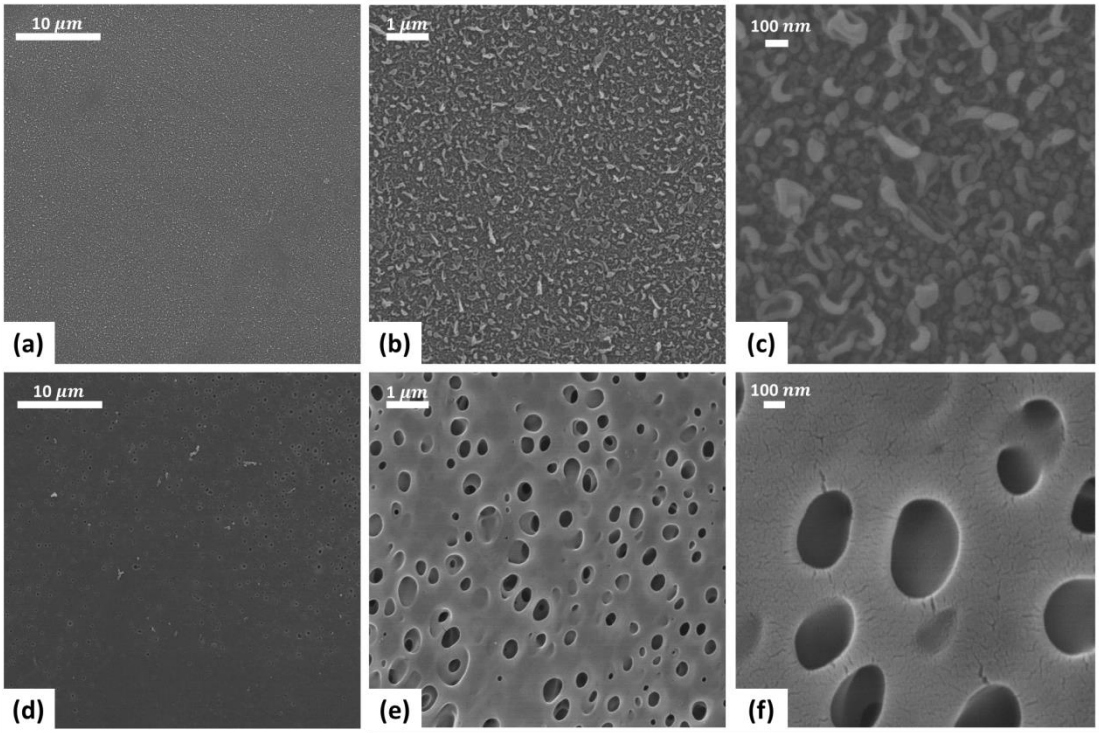

Figure 3.1. Top surface SEM images (a, b and c) and bottom surface FESEM images (d, e and f) of TFC membrane at magnifications of (a and d) 2000×, (b and e) 10,000×, and (c and f) 50,000×.

Figure 3.2 shows the cross-sectional SEM images of the TFC membrane. The thickness of the membrane is uniform at ~115μm while the diameter of the polyester fibers in the embedded mesh are ~50μm. This mesh provides most of the mechanical strength to the membrane, thereby eliminating the need for a thick porous support layer. A similar approach was used in the design of their CA membrane. Figure. 3.2c and 3.2d show that the selective layer adheres well to the denser part of the support layer. This layer accounts for the integrity and uniformity

of the polyamide layer [25].

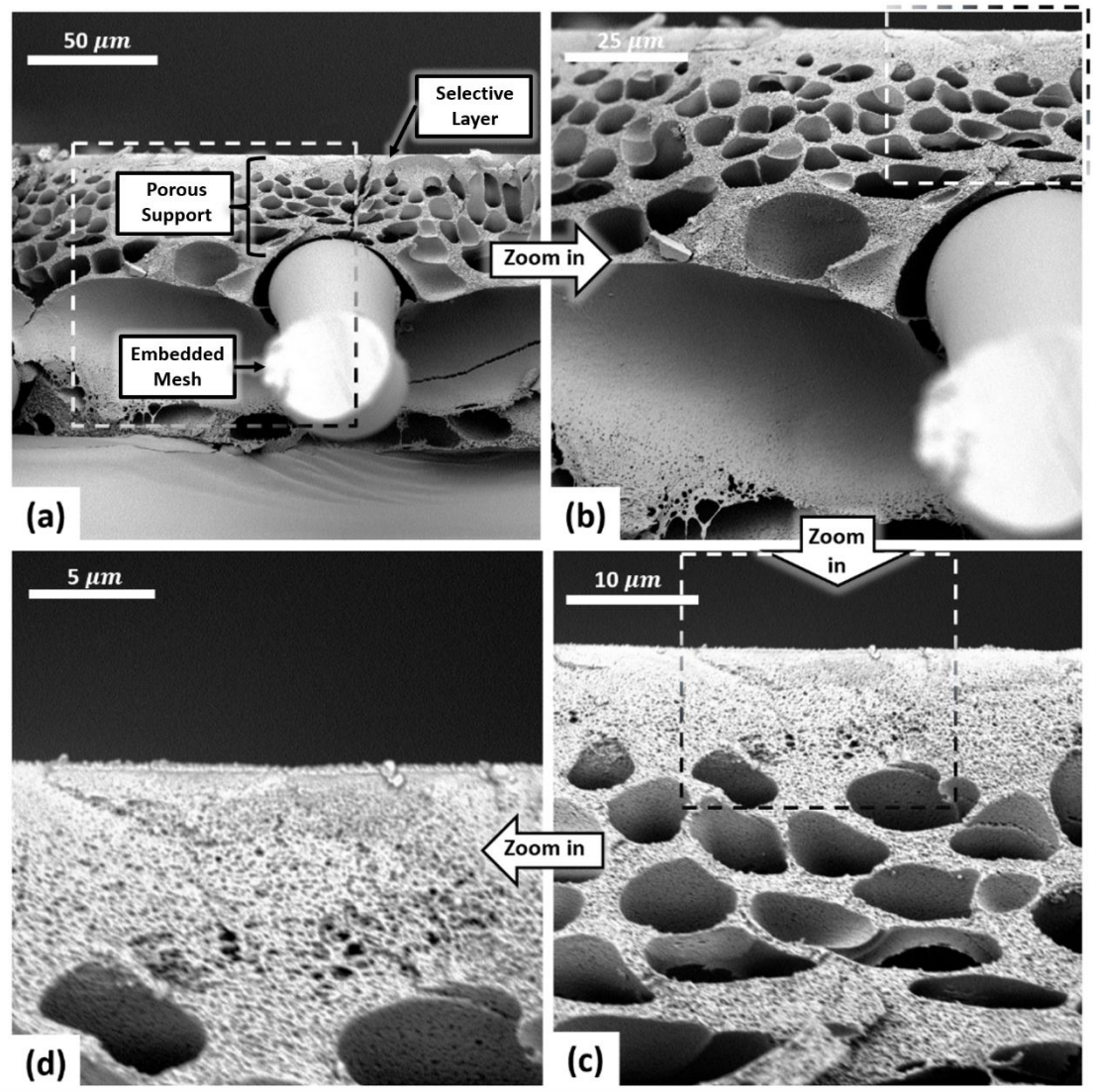

Figure 3.2. Cross-sectional SEM images of TFC membrane at magnifications of (a) 2000×, (b) 2020×, (c) 5800× and (d) 11,200×. Dotted boxes show the zooming sections.

3.3.1.2 Contact Angle

The relative hydrophilicity of both the selective layer and the support layer was measured by contact angle (Table 3.1). The selective layer showed a low contact angle (~14°) which implies a polyamide layer that is more hydrophilic than the CA membrane and other reported high performance FO membranes [25, 111, 137]. The contact angle of the support layer of the

TFC membrane was not shown here because the water droplet was absorbed during the measurement. This occurs on porous materials that are hydrophilic. We can assume that the material is hydrophilic, but a comparative contact angle cannot be measured. We can say, however, that support layer will wet easily when exposed to water.

Table 3.1. Measured contact angles of the selective and support layers of the membranes used.

Membranes	Contact angle (°)	
	Selective	Support
CA	62.0 ± 7.2	63.6 ± 13.0
TFC	14.3 ± 1.6	N/A

Selective and support layer contact angles are included for the CA [111] and the TFC membranes. Temperature during the measurements was 21±0.5℃.The contact angle of TFC support layer was not measureable using the sessile drop method because the droplet was adsorbed into the support layer during the measurement.

3.3.1.3 Attenuated Total Reflection Fourier-transform Infrared Spectroscopy

Figure 3.3 shows the ATR-FTIR spectra of both the support and selective layer of the TFC membrane. The spectrum of the selective layer shows peaks attributed to both the support and selective layer material. Arrows indicate the peaks that are specific to the selective layer [26, 51]. The selective layer spectrum displays the characteristic peaks of polyamide such as 1655 cm^{-1} (C=O stretching of amide), 1610 cm^{-1} (aromatic ring), and 1545 cm^{-1} (C-N stretching of amide) [26]. These peaks strongly suggest the likelihood that polyamide serves as the

functional selective layer material.

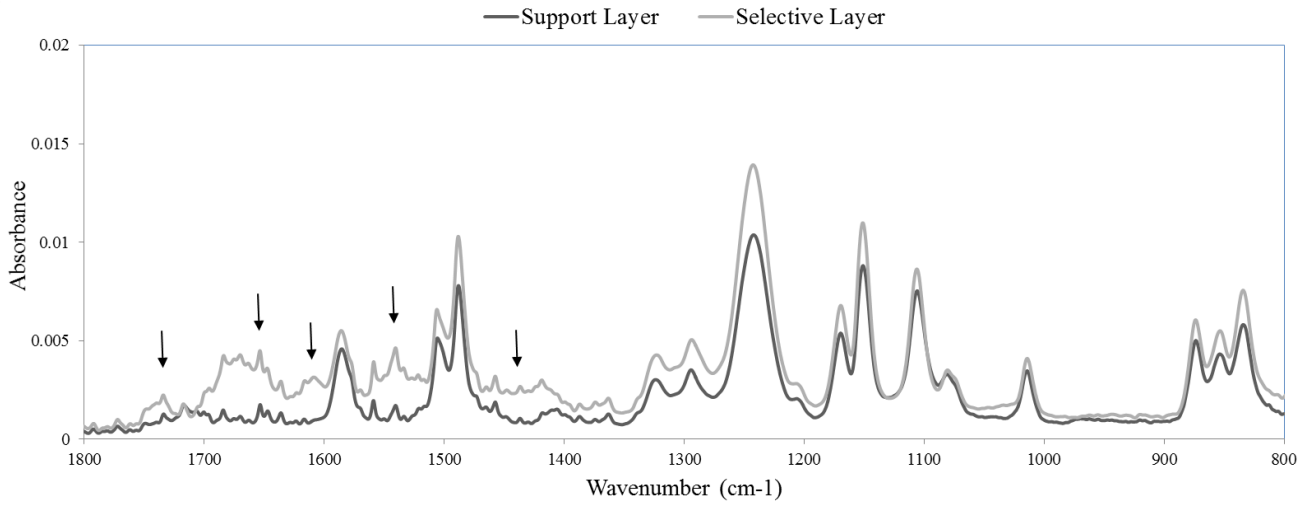

Figure 3.3. ATR-FTIR spectrum of the TFC membrane support (black curve) and selective layer (grey curve). Arrows indicate peaks specific to the selective layer.

3.3.2 Intrinsic Separation Properties

The intrinsic water permeance (A), salt permeability (B), and salt rejection of the CA, TFC and prewetted TFC membranes selective layer are reported in Figure 3.4 and 3.5. Figure 3.4 shows that the salt rejections of TFC membranes are slightly lower than that of CA membrane. This is an interesting result as most TFC type membranes normally exhibit far superior selectivity than their CA membrane counterparts. It is possible that the membrane properties have been optimized for FO and therefore not designed to be tested under the relatively high pressure of RO [91, 127]. However, it is still worth noting the potential of the TFC membrane for PRO applications since it was able to withstand the hydraulic pressure of 250 psi.

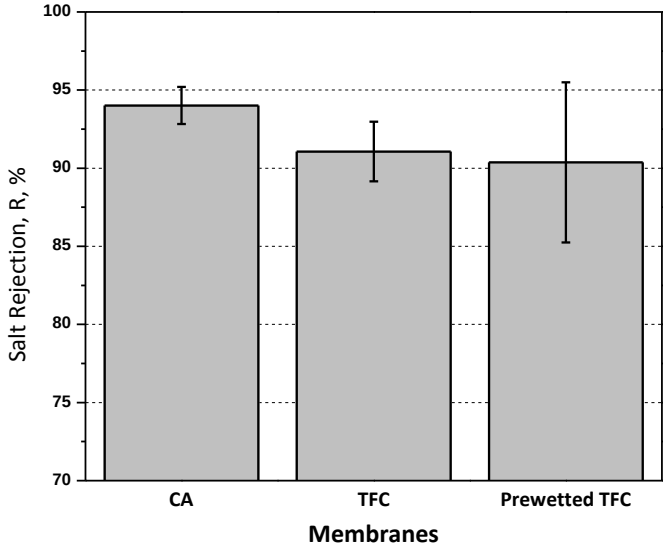

Figure 3.4. Salt rejections (%R) for the three membranes. Results are an average of four experiments with different coupons. Error bars indicate standard deviation.

Operating conditions: feed pressure 8.62 bars (125 psi), feed temperature 20 °C, feed flow velocity 0.25 m/s (for CA membrane) and 0.30 m/s (for TFC membranes). The Reynolds numbers for the flows in CA and TFC membranes were 1125 and 1350, respectively.

The water permeance of the TFC membrane is about two times that of the CA membrane. This is consistent with other TFC membranes for RO exhibiting higher water permeance compared to CA RO membranes. For the prewetted TFC, the water permeance is even higher, almost 50% higher than the virgin TFC and three times of the CA membrane. Along with this increase in water permeance, the salt permeability of the prewetted TFC membrane also increased. This is likely due to two possible affects that IPA has on the polyamide selective layer [138-141]. First, unreacted amine and low molecular weight products of the condensation reaction can be extracted by IPA from the selective layer. Removal these small molecules resulted in a more open structure in the polyamide layer [140]. Second, the physical swelling of the polyamide chains was exacerbated by the presence of IPA molecules. The lower polarity

of IPA compared with water engaged in hydrogen bonding and non-polar interactions with polyamide [140, 141]. Thus, the weaker and more flexible chain interactions within the polyamide caused the enlargement of pore, or free element, size. Meanwhile, it is not surprising to observe significant variability in the salt rejection and salt permeability of the prewetted TFC. Because small membrane samples were tested and DI water feeds were used, the deviation is large since the sensitivity of a conductivity measurement is relatively high. Furthermore, deviation in selectivity from coupon to coupon can cause substantial variability in salt flux, especially when these coupons are prewetted with an agent that may change membrane properties. Large variability in salt flux has been observed in some previous work on FO membrane investigations [25, 91].

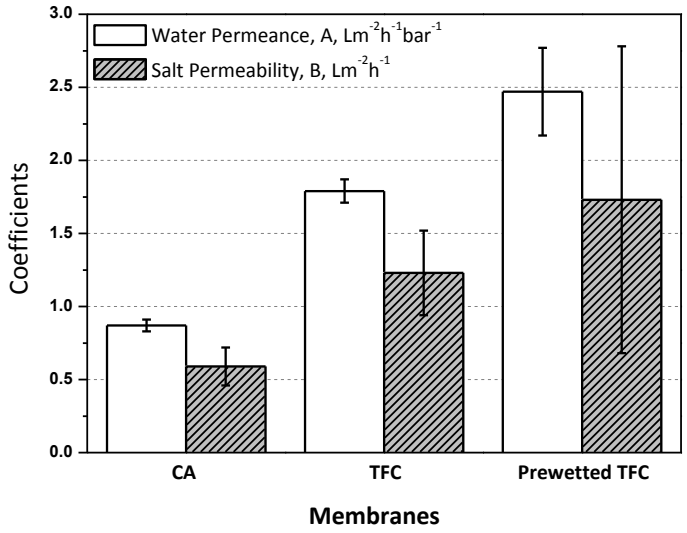

Figure 3.5. Pure water permeance (A) and salt permeability (B) for the three membranes.

Results are an average of four experiments with different coupons. Error bars indicate standard deviation. Operating conditions: feed pressure 8.62 bars (125 psi), feed temperature 20 °C, feed flow velocity 0.25 m/s (for CA membrane) and 0.30 m/s (for TFC membranes. The Reynolds numbers for the flows in CA and TFC membranes were 1125 and 1350, respectively.

3.3.3 Osmotic Flux Results

The osmotic water fluxes of TFC membranes are shown in Figure 3.6 for both FO and PRO modes. In the standard method tests, the two TFC membranes achieved nearly two times higher water fluxes than the CA membrane (Figure 3.6). This is consistent with the higher A values of TFC membranes and suggests a support structure that is more open and/or hydrophilic.

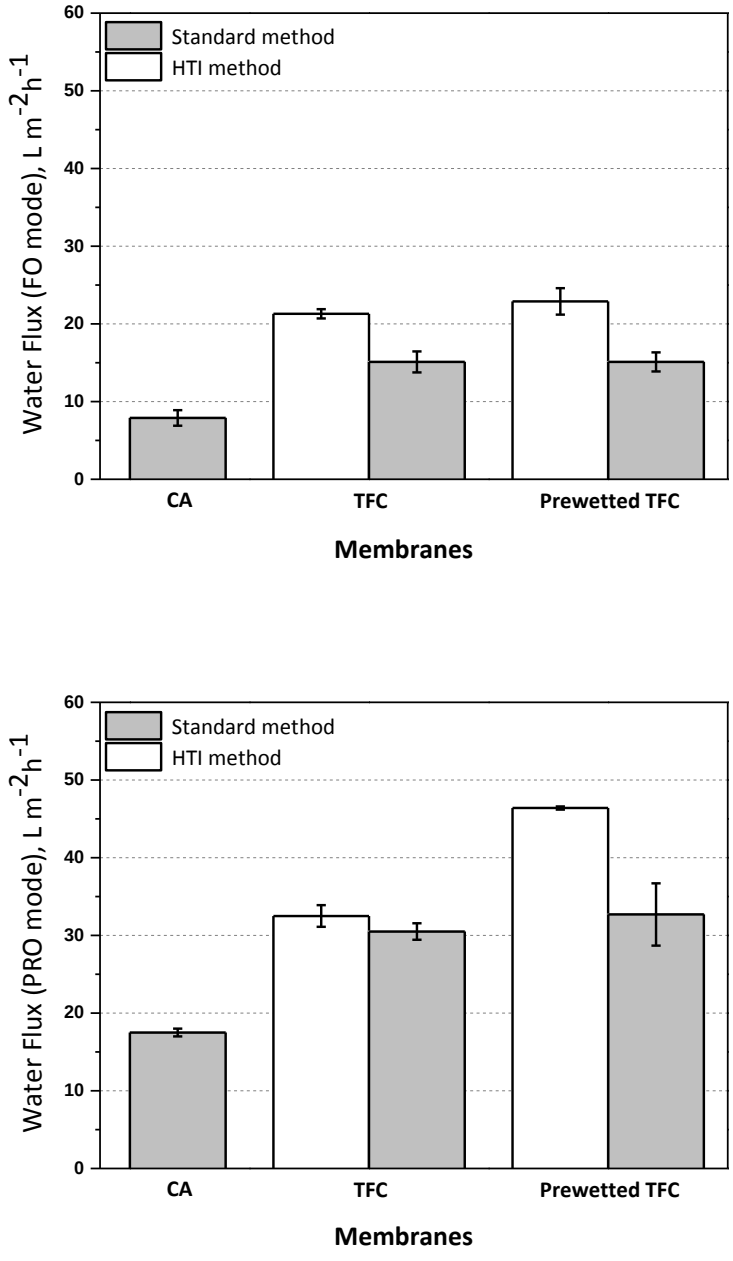

Figure 3.6. Water flux of FO and PRO tests with three membranes.

Results are an average of three experiments with different coupons. Error bars indicate standard deviation. Standard method operating conditions: 1 M NaCl draw solution, deionized water feed, 20 °C feed and draw solution temperature, 0.25 m/s feed and draw solution cross flow velocities, 0 transmembrane pressure and no spacers [133]. HTI method operating conditions: 1 M NaCl draw solution, deionized water feed, 0.30 m/s feed and draw solution cross flow velocities, 20 °C feed and draw solution temperature. Spacers were used on both sides. 1 and 5 psi hydraulic pressures (gauge pressures) on draw and feed sides in FO mode. 5 and 1 psi hydraulic pressures on draw and feed sides in PRO mode.

Prewetting preparation is normally used to ensure the membrane porous support is fully water saturated [111, 133]. This is especially true with more conventional TFC chemistries that use polysulfone or other hydrophobic polymers as support materials. Generally, prewetted membranes with hydrophobic supports show a higher water flux than the virgin membrane, consistent with other prewetting studies [138, 139]. In our study, we note that water fluxes are generally unchanged after prewetting with the one exception of the PRO mode testing using the HTI method. It is likely that the virgin TFC support is already easily saturated in water and the prewetting preparation is unnecessary. Another possible reason might be the negative effects of prewetting preparation on the membrane selective layer. As discussed in Section 3.3.2, the prewetting procedure might enlarge the pore or free element size of the polyamide layer. The resulting lower selectivity results in higher reverse salt flux and decreases the osmotic pressure difference across the membrane. It can also worsen ICP. Therefore, the unchanged water flux is a result of enhanced water permeance balanced with lower effective osmotic pressure and enhanced ICP.

Figure 3.7 shows the reverse salt fluxes of the three membranes in FO and PRO modes. It is worth noting that the TFC membrane, despite a two-fold higher water flux than CA

membrane, has a comparable reverse salt flux. For the prewetted TFC membrane, it is not surprising to see a much higher salt flux since it was shown to have a lower rejection in Figure 3.4.

By comparing the water flux tested by the two testing methods (Figure 3.6), the HTI method gives a higher water flux in both FO and PRO modes. While the slight transmembrane pressure difference in the HTI method might be part of the reason, the more likely cause is the reduced ECP in the method. The HTI method uses a higher cross-flow velocity and incorporates turbulence promoting spacers into the channel, both of which facilitate mass transfer and reduce ECP.

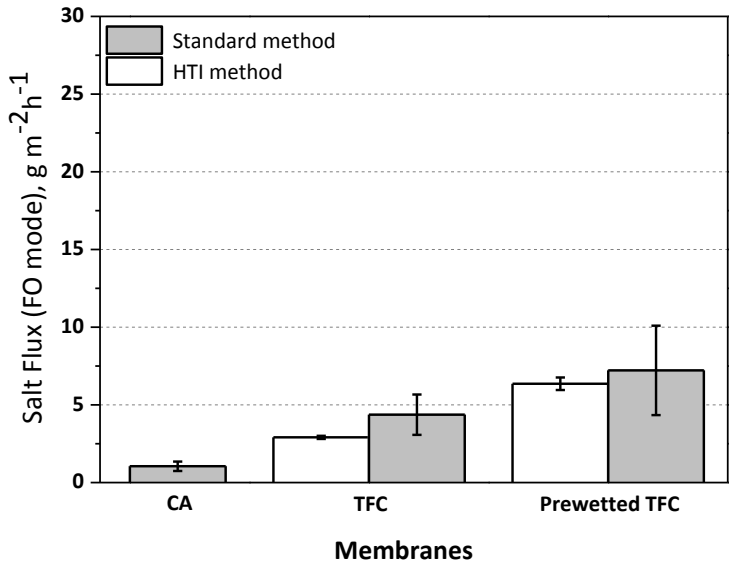

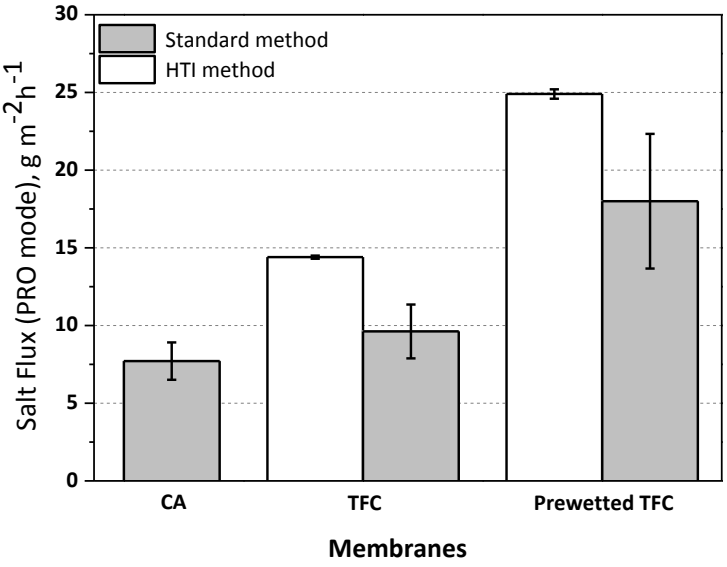

Figure 3.7. Salt flux of FO and PRO tests with three membranes.

Results are an average of three experiments with different coupons. Error bars indicate standard deviation. Standard method operating conditions: 1 M NaCl draw solution, deionized water feed, 20 °C feed and draw solution temperature, 0.25 m/s feed and draw solution cross flow velocities, 0 transmembrane pressure and no spacers [133]. HTI method operating conditions: 1 M NaCl draw solution, deionized water feed, 0.30 m/s feed and draw solution cross flow velocities, 20 °C feed and draw solution temperature. Spacers were used on both sides. 1 and 5 psi hydraulic pressures (gauge pressures) on draw and feed sides in FO mode. 5 and 1 psi hydraulic pressures on draw and feed sides in PRO mode.

3.3.4 Structural Parameters

The structure parameters for the three membranes were calculated according to Eq. 3.2 using the corresponding measured water flux data in FO mode. The S value for CA membranes was calculated as the lowest ~465μm. The TFC membrane, despite a thickness of more than twice of the CA membrane (~100 μm vs ~50 μm), shows a comparable structure parameter of

~533μm with CA. This suggests that the TFC membrane support has a higher porosity, lower tortuosity, or allows for more complete wetting of the structure.

The prewetted membrane exhibits a structural parameter of ~620μm. This is an interesting result since the structure parameter, which characterizes the ICP in support layer, should be decreased by the wetting procedure [111]. It is likely due to the increase of the support thickness which caused by the swelling of the support layer in the IPA. The pores in support layer may also shrink as the polymer swells, increasing the tortuosity and decreasing porosity. The IPA may also affect selective layer properties (A and B) and thus will impact the calculation of structural parameter when using empirical data.

3.4. Conclusions

In this study, we report the performance of an early generation TFC FO membrane from HTI. This membrane incorporates a selective barrier with a hydrophilic support structure with a low structural parameter, giving it improved performance over their existing CA membrane. This membrane represents the first TFC FO membrane manufactured on a 40-inch continuous production line and was shown to have superior performance when compared to the cellulose acetate membrane that has been often used in recent FO studies. Later generations of the TFC membrane platform will likely replace the CA membrane as a benchmark for FO, further pushing the bar higher for improving FO membrane performance with new membrane designs.

Chapter 4. Developing Sulfonated Polysulfone Based High Performance Thin Film Composite Membranes for Forward Osmosis

Published as

Ren, J., O'Grady, B., de Jesus, G., McCutcheon, J.R., "Sulfonated polysulfone-based high-performance thin film composite membranes for forward osmosis", *Polymer,* 103 (2016), 486-497. DOI: 10.1016/j.polymer.2016.02.058.

4.1. Introduction

Forward osmosis (FO) is an emerging membrane technology that utilizes osmotic pressure difference to drive water across a semipermeable membrane from a diluted feed solution, to a concentrated draw solution while rejecting most solutes [142-144]. FO has been touted as a high water recovery and low cost option for seawater desalination and wastewater concentration [7, 11, 39]. However, the large-scale commercialization of FO is in part hindered by the lack of a specifically designed cost-efficient membrane with high performance [13, 39, 145].

Thin film composite (TFC) membranes have become a popular platform for membrane design, as an ultra-thin selective layer could be supported on a chemically different porous support layer wherein the benefits of two separate layers can be combined [40, 41]. Unlike integrated asymmetric membranes, the TFC membrane selective layer and porous support layer

should be tailored independently towards a good FO performance. The selective layer needs to be extremely thin and have high water permeance and solute selectivity. On the other hand, support layers need to be thin, highly porous, and minimally tortuous (a low structural parameter [25, 43, 44, 146]) to minimize the mass transfer resistance, which is known as internal concentration polarization (ICP) [45, 46].

Today's TFC reverse osmosis (RO) membranes meet the selectivity criteria with their highly selective polyamide layers, but they fall short with regards to their support layers [47, 48]. They typically have high structural parameters and in fact are designed with thicker midlayer and polyester (PET) backing layer to maintain integrity under high pressure conditions [81, 147]. This has caused many researchers and companies to combine the selective polyamide layer with a tailored, low structural parameter support layer for FO [27, 148, 149].

Some of these tailored FO membranes strive to maintain robust mechanical properties by inheriting RO-type PET backing layers. However, these layers limit the further reduction of structural parameter [25, 146, 150, 151]. To offset the high structural parameter caused by PET backing fabric, optimization of the support midlayer alongside choice of the PET backing must be considered.

We propose here the consideration of sulfonated polymers as support midlayer materials for FO membranes. Sulfonated polymer is typically obtained by either directly introducing the sulfonic acid group onto the polymer backbone by modification or by polymerizing sulfonated monomers [152-154]. Sulfonated polymers have shown great promise as a material for membranes in water purification [155-157]. Their hydrophilic nature combined with impressive chemical stability has yielded unique membranes with desalination capacity combined with chlorine tolerance [157-161]. Our reasoning behind the use of sulfonated polymers lies in their intrinsic hydrophilicity, which was found to be essential to promote wetting and mass transfer in FO membranes support layer [81].

Previous studies in FO membrane development have shown that by employing sulfonated polymers, the support layer hydrophilicity could be tailored towards an improved FO performance [52, 92, 162, 163]. However, these membranes exhibited noticeable impaired mechanical strength, which calls into question the viability of these membranes under practical conditions.

In this study, PET nonwoven fabrics were employed to reinforce the sulfonated polymer membrane supports. Sulfonated polysulfone (SPSU) was blended with polysulfone (PSU) and cast on one of two PET nonwoven fabrics. The polymer solution had properties that enhanced the integration of the PET fabric layer with the polysulfone layer, creating what we refer to as a fabric integrated support layer. The polyamide selective layer was formed *in-situ* on the top surface of polysulfone via interfacial polymerization (IP). The resultant TFC membranes exhibited excellent performance while retaining enhanced strength because of the embedded fabric. This is the first time that sulfonated polymer was integrated with a PET nonwoven for the fabrication of low structural parameter TFC membranes for FO applications. Such efforts could lead to commercialization of membranes that utilize hydrophilic polymers with integrated nonwovens.

4.2. Experimental

4.2.1. Materials

Polysulfone (PSU, Udel P-3500 LCD MB7, M_w= 77,000-83,000 g/mol), sulfonated polysulfone-17 (SPSU-17, M_w= 56,023 g/mol, sulfonation degree= 9%) and sulfonated polysulfone-45 (SPSU-45, M_w= 58,495 g/mol, sulfonation degree= 16%) were kindly provided by Solvay Advanced Polymers (Alpharetta, GA). The sulfonation of PSU followed protocols in the literature. The reaction product was isolated by precipitation from a non-solvent,

followed by drying [164, 165]. The chemical structures of PSU and SPSU are illustrated in Figure 4.1. m-phenylene diamine (MPD, >99.0%), triethylamine (TEA, >99.0%), sodium dodecyl sulfate (SDS, >99.0%) and 1, 3, 5-benzenetricarbonyl trichloride (trimesoyl chloride, TMC, 98.0%) were purchased from Sigma Aldrich (St. Louis, MO). 1-methyl-2-pyrrolidone (NMP, laboratory grade), *n*-hexane (HPLC, >98.5%), 2-propanol (isopropyl alcohol, IPA, >99.5%) and sodium chloride (NaCl, crystalline, >99.0%) were purchased from Fisher Scientific (Pittsburgh, PA). Deionized water (DI) was obtained from a Milli-Q ultrapure water purification system (Millipore, Billerica, MA). Two commercial polyester nonwoven fabrics, Sanko PET 16-1 and Ahlstrom PET 3256, were acquired from the Sanko Junyaku Co., Ltd (Japan) and Ahlstrom Filtration LLC (Finland), respectively. The thick (107 μm) PET fabric Sanko has a relatively dense structure, while the thin (45 μm) PET fabric Ahlstrom has an open structure. Commercial TFC FO membranes were provided by Hydration Technology Innovations (HTI, Albany, OR) for comparison and these membranes were designated as HTI TFC hereafter.

(a)

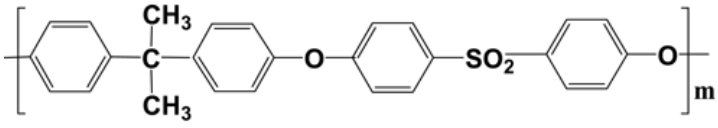

(b)

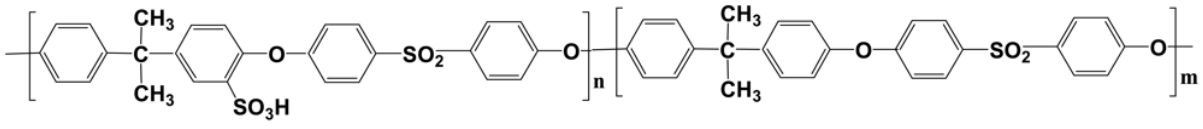

Figure 4.1. Chemical structures of: (a) Polysulfone (PSU); (b) Sulfonated polysulfone (SPSU).

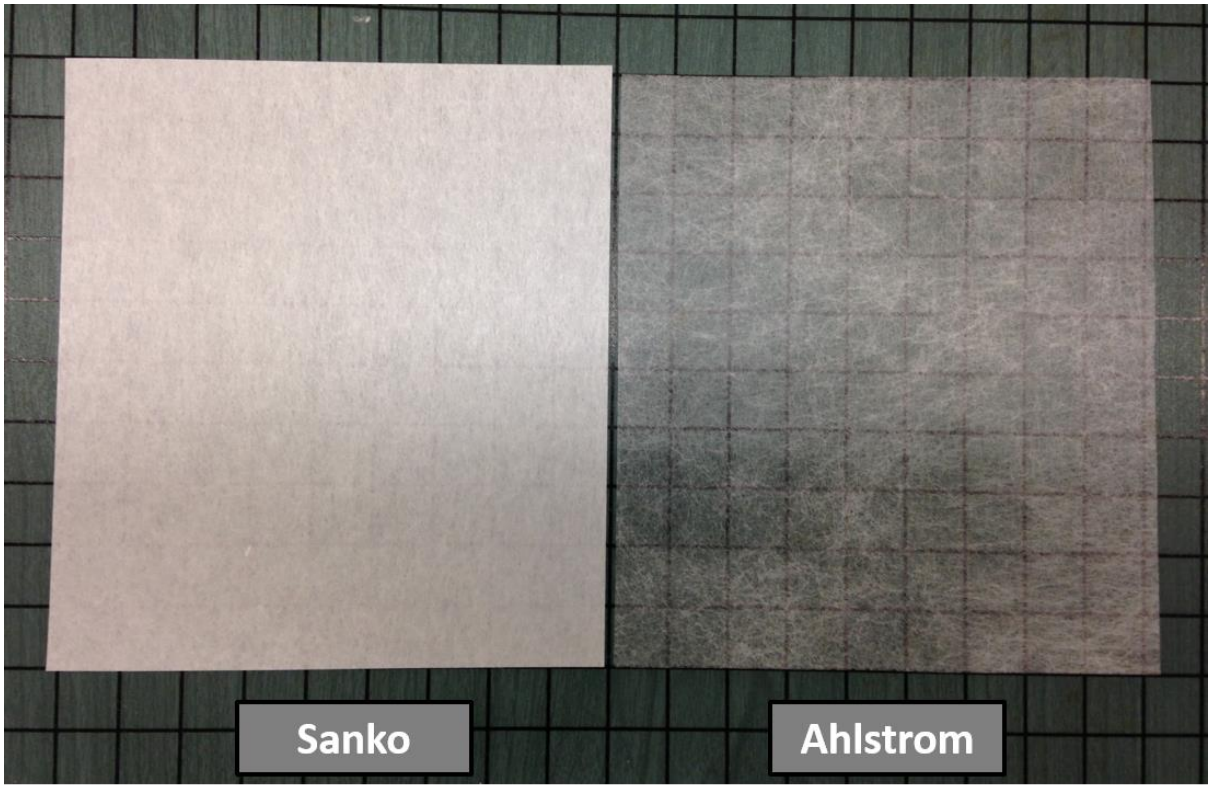

Figure 4.2. Photograph of two PET nonwoven fabrics on a grid background (0.5 inch grid size) to show fiber density. PET Sanko was acquired from Sanko Junyaku Co., Ltd (Japan). PET Ahlstrom was acquired from Ahlstrom Filtration LLC (Finland).

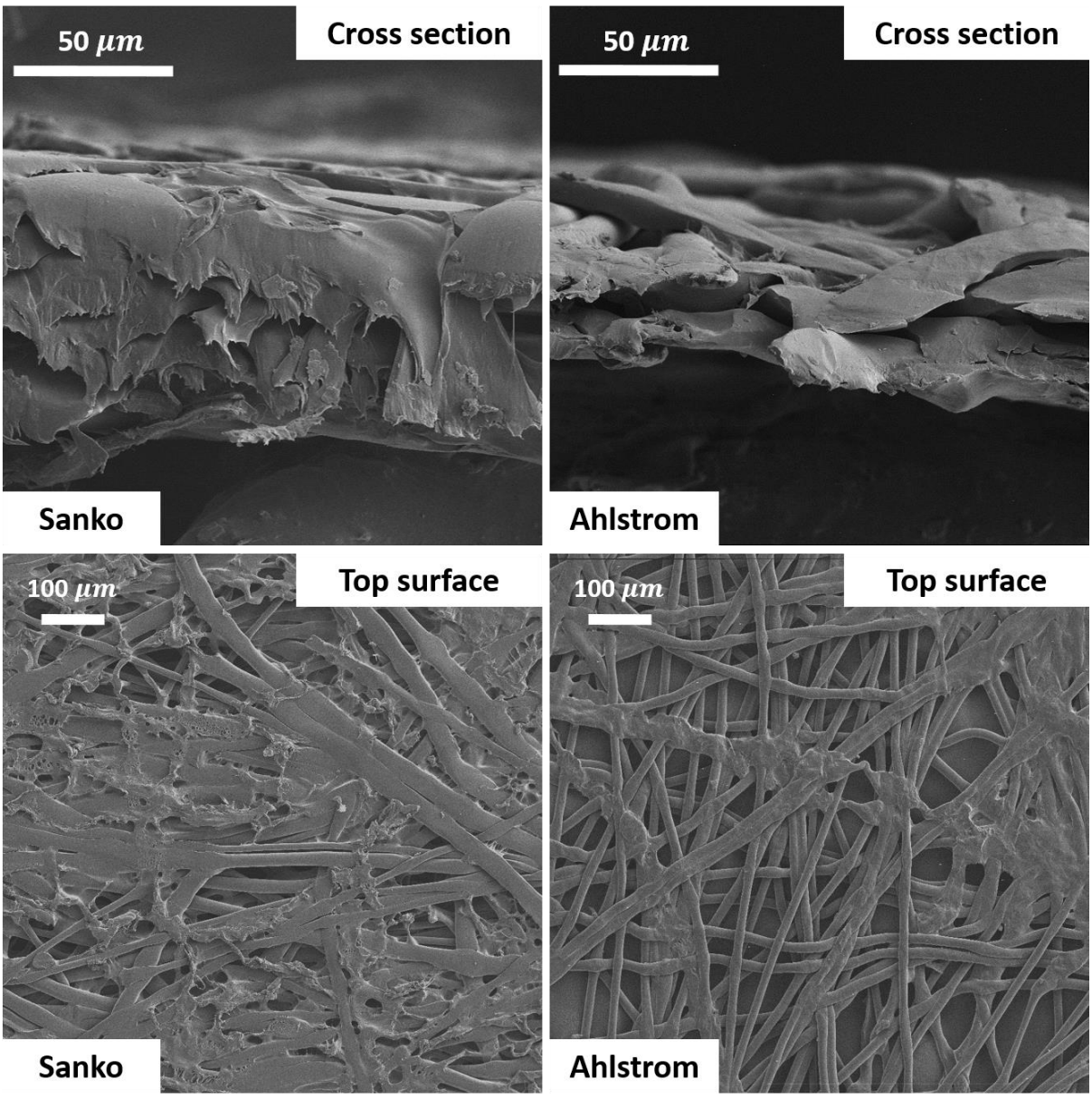

Figure 4.3. Cross-sectional and surface FESEM images of PET nonwovens. Cross-sections of Sanko and Ahlstrom at 500×. Top surfaces of Sanko and Ahlstrom at 100×.

4.2.2. Fabrication of membrane substrates

The membrane substrates were prepared by non-solvent induced phase separation. 16 wt. % polymer beads were dissolved in NMP with three formulations: pure PSU (SPSU-0), PSU blend with SPSU-17, and SPSU-45 at a ratio of 3:1 (*i.e.* 12 wt. % of PSU and 4 wt. % of SPSU),

respectively. The solutions were continuously stirred at room temperature for 24 h and then rested overnight to allow air bubbles to escape. PET Sanko and Ahlstrom nonwovens were taped onto glass plate and uniformly wetted out by spreading 3-4 mL of NMP evenly using a rubber roller [166]. Polymer solution was then cast on PET nonwoven with a 150 μm casting knife. The as-cast membrane substrates were evaporated in a fume hood for 10 sec and then immersed into a DI water bath for 10 min at room temperature. Afterwards, the membrane substrates were rinsed with DI water several times then stored at 5 ℃ until further use.

4.2.3. Synthesis of polyamide selective layer

The thin film polyamide layer was synthesized on the membrane substrate top surface via *in-situ* interfacial polymerization. First, the top surface of membrane substrate was wetted out with isopropyl alcohol (IPA) for 1 min, then rinsed with DI water for 30 min. The membrane substrate was then immersed in a 2/2/0.1 wt. % MPD/TEA/SDS aqueous solution for 5 min [167]. The excess MPD solution residual was removed by rubber roller then dried in a fume hood for 2 min. After that, a 0.1 wv. % TMC/hexane solution was brought into contact with the MPD-saturated membrane substrate for 1 min. After the reaction, the membrane top surface was rinsed with hexane to remove unreacted monomers and dried in air at room temperature for 1 min. Afterwards, the membrane was further cured in oven at 70 ℃ for 1 min. Finally, the membrane was dried in fume hood at room temperature for 3 min and then stored in DI water at 5 ℃ until further tests.

Two types of membranes with different PET nonwoven fabrics (PET Sanko and PET Ahlstrom) were fabricated. The polysulfone membranes with thick PET Sanko and thin PET Ahlstrom were designated as SPSU-0 Sanko and SPSU-0 Ahlstrom, respectively. For better FO performance, the thick PET Sanko nonwoven was peeled off from TFC membranes in some tests. Those membranes without PET nonwoven were designated as SPSU-0 No-PET. A similar

designation is used for the SPSU-17 and SPSU-45 blend membranes. It is worth noting that due to the open structure of PET Ahlstrom, the polymer solution can easily penetrate into the nonwoven fabric. This caused the fabric to be integrated into the membrane and therefore PET removal was impossible. As a result, there are no “No-PET” samples for membranes cast on PET Ahlstrom.

4.2.4. Characterization of substrates and TFC membranes

4.2.4.1. Cloud point measurement

The cloud point curves of ternary membrane forming systems were determined by rapid titration method at 21 ℃ for the three polymer solutions with the same formulation of casting solutions [168-170]. The blend solutions were used to conduct the determinations because the pure sulfonated polymer would form transparent gel during phase separation and was therefore difficult to distinguish at the cloud point. This is due to the presence of hydrophilic sulfonic groups, which are prone to form swollen gel phase rather than white polymer [171]. PSU, PSU and SPSU-17, PSU and SPSU-45 (both at the ratio of 3:1) were dissolved in NMP to obtain homogenous solutions. DI water was slowly added to the solution, while thorough mixing was applied by a magnetic stirrer. The cloud point composition was calculated from the mass balance in the system corresponding to the added volume at which permanent turbidity was detected visually [169].

4.2.4.2. Scanning electron microscopy

The morphology of the membrane substrates and TFC membranes were imaged with a cold cathode field emission scanning electron microscope JSM-6335F (FESEM, JEOL Ltd., Japan). To view the cross sections of the membrane substrates, the samples were submerged in liquid

nitrogen in order to preserve the pore structure and then cut with a razor blade. Prior to imaging, the samples were sputter coated with gold.

4.2.4.3. Contact angle

The contact angles of the top surfaces of the membrane substrates were measured using the sessile drop method on a CAM 101 series contact angle goniometer (KSV Company Linthicum Heights, MD). The values were taken as an average of six points with a droplet volume of 10 ± 1 μL. All measurements were taken at room temperature.

4.2.4.4. Porosity and moisture sorption

The membrane substrate porosity was determined using gravimetric measurements [172, 173]. The hydrated SPSU membrane substrates were cut into sample discs using a punch die. The volume of a membrane disc is determined via measuring its physical dimensions at hydrated state. Its diameter and thickness were measured with a coolant proof digital micrometer (IP65-MX, Mitutoyo, IL). The membrane discs were dried in a vacuum oven for 24 h and were periodically weighed until a constant weight was obtained. Then the discs were immersed in IPA at 25℃. IPA was selected as the wetting reagent because of its sufficient wetting property. The weights of dry and IPA wetted membrane substrates were measured at room temperature. The residual IPA on the surface of wetted membranes was quickly removed using tissue paper before weighing. The membrane porosity can be determined as the volume of wetting reagent (*i.e.* IPA) divided by the total volume of the membrane, defined as:

$$\varepsilon = \frac{m_{wet} - m_{dry}}{\rho_{IPA} \cdot A \cdot t} \qquad (4.1)$$

where m_{wet} is the weight of wet membrane; m_{dry} is the weight of dry membrane; ρ_{IPA} is the density of IPA (0.786 kg/m^3); A is the effective area of membrane sample disc; t is the

membrane substrate thickness.

To rule out the possible influence of wetting reagent moisture absorbed in membrane substrates, a moisture sorption study was conducted [161, 174]. The membrane substrates were vacuum dried for 24 h and then weighed (m_i). The dried membrane were placed in a sealed sorption cell as described in an early study with the exposure of pure IPA vapor at room temperature [174]. IPA vapor was used (rather than liquid IPA) to avoid having IPA fill the pores and bias the results. The membrane substrates were weighed every 12 h on an analytical balance until a constant saturated sorption weight (mf) was obtained after 96 h of IPA vapor exposure. The moisture sorption degree is defined at as:

$$moisture\ sorption\ degree = \frac{m_f - m_i}{m_i} \times 100\% \qquad (4.2)$$

where m_i and m_f are the initial and final mass of the membrane substrate sample.

4.2.4.5. Mechanical properties

The mechanical properties of TFC FO membranes were obtained from the tensile tests in air at 25℃ using a Dynamic Mechanical Analyzer 2980 (DMA, TA Instruments, New Castle, DE). Membranes were cut into 15 mm × 5 mm samples and stored in DI water before measurement. Tests were run at a preload force of 0.5 N and a ramp rate of 0.5 N/min and conducted on wet TFC membranes. Data acquisition and analysis was completed using Universal Analysis software from TA Instruments. Values presented are the average of four tests.

4.2.5. Osmotic flux performance of TFC membranes

4.2.5.1. Osmotic flux tests

Osmotic water flux and reverse salt flux through TFC membranes were characterized using a custom lab-scale cross-flow forward osmosis system. The similar experimental setup was described in earlier investigations [27, 148, 151, 175]. Osmotic flux tests were carried out with the membrane oriented in both FO mode (the membrane selective layer faces the feed solution) and PRO mode (the membrane selective layer faces the draw solution). The TFC membranes were tested under a previously provided standard method in which water and salt fluxes were measured at $20 \pm 0.5℃$ using DI feed and 1 M NaCl draw solution [176]. The hydraulic pressure and Reynolds number (1125) were equal on both sides of membrane. The osmotic water flux, J_w, was calculated by dividing the volumetric flux by the membrane area. By measuring the conductivity of the feed solutions at certain time points during the tests, the reverse salt flux, J_s, was calculated by dividing the NaCl mass flow rate by the membrane area. The specific salt flux is simply a ratio of salt flux to water flux, J_s/J_w.

4.2.5.2. Determination of transport and structural parameter

The water permeance (A), salt permeability coefficient (B) and structural parameter (S) of the TFC FO membranes were determined by adopting the Excel-based method developed by Tiraferri et al [177]. The method allows the simultaneous determination of A, B and S parameters of FO membranes by dividing the FO experiment into discrete number of stages. In this work, the experiments were carried out in four stages using different draw solution concentrations (0.5 M, 1 M, 1.5 M and 2 M).

4.3. Results and discussion

4.3.1. Phase separation properties

The ternary phase diagram with the binodal curves of the three polymer blends (pure PSU, PSU/SPSU-17=3/1, PSU/SPSU-45=3/1) is shown in Figure 4.4. It can be observed that in the sulfonated polymer blend systems, the area of the one-phase region would be bigger than that in the PSU system, which means the path taken by the polymer solution of fixed starting composition to reach the phase border line (binodal curve) will be longer for a more sulfonated polymer [171]. In other words, this suggests that the dope solution with a higher sulfonation degree would result in a slower phase separation rate. This is mainly due to the presence of hydrophilic sulfonic groups, which are prone to bond with water. The much greater affinity of the sulfonated materials to water (non-solvent) leads to a longer time for the solvent and non-solvent exchange [171].

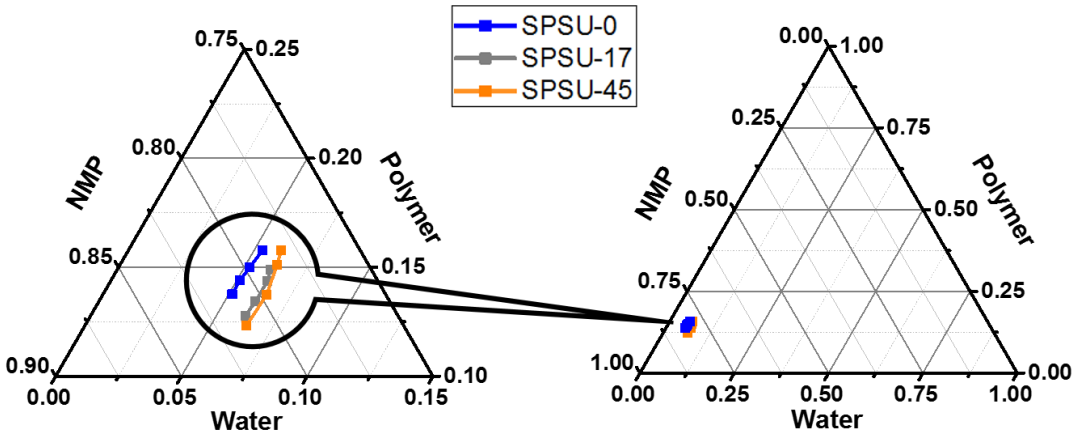

Figure 4.4. Ternary phase diagram showing binodal curves of three blend polymers (SPSU-0: pure PSU; SPSU-17: PSU/SPSU-17=3/1; SPSU-45: PSU/SPSU-45=3/1).

4.3.2. Morphology of membranes

4.3.2.1. Morphology of membrane substrates

For the ease of sample fracture, No-PET membrane films (*i.e.* Sanko PET nonwoven removed from membrane substrates) were used in FESEM imaging. Figure 4.5 shows the top surfaces, cross sections and bottom surfaces of three No-PET membranes. Due to the same polymer concentration in dope solution and same casting protocol, all the three membranes showed fixed thicknesses of about 60 μm. The top surfaces of the three membranes showed less difference because of the instantaneous demixing on the top skin layers.

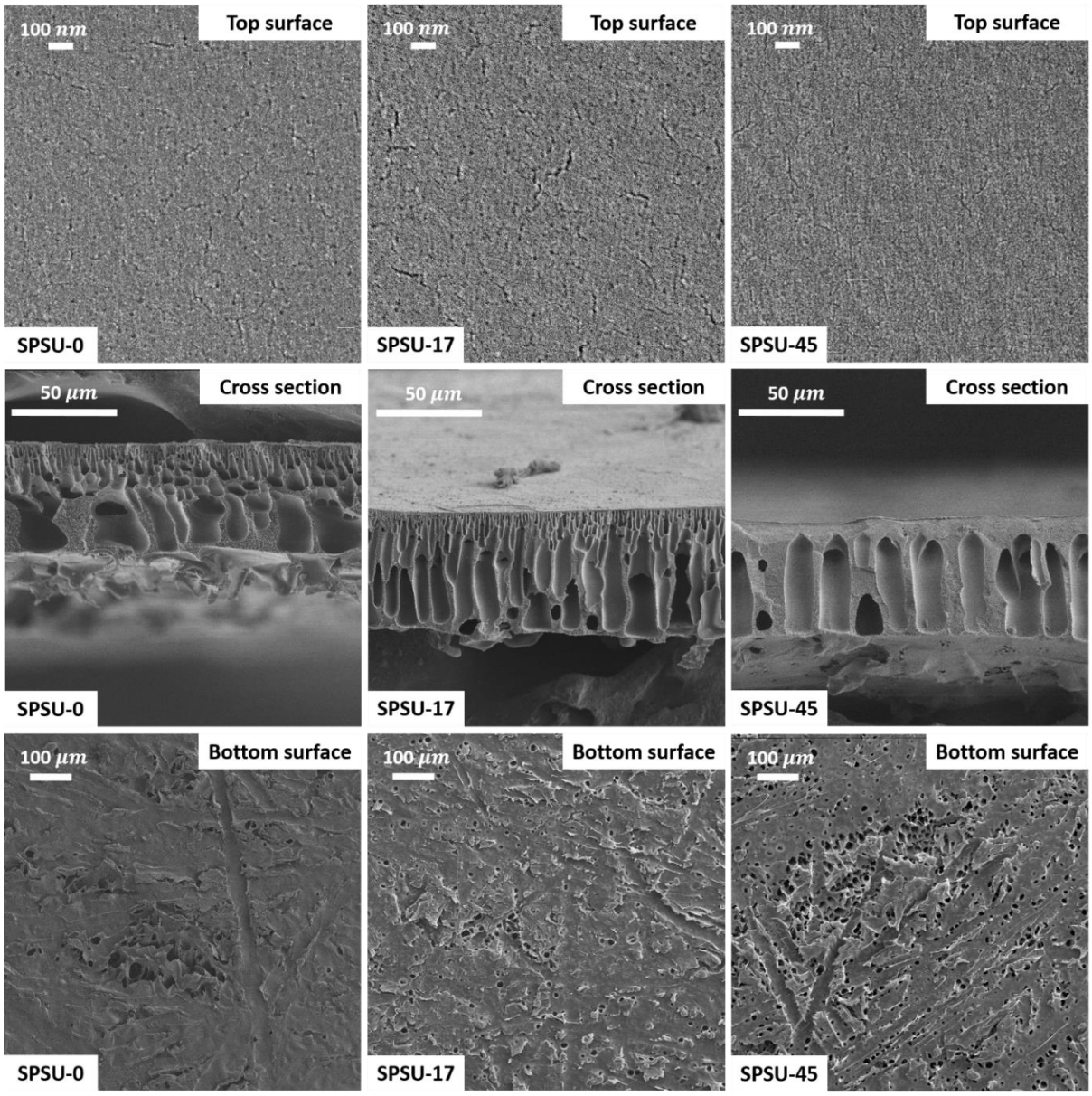

Figure 4.5. FESEM images of No-PET membranes films. Top surfaces of membrane films at 40,000×. Cross-sections of membrane films at 500×. Bottom surfaces of membrane films at 100×.

The influence of the SPSU polymer could be seen clearly from the cross section morphology changes with the increased sulfonation degree. For the SPSU-0, numerous small macrovoids were separated by a loose sponge-like porous medium in between. However, for the SPSU-17 and SPSU-45, as the sulfonation degree increased, the membranes showed fewer

larger, finger-like pores separated by denser sponge-like porous medium in between. As shown in the ternary phase diagram, the more sulfonated SPSU blend has a slower phase separation rate. Therefore, a longer time was required for solvent and non-solvent exchange in SPSU blended dope solution when immersed in water. A more developed process of polymer-lean phase growth and coalescence resulted in larger finger-like pores [171, 178]. Similarly, denser spongy-like structures were formed between finger-like structures in the SPSU blend membranes because the growth of the large finger-like structure extracted more solvent from the polymer dope surrounding the growing macrovoids. This was due to the longer phase separation time [171]. However, for the PSU membrane, the macrovoids were formed at a rapid phase separation rate while the sponge-like pores were formed at the same time by binodal phase separation.

The bottom surfaces of all three membranes exhibited an open and porous morphology with very large surface pores. It was inevitable that some polymer was removed when removing the PET Sanko nonwoven from the membrane, as the imprints of nonwoven fiber can still be seen on the bottom surface. Compared to other membranes cast on glass plates, our membranes have more open and porous morphology on the bottom surfaces [52, 137, 146]. This is because we brought additional solvent into the system and delayed the phase separation rate on the bottom surface. However this is favorable because the open structure on the bottom can facilitate water and solute transport during FO.

The morphology of three integrated membrane substrates cast on Ahlstrom PET nonwoven were shown in Figure 4.6. The membrane substrate thickness was about 95 μm due to the additional thickness from the embedded PET nonwoven. Similarly to the No-PET membrane samples, all three membranes showed dense and uniform top surfaces and finger-like cross-sectional structures. With higher sulfonation degree, the SPSU-45 sample has wider marcrovoids separated by denser sponge-like porous medium in between.

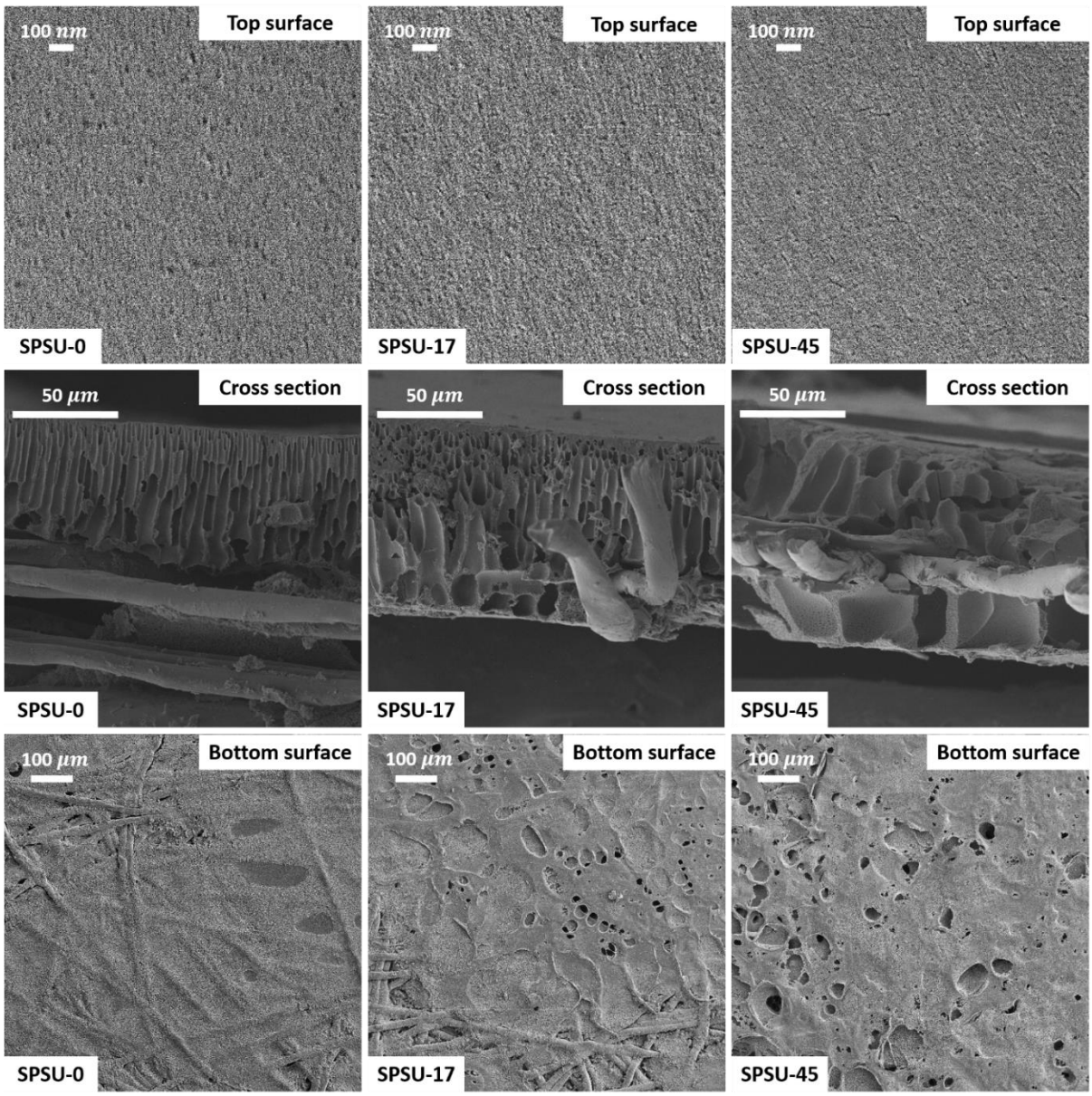

Figure 4.6. FESEM images of Ahlstrom membrane substrates. Top surfaces of membrane substrates at 40,000×. Cross-sections of membrane substrates at 500×. Bottom surfaces of membrane substrates at 100×.

4.3.2.2. Morphology of TFC membranes

Figure 4.7 and Figure 4.8 show the TFC membrane selective layer surface morphology of Sanko and Ahlstrom membranes, respectively. Uniform and defect-free thin polyamide selective layers were successfully formed onto each of the membrane samples. The polyamide

surface showed characteristic rough, ridge-and-valley morphology for the PSU samples and more leaf-like morphology for the SPSU samples. This may be due to the enhanced surface saturation of MPD molecules in the more hydrophilic surfaces of SPSU blend membranes [50, 179].

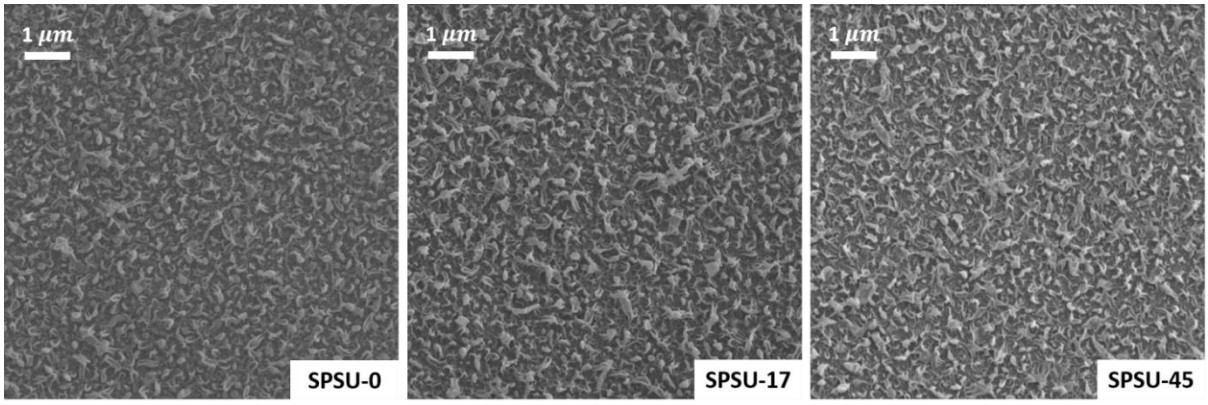

Figure 4.7. Top surface FESEM images of Sanko TFC membranes at 10,000×.

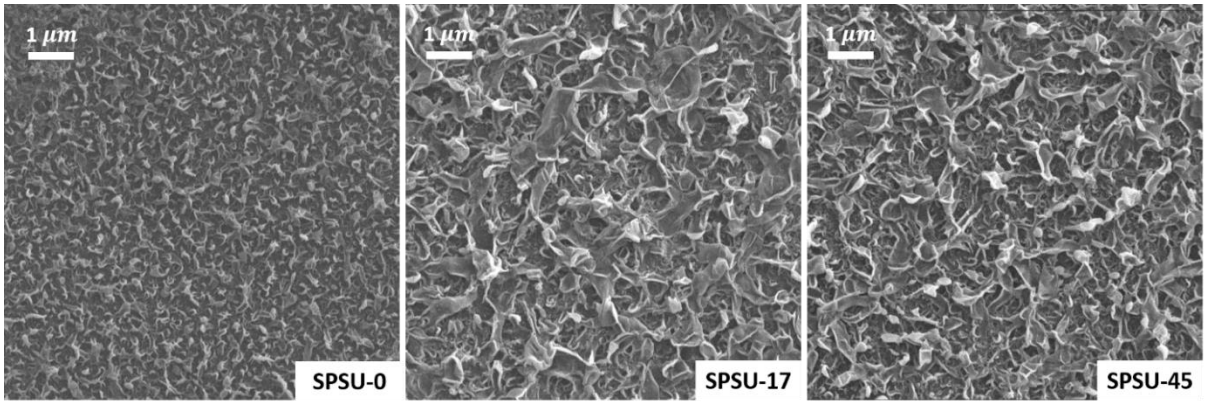

Figure 4.8. Top surface FESEM images of Ahlstrom TFC membranes at 10,000×.

4.3.3. Characterization of membranes

4.3.3.1. Contact angle

The contact angle data of the top and bottom surfaces of membrane substrates based on PET Sanko and PET Ahlstrom were tabulated in Table 4.1. Generally the SPSU membranes

have slightly lower contact angles, which indicates a more hydrophilic surface. This has also been reported in other sulfonated polymer studies and is also essential to promote wetting and mitigating ICP, thus facilitating water transport in following osmotic flux tests [52, 92, 112]. For the bottom surfaces, the three Sanko membranes showed similar results because of the same PET backing used. The Ahlstrom membranes showed a clear trend on the bottom surface due to the penetration of polymer solution into PET fabric, which changed the bottom surface properties.

Membranes	Sanko		Ahlstrom	
	Top	Bottom	Top	Bottom
SPSU-0	82.7 ± 2.2	72.5 ± 3.0	74.3 ± 3.6	102.7 ± 4.5
SPSU-17	79.0 ± 2.7	71.4 ± 2.5	71.3 ± 0.9	80.4 ± 5.7
SPSU-45	77.1 ± 1.7	70.9 ± 1.6	65.7 ± 4.4	79.5 ± 3.4

Table 4.1. Contact angles of top and bottom surfaces of Sanko and Ahlstrom membrane substrates from polymer blends SPSU-0, SPSU-17 and SPSU-45, respectively. Results are an average of 6 samples and the range is the standard deviation.

4.3.3.2. Porosity and moisture sorption degree

To rule out the possible influence of swelling issues on the SPSU, a moisture sorption study was conducted on the No-PET membrane films of SPSU-0, SPSU-17, and SPSU-45 polymer

blends. The results showed that the weight fraction of IPA vapor absorbed in the membrane films for the three polymer blend films were comparable as 5.3%, 6.3%, and 5.8%, respectively. While these results suggest that the uptake of the wetting reagent was generally low, the difference between the non-sulfonated and sulfonated polymers was negligible [161]. Therefore, the porosity measurement was minimally impacted by the different chemistries of the samples and can be compared side by side.

The porosity data of Sanko, Ahlstrom and No-PET membrane substrates cast from SPSU-0, SPSU-17, and SPSU-45 blend solutions are shown in Figure 4.9. The Sanko membranes generally exhibited a much lower porosity than the polymer film because of the dense, low-porosity PET backing. The fabric integrated membranes (PET Ahlstrom) exhibited comparable porosity with the polymer film because of its open structure, which facilitates the integration with polymer solution. SPSU-17 and SPSU-45 showed slightly higher porosity compared to the SPSU-0. This is probably due to the larger macrovoids from a slower phase separation rate.

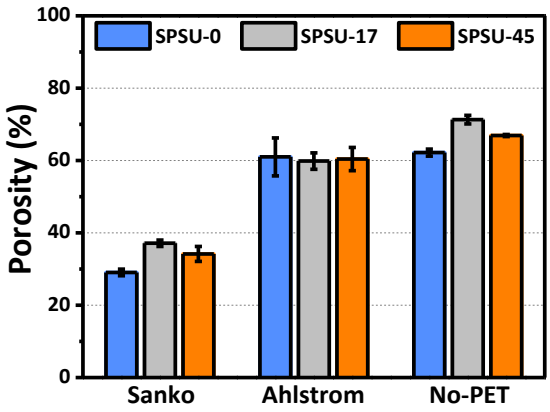

Figure 4.9. Porosity of Sanko, Ahlstrom and No-PET membrane substrates from SPSU-0, SPSU-17, and SPSU-45 polymer blends.

4.3.3.3. Mechanical properties

The mechanical properties of the No-PET and Ahlstrom TFC membranes from three polymer blends were measured at room temperature and presented in Figure 4.10. The mechanical properties of Sanko membranes were not presented since the results mainly showed the features of the Sanko PET nonwoven itself and were too high to be compared to the membrane films.

As expected, No-PET membrane samples showed low Young's modulus as well as tensile strength compared to the fabric integrated ones. The flat sheet TFC membranes fabricated in other studies were mainly cast on a glass plate to ensure a thinner structure and better FO performance [52, 137, 149]. These membranes, without PET supporting layer, are weak, fragile, and very similar to our No-PET samples. The mechanical properties were such that the membranes were very difficult to handle.

The Ahlstrom PET fabric integrated membranes showed significant enhancement in both rigidity and strength compared to No-PET samples. The Ahlstrom membrane samples generally exhibited 3-8 fold higher Young's modulus and 3-6 fold higher tensile strength than those with no embedded PET. Membranes that based on sulfonated polymers were widely considered as lack of mechanical properties. Previously reported sulfonated polymer based FO membranes generally exhibited moderate Young's modulus about 50-80 MPa and tensile strength around 3-4 MPa [52, 92, 162]. In this study, the fabric integrated sulfonated polymer based FO membranes exhibited remarkably high Young's modulus of 350-400 MPa as well as tensile strength of 10-12 MPa. This is about 5-7 times more rigid and 3-4 times stronger than their predecessors. These improved mechanical properties made the fabric integrated membrane a much better platform overall. It also allows one to use functional or modified polymers with interesting properties but insufficient mechanical strength.

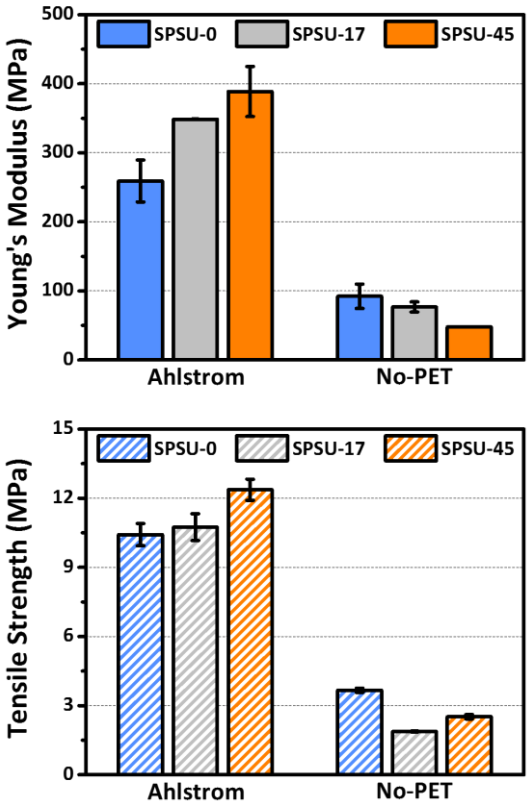

Figure 4.10. Young's modulus and tensile strength of Ahlstrom and No-PET TFC membranes from SPSU-0, SPSU-17, and SPSU-45 polymer blends.

4.3.4. Performance of TFC membranes

4.3.4.1. Osmotic flux performance of TFC membranes

The TFC membranes were evaluated under FO and PRO modes using DI water as the feed and 1 M NaCl as the draw solution. The osmotic water fluxes, reverse salt fluxes and specific salt fluxes (J_w,J_s, and J_s/J_w) are presented in Figure 4.11. The TFC membranes fabricated using different PET nonwovens showed great differences. The No-PET membranes exhibited 4-9 fold higher J_w compare to its Sanko counterparts. This is due to the substantial thinness

that reduced severe ICP. However, the No-PET membranes also showed a much higher J_s due to the membrane thinness (~60 μm) and possible damage to the selective layer because of the lack of support. The Ahlstrom membranes showed high J_w with reasonably low J_s. Again, this can be attributed to the thin and open support layer structure (~ 95 μm) with better overall mechanical integrity.

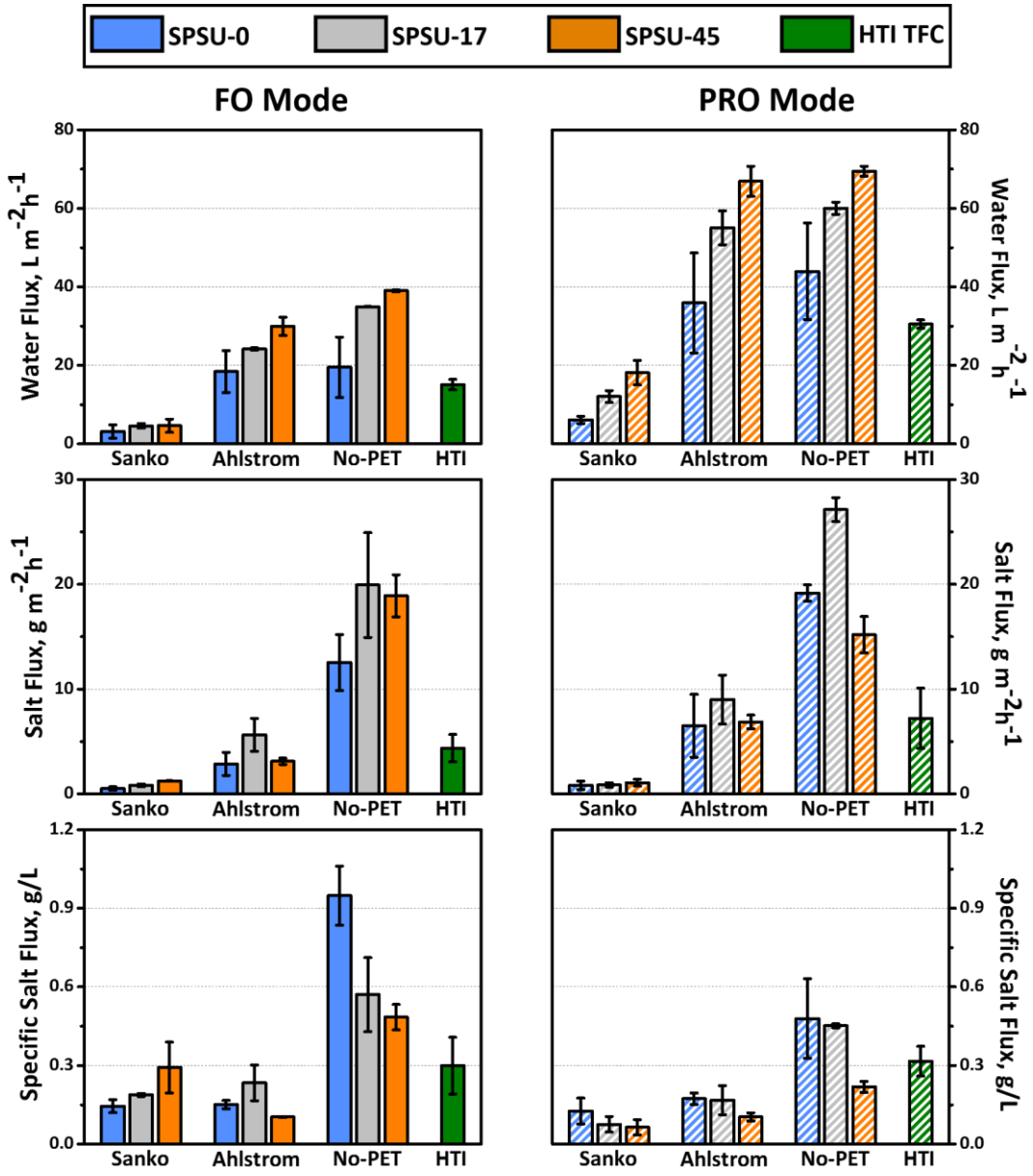

Figure 4.11. Water flux, reverse salt flux and specific salt flux (J_w, J_s and specific J_s) of FO and PRO tests for TFC membranes from SPSU-0, SPSU-17, and SPSU-45 polymer blends

and benchmark HTI TFC [151]. Results are an average of three experiments with different coupons. Error bars indicate standard deviation. Operating conditions: 1 M NaCl draw solution, DI water feed, 20 ℃ feed and draw solution temperature, 0.25 m/s feed and draw solution cross flow velocity, 0 transmembrane pressure.

The membranes fabricated from sulfonated polymer blends generally showed higher J_w and similar J_s when compared with the SPSU-0 membranes. Since the same selective layer formation protocol was used for all membranes, the difference in osmotic flux can be largely attributed to the difference in the support layer, including both the structural and chemical effects of SPSU. The more open and less tortuous finger-like structure in the SPSU membrane supports facilitated the water transport and resulted in a higher water flux. The increase of SPSU support layer hydrophilicity also promoted water transport during osmotic processes [81].

The commercial HTI TFC membranes were compared to the Ahlstrom membranes since both of them were fabricated on thin PET fabrics (~ 50 μm) and have comparable membrane thickness (115 μm and 95 μm) [151]. It is worth noting that the PET fabric used for the HTI TFC membranes was woven mesh, which is less cost-efficient than the PET nonwoven fabric used for our membranes. Our SPSU-0 Ahlstrom membranes exhibited slightly higher J_w and noticeably lower J_s than HTI TFC membranes in both FO and PRO modes. For SPSU-17 and SPSU-45, the Ahlstrom TFC membranes generally exhibited two times higher J_w and comparably low J_s when compared to HTI TFC membranes. SPSU-45 is better performing with a remarkably high J_w of 66.9 $L\,m^{-2}h^{-1}$ and low J_s of 6.9 $g\,m^{-2}h^{-1}$ in PRO mode. Again, the excellent performance of SPSU blend membranes is due to the finely tuned pore structure and increased hydrophilicity of the support layer.

Specific salt flux J_s/J_w is a metric that is used to determine the amount of draw solute loss

per unit of water passed. It has been used to compare membrane performance when different membranes and/or draw solutes are used [180]. Lower J_s/J_w is desirable to prevent the loss of draw solutes in FO and help to minimize ICP in PRO. As shown in Figure 4.11, the membranes generally exhibited higher J_s/J_w in FO mode which indicated more severe ICP (and hence lower water flux) than that in PRO mode. The high J_s/J_w of No-PET membranes was due to their considerably thinner structure, which allows more solute to diffuse through. In this case, the improved J_w does not surpass the increase in J_s. The SPSU-45 Ahlstrom membranes, with the specific salt flux of 0.10 g/L in both FO and PRO modes, which is just one third of that of HTI TFC membrane, represent our best performing TFC membrane based on this metric of performance.

4.3.4.2 Structural parameters

The structural parameters were calculated by Tiraferri's method and presented in Figure 4.12 [177]. The structural parameter gives insight to the extent of ICP, where a low S value correlates with less ICP. The high S values observed in Sanko TFC membranes are due to the thick and dense PET nonwoven backing layer, which exacerbated ICP during FO operation. The SPSU-45 membranes were observed to have the smallest S values among the three types of membranes due to the less tortuous finger-like morphology. This indicated that using a sulfonated polymer in the casting solution results in a membrane structure that helps alleviate ICP.

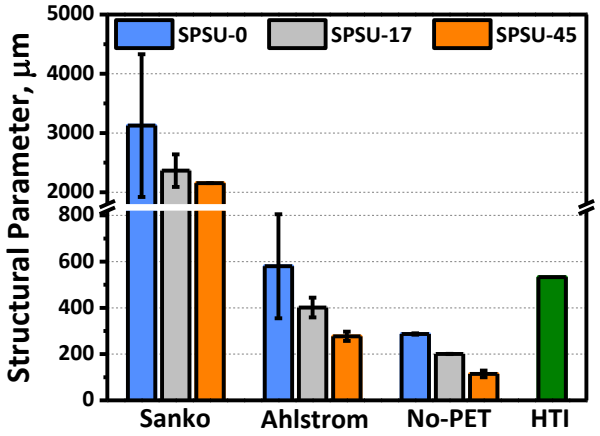

Figure 4.12. Structural parameters of TFC membranes from SPSU-0, SPSU-17, and SPSU-45 polymer blends. Structural parameters were calculated by the Excel-based algorithm developed by Tiraferri [177].

As a membrane with a three-tiered structure (selective PA layer, porous polymeric layer, and PET woven/nonwoven support), our SPSU-45 Ahlstrom membrane represented the lowest S value (277 µm) among all three-layer TFC FO membranes in the open literatures [25, 146, 150]. In addition, this membrane exhibited the S value about half of the commercial HTI TFC membrane (533 µm) with excellent mechanical strength and therefore shows great promise in industrial applications [151].

4.3.4.3 Performance comparison with existing TFC FO membranes reported in literatures

Since the membranes fabricated in this study have two major benefits – adopting novel SPSU material and using an inexpensive nonwoven support – our membranes were compared with existing flat sheet FO membranes with similar features.

Table 4.2 summarizes the osmotic flux performance of sulfonated materials based TFC FO

membranes in this study and open literatures [52, 92, 112, 162, 163, 181]. The No PET membranes have similar configuration with the glass plate cast TFC FO membranes in literatures and were therefore taken into comparison. All of the TFC FO membranes were tested under a 1 M NaCl draw solution and DI water feed condition. The water flux of our membranes surpassed almost all the other membranes in both FO and PRO modes. Since all of these membranes showed improved hydrophilicity due to the use of sulfonated polymer, we attribute the high performance of the No-PET membranes to the support structure differences. The No-PET membrane support layer exhibited substantial thinness, a porous bottom surface as well as open and straight finger-like morphology. All these contribute to a reduced mass transfer resistance in the support layer (i.e. ICP) and result in lower structure parameters compared to other sulfonated polymeric membranes in previous work. The low structural parameters of the No-PET membranes also resulted in higher reverse salt flux in this work. This is because the draw solutes can diffuse through the thin support structure rapidly and cause relatively higher reverse salt flux.

Membranes	Feed	Draw	Water flux ($L\ m^{-2}h^{-1}$)		Salt flux ($g\ m^{-2}h^{-1}$)		Specific salt flux (g/L)		Structural parameter (μm)	Reference
			FO mode	PRO mode	FO mode	PRO mode	FO mode	PRO mode		
SPSU-17 No PET	DI	1 M NaCl	34.92	60.02	19.93	27.12	0.57	0.45	201	This work
SPSU-45 No PET	DI	1 M NaCl	39.00	69.44	18.90	15.19	0.48	0.22	114	This work
50 wt. % sulfonated polymer	DI	1 M NaCl	20.00	27.47	4.04	3.60	0.20	0.13	324	[92]
50 wt. % SPEK	DI	1 M NaCl	22.65	32.24	4.73	6.10	0.21	0.19	107	[162]
PES/SPSf	DI	1 M NaCl	17.81	32.25	5.44	7.59	0.31	0.24	238	[163]
sPPSU-2.5	DI	1 M NaCl	41.50	44.86	7.21	6.85	0.17	0.15	652	[52]
SPPO/PSf (50:50)-45	DI	1 M NaCl	26.67	38.30	5.18	5.34	0.19	0.14	293	[181]
1.5 mol. % sPPSU HFM	DI	1 M NaCl	28.15	69.63	6.30	12.37	0.22	0.18	163	[112]

Table 4.2. Comparison with sulfonated material based TFC FO membranes reported in literatures.

Along with the comparison to other sulfonated polymer based membranes, our fabric integrated Ahlstrom membranes were also compared with three layer TFC FO membranes in the literatures (*i.e.* TFC FO membrane with PET fabric in the structure) [25, 146, 150, 151, 182, 183]. The comparison is summarized in Table 4.3. Even for the non-sulfonated polymer based membrane, our SPSU-0 membrane exhibited reasonably high water flux yet low reverse salt flux when compared to other literatures. Although it showed slightly lower PRO and FO water fluxes when compared to TFC/PSF9 and 9 wt. % PSf in 100 wt. % DMF, respectively. It is worth noting that these two membranes were fabricated with 9 wt. % casting solution, which was much lower than that of 16 wt. % in this study. This low concentration allowed for a looser pore structure to form and was supposed to result in higher porosity as well as FO performance [146, 150, 184]. Not to mention the performance of our SPSU-45 membranes surpassed all the other three layer TFC membranes in the open literature. These results suggest that the combination of sulfonated polymer midlayers with appropriate PET nonwovens could serve to inform future membrane designs for forward and pressure retarded osmosis.

Membranes	**Feed**	**Draw**	**Water flux ($L\ m^{-2}h^{-1}$)**		**Salt flux ($g\ m^{-2}h^{-1}$)**		**Specific salt flux (g/L)**		**Structural parameter (μm)**	**Reference**
			FO mode	**PRO mode**	**FO mode**	**PRO mode**	**FO mode**	**PRO mode**		
Integrated SPSU-0	DI	1 M NaCl	18.40	35.91	2.86	6.51	0.15	0.17	580	This work
Integrated SPSU-17	DI	1 M NaCl	24.17	55.05	5.64	9.01	0.23	0.17	401	This work
Integrated SPSU-45	DI	1 M NaCl	29.95	66.89	3.11	6.87	0.10	0.10	277	This work
HTI CTA nonwoven	DI	0.6 M NaCl	7.1	N/A	N/A	N/A	N/A	N/A	N/A	[182]
HTI CTA mesh	DI	1 M NaCl	7.89	17.50	1.05	7.71	0.13	0.44	465	[151]

HTI TFC	DI	1 M NaCl	15.10	30.50	4.37	9.62	0.30	0.32	533	[151]
9 wt. % PSf in 100 wt. % DMF	DI	1 M NaCl	25.00	N/A	N/A	N/A	N/A	N/A	312	[146]
TFC/PSF9	DI	1 M NaCl	17.10	49.4	6.00	7.10	0.35	0.14	314	[150]
TFC-FO	DI	1.5 M NaCl	18.16	N/A	N/A	N/A	N/A	N/A	492	[25]
PAI 2#	DI	0.5 M $MgCl_2$	19.20	23.90	9.41	36.33	0.49	1.52	N/A	[183]

Table 4.3. Comparison with PET fabric integrated TFC FO membranes reported in literature.

4.4. Conclusions

Hydrophilic sulfonated polymers and appropriate PET nonwovens were combined towards an optimized design of high performance thin film composite membrane for forward osmosis. The PET nonwoven fabrics enable the use of delicate sulfonated polymers by reinforcing the mechanical properties for industrial conditions. Meanwhile, the sulfonated polymers enable the use of hydrophobic PET fabric by integrating it into the support without enhancing mass transfer resistance. These results exhibited great promise of combining sulfonated polymers with appropriate PET nonwoven fabrics for future membrane design for forward and pressure retarded osmosis.

Chapter 5. Relating osmotic performance of thin film composite hollow fiber membranes to support layer structure

Published as

Ren, J., McCutcheon, J.R., "Polyacrylonitrile supported thin film composite hollow fiber membranes for forward osmosis", *Desalination*, 372 (2015) 67-74.

DOI: 10.1016/j.desal.2015.05.018.

5.1. Introduction

Forward osmosis (FO), a platform technology that utilizes osmotic pressure difference to drive water across a semipermeable membrane from a dilute feed solution to a concentrated draw solution while rejecting most solutes, has been touted as a high water recovery and low cost option for seawater desalination and wastewater purification [7, 11, 65, 129, 143]. As an osmotically driven membrane process (ODMP), the commercial development of FO has long been hampered by membrane design [10, 12, 13]. Therefore, the developments of high performance membranes specifically for FO have been intensively studied in both academic laboratories and industry during the past decade [10, 25, 26, 29, 32].

As new membranes are considered for FO, specific design criteria must be met. The selective layer needs to have good permeance and selectivity. The support layer needs to be thin and have an open and interconnected pore structure. These characteristics contribute to the

structural parameter, S, defined as the product of the thickness (t) and tortuosity (τ), divided by the porosity (ε) (i.e., $S = t\tau / \varepsilon$). S must be minimized in order to minimize internal concentration polarization (ICP) [43, 44, 132].

Hollow fiber membranes are desired in many membrane applications because of their high packing densities relative to flat sheet and spiral wound configurations. This higher packing density allows for small footprint systems and makes low flux performance more tolerable. These benefits have translated well for FO, making them a preferred platform for many academic groups [12, 34, 115]. A number of hollow fiber membranes have been developed for FO in academic laboratories, with many showing some promise of high performance [29, 53, 54, 103]. Only recently have some companies designed new hollow fiber FO membranes and manufactured on a large scale. But those membranes, with moderate performance, are still largely unavailable to academic researchers or industrial operations [98].

Amongst the first hollow fiber membranes developed for FO were integral asymmetric membranes. Polybenzimidazole (PBI) and cellulose acetate (CA) were chosen because of their excellent nanofiltration (NF) characteristics [53, 87, 88]. Thermal and chemical treatments were used to enhance their selectivity and the resultant membranes showed good rejection to divalent ions. However, the relatively low selectivity to monovalent ions limited their capabilities in desalination applications. Follow-up work was focused on enhancing the water flux for FO applications using dual-layer composite membranes comprised of polybenzimidazole/polyethersulfone/polyvinylpyrrolidone (PBI/PES/PVP) [54]. Another study utilized polyamide-imide (PAI) as hollow fiber substrate material followed by polyelectrolyte post-treatment with ployethyleneimine (PEI) to achieve a NF-like selective layer [103]. Similarly, a dual-layer composite membrane comprised of PAI/PES was also investigated [105]. These membranes all exhibited good flux performance, but were still limited to nanofiltration selectivity.

A leap forward in composite hollow fiber membrane occurred when Wang et al first synthesized a reverse osmosis (RO)-like thin film composite (TFC) hollow fiber membrane in 2010 [29]. The polyamide (PA) selective layer was formed via *in-situ* interfacial polymerization on a porous polyethersulfone (PES) hollow fiber substrate. Since then, a number of studies have been focused on investigating the structure-performance relationships of TFC hollow fiber membranes. Shi et al has investigated the effect of substrate structure on the FO performance of PES hollow fiber membranes. The substrate surface structure was proved to be essential for forming the TFC layer and it should possess a MWCO of less than 300 kDa in order to achieve a desirable performance. Cross-section structures with different proportions of needle-like pores, sponge-like pores and large macrovoids were investigated, but no significant difference were found in their FO performances [114]. Based on the same substrate material (PES), Sukitpaneenit et al designed a macrovoid-free fully sponge-like structure. This macrovoid-free TFC hollow fiber membrane showed slightly inferior FO performance but enhanced strength, which resulted in a more stable operation process [31]. Moreover, novel substrate materials were studied and aimed for a lower structural parameter and greater hydrophilicity. Zhong et al used direct sulfonated polyphenylenesulfone (sPPSU) as substrate material for TFC hollow fiber membrane. With increased degree of sulfonation, the hydrophilicity of substrate was increased and resulted in higher FO performance [112].

A hydrophilic support layer is favored in TFC membrane design for FO as support layer wetting was found to be essential for osmotic flow. The solutes can only diffuse through the wetted porosity of the support layer and an intrinsically hydrophilic support can effectively minimize ICP [111]. A number of studies on TFC FO flat sheet membranes have shown high performance by utilizing intrinsically hydrophilic material or physically wetting membrane support [27, 91, 127]. For hollow fiber membranes, intrinsically hydrophilic materials have been only investigated as integral asymmetric membranes with NF selectivity [88].

In this study, an intrinsically hydrophilic polymer -- polyacrylonitrile (PAN) -- was selected as the support material for TFC hollow fiber membranes for FO because it is hydrophilic, inexpensive and easy to spin. Different structures were considered by altering the fabrication technique. The polyamide selective layer was formed *in-situ* on the shell side surface of hollow fiber substrates. In comparison to the lumen-selective hollow fiber membranes, the shell-selective hollow fiber membrane has more surface area per module and less propensity for serious fouling [34, 102]. However, forming a perfect PA layer on fiber shell surface is more challenging than on lumen surface. Neither an air purge nor solvent can be applied for removing excess amine from the shell surface. Therefore, the preferred method in the literature is lumen side selective layer formation [29, 49]. Recent studies show that when interfacial polymerization is conducted on fiber shell surface in bundle, the PA tends to form between fibers and induce defects if the excess monomer solution is not sufficiently removed. In a continuous process, submerging fiber through several monomer solutions to synthesize the selective layer is troublesome since the fiber shell surface will contact multiple rollers during the process, thereby inducing defects on the PA layer [102]. In this work, we developed a batch coating method for fiber shell-selective layer synthesis. The TFC FO hollow fiber membranes exhibited reasonable osmotic fluxes in both FO and PRO modes and demonstrated the potential of PAN being a suitable substrate polymer for TFC hollow fiber membranes with shell side selective layers.

5.2. Experimental

5.2.1 Materials

Polyacrylonitrile (PAN, M_w= 150,000 g/mol), m-phenylene diamine (MPD, >99.0%), triethylamine (TEA, >99.0%), sodium dodecyl sulfate (SDS, >99.0%) and 1, 3, 5-

benzenetricarbonyl trichloride (TMC, 98.0%) were purchased from Sigma Aldrich (St. Louis, MO). N, N-dimethylformamide (DMF, anhydrous, >99.8%), glycerol (certified ACS, >99.5%), *n*-hexane (HPLC, >98.5%), 2-propanol (IPA, >99.5%) and sodium chloride (NaCl, crystalline, >99.0%) were purchased from Fisher Scientific (Pittsburgh, PA). Deionized water (DI) was obtained from a Milli-Q ultrapure water purification system (Millipore, Billerica, MA).

5.2.2 Fabrication of hollow fiber substrates

16 wt. % of PAN was dissolved in DMF at 60℃ to obtain homogeneous solutions. The solutions were continuously stirred at room temperature for 24 h and then rested to allow air bubbles to escape. Hollow fiber membranes were prepared via dry-jet wet-spinning process. Similar method has been reported in our previous studies [185, 186]. The degassed polymer solutions and bore fluids were extruded through the spinneret. Three bore fluids: DI water, 30 and 60 wt. % DMF aqueous solutions were used and delivered by syringe pump KDS220 (KD Scientific, Holliston, MA) at a flow rate of 4 mL/min. The hollow fiber membranes formed were designated as PAN-0, PAN-30 and PAN-60, respectively. The nascent fiber went through an air gap of 2 cm before immersing into an external coagulation bath. Tap water was used as the external coagulant and circulated throughout the spinning processes. Fibers were taken up by a rotating drum at a linear speed of 2 m/min. To remove residual solvent, the hollow fiber substrates were stored in DI water for at least two days. Afterwards, the fibers were post-treated by 50 wt.% glycerol aqueous solution for 24 h to prevent the collapse of porous structures when they were dried [185, 187].

5.2.3 Synthesis of polyamide selective layer

The thin film polyamide selective layer was synthesized on the shell side surface of hollow

fiber substrates via *in-situ* interfacial polymerization. First, the glycerol treated PAN hollow fiber substrates were taped on a rubber frame with sufficient fiber length and space between adjacent fibers. The whole fiber frame was immersed in DI water for 1 h to remove surface glycerol. Then the fibers were sealed at both ends and immersed in a 2/2/0.1 wt. % MPD/TEA/SDS aqueous solution for 3 min. The excess MPD solution residual were removed by filter paper then dried in fume hood for 3 min. After that, a 0.1 wv. % TMC/hexane solution was brought into contact with the MPD-saturated fiber shell surface for 1 min. After the reaction, the fibers were rinsed with hexane to remove unreacted monomers and dried in air at room temperature for 1 min. Similarly, the effective part of TFC hollow fiber membranes were cut off from rubber frame and post-treated by 50 wt. % glycerol aqueous solution overnight.

After drying in air at room temperature, both hollow fiber substrates and TFC membranes were bundled and inserted into clear 6-inch PVC tubes, respectively. Epoxy resin (Cytec Industries, Olean, NY) was employed as potting material and prepared modules for further testing.

5.2.4 Hollow fiber membrane characterization

All the dimensions of the fibers were obtained based on physical measurements on water saturated fibers at five different locations for each membrane sample. The fiber diameter and fiber wall thickness were measured with coolant proof digital micrometer (IP65-MX, Mitutoyo, IL) on wetted membranes. The effective fiber length in module is measured with solar digimatic caliper (Absolute 500, Mitutoyo, IL).

The morphology of the hollow fiber substrates and TFC membranes were imaged with a cold cathode field emission scanning electron microscope JSM-6335F (FESEM, JEOL Ltd., Japan). To view the cross sections of the membranes, the samples were submerged in liquid nitrogen to preserve the pore structure and cut with a razor blade. Prior to imaging, the samples

were sputter coated with gold.

Dynamic contact angle (DCA) measurements were performed using a Cahn 322 dynamic contact angle analyzer (Thermo Scientific, Newington, NH) to determine the hydrophilicity of the hollow fiber membranes [29]. Each hollow fiber was tested by a single cycle-single loop method with a moving rate of 80μm/s and an immersion depth of 4mm. The values were taken as an average of four advancing contact angles. All measurements were taken at room temperature.

A bench-scale ultrafiltration testing unit was used to evaluate the pure water permeance of hollow fiber substrates at $20\pm 1℃$. DI water was circulated through the shell side of the membrane module at a transmembrane pressure of 0.07 bar with a fixed cross-flow velocity of 0.06 m/s. Similar apparatus was described in our earlier studies [185, 187].

The mechanical properties of hollow fiber substrates and TFC hollow fiber membranes were obtained from the tensile tests in air at 25℃ using a Dynamic Mechanical Analyzer 2980 (DMA, TA Instruments, New Castle, DE). Hollow fibers were cut into 15 mm sample segments and stored in DI water before measurement. Tests were run at a ramp rate of 1 N/min and conducted on wet hollow fiber substrates and TFC membranes. Data acquisition and analysis was completed using Universal Analysis software from TA Instruments. Values presented are the average of four tests.

5.2.5 Membrane performance tests

5.2.5.1 Pure water permeance of TFC membranes

Pure water permeances (A, $L\,m^{-2}h^{-1}bar^{-1}$) of the TFC hollow fiber membranes were evaluated in a lab-scale cross-flow RO test unit designed for hollow fibers. The hydraulic pressure was applied on the shell side of TFC hollow fiber membrane during the RO

experiments. The A value was obtained from pure water flux with applied pressure of 1 bar at 20±0.5℃. The salt permeability coefficients (B, $L\,m^{-2}h^{-1}$) were determined by testing the membrane under the RO mode following a method described elsewhere [29]. A feed solution of 100 ppm NaCl and a feed pressure of 0.5 bar was used and the salt permeability B was derived using methods previously described [25, 29, 31].

5.2.5.2 Osmotic flux tests of TFC membranes

Osmotic water flux and reverse salt flux through TFC membranes were characterized using a custom lab-scale cross-flow forward osmosis system. The similar experimental setup was described in earlier investigations [32, 91]. Osmotic flux tests were carried out with the membrane oriented in both FO mode (the membrane selective layer faces the feed solution) and PRO mode (the membrane selective layer faces the draw solution). The TFC membranes were tested under a previously provided standard method in which water and salt fluxes were measured at 20±0.5℃ using DI feed and 1 M NaCl draw solution [133]. The hydraulic pressure was equal on both sides of membrane while the Reynolds numbers of the fluid flowing in the fiber lumen and shell were 1100 and 800, respectively [188]. The osmotic water flux, J_w, was calculated by dividing the volumetric flux by the membrane area. By measuring the conductivity of the feed solutions at certain time points during the tests, the reverse salt flux, J_s, was calculated by dividing the NaCl mass flow rate by the membrane area. The specific salt flux is simply a ratio of salt flux to water flux, J_s/J_w. The structural parameters (S, μm) were empirically determined by solving the following set of equations when membranes were oriented in FO mode [177]:

$$J_w = A\left\{\frac{\pi_D \exp(-\frac{J_w S}{D}) - \pi_F \exp(\frac{J_w}{k})}{1+\frac{B}{J_w}\left[\exp(\frac{J_w}{k}) - \exp(-\frac{J_w S}{D})\right]}\right\} \qquad (5.1)$$

$$J_s = B\left\{\frac{c_D\exp(-\frac{J_w S}{D}) - c_F\exp(\frac{J_w}{k})}{1+\frac{B}{J_w}\left[\exp(\frac{J_w}{k}) - \exp(-\frac{J_w S}{D})\right]}\right\} \qquad (5.2)$$

where J_w and J_s are the water and reverse salt flux in FO mode. *k* is the mass transfer coefficient for the feed channel (*i.e.* shell side) of hollow fiber module [35]. D is the bulk diffusion coefficient of the draw solute. The water permeance A and salt permeability coefficient B are determined from the RO tests. Other parameters: draw solution concentration c_D, feed solution concentration c_F, and the corresponding osmotic pressures, π_D and π_F, are all experimentally accessible. Once all of these known values are input into the model, S can be determined numerically.

5.3. Results and discussion

5.3.1 Morphology of hollow fiber membranes

The TFC hollow fiber membranes are designed with a shell-selective layer and three different interior structures to investigate their effects on performance. Figure 5.1 shows the cross-sectional structure of the three hollow fiber substrates. These fibers were designed to have a fixed outer diameter of about 1100 ± 50 μm. A sponge-like dense layer was observed underneath the fiber shell surface for each fiber. This is due to an instantaneous de-mixing induced by the non-solvent external coagulant (*i.e.* tap water) [34, 36]. Figure 5.2 shows the surface morphology of hollow fiber substrates and TFC membranes. A smooth and uniform shell surface morphology was observed for all three fibers. This is critical for interfacial polymerization to form a robust and defect-free PA selective layer on the shell surface of hollow fiber substrates [25].

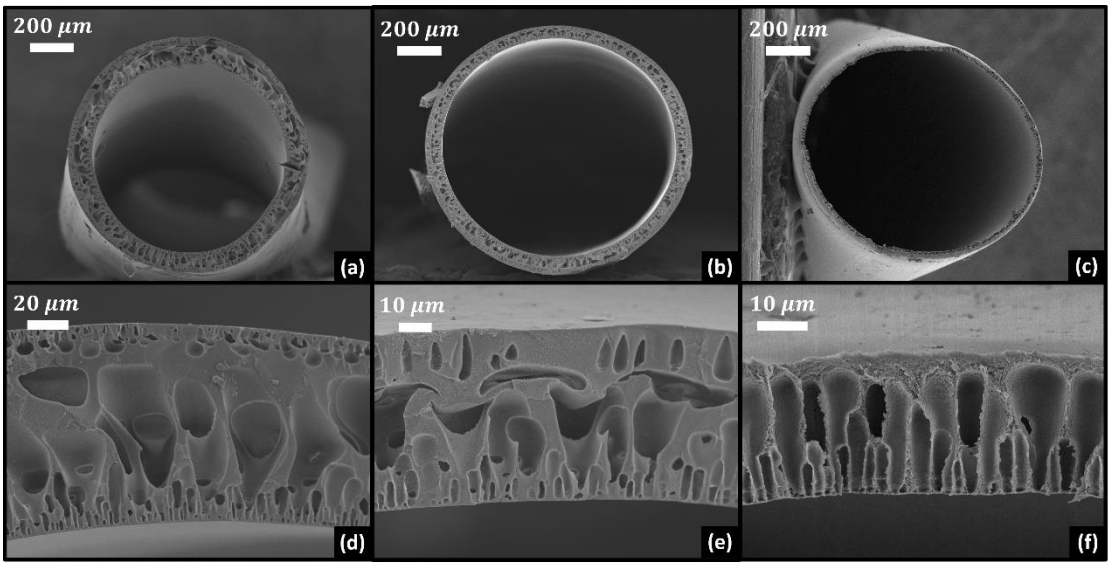

Figure 5.1. Cross-sectional FESEM images of hollow fiber substrates. (a), (b) and (c) PAN-0, PAN-30 and PAN-60 at 65×, respectively. (d) PAN-0 at 600×, (e) PAN-30 at 950×, (f) PAN-60 at 1000×.

As expected, the lumen surfaces and cross-section morphologies underneath the lumen surfaces of the hollow fibers were varied with different fabrication conditions. As the concentrations of solvent (DMF) in bore fluids changed from 0 to 60%, the polymer precipitation rate during phase separation was delayed and resulted in varied wall thickness. The PAN-0 had the thickest wall at ~ 100 μm and the PAN-60 had the thinnest at ~ 50 μm based on the micrometer measurement. PAN-0 and PAN-30 showed similar cross-sectional structure: a thick region of macrovoid structure adjacent to a relatively thin region of finger-like structure underneath the lumen surface of hollow fiber. This is due to the instantaneous polymer precipitation induced by the non-solvent-rich bore fluid for PAN-0 and PAN-30 (pure DI water and 70 wt. % DI water, respectively) [34, 36] .

However, PAN-60 hollow fiber fabricated from a solvent-rich bore fluid (60 wt. % DMF)

exhibit a porous interior structure with straight and open finger-like pores throughout the membrane (Figure 5.1f). Again, DMF in the bore fluid reduced the solvent/non-solvent de-mixing rate, which provided time for the nuclei and surface pore formation [133].

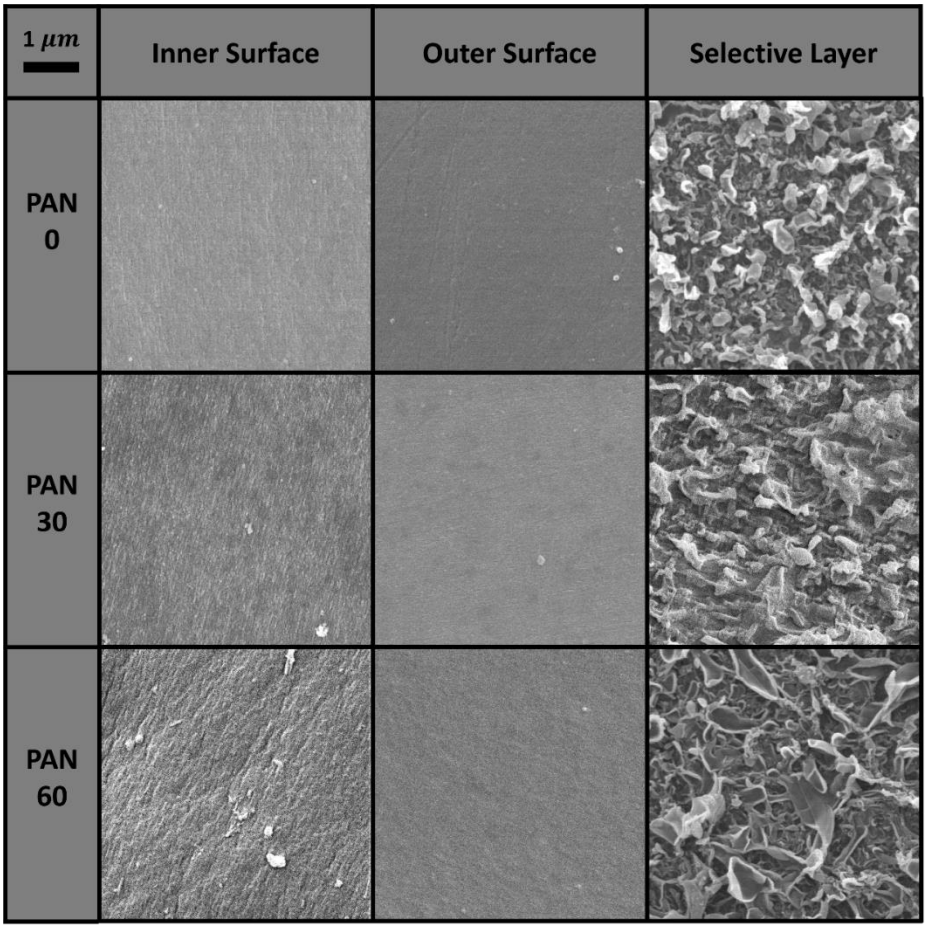

Figure 5.2. Inner and outer surface FESEM images of hollow fiber substrates and selective layer surface FESEM images of TFC hollow fiber membranes at magnifications of 10,000×.

Figure 5.2 also shows the three TFC membranes selective layer surface morphology. The TFC membrane lumen surface showed uniform and defect-free ridge-and-valley morphology which is typical for polyamide synthesized using the interfacial polymerization method [50]. This suggests that thin polyamide selective layers were successfully formed onto each of the PAN hollow fiber substrates.

5.3.2 Characterization of hollow fiber membranes

The dynamic contact angle and pure water permeability of the PAN hollow fiber substrates were tabulated in Table 5.1. The contact angles of three substrates were ~ 50°, indicating their reasonably good hydrophilicity and is consistence with a flat-sheet cast PAN membrane [189].The pure water permeabilities for PAN-0, PAN-30 and PAN-60 were 154.4, 231.6 and 304.7 $L\,m^{-2}h^{-1}bar^{-1}$, respectively.

Table 5.1. Dynamic contact angles and pure water permeances of the hollow fiber substrates.

Substrates	Contact angle (degree)	Pure water permeance ($L\,m^{-2}h^{-1}bar^{-1}$)
PAN-0	52.0 ± 3.4	154.4 ± 6.8
PAN-30	54.8 ± 6.4	231.6 ± 9.4
PAN-60	56.2 ± 3.6	304.7 ± 13.3

Temperature during the measurements was 20±0.5℃.

The mechanical properties of the hollow fiber substrates and TFC membranes were measured at room temperature. The stress-strain curves of representative membrane samples are presented in Figure 5.3. All the substrates and TFC membranes exhibited reasonable stiffness and excellent stretch resistance. It is worth noting that the PAN-60 membranes, with the thinnest wall, possess the highest tensile strength and elastic modulus among all three membranes. This is expected since the material mechanical properties were normalized as force per unit area and PAN-60 has smallest cross section area [29, 102, 190, 191]. By comparing the substrates with TFC membranes, it can be seen that the TFC membranes exhibit comparable or better mechanical properties than their substrate bases. This suggests that the interfacial

polymerization may not jeopardize the membrane mechanical properties. Instead, the strength and stiffness of TFC hollow fiber membranes could be enhanced by PA thin film [27, 91]. This is most obvious for PAN-60 TFC membrane, where the PA thin film occupies the highest proportion of the TFC membrane thickness.

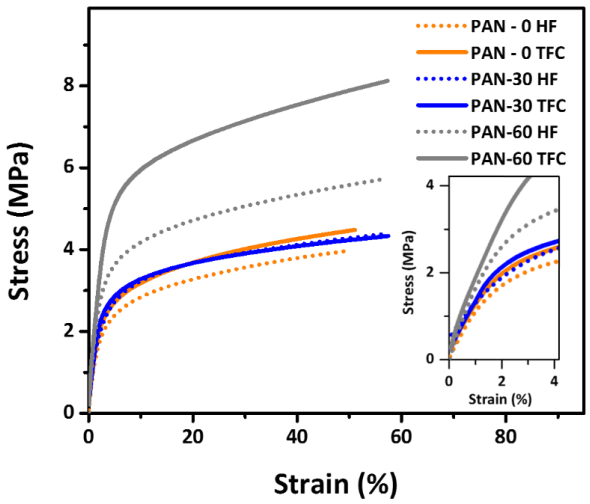

Figure 5.3. Representative stress-strain curve of hollow fiber substrates (HF) and TFC membranes for PAN-0, PAN-30 and PAN-60.

5.3.3 Performance of TFC membranes

5.3.3.1 Permselectivity of polyamide selective layers

The intrinsic water permeance (A) and salt permeability (B) of the TFC membranes selective layer are reported in Figure 5.4. Based on the pure water permeance test, the PAN-0, PAN-30 and PAN-60 showed comparable A values of 2.05, 1.96 and 2.15 $L\,m^{-2}h^{-1}bar^{-1}$, respectively, which are also comparable with the commercial TFC FO membrane from Hydration Technology Innovations [32]. The B values were found to be 0.67 and 0.70 $L\,m^{-2}h^{-1}$ for PAN-0 and PAN-30 and 1.56 $L\,m^{-2}h^{-1}$ for PAN-60 when using 100 ppm NaCl as feed solution. Even at the low pressures, the PAN-60 membranes were observed to be

collapsed during the test. This collapse is possibly caused by its thin thickness, large radius, and greater rigidity [192, 193].

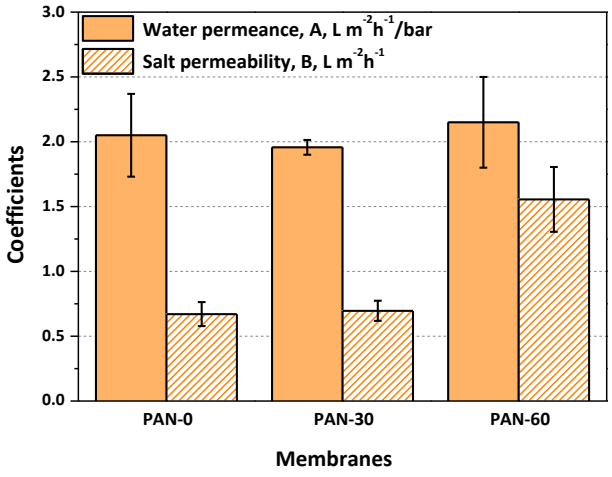

Figure 5.4. Pure water permeance (A) and salt permeability coefficients (B) for the three TFC membranes. Results are an average of three experiments with different modules. Error bars indicate standard deviation. Rejection test operating conditions: feed 100 ppm NaCl, feed pressure 0.5 bar, feed temperature 20 °C, feed flow velocity 0.08 m/s, Reynolds number 800.

5.3.3.2 Osmotic flux performance of TFC membranes

The osmotic water fluxes and reverse salt fluxes of the TFC membranes are presented in Figure 5.5. The membranes with the thinnest walls exhibited the highest water flux for both FO and PRO modes. PAN-60 achieved fluxes ~ 50% higher than those of PAN-0 and PAN-30 in both FO and PRO modes. Meanwhile, the reverse salt flux of PAN-60 is 19.2 $g\ m^{-2}h^{-1}$ in FO mode, which is about 3 times higher than those of PAN-0 and PAN-30. This can be attributed to the thinness of PAN-60 membranes because the reverse draw solutes can diffuse through the thin supporting structure to the selective layer relatively easy.

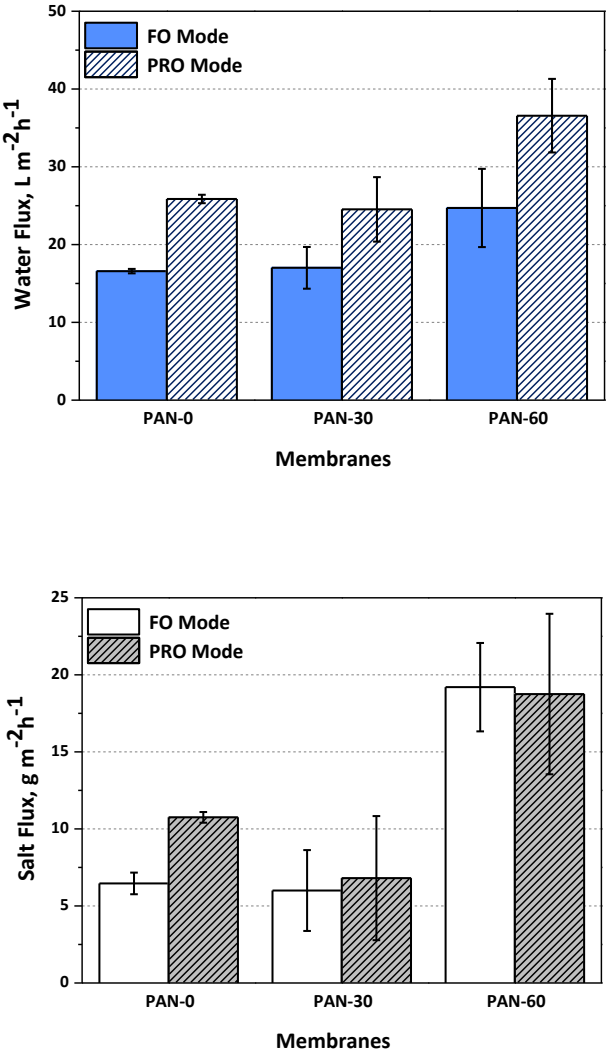

Figure 5.5. Water and reverse salt fluxes (J_w and J_s) of FO and PRO tests for three membranes. Results are an average of three experiments with different modules. Error bars indicate standard deviation. Operating conditions: 1 M NaCl draw solution, deionized water feed, 20 °C feed and draw solution temperature. Reynolds number 1100 and 800 on lumen and shell sides, respectively.

Compared to the commercial HTI TFC membrane [32], our TFC membranes generally yield comparable or higher water and reverse salt flux in both modes. Our highest water flux membrane, the PAN-60, exhibited higher reverse salt flux despite 30% higher water flux in

PRO mode and 70% higher water flux in FO mode. The PAN-30 membrane has 2 times lower reverse salt flux than HTI TFC in PRO mode and about equal in FO mode. For the PAN-0, both water and reverse salt fluxes are about equal with the HTI TFC membrane in both modes.

The structural parameters of PAN-0, PAN-30 and PAN-60 membranes were empirically determined from Eq (5.1) and (5.2) as 549, 499 and 305 μm, respectively. It is not surprising to see a comparable structural parameter of PAN-0 (549 μm) with the HTI TFC (533 μm) since the osmotic flux performance is in good agreement. Also, the membrane thicknesses of these two membranes are comparable (~ 100 μm). Meanwhile, we obtained a low S value of 305 μm for the PAN-60 which can be attributed to the thinness of hollow fiber wall (~ 50 μm). However, the empirically calculated S value might be slightly larger than the real S value. This is because the lumen surface area is smaller than that of shell selective surface. It may result in mildly dilution of local concentration of draw solute at the interface of selective and support layer. This would be reflected as a slightly larger S than the real value.

Specific salt flux J_s/J_w is a metric that is used to determine the amount of draw solute loss per unit of water passed. It has been used to compare membrane performance when different membranes and/or draw solute are used [180]. Lower J_s/J_w is desirable to prevent the loss of draw solutes in FO and help to minimize ICP in PRO. As shown in Figure 5.6, the high J_s/J_w of PAN-60 is due to its considerably high salt permeability. In this case, the improved water flux does not surpass the increase in salt flux. The PAN-30 membrane, with the specific salt fluxes of 0.34 and 0.26 g/L in FO and PRO modes, represent our best performing TFC membrane based on this metric of performance.

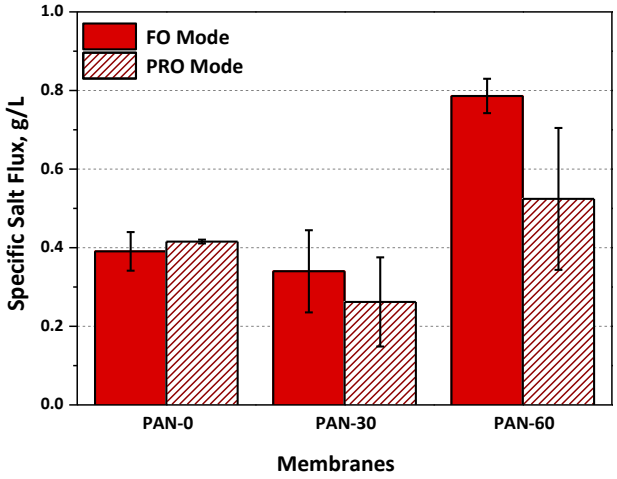

Figure 5.6. Specific salt fluxes J_s/J_w of FO and PRO tests for three membranes. Results are an average of three experiments with different modules. Operating conditions: 1 M NaCl draw solution, deionized water feed, 20 °C feed and draw solution temperature. Reynolds number 1100 and 800 on lumen and shell sides, respectively.

Along with comparison to commercial benchmark HTI TFC membrane, the PAN supported TFC hollow fiber membranes were also compared to other PAN based flat sheet TFC FO membranes [179], layer-by-layer membranes[189], other shell selective hollow fiber FO membranes [29], PRO membranes [102], and lumen selective FO hollow fiber membranes from academic research groups [29, 31, 112] and industrial company [98]. As shown in Table 5.2, our hollow fiber membranes exhibit significantly better water flux combined with a lower specific salt flux in both modes than PAN flat sheet TFC membranes. Compared to layer-by-layer assembled flat sheet membranes which were targeted for nanofiltration solute rejection, our membranes showed comparable water flux and lower specific salt flux, especially in PRO mode [45]. It is worth noting that the draw solution in our tests (1 M NaCl) provided a lower osmotic driving force than that in the LbL work (1 M $MgCl_2$). Moreover, Mg^{2+} ions are more

easily retained which results in lower reverse salt flux.

When compared with another shell-selective hollow fiber FO membrane based on PES, all of our membranes exhibited higher performance in both FO and PRO modes [11]. This is due to employing hydrophilic PAN as the support layer material. The supporting structure wetting was promoted, the effective porosity was increased and the internal concentration polarization was mitigated. Meanwhile, the reverse salt flux of PAN hollow fiber membrane is slightly higher because it is relatively easy for the draw solute to diffuse through a hydrophilic supporting structure to the interface of selective and support layer in FO tests. While comparing with shell-selective hollow fiber PRO membranes fabricated via a vacuum-assisted interfacial polymerization in PRO mode, our membranes exhibited comparable water fluxes but much lower salt fluxes. However, our membranes showed inferior performance when compared with the lumen selective FO hollow fiber membranes. We attribute this to the general challenges of obtaining high quality shell side selective layers using current methods, even though our batch method shows promise. However, with the same packing density, shell-selective TFC hollow fiber membranes would yield higher water flux per module.

Table 5.2. Comparison of osmotic flux performance with TFC FO membranes reported in literature.

Membrane	Configuration	Mode	Feed	Draw solution	Water flux	Salt flux	Specific salt flux	Reference
					$L\,m^{-2}h^{-1}$	$g\,m^{-2}h^{-1}$	g/L	
PAN-0	Shell selective hollow fiber	FO	DI	1 M NaCl	16.58	6.46	0.39	This work
PAN-30	Shell selective hollow fiber	FO	DI	1 M NaCl	17.01	6.00	0.34	This work
PAN-60	Shell selective hollow fiber	FO	DI	1 M NaCl	24.71	19.20	0.79	This work
HTI TFC	Flat sheet	FO	DI	1 M NaCl	15.10	4.40	0.29	[32]
H-PAN	Flat sheet	FO	DI	0.5 M NaCl	9.25	6.43	0.69	[179]
6#LbL-PAN	Flat sheet	FO	DI	1 M $MgCl_2$	22.00	6.65	0.30	[189]
#A-FO HF	Shell selective hollow fiber	FO	DI	0.5 M NaCl	5.00	2.12	0.42	[29]
#B-FO HF	Lumen selective hollow fiber	FO	DI	0.5 M NaCl	14.00	1.75	0.13	[29]
#C-FO HF	Lumen selective hollow fiber	FO	DI	0.5 M NaCl	18.50	1.50	0.08	[30]
FO-PES_{water}	Lumen selective hollow fiber	FO	DI	1 M NaCl	26.00	4.30	0.17	[31]
1.5 mol % sPPSU	Lumen selective hollow fiber	FO	DI	0.5 M NaCl	22.51	5.49	0.24	[112]
Samsung Cheil HFFO	Lumen selective hollow fiber	FO	DI	1 M NaCl	10.00	3.60	0.36	[98]
PAN-0	Shell selective hollow fiber	PRO	DI	1 M NaCl	25.86	10.75	0.42	This work
PAN-30	Shell selective hollow fiber	PRO	DI	1 M NaCl	24.53	6.80	0.26	This work
PAN-60	Shell selective hollow fiber	PRO	DI	1 M NaCl	36.57	18.75	0.52	This work
HTI TFC	Flat sheet	PRO	DI	1 M NaCl	30.05	11.2	0.37	[32]
H-PAN	Flat sheet	PRO	DI	0.5 M NaCl	13.88	6.43	0.46	[179]
6#LbL-PAN	Flat sheet	PRO	DI	1 M $MgCl_2$	25.09	14.25	0.57	[189]
#A-FO HF	Shell selective hollow fiber	PRO	DI	0.5 M NaCl	12.90	5.03	0.39	[29]
#B-FO HF	Lumen selective hollow fiber	PRO	DI	0.5 M NaCl	32.20	3.54	0.11	[29]

#C-FO HF	Lumen selective hollow fiber	PRO	DI	0.5 M NaCl	42.60	4.00	0.09	[30]
FO-PES_{water}	Lumen selective hollow fiber	PRO	DI	1 M NaCl	37.50	5.10	0.14	[31]
1.5 mol % sPPSU	Lumen selective hollow fiber	PRO	DI	0.5 M NaCl	49.39	11.00	0.22	[112]
Samsung Cheil HFFO	Lumen selective hollow fiber	PRO	DI	1 M NaCl	19.00	8.88	0.47	[98]
M1IP1 HF-PRO	Shell selective hollow fiber	PRO	DI	1 M NaCl	21.78	12.85	0.59	[102]
M1IP2 HF-PRO	Shell selective hollow fiber	PRO	DI	1 M NaCl	36.29	33.75	0.93	[102]
M2IP2 HF-PRO	Shell selective hollow fiber	PRO	DI	1 M NaCl	33.17	23.88	0.72	[102]

5.4. Conclusions

In this work, we investigated polyacrylonitrile supported TFC hollow fiber membranes for use in forward osmosis. The intrinsically hydrophillic PAN substrate material was used to mitigate ICP by ensuring wetting of the supporting structure. We also described a simple way to adjust the structure of the fibers in order to elucidate the structure-performance relationships of TFC hollow fiber membranes during osmosis. While exhibiting good osmotic performance overall, our best performing membrane exhibited one of the lowest structural parameter of TFC hollow fiber membranes reported in the open literature. Our thinnest membrane had a wall thickness of ~ 50 μm and was shown to have excellent performance when compared to the flat sheet counterparts and other shell-selective hollow fiber membranes reported in the literature.

Chapter 6. Relating osmotic performance of thin film composite hollow fiber membranes to support layer surface pore size

To be published as

Ren, J., Chowdhury, M.R., Qi, J., Xia, L., Huey, B.D., McCutcheon, J.R., "Relating osmotic performance of thin film composite hollow fiber membranes to support layer surface pore size".

6.1 Introduction

Forward osmosis (FO) exploits the natural osmotic pressure difference to drive water across a semipermeable membrane from a diluted feed solution to a concentrated draw solution while rejecting most solutes [10, 60]. FO requires no applied hydraulic pressure and has been considered for applications involving the treatment of waters with high salinity and fouling propensity [12-14]. The promise of FO has been demonstrated in various applications such as wastewater treatment [15, 16], seawater desalination [17, 18], brine/product concentration [19, 20] and combined with other membrane processes (such as reverse osmosis and membrane distillation) for better system performance [21-24].

As the field of FO experienced development during the past decade, high performance FO membranes have been developed in both academia and industry [25-33]. Among them, hollow fiber FO membranes showed great promise due to the high performance, high packing density, as well as the self-supported structure [29, 30]. These membranes were largely based on a thin

film composite (TFC) membrane design platform, where an ultra-thin selective layer could be supported on a chemically different porous support layer. The two layers could be tailored independently to specifically address membrane structure and chemical needs for good FO performance [40-42]. For making good FO membranes, previous studies have shown that the selective layer needs to have high water permeance and solute selectivity while the support layer needs to be thin, highly porous, and minimally tortuous (*i.e.* a low structural parameter [25, 43, 44]) to minimize the internal concentration polarization (ICP) [45, 46]. A majority of the effort to make TFC hollow fiber FO membranes has focused on the design of these two layers [31, 101, 103, 105, 112-114, 116] as independent features of the membrane. However, the formation of the selective layer *is dependent* on the support layer properties. This interdependency has been largely overlooked by the researchers, especially for the hollow fiber platform.

The selective layer is typically formed via *in-situ* interfacial polymerization on the support layer, thus its formation is impacted by the support layer surface properties [41, 194, 195]. These include physical properties such as pore size, and porosity, and chemical properties such as hydrophilicity and surface charge [195]. The impact of these properties on overall membrane performance (permeance and selectivity) have been studied for flat sheet RO membranes previously. Singh et al. investigated the impact of polysulfone support layer surface pore dimension on the membrane RO performance [194]. Similarly, Ghosh et al. studied the impacts of polysulfone support layer surface pore size, porosity and hydrophilicity on membrane RO performance and proposed a conceptual model describing the formation of polyamide selective layer [195]. It showed that support layer surface pore size tends to have the most influence on the formation of selective layer, as well as the overall membrane performance [195]. Alongside these experimental efforts, Ramon et al. developed 2D and 3D models to study the direct effects of support pore size and porosity on TFC membrane performance [196, 197]. These works

provided insight to the effect of support layer pore size on selective layer formation and its ultimate properties, but were confined to RO membranes only. In the field of FO, Huang et al. reported the impact of support layer pore size on the osmotic flux performance [198]. This study was, however, limited to a microfiltration nylon 6,6 flat sheet support. Shi et al. conducted a study on elucidating structure-performance relationship for hollow fiber TFC membranes in FO, but these were based on cross sectional structures, and not surface pore sizes, of the support layer [114].

In this study, we systematically studied the impact of the support layer surface pore size on the osmotic performance of TFC hollow fiber membranes. We used a series of four commercially available polysulfone hollow fiber ultrafiltration (UF) membranes as supports for making TFC membranes. Using such commercial platform allowed us to maintain the consistency of the membrane structure while varying the support pore size as an independent variable over a relatively wide range. A thin polyamide film was synthesized on the lumen surface of hollow fibers using the conventional interfacial polymerization procedure. Results show that support layer pore size plays an important role in selective layer formation and differences in surface morphology can lead to substantial changes in membrane performance. This work also demonstrates an option to simply and efficiently make high performance TFC hollow fiber FO membranes using commercially available platforms.

6.2. Materials and methods

6.2.1 Materials

A series of special grade commercial hollow fiber ultrafiltration membranes were provided by Koch Membrane Systems Inc. (KMS, Wilmington, MA). The hollow fiber UF membranes

were made of polysulfone with different inner surface molecular weight cut-off (MWCO) ranging from 10, 50, 100 to 500 kDa. The details of membrane structure and other characteristics will be discussed in Section 3.1.

M-phenylene diamine (MPD, >99.0%) and 1, 3, 5-benzenetricarbonyl trichloride (trimesoyl chloride, TMC, 98.0%) were purchased from Sigma Aldrich (St. Louis, MO). *n*-hexane (HPLC, >98.5%), 2-propanol (isopropyl alcohol, IPA, >99.5%) and sodium chloride (NaCl, crystalline, >99.0%) were purchased from Fisher Scientific (Pittsburgh, PA). Deionized (DI) water was used throughout the study and obtained from a Milli-Q ultrapure water purification system (Millipore, Billerica, MA).

6.2.2 Synthesis of polyamide selective layer

The thin film polyamide selective layer was synthesized on the inner surface of hollow fiber membranes via *in-situ* interfacial polymerization (IP). The hollow fiber modules were prepared by potting 10 fibers into clear 6-inch PVC tubes using epoxy resin (Cytec Industries, Olean, NY). To ensure a thorough water saturation of the polysulfone membranes when exposed to aqueous solution, an isopropyl alcohol (IPA) wetting pretreatment was conducted prior to the IP process [127, 199]. Pure IPA was circulated within the module for 2 min to prewet the inner surface of hollow fiber membranes. The hollow fiber module was then thoroughly rinsed with DI water for 3 times and stored in DI water for 1 h prior to the IP process.

The IP process was conducted at room temperature as follows. First, the wetted hollow fiber modules were mounted vertically on a module holder. 2.0% (wt/v) m-phenylene diamine (MPD) aqueous solution was circulated using a pump through the lumen of the hollow fiber module (from the bottom to remove air) for 6 min at a flow rate of 5 mL/min. Excess MPD solution was removed by purging with compressed air, followed by 5 min of air-drying in fume hood at room temperature. 0.1% (wt/v) trimesoyl chloride (TMC) hexane solution was then

pumped into the lumen side of the module from the bottom for 6 min at a flow rate of 5 mL/min to form an ultrathin polyamide film. After the reaction, the modules were air dried for 2 min and subsequently cured in an oven at 65 ℃ for 5 min. Finally, the resulting TFC hollow fiber modules were dried in fume hood at room temperature for 1 min and then stored in DI water at 5 ℃ until further tests.

6.2.3 Characterization of support layer

All the dimensions of the hollow fibers were obtained based on physical measurements at five different locations for each membrane sample. The fiber diameter and fiber wall thickness were measured with coolant proof digital micrometer (IP65-MX, Mitutoyo, IL). The effective fiber length in module is measured with solar digimatic caliper (Absolute 500, Mitutoyo, IL).

The hollow fiber support bulk porosity was determined using gravimetric measurements at room temperature [28, 29, 56]. The dry hollow fibers were cut into 1 cm segments and weighed. The segments were then immersed in IPA until saturation and weighed. IPA was selected since it readily wets the complete structure and will not swell the polymer substantially. The membrane porosity can be determined as the volume of wetting reagent (*i.e.* IPA) divided by the total volume of the membrane, defined as:

$$\varepsilon = \frac{(m_w - m_d)/\rho_w}{(m_w - m_d)/\rho_w + m_d/\rho_m} \times 100\% \qquad (6.1)$$

where m_w is the weight of wet membrane; m_d is the weight of dry membrane; ρ_w is the density of wetting agent IPA (0.786 kg/m^3); ρ_m is the density of membrane material polysulfone (1.240 kg/m^3).

The cross-section morphology of the hollow fiber membranes was imaged with a cold cathode field emission scanning electron microscope (FESEM, JSM-6335F, JEOL Ltd., Japan) at the magnification of 30 ×. To preserve the cross section pore structure, the samples were

submerged in liquid nitrogen and then freeze fractured. Before imaging, the samples were sputter coated with gold.

The surface morphology of the lumen surface of four types of membranes was observed with a low vacuum scanning electron microscope (LVSEM, Teneo, FEI, Hillsboro, OR) at $100{,}000\times$ magnification. The surface porosity was determined using the image processing software ImageJ (Version 1.50, National Institutes of Health, NIH) on the LVSEM images of the lumen surface of the hollow fibers. The values presented are the average of five sample images at different locations on the membranes.

6.2.4 Characterization of selective layer

The surface and cross section morphology of the thin polyamide layer was imaged with FESEM at a magnification of $20{,}000\times$. The thickness of the polyamide selective layer was measured using ImageJ [200, 201]. The area and length of the polyamide film in the field of view were obtained, and the thickness was then calculated as the ratio of the area over length. The results are average values of at least three sample images of different locations.

The surface roughness of the polyamide thin film was studied using Asylum Research MFP-3D atomic force microscope (AFM, Santa Barbara, CA) equipped with silicon tips (Pointprobe, Nanoworld Innovative Technologies, Switzerland). In the operation of AFM, non-contact mode was used on a $10\times 10\ \mu m^2$ scan size at 1.0 Hz [202]. Values presented are at least the average of three samples.

6.2.5 Osmotic flux performance of TFC hollow fiber membranes

Osmotic water and reverse salt flux through TFC hollow fiber membranes were characterized using a custom lab-scale cross-flow forward osmosis system. The similar

experimental setup was described in our earlier investigation [101]. Osmotic flux tests were carried out with the membrane oriented in both FO mode (the selective layer faces the feed solution) and PRO mode (the selective layer faces the draw solution). The TFC membranes were tested under a previously provided standard method in which water and salt fluxes were measured at 20±0.5℃ using DI feed and 1 M NaCl draw solution [101, 133]. The hydraulic pressure was equal on both sides of the membrane while the Reynolds numbers of the fluid flowing in the fiber lumen and shell were 1500 and 580, respectively. The osmotic water flux, J_w, was calculated by dividing the volumetric flux by the membrane area. By measuring the conductivity of the feed solutions at certain time points during the tests, the reverse salt flux, J_s, was calculated by dividing the NaCl mass flow rate by the membrane area. The specific salt flux is simply a ratio of salt flux to water flux, J_s/J_w.

6.3. Results and discussion

6.3.1 Characterization of UF support layer

The molecular weight cut-off (MWCO), dimensions, surface and bulk porosity, and surface pore size of the hollow fiber membrane platforms are presented in Table 6.1. The four types of hollow fiber UF membranes are designated based on their MWCOs (10, 50, 100, and 500 kDa). They all share similar dimensions with inner diameter ~ 1.0 mm and wall thickness of ~ 0.4 mm. The bulk porosity of the four types of membranes are also similar, ranging from 52 to 59%. This wall is relatively thick and less porous than other lab-made hollow fiber FO membranes. Those studies describe hollow fiber membranes with a wall thickness of ~ 0.2 mm and a porosity of 60-80% [30, 31, 101, 112-114]. However, these UF membranes are not designed for this purpose and should not be expected to be as tailored as these academically produced membranes.

It is important to note, however, that the cross sectional images of the UF membranes (Figure 6.1 (a-d)) show an almost identical structure between the different membranes. This enables an independent evaluation of the support layer pore size. Moreover, while unintended, the pore structure has some favorable features for FO performance. The relatively thin and dense layer on the lumen of the membrane, which serves to provide selectivity when used for UF, provides adequate support for the polyamide layer. The open and non-tortuous pores that traverse the membrane wall can facilitate mass transport and reduces ICP [25].

Figure 6.1 (e-h) show the surface morphology and Table 6.1 presents the surface characteristics of these hollow fiber membranes. The 10, 50, and 100 kDa membranes exhibited similar surface porosity ranging from ~ 12 to 14%. The 500 kDa membranes exhibited a higher surface porosity of ~ 26%, presumably due to the larger surface pore size. Note that a higher surface porosity might help to improve the osmotic water flux because selective layer area is less shadowed by the support [198]. The surface mean pore size was determined based on the MWCO relationship provided by Ren et al. [203]. These membranes demonstrated mean pore size varying from ~ 4 to 28 nm, such range of pore size has not been studied in previous investigations [114, 194, 195, 198].

Table 6.1. Characteristics of polysulfone hollow fiber ultrafiltration membranes.

Membrane ID	10 kDa	50 kDa	100 kDa	500 kDa
Molecular weight cut-off (kDa)	10	50	100	500
Inner diameter (mm)[a]	1.07 ± 0.03	1.10 ± 0.02	1.00 ± 0.03	1.05 ± 0.02
Wall thickness (mm)[a]	0.41 ± 0.02	0.39 ± 0.03	0.40 ± 0.01	0.40 ± 0.02
Bulk porosity (%)[b]	58.8 ± 0.8	55.4 ± 1.1	52.3 ± 3.4	54.3 ± 0.9

Surface porosity (%)[c]	11.9 ± 0.8	14.0 ± 0.9	13.0 ± 0.3	26.4 ± 1.4
Surface mean pore size (nm)[d]	4.57	9.57	13.2	27.6

[a] Physical dimensions measured using micrometer.

[b] Bulk porosity measured using the gravimetric method.

[c] Inner surface porosity determined by image analysis on the LVSEM images.

[d] Surface mean pore size calculated based on MWCO [203].

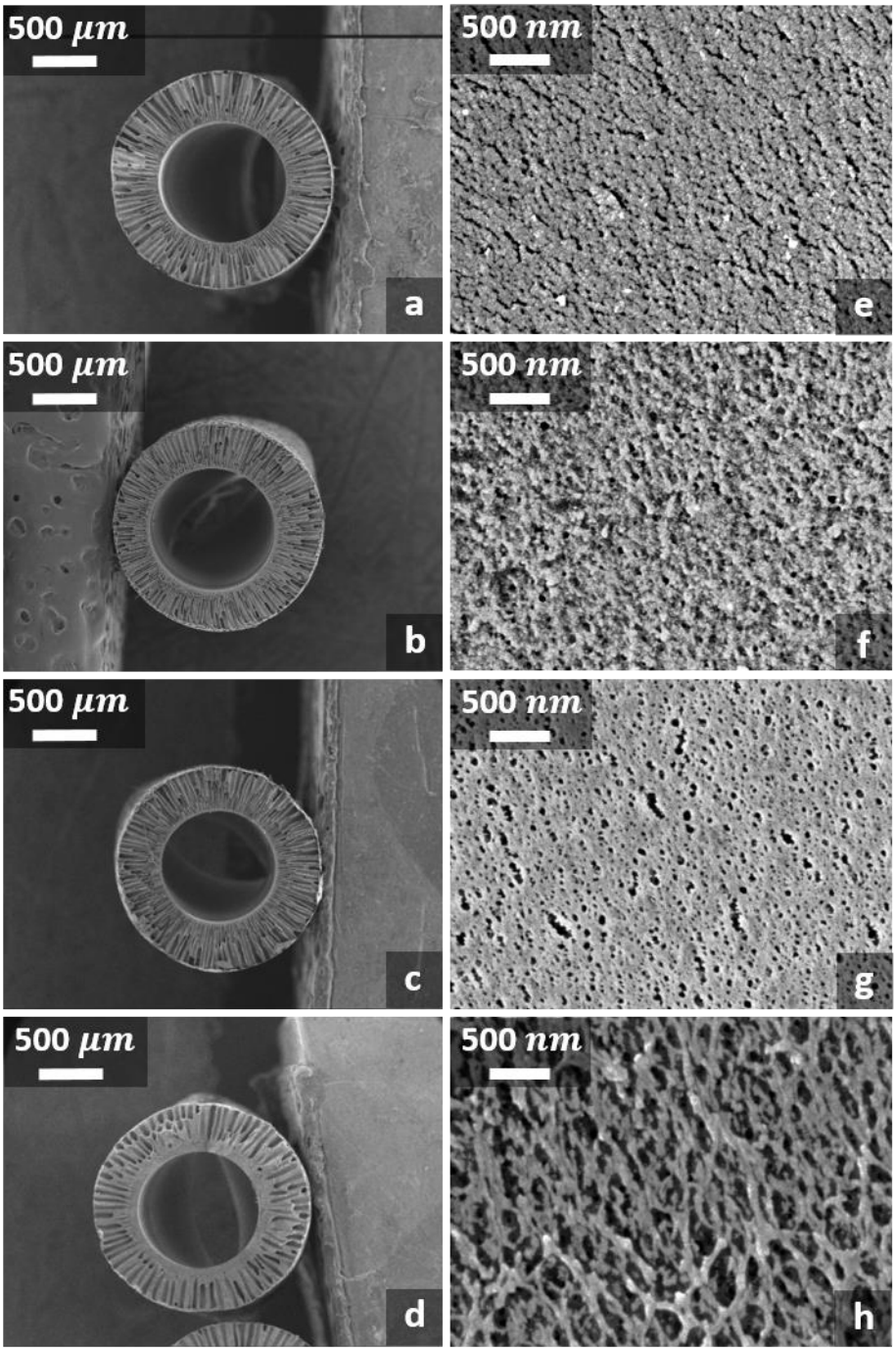

Figure 6.1. Cross-sectional FESEM images of hollow fiber membranes at magnification of 30×: (a) 10 kDa, (b) 50 kDa, (c) 100 kDa, (d) 500 kDa. Surface LVSEM images of hollow fiber membranes at magnification of 100,000×: (e) 10 kDa, (f) 50 kDa, (g) 100 kDa, (h) 500 kDa.

6.3.2 Characterization of selective layer

The surface morphology of the selective layer of the TFC membranes are shown in Figure 6.2 (a-d). The polyamide is formed on the lumen (selective surface) of the UF membrane and exhibited different morphology for different support layers. For 10 and 50 kDa membranes, the polyamide had protuberances that were relatively small and worm-like. For the 100 and 500 kDa membranes, large and irregular protuberances were observed and the morphology was more likely to be ridge-and-valley or even leaf-like [204]. These were most noticeable on the 100 kDa membrane. Similar structures have been observed in previous investigations suggesting a multi-level structure of polyamide [204-206].

The cross-section views of the four TFC membranes are shown in Figure 6.2 (e-h). By using ImageJ image analysis on the cross section FESEM images, the thickness of the four membranes were estimated (Table 6.2). The analysis revealed a trend that the selective layer thickness increased with varying support pore size. The 10 kDa support showed a polyamide thickness of ~ 290 nm to 100 kDa support showed a thickness of ~ 500 nm. The 500 kDa support had polyamide thicknesses that were slightly less at ~ 430 nm. Meanwhile, the standard deviation of the selective layer thickness also varied from 60 nm at 10 kDa to 145 nm at 100 kDa to 84 nm at 500 kDa, which suggests the surface roughness is also impacted by the support layer pore size.

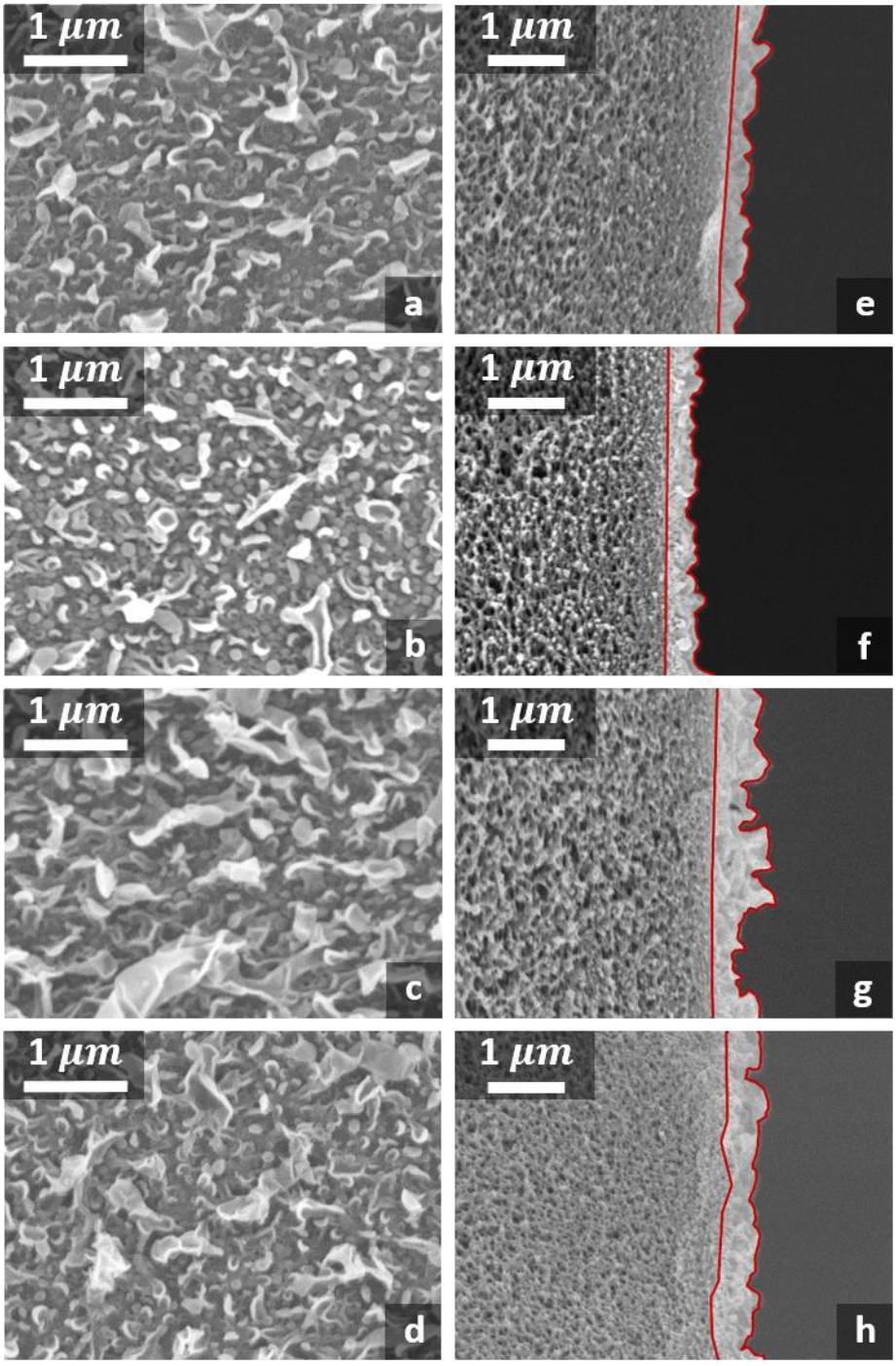

Figure 6.2. FESEM images of the surface (a-d) and cross section (e-h) of the selective layer formed on 10, 50, 100, and 500 kDa hollow fiber membranes at a magnification of 20,000×. The selective layer is outlined in red in cross section images.

Table 6.2. Characteristics of selective layer of four types of TFC hollow fiber membranes

Membrane ID	10 kDa	50 kDa	100 kDa	500 kDa
Thickness (nm)[a]	291.7 ± 60.2	365.8 ± 63.2	506.5 ± 145.8	427.9 ± 83.6
RMS surface roughness (nm)[b]	82.7 ± 7.2	88.0 ± 3.8	127.7 ± 6.3	96.3 ± 3.9
Average surface roughness (nm)[b]	65.7 ± 5.7	69.1 ± 2.8	101.0 ± 3.7	76.9 ± 3.3
Surface area percent (%)[c]	33.1 ± 3.7	37.6 ± 0.9	46.8 ± 1.2	39.5 ± 3.6

[a] Selective layer thickness determined based on image analysis using cross-sectional FESEM images.

[b] Root mean square (RMS) and average surface roughness determined using AFM.

[c] Surface area percent is defined as the three-dimensional area over the two-dimensional area of the sample scan size, obtained from AFM.

AFM was used to quantitatify surface roughness of the polyamide selective layers, and the results are shown in Figure 6.3 and Table 6.2. The 100 kDa membrane showed the roughest surface while the other three membranes showed more modest differences. By comparing the results in Table 6.2, the root mean square (RMS) and the average surface roughness increased from 10 to 100 kDa, and then dropped at 500 kDa. The surface area percentage, which is defined as the difference of three-dimensional area over the two-dimensional area of the sample scan size, showed the same trend [202]. The largest three-dimensional surface area of the selective layer (147%) was exhibited in the membranes with the 100 kDa support membranes. This result has similarities and differences with previous observations on flat sheet membranes which suggest small support layer surface pores produce smoother polyamide layers [113, 195]. In our work, we see rougher polyamides with increasing pore sizes *to a point*, but then the

polyamide becomes smoother.

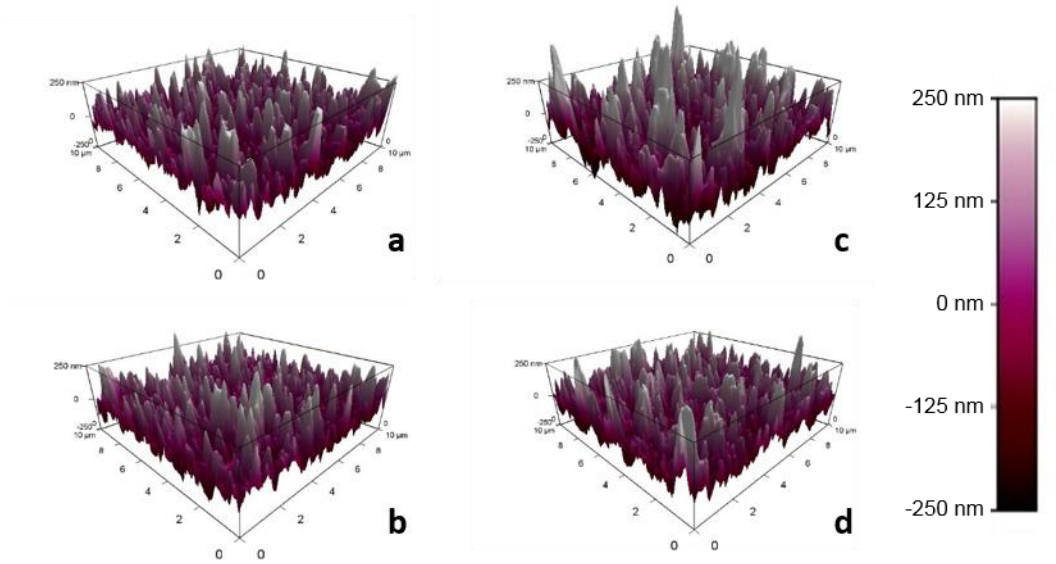

Figure 6.3. AFM images of selective layer surface of (a) 10 kDa, (b) 50 kDa, (c) 100 kDa, and (d) 500 kDa TFC hollow fiber membranes. Sample scan size is $10 \times 10\ \mu m^2$.

6.3.3 Elucidating selective layer formation mechanisms

Previous investigations have demonstrated that a number of factors could affect the formation of polyamide during interfacial polymerization. Using different monomers, concentrations of monomers, additives, experiment conditions (reaction time, curing temperature, etc.), and support layer chemistry and structure have all been demonstrated as a way to change selective layer properties [50, 194, 195, 207]. This work was designed to hold all variables constant except for support layer pore size by using commercialized UF membranes as supports for making the TFC membranes. However, due to the limitations during the manufacture, the porosity of 10, 50 and 100 kDa membranes shared high consistency while the 500 kDa membrane exhibited inconstant porosity which may played a role in the selective layer formation which will be further discussed in this section.

A number of conceptual models have attempted to clarify the potential effects of support

pore size on polyamide formation in flat sheet membranes [113, 194, 195, 198]. Some of these models were proposed based on the belief that the polyamide layer is a dense film and therefore focused on the polyamide thickness variation dependence on support structure [194, 195, 198]. However, recent advanced characterizations of the polyamide selective layer have revealed that voids exist in the polyamide, and some of these voids are even open to the support layer [201, 204, 208]. These findings suggest that the dense film hypothesis in these models may not be accurate.

We therefore propose an updated conceptual model which incorporates the formation of voids as a hypothesis to attempt to clarify the impacts of support pore size on polyamide formation based on the observation in this study. Figure 6.4 illustrates the conceptual model of polyamide formation mechanism on supports with various pore sizes. The interfacial polymerization occurs when the aqueous MPD/water saturated support is contacted with the organic TMC/hexane solution. The film grows into the organic phase because the diamine has greater solubility in the hexane than TMC in water [100, 209]. The MPD diffuses from the water phase into the organic phase to form the polyamide nuclei. As the MPD continuously diffuses from the pores and partitions into the organic phase, the polyamide nuclei diffuse laterally to create a continuous polyamide film across the regions spanning one or more pore openings [195, 204]. The film formation is self-limiting since the formation of the film slows down the diffusion of MPD into the organic phase until the reaction ultimately terminates. It has been proposed that the upper bound limit of PA thickness in the MPD/water-TMC/hexane system is around 20 nm [204, 205], while the PA film crumpled and folded to exhibit an overall thickness of hundreds of nanometers, as observed in Figure 6.2.

For the small pore membranes (i.e. 10 kDa), the amount of MPD is less and therefore will more rapidly dilute as it diffuses into the organic phase. This dilution lessens the concentration gradient and reduces diffusive flux rapidly, leading to relatively small and shallow

protuberances of polyamide. For a larger pore membranes (i.e. 100 kDa), the dilution of MPD is lessened and diffusion is therefore more rapid, which causes a more violent and “eruption” into the organic phase. This results in larger and rougher polyamide protuberance formed spanning over multiple pore openings.

Based on these results, one would expect that even larger pores would yield even rougher surfaces. However, in this work, that was not the result. The 500 kDa membrane supports yielded rougher polyamide layers than the smallest pore sizes measured (10 kDa), but smoother than the medium pore size measured (100 kDa). While we see little literature evidence for this phenomenon over the ranges of pore sizes tested, we hypothesize that the pore spacing may play a role. We must recall that the 500kDa membrane has a larger pore size and a higher surface porosity than the others tested, meaning that the distance between pores is smaller. Thus the MPD diffusing out of one pore is more likely to interact with MPD diffusing out of a nearby pore, changing the direction of the MPD diffusion because of the concentration gradient. The nearby pores are more able to “fill in the gaps” in the film that would be more prominent for films formed on supports where the pores were widely spaced. The result is a somewhat smoother, but still thick film. The authors emphasize that this is only a hypothesis, and an intricate study on pore spacing and its effect on polyamide film formation would be prudent, though such an effort is beyond the scope of this study.

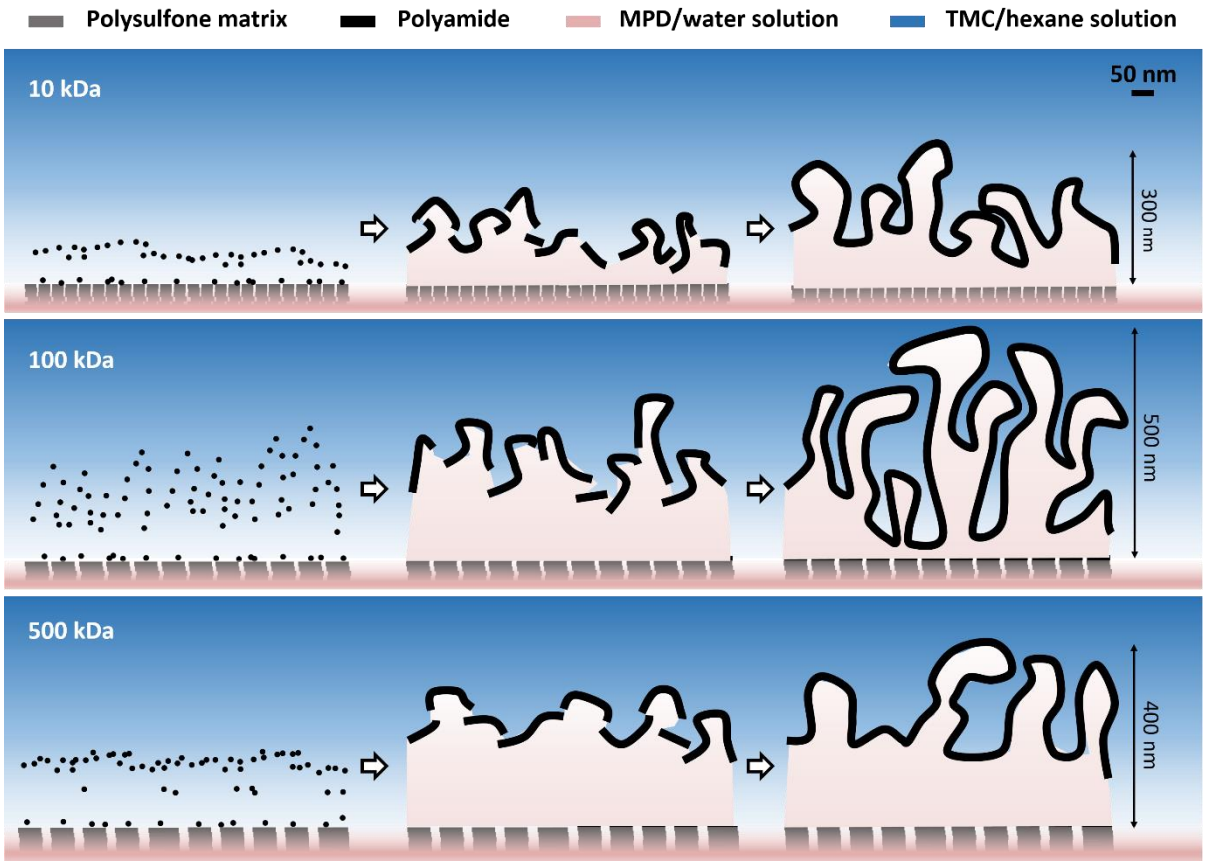

Figure 6.4. Conceptual model illustrating the role of polysulfone support pore size during interfacial polymerization of MPD-TMC thin films.

6.3.4 Osmotic flux performance of TFC hollow fiber membranes

The TFC membranes were evaluated under FO and PRO modes using DI water as the feed and 1 M NaCl as the draw solution. The osmotic water and reverse salt flux (J_w and J_s) of the four TFC hollow fiber membranes is presented in Figure 6.5. Water and salt flux performance was compared with the commercial TFC hollow fiber FO membrane from Samsung Cheil Industries reported in the literature [73, 98]. Generally, our membranes exhibit a comparable or higher water flux and much lower reverse salt flux than the commercial membrane in both FO and PRO mode. Our best membrane, the 100 kDa, showed ~ 70% and ~ 15% higher J_w

than the Cheil membrane in PRO and FO mode, respectively. For the J_s, the 100 kDa membrane showed J_s of 3.3 and 2.1 gmh in PRO and FO mode, which was ~ 2 to 3 times lower than the commercial benchmark.

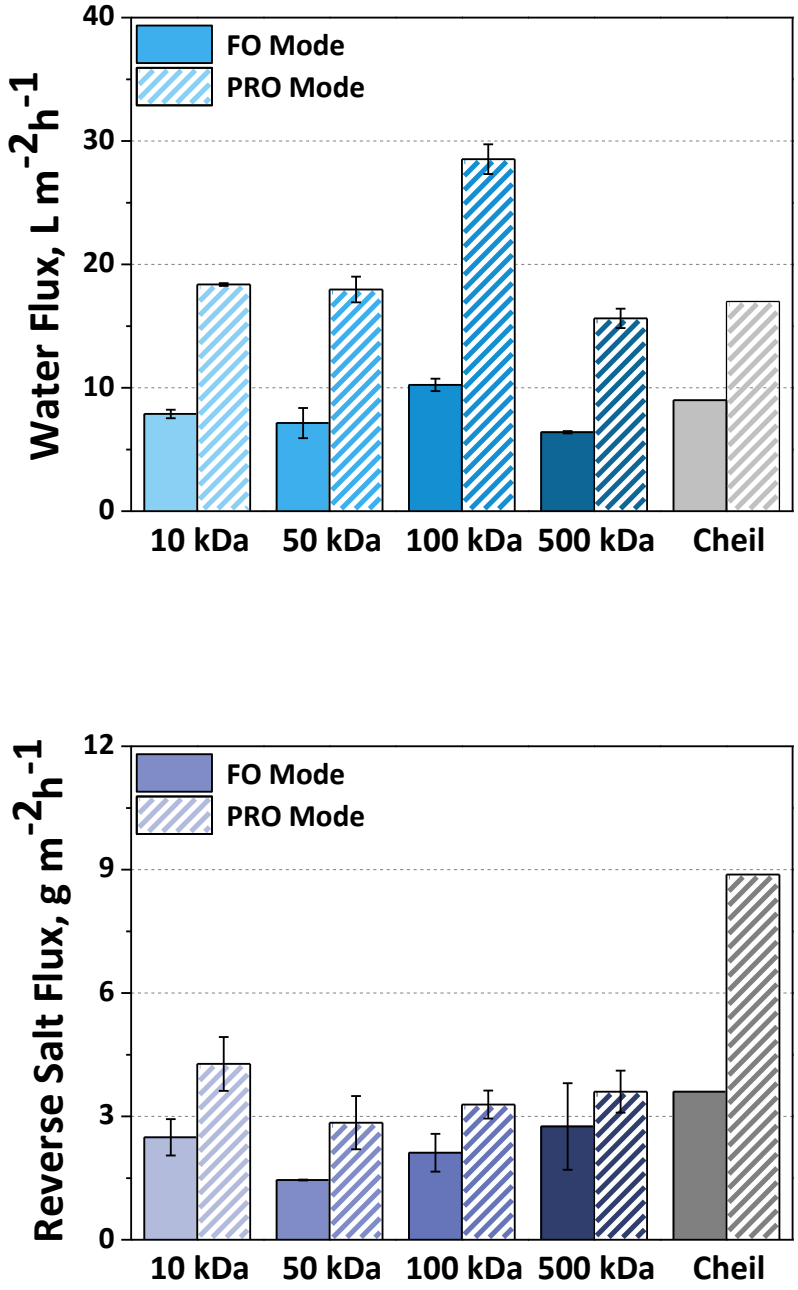

Figure 6.5. Water flux and reverse salt flux (J_w and J_s) of FO and PRO tests for 10, 50, 100, and 500 kDa TFC membranes and commercial TFC hollow fiber membranes from Chiel

Industries [73, 98]. Results of lab-made membranes are an average of three experiments with different modules. Error bars indicate standard deviation. Operating conditions: 1 M NaCl draw solution, DI water feed, 20 ℃ feed and draw solution temperature, 0 transmembrane pressure.

Aside from the water and salt flux results, the specific salt flux (J_s/J_w) was also evaluated (Figure 6.6). J_s/J_w is a practical metric that is used to determine the amount of draw solute loss per unit of water pass through. Lower J_s/J_w is desirable to prevent the loss of draw solutes in FO mode and help to minimize ICP in PRO mode. Again, all our membranes outperformed the commercial membrane from Cheil under this performance metric. It worth noting that with a similar lumen dimension (1 mm vs. 0.9 mm), the membrane supports used in this work are two times thicker than Cheil membrane benchmark (0.4 mm vs. 0.15 mm). Remarkably, even with this feature, the membranes still outperformed the benchmark. This is presumably due to the needle-like long and open pore structure traverse the membrane wall that reduces mass transfer resistance and ICP [114].

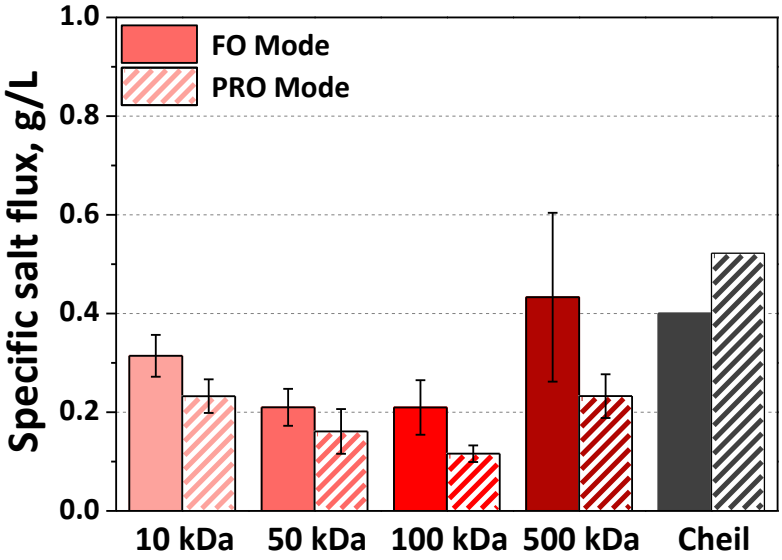

Figure 6.6. Specific salt flux (J_s/J_w) of FO and PRO tests for 10, 50, 100, and 500 kDa

TFC membranes and commercial TFC hollow fiber membranes from Chiel Industries [73, 98]. Operating conditions: 1 M NaCl draw solution, DI water feed, 20 ℃ feed and draw solution temperature, 0 transmembrane pressure.

6.3.5 Impact of support layer pore size on osmotic flux performance

Figure 6.5 also shows that water and salt flux both varied for membranes formed on different pore size supports. Comparable low water and salt flux membranes were formed on the 10 and 50 kDa supports. The highest water flux membrane was formed on the 100 kDa support. Interestingly, the lowest water flux and highest salt flux was exhibited by the TFC membrane formed on the 500 kDa support. Such a trend in water flux correlates well with selective layer roughness, especially in the PRO mode. It has been reported that a rough or crumpled polyamide surface in RO and NF membranes provides a greater effective permeable area than the smooth surface, thus results in a permeance enhancement [209-212]. The water permeance was difficult to determine because of the potential polyamide deformation induced by the high lumen pressure in RO tests [122]. We can nevertheless assess how roughness affects performance of these membranes in osmotic tests. The 10, 50, and 500 kDa membranes exhibited similar water flux and had similar roughnesses (500 kDa was a little rougher, but it also exhibited higher salt flux). The 100 kDa membrane with the highest roughness (about 45% rougher than the other three membranes) had the highest water flux (about 65% higher than the other membranes) in both the FO and PRO mode. The PRO mode performance was most notable, though. Rough selective layers benefit PRO mode operation because the draw solution may "act" upon a larger surface area. The roughness effect is lessened in the FO mode, however, since the draw solution is diluted within the support layer of the membrane due to the ICP. In

the cases where the polyamide film protuberances are “hollow” or full of void spaces, roughness may actually enhance ICP effects near the selective layer interface in the FO mode [201, 208]. Thus the roughness demonstrates distinct effects on the osmotic flux performance of TFC hollow fiber membranes.

6.4. Conclusions

In this work, we first identified that the support layer surface pore size has a significant impact on the formation of TFC membrane formation on the hollow fiber platform. Using a commercial UF hollow fiber platform allowed for the independent assessment of pore size as a variable that impacts polyamide layer formation. It was clear from the findings that the pore size could greatly impact polyamide roughness. This roughness, in turn, had distinct impacts on water and salt flux performance of the membrane.

An unanticipated finding of this work was the simple fact that a commercial UF hollow fiber could serve as a support for a TFC membrane used in FO. While UF membranes are not designed with FO specifications in mind, these membranes not only performed well as supports for TFC membranes, they outperformed the only commercial benchmark in the literature. Such a finding may have ramifications across FO research groups since now they have the ability to fabricate TFC hollow fiber membranes via a simple and facile interfacial polymerization process. The ability to fabricate membranes, especially those that can exhibit high packing density, is essential to applied research in osmotic processes given the challenges in finding stable and consistent supplies of commercial FO membranes.

Chapter 7. Developing Thin Film Composite Hollow Fiber Forward Osmosis Membranes at the Module Scale

To be published as

Ren, J., McCutcheon, J.R., "Making thin film composite hollow fiber forward osmosis membranes at the modules scale using commercial ultrafiltration membranes", *Industrial & Engineering Chemistry Research.*

7.1. Introduction

Forward osmosis (FO) offers a unique solution to some of our most challenging water treatment processes [10, 13, 39, 145, 213]. Water reuse[16, 214], produced water treatment [65, 66], brine dewatering [19, 215], and zero liquid discharge systems [9, 213] are all enabled by FO technology. Progress in the field of FO has previously been hampered by poor membrane performance [12, 13, 17]. Over the past decade, research groups all around the world have been focused on developing high performance membranes specifically for FO [25, 27, 31, 91, 216]. Industry joined the effort and companies like Fluid Technology Solutions (formerly Hydration Technology Innovations, HTI) [32], Oasys Water [33, 94], Modern Water [217], and Porifera [96] emerged with their own brand of membrane technology. These achievements enabled the advancement of FO since the lack of membranes were no longer preventing it from commercial opportunities.

However, FO membrane technology is still far from performing at a level that would spur rapid acceptance by the broader membrane community. This is evident in the fact that companies have settled on neither a membrane nor a module that can serve as a standard for FO [39, 218]. The lack of agreement on these two features strongly suggests that further improvement in membrane design and demonstration, especially *at scale*, is needed for the field. In the reverse osmosis (RO) industry, nearly all companies use the same type of element: spiral wound 4040 and 8040 elements, with 16 and 18-inch elements now emerging [219-221].This standardization has taken place over decades of optimization that finally honed in on the necessary packing density required to make RO the most profitable. These membranes also are made with very similar chemistries (polyamide based thin film composites，TFC), because this chemistry has been determined to be one of the best for combined selectivity and permeance performance [222]. Looking at the fledgling FO industry today, no such standardization exists. Porifera uses a flat sheet plate-and-frame module with a TFC membrane [96, 223]. FTS uses a spiral wound element with the same dimensions as today's RO elements but incorporates a cellulose acetate membrane [135, 136, 224, 225]. Oasys Water and Toray both use spiral wound elements with their own brand of TFC membranes [94, 95]. Toyobo offers a hollow fiber cellulose acetate module [97]. Recently, Aquaporin A/S and Samsung Cheil Industry are emerging with TFC hollow fiber membrane modules [73, 98, 226].

This last platform is of particular interest to FO. Hollow fiber membranes have long been considered a valuable platform for membrane separations because of their higher packing densities than any flat sheet configurations [34]. This has made hollow fibers the preferred configuration for many membrane contactor applications and some academic groups have seized upon these same benefits for FO [12, 29, 30, 115]. A number of TFC hollow fiber membranes have been developed for FO in academic laboratories, with many showing promise of high performance [29-31, 112, 114].

The TFC membrane is a preferred platform since an ultra-thin selective layer is supported on a chemically different porous support layer allowing for the two layers to be designed for specific purposes [40-42]. The selective layer is designed to have a high water permeance and solute selectivity. This criterion can be met with today's TFC RO membranes' polyamide chemistry formed through interfacial polymerization [25, 47]. The support layer is designed to be thin, highly porous, and minimally tortuous (*i.e.* a low structural parameter) [25, 43, 44] to minimize the mass transfer resistance, which manifests as internal concentration polarization (ICP) [45, 46]. Since the polyamide chemistry is seen as the standard and best available selective layer chemistry, most efforts in FO membrane design have been focused on the design of low structural parameter supports [31, 101, 112, 113, 116]. Some of these membranes exhibited beautifully crafted pore structures with low structural parameter and correspondingly excellent FO performance. However, many require the use of costly polymers, difficult fabrication methods, or intricate module designs that make commercialization challenging.

This study seeks a shortcut by simply employing existing commercial hollow fiber ultrafiltration (UF) modules as support for TFC FO membranes. A series of commercial hollow fiber modules with different fiber dimensions were selected as supporting materials from Koch Membrane Systems Inc. (KMS). These membranes were designed for UF applications but can serve as adequate supports for a TFC FO membrane. A selective polyamide film was synthesized on the inner surface of hollow fibers via interfacial polymerization using conventional approaches. Testing was conducted over a range of operating conditions (membrane orientation, draw solution concentration, cross flow arrangement, and cross flow velocity) to elucidate the effect of operation parameters on FO performance of hollow fiber membranes at a module scale. Moreover, this work justifies the simplicity of making TFC hollow fiber modules for FO with reasonable performance using off-the-shelf UF membranes.

7.2. Materials and methods

7.2.1 Materials

Two special grade commercial hollow fiber ultrafiltration modules were provided by Koch Membrane Systems Inc. (KMS, Wilmington, MA). Figure 7.1 is a photograph of the module showing the dimensions. Table 7.1 presents the specifications of the two types of modules. The hollow fiber UF membranes in the modules were made of polysulfone with different fiber diameters. The module with small diameter fibers (I.D. 467μm) was designated as HFM-A while the one with large diameter fibers (I.D. 1023μm) was HFM-B. The selective skin layer of the hollow fiber UF membrane was on the inner surface with a molecular weight cut-off (MWCO) of 10 kDa for both HFM-A and HFM-B.

m-phenylene diamine (MPD, >99.0%) and 1, 3, 5-benzenetricarbonyl trichloride (trimesoyl chloride, TMC, 98.0%) were purchased from Sigma Aldrich (St. Louis, MO). *n*-hexane (HPLC, >98.5%), 2-propanol (isopropyl alcohol, IPA, >99.5%) and sodium chloride (NaCl, crystalline, >99.0%) were purchased from Fisher Scientific (Pittsburgh, PA). Deionized water (DI) was used throughout the study and obtained from a Millipore Integral 10 water purification system (Millipore, Billerica, MA).

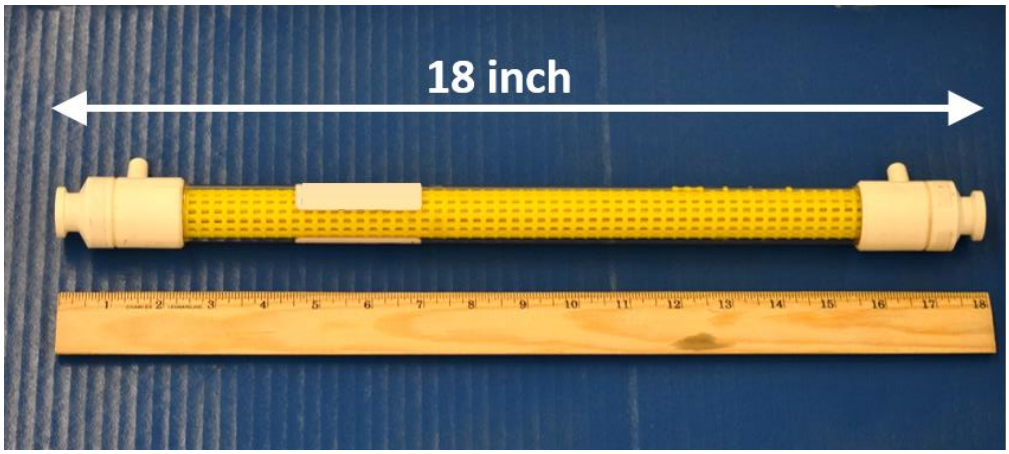

Figure 7.1. Photograph of a special grade commercial hollow fiber ultrafiltration membrane module provided by KMS.

Table 7.1. Specifications of the special grade commercial hollow fiber membrane (HFM) modules.

Membranes	Fiber inner diameter (μm)	Fiber outer diameter (μm)	Molecular weight cut-off (kDa)	Fiber length ($inch$)	Number of fibers	Packing density (%)	Effective membrane area (m^2)
HFM-A	467	906	10	18	300	38.5	0.18
HFM-B	1023	1818	10	18	60	30.7	0.09

7.2.2 Synthesis of selective polyamide layer

The aromatic polyamide layer was synthesized on the hollow fiber membrane inner surface via in-situ interfacial polymerization (IP). This is a condensation polymerization involves monomers from aqueous and organic phases react at the aqueous-organic phase interface. The aqueous solution was 2.0% (wt/v) m-phenylene diamine (MPD) dissolved in DI water. The organic solution was 0.1% (wt/v) trimesoyl chloride (TMC) dissolved in hexane.

To ensure a thorough water saturation of the polysulfone hollow fiber membranes when exposed to MPD aqueous solution, an isopropyl alcohol (IPA) wetting pretreatment was conducted prior to the IP process [127, 199]. Pure IPA was circulated through the fiber lumen for 2 min to wet out the inner surface of hollow fiber membranes in the module. The hollow fiber lumen side was then thoroughly rinsed and stored in DI water overnight at room temperature to remove the residual IPA.

The IP process was conducted within the module at room temperature. The modules were mounted vertically and aqueous MPD solution was pumped into the wetted membrane (lumen side) from the bottom for 10 min at a flow rate of 0.75 L/min using a peristaltic pump (Thermo Fisher Scientific, Waltham, MA). Residual MPD solution in the lumen was then removed using filtered compressed air for 5 min. The membranes were then dried for 15 min in a fume hood. The TMC hexane solution was then pumped into the lumen from the bottom for 10 min at a flow rate of 0.75 L/min. After the reaction, residual TMC solution was removed by compressed air for 5 min. The module was subsequently cured in oven at 70 ℃ for 8 min. Finally, the module was dried at room temperature for 3 min and then stored in DI water at 5 ℃ until testing.

7.2.3 Morphology of hollow fiber membrane substrates

The surface and cross-sectional morphology of the hollow fiber UF membranes were imaged with a cold cathode field emission scanning electron microscope JSM-6335F (FESEM, JEOL Ltd., Japan). To view the cross-sections of the membrane substrates, the samples were submerged in liquid nitrogen to preserve the pore structure and then fractured. Before imaging, the samples were sputter coated with gold.

7.2.4 Osmotic flux performance of TFC hollow fiber membranes

7.2.4.1 Osmotic flux tests

Osmotic water and reverse salt flux of TFC hollow fiber membranes were characterized using a custom lab-scale cross-flow FO system shown in Figure 7.2. This system is similar to the system described in our earlier investigations [101, 185], but was modified to accommodate a larger volume of draw solution (10 L) to avoid significant draw dilution due to the large membrane area in the module. Osmotic flux tests were carried out with the hollow fiber module oriented in both FO mode (the selective layer faces the feed solution, *i.e.* feed in the lumen) and PRO mode (the selective layer faces the draw solution, *i.e.* draw in the lumen). DI water was used as feed and NaCl solution was used as draw. The effect of NaCl draw solution concentration on osmotic flux performance was studied with various NaCl concentrations (0.3M, 0.6M, 1M and 1.5M). The membrane modules were tested at $20\pm0.5℃$ in both co-current and counter-current flow arrangements. The cross flow velocity (CFV) could be independently varied to evaluate the impact on water and solute flux. In all tests, the Re was the same on both shell and lumen sides. For the HFM-A, the Re ranged from 80 to 160. For the HFM-B, the Re varied from 240 to 480. The osmotic water flux, J_w, was calculated by dividing the volumetric flux by the membrane area. By measuring the conductivity of the feed solutions at certain time during the tests, the reverse salt flux, J_s, was calculated by dividing the NaCl mass flow rate by the membrane area. The specific salt flux is simply a ratio of salt flux to water flux, J_s/J_w.

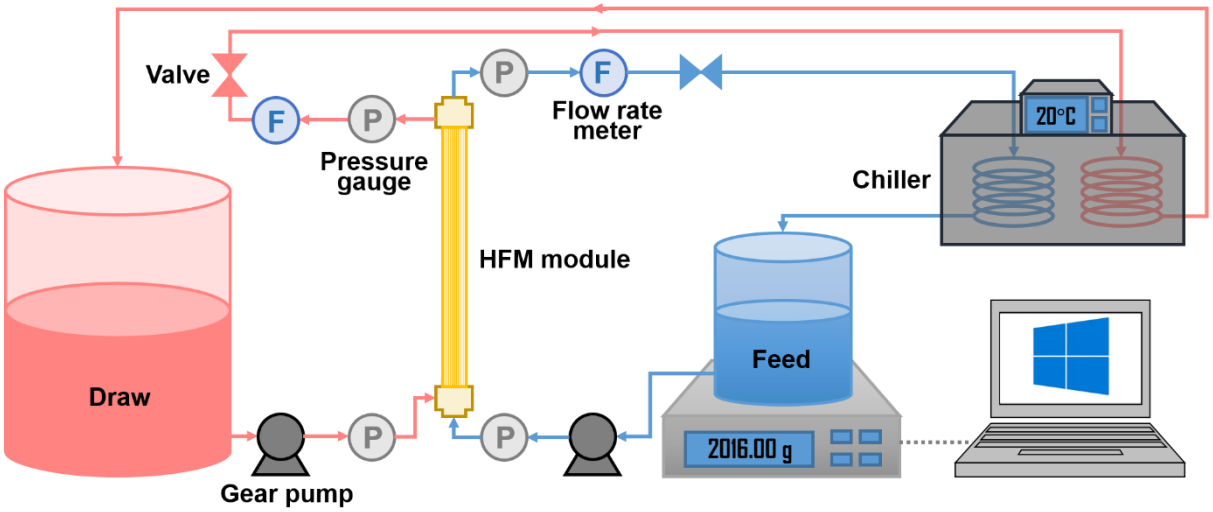

Figure 7.2. Schematic diagram of FO testing apparatus for the hollow fiber membrane modules.

7.2.4.2 Determination of structural parameter

The water permeance (A), salt permeability coefficient (B) and structural parameter (S) of the TFC FO membranes were determined by adopting the empirical method developed by Tiraferri et al. [177]. The method allows the simultaneous determination of A, B and S parameters of FO membranes by dividing the FO experiment into a discrete number of stages. In this work, the experiments were carried out in four stages using different draw solution concentrations in FO mode (0.3M, 0.6M, 1M, 1.5M).

7.3. Results and discussion

7.3.1 Morphology of hollow fiber membrane substrates

Figure 7.3 shows the cross-sectional structure of the two hollow fiber membranes selected for this work. These two membranes showed a similar cross-sectional structure with a spongy-like layer close to the lumen surface and aligned dendritic pores throughout much of the

membrane wall. Figure 7.4 shows the outer and inner surface structures of HFM-A (the surface morphology of HFM-B is identical with HFM-A). The outer surface showed a rough and open structure with large pores at the scale of ~10 μm. The inner surface showed a uniform porous structure with small pores that corresponding to the MWCO of 10 kDa [203]. While unintended, this structure has some desirable features for FO performance. The majority of the pore structure is open and non-tortuous, which facilitates mass transport and reduces ICP. The relatively thin and dense layer on the lumen of the membrane, which serves to provide selectivity when used for UF, has smaller pores and provides adequate support for the polyamide layer [25, 146].

Since these membranes were designed for ultrafiltration, the fiber walls were relatively thicker (~220 and ~400 μm for HFM-A and HFM-B) compared to others that have been designed for FO (typically less than 200 μm) [31, 101, 103, 112]. However, because of the favorable cross-sectional structure, these membrane modules still showed solid FO performance which is discussed in the following sections.

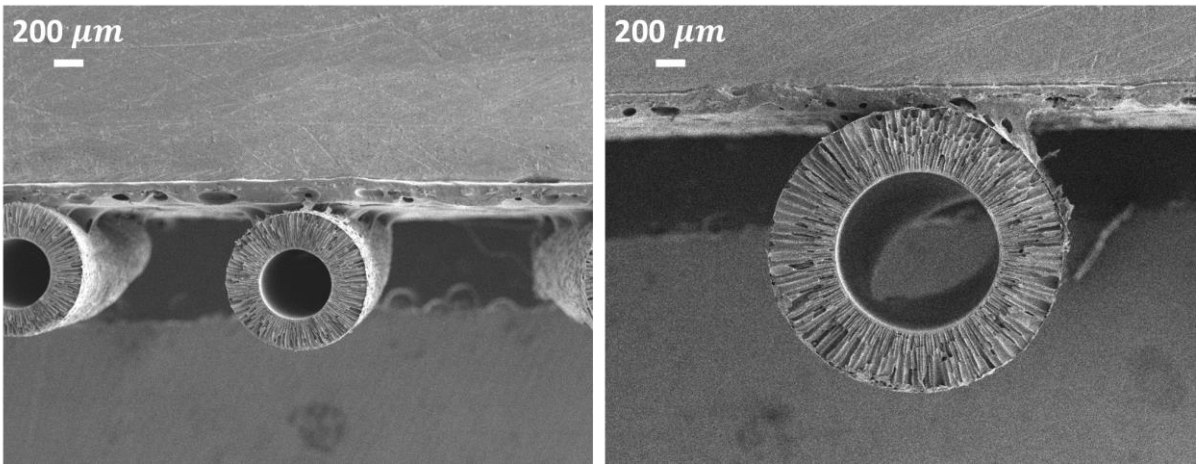

Figure 7.3. Cross-sectional FESEM images of KMS hollow fiber membranes at 30×. Left: HFM-A. Right: HFM-B.

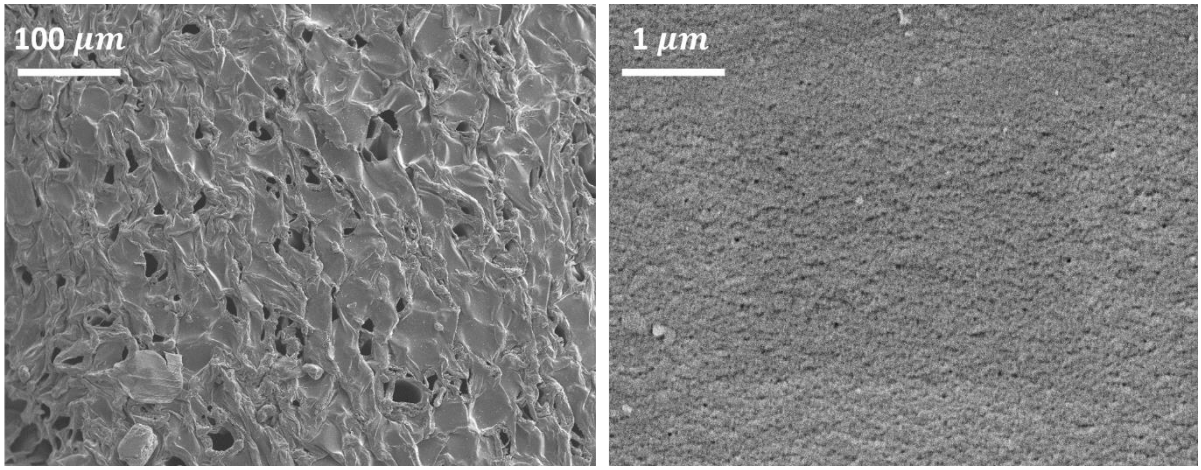

Figure 7.4. FESEM images of outer and inner surfaces of HFM-A. Left: outer surface at 200×. Right: inner surface at 20,000×.

7.3.2 Osmotic flux performance of hollow fiber membranes

In the osmotic flux tests, NaCl was used as the draw solute, and DI water was used as the feed. The water and reverse salt flux are depicted in Figure 7.5. As has been noted in most studies on FO, higher draw solution concentration yielded higher water fluxes with a maximum J_w of 20 LMH measured at 1.5M draw solution concentration in the PRO mode. While this flux does not match the highest performing hollow fiber and flat sheet membranes in the literature, the performance is impressive given that a larger scale module was used and the membrane supports are not specifically designed or modified for use in FO [31, 112].

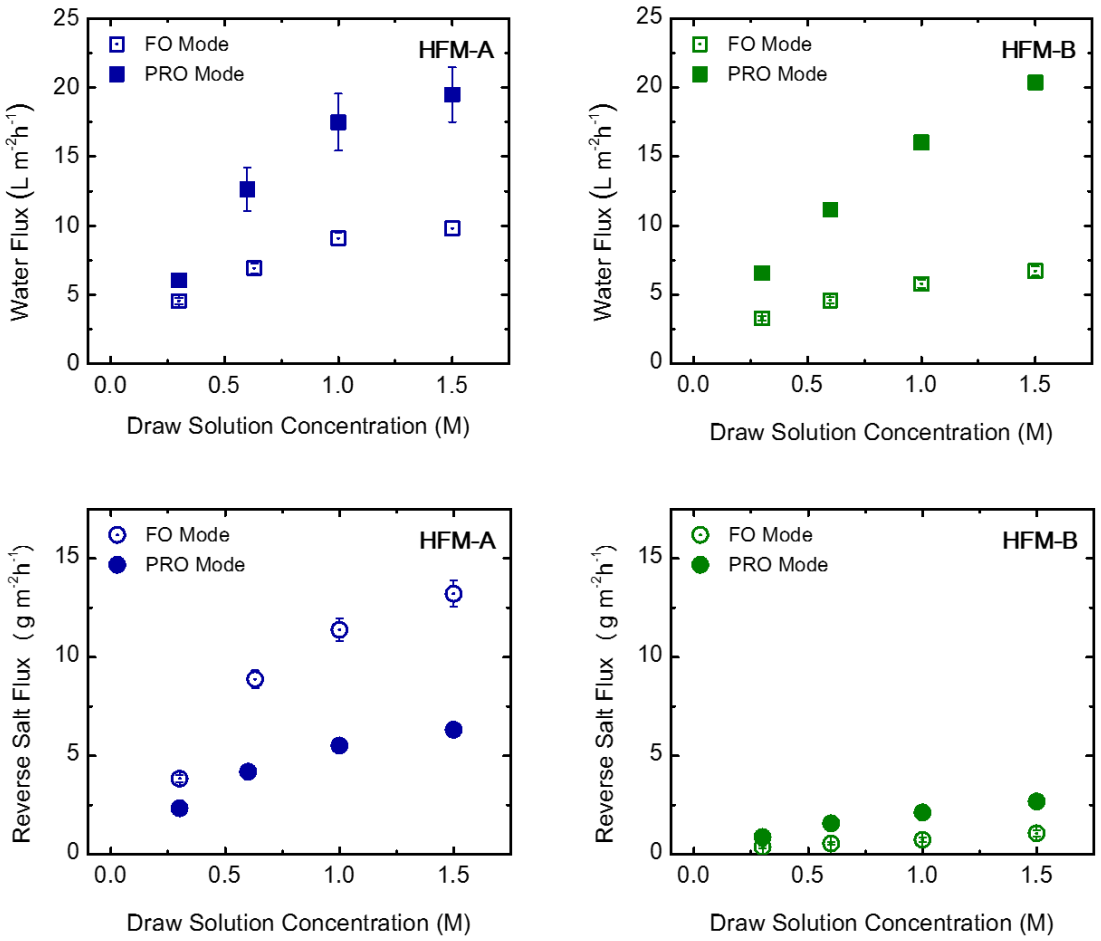

Figure 7.5. Water and reverse salt flux in FO and PRO modes of hollow fiber membrane modules with various draw solution concentrations. Operating conditions: NaCl draw solution, DI water feed, 20 ℃ feed and draw temperature, 0 transmembrane hydraulic pressure, counter-current flow arrangement, Reynolds number 160 for HFM-A and 480 for HFM-B.

The HFM-A membranes showed slightly higher J_w than HFM-B in both FO and PRO modes. This is a result of a reduced ICP due to a thinner wall (~220 μm compared to ~400 μm). It was interesting to note, however, that even though the thickness of the HFM-A membrane walls was about half of HFM-B, the HFM-A water flux was just marginally higher.

This is partially explained when comparing the reverse salt flux of the two membranes. HFM-A exhibited significantly higher J_s compared to the HFM-B. Higher reverse salt flux

causes the feed solution to increase in concentration and loss of driving force along the module. This would have substantial impact on the module averaged water flux, especially in the FO mode where the small-volume lumen feed would be susceptible to large changes in concentration. While in the PRO mode, the concentration change in shell feed would be less, but a high J_s would result in more severe ICP and hence reduce water flux [132].

High J_s of the HFM-A is attributed to the difficulty in forming the selective layer on the lumen of a large amount of smaller fibers. The same procedures and conditions were used to form the polyamide layer in both modules, but the pressure drop along the membrane is substantially higher in the smaller fibers (~ 2 psi in HFM-A while ~ 0.5 psi in HFM-B) [227]. Such pressure drop in the solution flows may impact the formation of polyamide and result in loose cross-linked polyamide towards the outlet of the module [102]. Meanwhile, HFM-A was densely packed with 300 fibers, and having air to flow through each of the 300 small fibers is challenging, as preferential flow through open fibers may exclude others from complete removal of residual reactant. Lack of complete fluid removal could cause an irregular surface or even defects in some fiber lumens [102]. While none of these defects is bad enough to cause complete breakthrough of the NaCl draw solute (no evidence in the data), it is possible that a few of the locations in the 300-fiber module may exhibit poor polyamide formation and cross linking which could lead to a measurable increase in solute flux.

Specific salt flux J_s/J_w is a metric that is used to determine the membrane selectivity defined as the amount of draw solute loss per unit of water passed [39]. It has been used to compare membrane performance when different membranes and/or draw solutes are used [180]. Lower J_s/J_w is generally desirable as it indicates that little salt is lost per unit of water permeated. Figure 7.6 shows that the specific salt flux results of HFM-A and HFM-B fibers. The HFM-B showed consistent low J_s/J_w of about 0.14 g/L regardless of the orientation of the membrane. This is expected given the osmotic flux performance and better polyamide layer

formed in the large HFM-B fibers. The HFM-A module, however, showed substantially higher J_s/J_w, especially in the FO mode. We attribute the higher specific salt flux to the likelihood of a poorly cross-linked selective layer caused by the reasons mentioned above. The significantly higher J_s/J_w in FO than PRO mode has been reported in some TFC hollow fiber FO membrane studies [31, 103, 109, 116]. It is likely that for loose selective membranes in PRO mode, the higher J_w could possibly help to prevent salt from back diffusing into feed and relief the reverse salt flux (a reverse coupling effect). Moreover, a the curvature of the fiber may play a role since salt flux into the smaller volume lumen in the FO mode may lead to higher J_s/J_w.

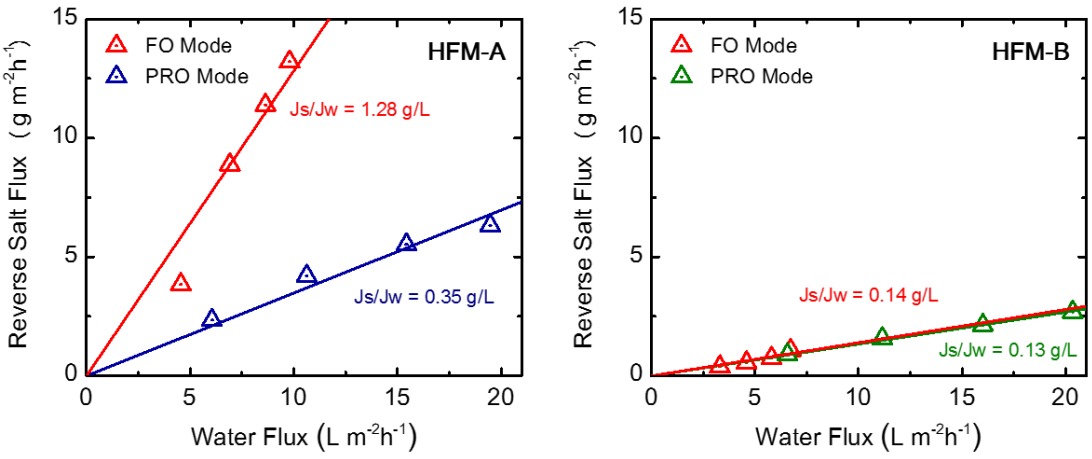

Figure 7.6. Specific reverse salt flux in FO and PRO modes of hollow fiber membrane modules. Operating conditions: NaCl draw solution, DI water feed, 20 ℃ feed and draw temperature, 0 transmembrane hydraulic pressure, counter-current flow arrangement, Reynolds number 160 for HFM-A and 480 for HFM-B.

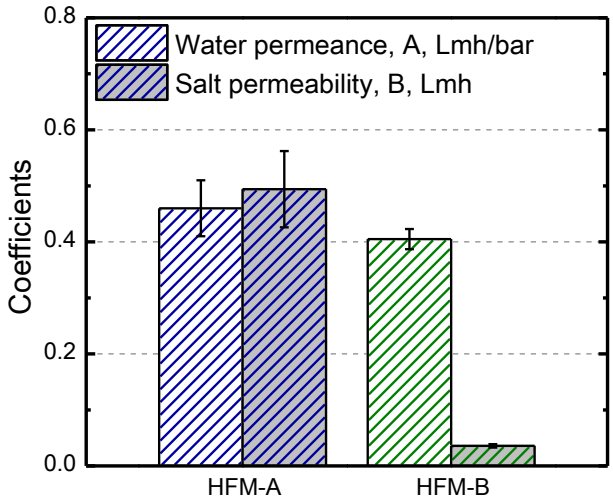

Figure 7.7. Water permeance (A) and salt permeability coefficient (B) for two modules. Values were evaluated by the empirical model developed by Tiraferri et al. [177].

Table 7.2. Selective and support layer properties

Membranes	A/B ratio (bar^{-1})	Structural parameter (μm)
HFM-A	0.93	539
HFM-B	11.31	651

The water permeance (A), salt permeability coefficient (B) and structural parameter (S) were evaluated using an empirical FO testing method proposed by Tiraferri et al. [177]. The A and B values of two modules are shown in Figure 7.7 while the A/B ratios and structural parameters were exhibited in Table 7.2. The two modules showed comparable A values of ~ 0.4 Lmh/bar. The B values revealed a higher salt permeability of HFM-A, which is consistent with osmotic flux results. The ratio of A/B, which is indicative of the permselectivity of the TFC membrane selective layer [39], was also calculated for both membrane modules. The HFM-A exhibited a relatively low A/B ratio of 0.93 while the HFM-B showed a high A/B ratio

of 11.31. Again, the lower permselectivity of HFM-A was due to the difficulty in the formation of a perfect polyamide selective layer in small fiber lumen. However, the HFM-B exhibited higher A/B ratio than commercial flat sheet FO membranes reported in literature thus demonstrated practical applications [32, 33]. The HFM-A showed a S value of 539 μm, which is lower than the HFM-B value of 651 μm. This is due to the substantially thinner supporting structure (~220 μm to ~400 μm). Both membranes showed relatively low S values (given their thicknesses) due to the open and non-tortuous pore structure. These results are also comparable to the S value of a commercial benchmark TFC flat sheet membranes from HTI [32]. These values are acceptable given that these membranes were not specifically designed or modified for use in FO.

It worth to note that FO technology is capable of treating challenging water with high salinity and fouling propensity due to the low hydraulic pressure used in the process. Though these two modules have relatively lower A values compared to most of lab-scale FO membranes from academic groups [29-31, 112], these A values are high enough to be suitable for the FO application with high salinity feeds. As suggested by Werber et al. [228], further increasing the water permeance for a membrane with structural parameter of 400-800 μm would not further improve the water flux in osmotic process when treating high salinity feeds. Therefore, both modules showed more than capable water permeance (A values) for the real world FO application.

7.3.3 Effect of cross-flow arrangement on water flux in FO tests

The osmotic water flux of the HFM-A and HFM-B TFC membrane modules under co-current and counter-current cross-flow arrangement are presented in Figure 7.8. Both the two modules demonstrated clearly that the J_w under counter-current mode was higher than that

under co-current mode. This result showed deviation from some experimental studies on both hollow fiber and flat sheet FO membranes, where the overall J_w was almost identical regardless of the flow arrangement [98, 229]. However, it worth to note that the modules tested in this study were much longer (18 inch) than those at bench scales (typically 3 to 6 inches). In fact, the experimental results in this study coincide well with previous modeling work at module scale (40 inch) [230]. In co-current mode, the J_w variation along the module is normally more evident as the draw solution dilutes and the feed solution concentrates along the module. In counter-current mode, J_w is relatively constant along the module. As a result, the overall J_w is lower in the co-current mode than that in counter-current mode.

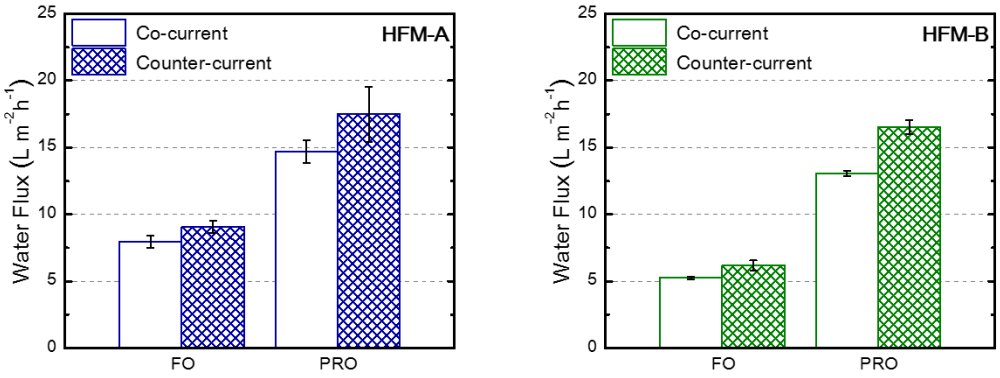

Figure 7.8. Water flux in FO and PRO modes of hollow fiber membrane modules with co-current and counter-current flow arrangements. Results are an average of two to three tests. Error bars indicate standard deviation. Operating conditions: 1 M NaCl draw, DI water feed, 20 ℃ feed and draw temperature, 0 transmembrane hydraulic pressure, Reynolds number 160 for HFM-A and 480 for HFM-B.

It was interesting to note that the difference between water flux under co- and counter-current mode was more severe in PRO mode. In FO mode, both modules showed ~15% less J_w in co-current than counter-current mode, while the difference was ~25% in PRO mode. The

PRO mode is more prone to these changes because the fluxes are higher and dilution/concentration effects are more prominent and thus lead to more substantial changes driving forces along the length of the module.

7.3.4 Effect of cross-flow velocity on water flux in FO tests

Osmotic flux tests were operated under various feed and draw cross flow rates in the counter-current mode to evaluate the effect of flow velocity on the overall FO performance. Two sets of cross flow rates representing lower cross-flow velocity (low CFV) and higher cross-flow velocity (high CFV) were used. Due to the difference in fiber size, the Reynolds numbers (Re) of the flows in two modules were different. For the HFM-A, low and high CFVs corresponded to Re of 80 and 160, respectively. For the HFM-B, low and high CFVs corresponded to Re of 240 and 480, respectively.

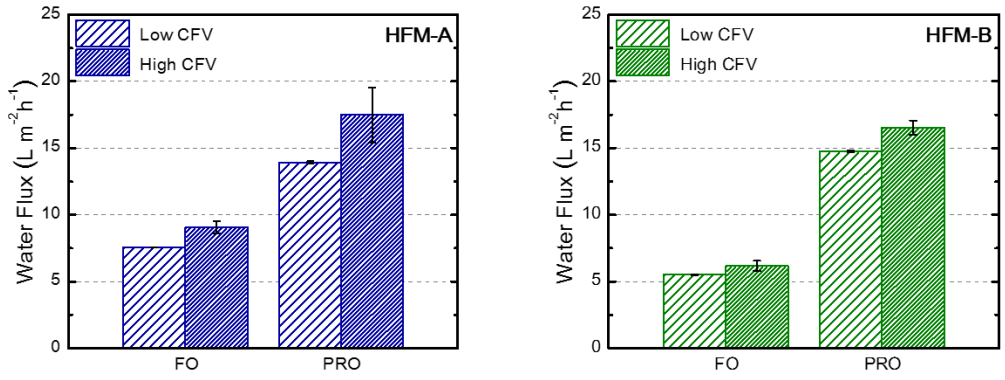

Figure 7.9. Water flux in FO and PRO modes of hollow fiber membrane modules with low and high cross flow velocities. HFM-A, Re 80 for low CFV, Re 160 for high CFV. HFM-B, Re 240 for low CFV, Re 480 for high CFV. Results are an average of two to three tests. Error bars indicate standard deviation. Operating conditions: 1 M NaCl draw, DI water feed, 20 ℃ feed and draw temperature, 0 transmembrane hydraulic pressure, counter-current flow arrangement.

Figure 7.9 presents the effect of cross-flow velocity on the water flux for the two types of modules in both FO and PRO modes. The results suggest moderately higher J_w at higher CFV in both modes for both modules. Higher crossflow velocity reduces external concentration polarization (ECP) on both sides of the fiber [29, 43]. Recent work also suggests that higher crossflow velocity along the porous support layer of a membrane may also reduce ICP as well due to induced mixing in the support layer [231]. Higher crossflow velocity also decreases the residence time of liquid in the module, meaning that dilution/concentration effects, which reduce driving force, are mitigated somewhat at higher CFV. This effect was more pronounced for the HFM-A because of the smaller dimensions of the fiber lumen which makes it more susceptible to dilution effects.

7.3.5 Comparison of overall module performance

Most membrane performance metrics are presented as area normalized fluxes. With modules, we are also able to summarize results using volume and module based normalization. Table 7.3 shows the osmotic flux performance of the two modules tested here, along with some commercial pilot scale FO elements in different configurations. These commercial FO elements include a semi-pilot scale TFC hollow fiber module from Samsung Cheil Industry [73], cellulose tri-acetate (CTA) based 4040 and 8040 spiral wound modules from HTI [136, 225], and TFC plate-and-frame module from Porifera [223].

In this comparison, packing density was defined by normalizing the effective membrane area by the module volume (m^2/m^3) [34]. The HFM-A module possessed the highest packing density of 778 m^2/m^3. This is more than twice of the other module configurations, demonstrating the benefit of high packing density of hollow fibers. The HFM-B module and its larger fibers exhibits lower parking density of 389 m^2/m^3. Though still higher than the spiral wound and plat-and-frame FO modules, it is on par with a semi-pilot TFC hollow fiber

module from Samsung Cheil Industry. However, considering that the HFM-A and HFM-B modules were just loosely packed (packing percentage 38.5% and 30.7%), there is substantial opportunity for improvement even if the same, non-optimized membranes are used.

Both HFM-A and HFM-B modules showed comparable area-normalized water flux ($J_w\ per\ m^2$) when compared with other membrane modules. However, the high packing density compensated a mediocre area-normalized water flux and resulted in good volume-normalized water flux. This packing density effect is especially noticeable when to compare the HFM-A to the plate-and-frame Gen 1 module from a patent filed by Porifera [223]. This Porifera module has one of the highest performance FO membranes available stacked in a plate-and-frame system and demonstrates high water flux of ~ 30 $Lm^{-2}h^{-1}$ in FO mode under 1M NaCl draw and DI feed, which is more than three times of the HFM-A membranes. But the two modules resulted in comparable overall module performance of ~ 7000 $Lm^{-3}h^{-1}$. Though higher salt flux was observed for the HFM-A module, one must to keep in mind that these modules had undergone no modification or optimization for use in FO.

Table 7.3. Performance parameters of the modules for FO process

Membrane	Membrane area (m^2)	Packing density (m^2/m^3)	Draw	Feed	Mode	Membrane water flux		Membrane salt flux		Ref.
						$per\ m^2$ ($Lm^{-2}h^{-1}$)	$per\ m^3$ ($Lm^{-3}h^{-1}$)	$per\ m^2$ ($gm^{-2}h^{-1}$)	$per\ m^3$ ($gm^{-3}h^{-1}$)	
HFM-A Hollow fiber	0.18	778	1 M NaCl	DI water	FO	9.08	7060	11.38	8848	This work
					PRO	17.49	13600	5.52	4290	
HFM-B Hollow fiber	0.09	389	1 M NaCl	DI water	FO	6.18	2400	0.75	292	This work
					PRO	16.54	6430	2.13	830	
Cheil Hollow fiber	1.00	453	1 M NaCl	Tap water	FO	12.00	5435	6.00	2718	[73]

HTI CTA 4040 MS Spiral wound	3.20	389	0.85 M NaCl	Tap water	FO	10.9	4237	N/A	N/A	[136]
HTI CTA 8040 CS Spiral wound	9.00	274	0.85 M NaCl	Pretreated tap water	FO	4.00	1095	N/A	N/A	[225]
HTI CTA 8040 MS Spiral wound	11.2	340	0.85 M NaCl	Pretreated tap water	FO	6.00	2043	N/A	N/A	[225]
Porifera's Gen 1 TFC plate-and-frame	7.00	233	0.94 M NaCl	DI water	FO	30.00	7000	12.00	2800	[223] *

* Data source from a patent filed by Porifera, Inc.

7.4. Conclusions

In this study, commercial hollow fiber ultrafiltration modules were used as a platform to make TFC hollow fiber FO membranes. Polyamide selective layers were formed *within the module* using a facile approach that employed conventional membrane chemistries. This approach, though having been done for lab-scale modules, had never been done at this scale. The results demonstrate that TFC hollow fiber FO membranes with reasonable performance can be produced at scale with relative ease using off-the-shelf UF modules. Further improvements could be realized if such a commercially produced module could incorporate fibers with a tailored support designed specifically for FO applications. Even without a tailored membrane, this study demonstrates that module-scale FO testing is possible in an academic laboratory without needing to resort to costly and difficult fiber spinning. Easy access to modules may enable continuation of the work on module- and volume- normalized

performance metrics that may become more important to industry in the coming years as new FO applications emerge into the marketplace.

Chapter 8. Developing Computational Fluid Dynamics Model to Optimize Design Parameters for Hollow Fiber Membranes and Modules for Forward Osmosis

To be published as

Ren, J., Ma, C., Chowdhury, M.R., Xia, L., Bollas, G.M., McCutcheon, J.R., "Developing Computational Fluid Dynamics Model to Optimize Design Parameters for Hollow Fiber Membranes and Modules for Forward Osmosis".

8.1 Introduction

The field of forward osmosis (FO) has been an academically active field for the past 10 years. Since a seminal paper on the subject in 2005 [17], hundreds of papers have been published on FO in numerous refereed journals. Motivated by applications in water reuse, desalination and power production (pressure retarded osmosis), a bevy of research on new membrane materials and structures [25, 26, 29, 52, 91-93], designer draw solutions [62, 232-234], transport modeling [43, 132, 177, 180, 235-237], and thermodynamics [230, 238, 239] have emerged.

A majority of the research published on FO during the past decade has focused on elucidating structure-performance relationships across asymmetric membranes and developing

new membranes that exploit those relationships. Much of the membrane development work focused on novel materials or structures [25, 26, 29, 52-57]. These membranes, while performing well in the lab, have not translated well to the commercial applications. Barriers to commercialization are rooted in the fact that "academic" membranes are often made using unconventional methods or with new materials. Risk averse companies are less likely to bring an unconventional membrane to market as they may be difficult to fabricate or place into modules. Companies, therefore, are likely to fall back on conventional membrane fabrication approaches (similar to those used to make reverse osmosis (RO) membranes) and module designs (such as spiral wound elements) [94, 95, 240].

FO companies like Oasys Water [33, 94], Fluid Technology Solutions (FTS, formerly Hydration Technology Innovations, HTI) [32], Toray [95] and Porifera [96] developed their own proprietary thin film composite (TFC) membranes that were largely based on conventional RO TFC membranes. The support layers of these membranes were simply altered to make them thinner, more porous, and hydrophilic in order to lessen internal concentration polarization [111, 132]. Interestingly, a vast majority of the commercial and academic work on FO has been limited to flat sheet membranes. This is largely driven by the fact that the development of FO membranes were initially based on the modifications of RO membranes, which were dominantly flat sheet configuration [17].

However, hollow fiber and capillary membranes can offer dramatic benefits in packing density over flat sheet elements. This has made hollow fibers a preferred geometry for membrane contactor applications (dialysis, gas-liquid contactors) [34]. Since osmosis is in some ways another contactor application with mass transfer between two streams, it would seem that such a configuration would be preferred in FO. Those who have developed custom hollow fiber FO membranes have made that argument as well [29, 30, 54, 114]. Academic groups in Singapore have developed TFC hollow fiber membranes for FO with high

performance [29-31, 103, 112, 114, 116]. Again, these membranes performed well in the lab but have not been translated to the commercial applications. Toyobo offers a full scale hollow fiber module, but the membrane is based on asymmetric cellulose acetate platform known with moderate performance and hydrolysis issue [97]. Samsung Cheil Industries does claim to have a semi-pilot TFC hollow fiber module, but it is unclear if a product is available [73, 98]. Aquaporin A/S in Denmark is advertising a TFC hollow fiber FO membrane that incorporates biological proteins into its structure, though this is a relatively new product and not much is known.

Looking at the jungled picture of FO, companies like Oasys, FTS, Porifera, Toray, Toyobo, and Aquaporin all claim to have game-changing FO technology, yet no one can agree on something as simple as the type of membrane or element to use. That makes the field seem as though it has not found its way to an optimum position. While some of this lack of agreement can be attributed to the fact that FO covers a wide swath of separations (desalination, brine concentration, food, dewatering, reuse), much of the problem exists because the field lacks tools to optimize both membrane and element configurations for different osmotic processes.

To bridge the gap between academic laboratories and the commercial sector, a comprehensive understanding of how new membranes can impact performance at the module/element level is needed. Since the experimental would be costly and time-consuming, a good way to do this is via computational modeling. In this study, we developed a *comprehensive* and *experimentally verified* computational fluid dynamics model that established relationships between both membrane properties and module design and overall performance (water flux and draw solute flux). Such a model would enable proper design of a module based on numerous factors that apply to the entire spectrum of forward osmosis.

While three basic module platforms are available (plate and frame, spiral wound, and hollow fiber), the focus of this study was hollow fiber modules. Hollow fiber modules were

selected for a number of reasons. First, their packing density benefits for numerous membrane applications are well documented [34]. Second, for experimental verification of our model, hollow fibers modules are easy to prototype in an academic lab. This is possible by applying a selective polyamide layer via interfacial polymerization to the lumen of a supporting fiber after it is already in the module. Lastly, commercial hollow fiber ultrafiltration membranes could be used as the supporting fibers for verification of the model at different module scales which would not be possible through academic lab fabrication techniques [241]. With membrane properties and module parameters that collected in academic laboratories, the osmotic flux performance would be simulated and evaluated at module scale. Such a model will serve as an important tool to guide research for membrane and module development. To benefit the scientific and industrial community, the model is released as an open source application through the supporting information.

8.2 Model development

A CFD model was developed for hollow fiber membrane process for FO. To simplify the model as well as to line up with the experimental verifications, we considered lumen-selective hollow fiber membranes in osmotic process using sodium chloride (NaCl) as draw solution. Though the modeling renders flexibility of changing such settings.

8.2.1 Model geometry

A simplified CFD model is created to predict concentration and velocity profiles in a hollow fiber module by only considering a single fiber. We assume that the fibers in the module were uniformly distributed and packed within a circular tube. As shown in Figure 8.1, the cross section of the module would be divided into hexagon elements with a single fiber in it. This

single fiber can be modeled using a circular approximation that describes the fluid inside fiber lumen, the membrane itself (inclusive of the support and selective layers), and the fluid surrounding the fiber. The dimensions of such unit cell can be determined from the actual fiber dimensions (inner radius (r_1), outer radius (r_2)) and fiber spacing (cell radius (r_3)). The inner and outer radii are easily measured on membranes while the cell radius is determined by the fiber packing density:

$$r_3 = N^{-0.5} \cdot R \quad (8.1)$$

Where N is the packing number and R is the inner radius of module.

Due to the axis-symmetric nature of the hollow fibers, the model can be simplified to a 2D representation with three domains (lumen channel, membrane support, shell channel) and one interface boundary (selective layer). The development of the model geometry is illustrated in Figure 8.1. As shown, a lumen selective layer is considered, though this is easily changed for shell selective layers if desired.

When building the model, we also considered a number of assumptions:

1. Incompressible, laminar flow in the lumen and shell channels;
2. Homogeneous, isotropic pore structure in the membrane support; and

3. Steady state condition

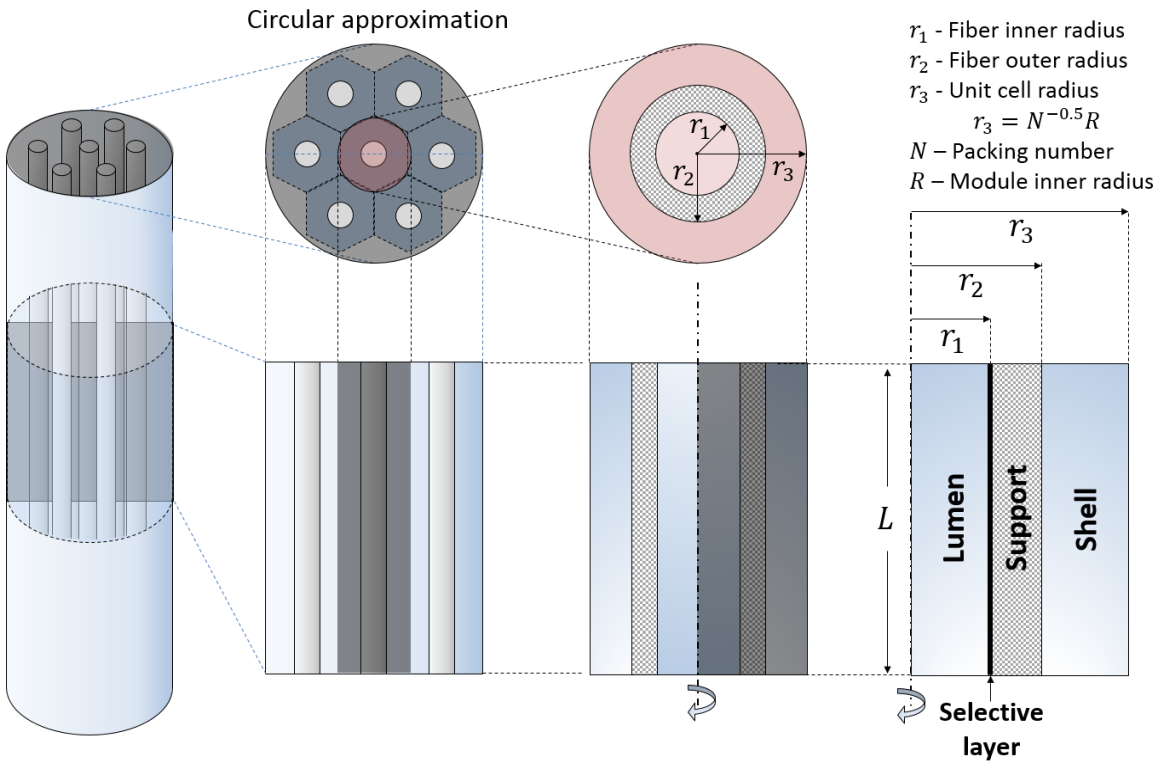

Figure 8.1. Illustration of model domains and dimensions. Please note the picture is best viewed in color.

8.2.2 Parameters and variables

The parameters and variables were divided into three major categories: solution properties, membrane properties, and operational variables. To accurately simulate the osmotic process in hollow fiber modules, all the parameters and variables that used in the model need to be carefully accounted.

8.2.2.1 Solution properties

A number of solution properties of NaCl solution are summarized in Table 8.1. All these parameters are dependent on the solution concentration and temperature. In most simulations, temperature was considered as constant throughout the model (in this work, 20 ℃ was used).

The solution concentration was considered as an operational variable in model. Thus in the model, solution concentration only reflects the local concentration and varies throughout the model.

Symbol	Parameter	Expression	Unit
ρ	Density	$\rho = (-1.55c^2 + 45.5c + 1123.3) \times \exp(-0.004T)$	kg/m^3
μ	Dynamic viscosity	$\mu = 0.4599 \times \exp(0.10495c) \times \exp(-0.021T)$	$Pa \cdot s$
D	Diffusivity	$D = (0.000182c^5 - 0.00172c^4 - 0.00142c^3 + 0.0497c^2 - 0.0987c + 1.0263) \times 9.32 \times 10^{-9}\exp(-2.63 \times 10^9/T^{3.7})$	m^2/s
π	Osmotic pressure	Fit to Pitzer's model: $\pi = (9.5508c^2 + 32.895c + 0.5081) \times 10^5$	Pa

Table 8.1. Summary of solution properties.

8.2.2.2 Membrane performance and properties

Osmotic water flux and reverse salt flux through TFC hollow fiber membranes was measured using a custom lab-scale cross-flow forward osmosis system shown in Figure 8.2. This system has been used in our previous investigations on hollow fiber membranes [101, 241]. Osmotic flux tests were carried out with the hollow fiber module oriented in both FO mode (the membrane selective layer oriented toward the feed solution, *i.e.* the feed in the lumen) and PRO mode (the membrane selective layer oriented toward the draw solution, *i.e.* the draw in the lumen). NaCl was used in the draw solution that varies from 0.1M to 5M to capture the entire range of osmotic performance (as well as to maximize and minimize dilution of the draw solution). Temperature was typically kept at 20 ± 0.5℃. Transmembrane hydraulic pressure was monitored for all tests and kept as close to zero as possible using back pressure valves on the system.

Three primary measurements were made. First, the area normalized osmotic water flux, J_w, was calculated by dividing the volumetric flux by the membrane area. Reverse solute flux, J_s,

was measured by monitoring the conductivity of the feed solutions during the tests (for DI water feeds) and correlating that to a salt flux (also area normalized). These two fluxes can be used to calculate the structural parameter (S), which is a support layer property for FO membranes. The S value is commonly defined in FO as the product of the thickness (t) and tortuosity (τ), divided by the porosity (ε). It is an indicator of the severity of the mass transfer resistance within the supporting structure of the membrane (internal concentration polarization, ICP) [43, 132]. The S value can be determined using Equation 8.2 and 8.3 using an Excel-based method developed by Tiraferri et al. and released through his publication [177],

$$J_w = A\left\{\frac{\pi_D \exp\left(-\frac{J_w S}{D}\right) - \pi_F \exp\left(\frac{J_w}{k}\right)}{1+\frac{B}{J_w}\left[\exp\left(\frac{J_w}{k}\right) - \exp\left(-\frac{J_w S}{D}\right)\right]}\right\} \quad (8.2)$$

$$J_s = B\left\{\frac{c_D \exp(-\frac{J_w S}{D}) - c_F \exp(\frac{J_w}{k})}{1+\frac{B}{J_w}\left[\exp(\frac{J_w}{k}) - \exp(-\frac{J_w S}{D})\right]}\right\} \quad (8.3)$$

In these equations, the water flux (J_w) and the salt flux (J_s) are directly measured. The concentrations of the draw (c_D) and feed solutions (c_F) are known. The mass transfer coefficient (*k)* can be calculated from the Sherwood Number correlations for both sides of the membrane. Diffusivity (*D*) and osmotic pressures of the feed (π_F) and draw (π_D) can be determined using equations in Table 8.1. This leaves the structural parameter (*S*), water permeance (*A*), and salt permeability (*B)* as the only unknowns. The method divides the FO experiment into a discrete number of stages, which requires four water and salt flux measurements to be carried out with four different draw solution concentrations with a DI water feed. Once all four data points are captured, the model allows the user to input the other known values, and then solves for the three unknown parameters to fit the data simultaneously.

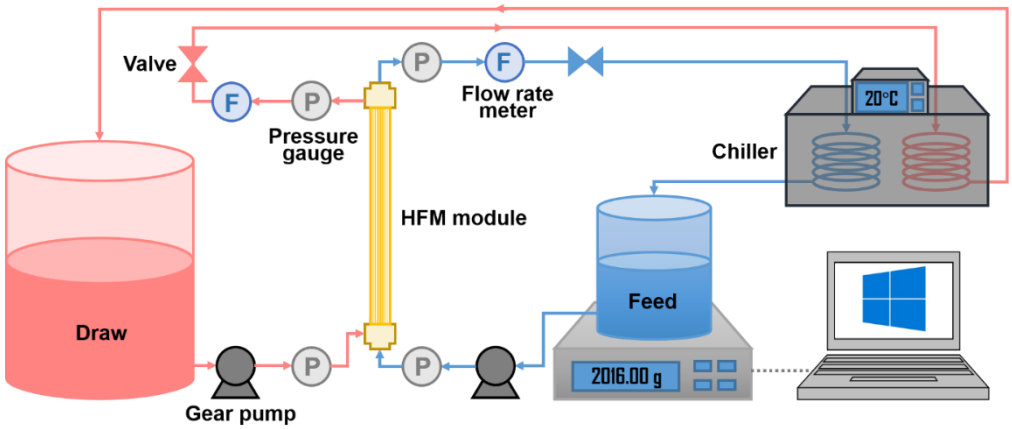

Figure 8.2. Schematic diagram of FO testing apparatus for hollow fiber modules.

These intrinsic properties, along with the support layer permeability (κ), were determined from experimental measurements as shown in Table 8.2. Selective layer pure water permeance (A), salt permeability (B) and support layer structural parameter (S) were determined from the forward osmosis test described above. Wall thickness of the hollow fibers (t) were obtained based on physical measurements at five different locations for each membrane sample using a coolant proof digital micrometer (IP65-MX, Mitutoyo, IL). The hollow fiber support bulk porosity (ε) was determined using gravimetric measurements at room temperature [29, 56, 101]. Support layer pore tortuosity (τ) was calculated from the S value obtained from forward osmosis test:

$$S = \frac{t\tau}{\varepsilon} \qquad (8.4)$$

Pure water permeability of the support layer (κ), was determined by conducting ultrafiltration tests of the supporting hollow fiber membranes [185, 187].

Properties		Determination	Unit
Selective layer properties	A	Forward osmosis test	$m/s/Pa$
	B		m/s
Support layer properties	S	Forward osmosis test	m
	t	Physical measurement	m

ε	Gravimetric measurement	%
τ	Forward osmosis test Effective diffusion coefficient	N/A
κ	Pure water permeability	m^2

Table 8.2. Summary of determinations of membrane properties.

8.2.2.3 Operational variables.

A number of operational variables are used in the model, including the lumen/shell inlet and outlet flow velocities (v_{lumen} and v_{shell}), feed and draw inlet concentration (c_{feed} and c_{draw}), and lumen and shell channel inlet and outlet pressure ($p_{lumen,\ in/outlet}$ and $p_{shell,\ in/outlet}$).

8.2.3 Governing equations and boundary conditions

The model incorporated governing equations and boundary conditions that applied to the different domains and boundaries of the axisymmetric system. These governing equations are available in COMSOL Multiphysics to define the types of transport in different domains of the system [242].

8.2.3.1 Momentum transfer equations.

In the lumen and shell. Navier-Stokes equations was used to describe the steady state flow in the open lumen/shell channels [243].

$$\rho(\boldsymbol{u}\cdot\nabla)\boldsymbol{u} = \nabla\cdot[-p\boldsymbol{I} + \mu(\nabla\boldsymbol{u} + (\nabla\boldsymbol{u})^T)], \qquad \nabla\cdot\boldsymbol{u} = 0 \qquad (8.5)$$

Where density (ρ) and dynamic viscosity (μ) are solution properties; pressure (p), and 2D

velocity vector $\boldsymbol{u}=(u,v)$ are operational variables inclusive of velocity in the axis direction (v) and perpendicular to the axis direction (u); $\boldsymbol{I}$ is a unit matrix; superscript T indicates transpose of matrix [242].

In membrane support. Brinkman equations was used to govern the incompressible flow of solution in the porous support.

$$0 = \nabla \cdot \left[-p\boldsymbol{I} + \frac{\mu}{\varepsilon}(\nabla \boldsymbol{u} + (\nabla \boldsymbol{u})^T)\right] - \frac{\mu}{\kappa}\boldsymbol{u}, \qquad \nabla \cdot \boldsymbol{u} = 0 \qquad (8.6)$$

Where porosity of support (ε), permeability of the support (κ) are membrane properties. Here we assume homogenous pore structure thus used isotropic porous material setting.

8.2.3.2 Mass transfer equations.

In the lumen and shell. The mass transfer of solute in both feed and draw solution channels are composed of convection and diffusion [243]. The governing convection and diffusion equation is:

$$\nabla \cdot (D\nabla c) = u \cdot \nabla c \qquad (8.7)$$

Where diffusion coefficient (D) is dependent on concentration (c) at a certain temperature. The dependency of D on c will be discussed in Section 2.3.

In membrane support. The mass transfer of solute in the porous support is also composed of convection and diffusion.

$$\nabla \cdot \left(\frac{\varepsilon}{\tau} D\nabla c\right) = u \cdot \nabla c \qquad (8.8)$$

Where porosity of support (ε) and tortuosity of the support (τ) are membrane properties.

8.2.3.3 Osmosis governing equations.

Osmotic water and reverse salt flux through TFC hollow fiber membranes were studied in both FO mode (the selective layer faces the feed solution) and PRO mode (the selective layer

faces the draw solution). The osmotic water flux, J_w, across the selective layer was determined by the following equations:

FO mode: $J_w = A(\pi_{p,m} - \pi_{f,m})$ PRO mode: $J_w = A(\pi_{d,m} - \pi_{p,m})$ (8.9)

Similarly, reverse salt flux, J_s, was also given by:

FO mode: $J_s = B(c_{p,m} - c_{f,m})$ PRO mode: $J_s = B(c_{d,m} - c_{p,m})$ (8.10)

Where water permeance A, and salt permeability B are membrane properties. Osmotic pressure (π) and concentration (c) are both solution properties. Subscript p, f, and d indicate porous support, feed and draw, respectively. Subscript m indicates the property at membrane surface.

8.2.3.4 Boundary conditions

Boundary conditions were set for all three domains (lumen flow channel, membrane porous support, and shell flow channel). Figure 8.3 shows the illustration of 2D model boundary conditions and boundary components at the selective layer interface in FO mode. A detailed boundary condition setting is tabulated in Table 8.3. The boundary conditions would be altered with the orientation of the membranes (FO or PRO mode). In all simulations, we used counter-current flow pattern. The boundary between domain m and d is considered as the interface of the porous support and shell flow channel, with continuous concentration profile at interface.

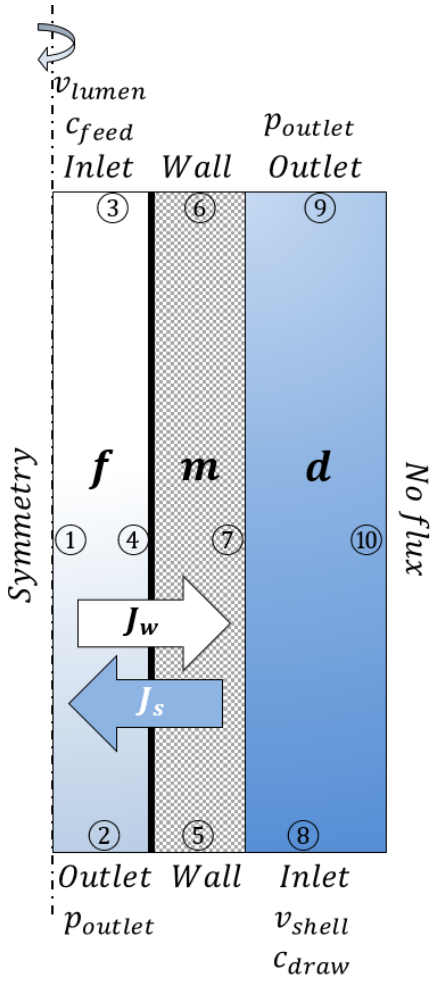

Figure 8.3. Illustration of model boundary conditions in FO mode

	FO mode		PRO mode	
Boundary	**Momentum**	**Mass**	**Momentum**	**Mass**
1	Symmetry	Symmetry	Symmetry	Symmetry
2	Outlet, p_{outlet}	Outflow	Outlet, p_{outlet}	Outflow
3	Inlet, v_{lumen}	Inflow, c_{feed}	Inlet, v_{lumen}	Inflow, c_{draw}
4	Left: outlet, J_w	Left: inward flux, J_s	Left: inlet, J_w	Left: outward flux, J_s
	Right: inlet, J_w	Right: outward flux, J_s	Right: outlet, J_w	Right: inward flux, J_s
5	No-slip wall	No flux	No-slip wall	No flux
6	No-slip wall	No flux	No-slip wall	No flux
7	Continuous interface	$c_{left} = c_{right}$	Continuous interface	$c_{left} = c_{right}$
8	Inlet, v_{shell}	Inflow, c_{draw}	Inlet, v_{draw}	Inflow, c_{feed}
9	Outlet, p_{outlet}	Outflow	Outlet, p_{outlet}	Outflow
10	Slip wall	No flux	Slip wall	No flux

Table 8.3. Summary of boundary conditions for FO and PRO modes.

8.2.4 Mesh geometry

A user-controlled mesh was built with COMSOL Multiphysics [242]. We used finer mesh size at the boundaries and selective layer to provide better resolution of velocity and concentration gradients. To create finer mesh at inlet/outlet boundaries, an arithmetic sequence with up to 25 element ratio (25 times finer at the inlet/outlet than the bulk) distribution was

used as the distribution method for the entire length of the domain. Similarly, to create finer mesh close to the selective layer, an arithmetic sequence with reverse distribution of 3 element ratio was used in the porous support, feed and draw channels. An estimated of 25000 element units would be appropriate for such simulation.

8.3 Experimental verification of model

8.3.1 Materials

A series of special grade commercial hollow fiber ultrafiltration membranes were provided by Koch Membrane Systems Inc. (KMS, Wilmington, MA). The hollow fiber UF membranes were made of polysulfone with different inner surface molecular weight cut-off (MWCO) of 10 kDa. The details of membrane structure and other characteristics are presented in Table 8.4.

Membranes	Fiber inner diameter (mm)	Wall thickness (mm)	Molecular weight cut-off (kDa)	Bulk porosity (%)
KMS	1.07 ± 0.03	0.41 ± 0.02	10	58.8 ± 0.8

Table 8.4. Characteristics of hollow fiber ultrafiltration membrane.

M-phenylene diamine (MPD, >99.0%) and 1, 3, 5-benzenetricarbonyl trichloride (trimesoyl chloride, TMC, 98.0%) were purchased from Sigma Aldrich (St. Louis, MO). *n*-hexane (HPLC, >98.5%), 2-propanol (isopropyl alcohol, IPA, >99.5%) and sodium chloride (NaCl, crystalline, >99.0%) were purchased from Fisher Scientific (Pittsburgh, PA). Deionized (DI) water was used throughout the study and obtained from a Milli-Q ultrapure water purification system (Millipore, Billerica, MA).

8.3.2 Synthesis of polyamide selective layer

The thin film polyamide selective layer was synthesized on the inner surface of hollow fiber membranes via *in-situ* interfacial polymerization (IP). The hollow fiber modules were prepared by potting fibers into clear PVC tubes using epoxy resin (Cytec Industries, Olean, NY). The hollow fiber membranes were loose fibers and PVC tubes were house machined thus the modules can be made at various lengths. The IP process was conducted at room temperature on the inner surface of hollow fiber membranes. 2.0% (wt/v) m-phenylene diamine (MPD) aqueous solution and 0.1% (wt/v) trimesoyl chloride (TMC) hexane solution were used to form an ultrathin polyamide film. Similar IP process has been reported in our previous studies [fourth paper].

8.3.3 Osmotic flux performance of TFC hollow fiber membranes

Osmotic water flux and reverse salt flux through TFC hollow fiber membranes were characterized using a lab-scale forward osmosis system described in Section 8.2.2.2. The system could be modified to accommodate higher volume of draw and feed solutions for long modules. The osmotic water flux, J_w, and reverse salt flux, J_s, were used as two performance metrics to be compared with the simulation results.

8.3.4 Model verification

The model accuracy was verified by experimental data generated from the osmotic flux tests based on two sets of easy to adjust independent variables. First, a pilot scale hollow fiber FO module with selective layer on the lumen surface was simulated and tested [241]. Osmotic water flux and reverse salt flux as two performance metrics were tested in FO tests under various conditions. DI water was used as feed solution while NaCl solution with various

concentrations were used as draw solution. The fiber module was tested in both FO and PRO modes. The experimental and simulation results are shown in Figure 8.4. As shown, both the water flux and reverse salt flux showed good agreement between the experimental data and modeling simulation which is indicative of a high accuracy of the developed model.

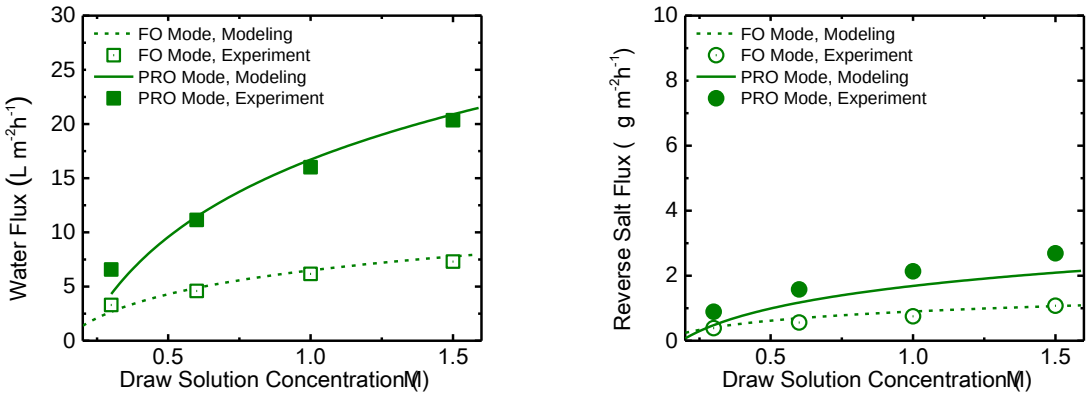

Figure 8.4. Experiment and modeling result of TFC hollow fiber FO module water flux and reverse salt flux at various draw concentrations. Lines are modeling results. Dots are data based on osmotic flux experiments. Operating conditions: NaCl draw solution, DI water feed, 20 ℃ feed and draw temperature, counter-current flow arrangement, Reynolds number 480.

The model was further verified with same testing condition yet various modules. A series of modules with same hollow fiber membranes were made into various length, ranging from ~ 7 cm to 457 cm. All fiber modules were tested and simulated individually and the results are shown in Figure 8.5. Though the water and reverse salt flux did not show significant variation as the module length varied from 7 cm to 457 cm, it worth the note that the overall water flux was relatively low (less than 10 and 20 LMH in FO and PRO mode, respectively), thus no significant dilution of the concentration or driving force variation along the module would be caused. Again, the modeling and experimental results showed good agreement. With the model

showing high accuracy, the further section will be focused on studying the effect of independent variables in the hollow fiber membrane design and operation.

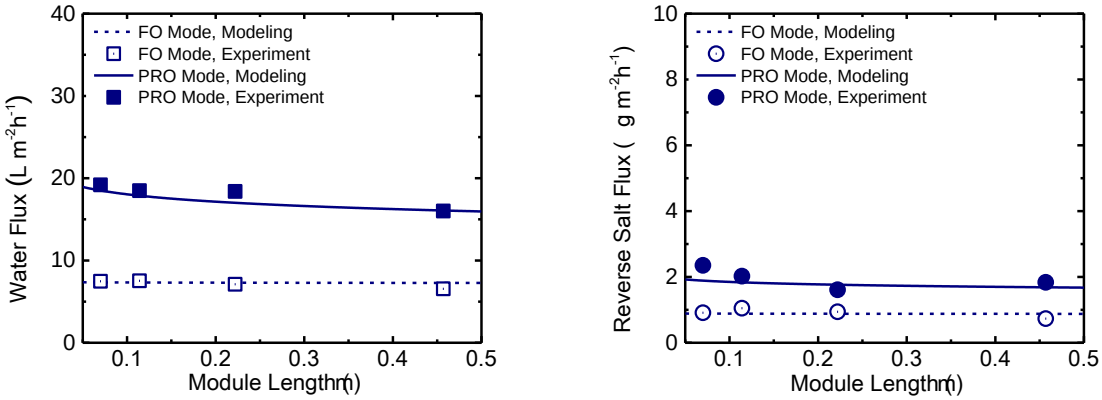

Figure 8.5. Experiment and modeling result of TFC hollow fiber FO module water flux and reverse salt flux at various module length. Lines are modeling results. Dots are data based on osmotic flux experiments. Operating conditions: 1 M NaCl draw solution, DI water feed, 20 ℃ feed and draw temperature, counter-current flow arrangement, Reynolds number 480.

8.4 Results and discussion

In this section, we conducted a series of simulations that would enable us to elucidate the membrane and module property-performance relationships. Understanding these relationships would quantify the interdependencies between membrane performance and module design in order to better match a particular type of membrane with an appropriately design module for a specific osmotic process.

The independent variables that can be studied in the model are listed in Table 8.5. These variables can be divided into membrane variables and module variables. Membrane variables include both selective layer and support layer properties. Selective layer properties are distinguished by traditional water permeance (A) and salt permeability (B) values. Support layer properties are governed by structural properties including porosity (ε), tortuosity (τ),

water permeability (κ) and support membrane dimensions (r, t). Module specific variables are distinguished by module design and operating variables. Design parameters include the module length (L), inner diameter (R), and packing number. Operating condition variables include flow velocities, inlet/outlet pressures in the lumen and shell channels, and the feed and draw concentrations. In this study, four independent variables (pure water permeance A, membrane thickness t, module length L, and draw concentration c_{draw}) were selected from each of the four categories to study their effects on the overall osmotic performance. The default values used in the modeling are also shown in Table 8.5. These default values are based on the typical membrane characteristics and operation parameters from literatures [177, 236, 244].

Parameters			Symbol	Value	Unit
Membrane Design	Selective layer properties	Pure water permeance	$\boldsymbol{A}$	1	$Lm\text{h}/bar$
		Salt permeability	$\boldsymbol{B}$	0.2	$Lm\text{h}$
	Support layer properties	Porosity	$\boldsymbol{\varepsilon}$	60	%
		Tortuosity	$\boldsymbol{\tau}$	1.2	N/A
		Pure water permeability	$\boldsymbol{\kappa}$	2×10^{-5}	m^2
		Fiber inner diameter	$\boldsymbol{r_1}$	5×10^{-4}	m
		Membrane thickness	$\boldsymbol{t}$	1×10^{-4}	m
Module Operations	Module design parameters	Module length	$\boldsymbol{L}$	0.5	m
		Module inner diameter	$\boldsymbol{R}$	0.025	m
		Fiber packing number	$\boldsymbol{N}$	60	N/A
	Module operating parameters	Lumen velocitiy	$\boldsymbol{v_{lumen}}$	0.25	m/s
		Shell velocity	$\boldsymbol{v_{shell}}$	0.25	m/s
		Lumen & shell outlet pressures	$\boldsymbol{p_{outlet}}$	0	Pa
		Feed concentration	$\boldsymbol{c_{feed}}$	0	mol/L
		Draw concentration	$\boldsymbol{c_{draw}}$	5	mol/L

Table 8.5. Summary of independent variables as hollow fiber FO membrane and module design and operation parameters.

8.4.1 Effect of selective layer pure water permeance

The effect of selective layer pure water permeance (A) was studied with values ranging from 0.5 to 2 LMH/bar. The 2D modeling results of NaCl concentration distribution in the membrane module domains are shown in Figure 8.6. The channel domains distribution is consistent with the domain illustration in Figure 8.3.

As shown in Figure 8.6, the A value plays a role as it impacts the concentration distribution in the channels and membrane support. The concentration gradient within the membrane support, which is more substantial in FO mode, is indicative of internal concentration polarization (ICP). It has been proved as the major mass transfer resistance in the osmotic process [43, 132] and can be illustratively seen in the 2D figures. Again, as shown in Figure 8.6, the ICP effect in the PRO mode is less severe due to the fact that DI water was used as the feed facing the support layer. However, we do see a thicker boundary layer formed when A value is high. This is due to the promoted water flux accompanied with the increase A value, which exacerbated the boundary layer formation in the flow channel, known as external concentration polarization (ECP) [132, 231]. Since same flow conditions were used for the simulations, the higher axial flow velocity (water flux) caused by the higher A value impaired the mixing at the lumen surface thus caused such inhabitation of driving force.

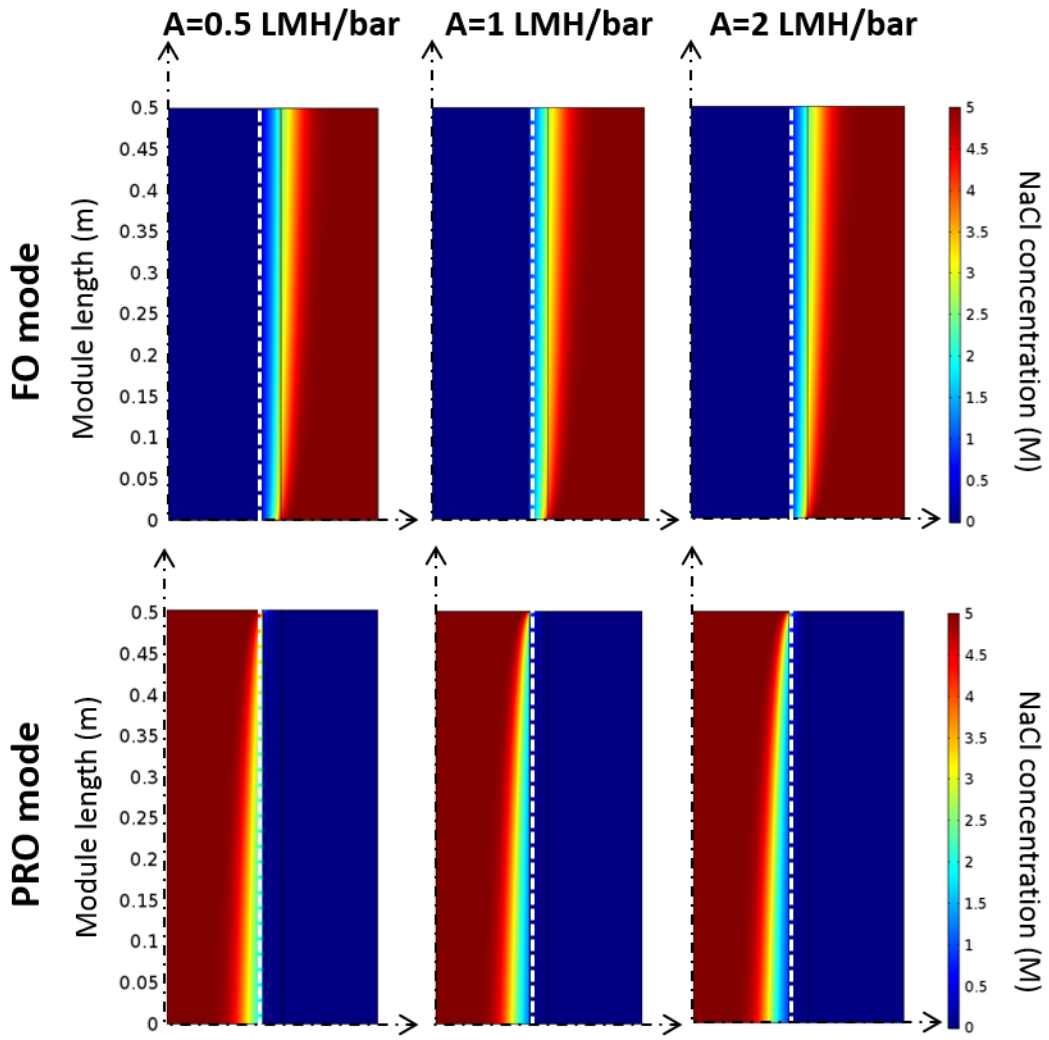

Figure 8.6. Two dimensional NaCl concentration distribution in 0.5 m long axisymmetric hollow fiber element with various A value in both FO and PRO modes. White dash line is indicative of selective layer, light black line is indicative of domain boundary and interfaces. Illustration figure is not drawn to scale.

To quantitatively study the impact of individual variables, the water flux variation as a function of position in the membrane module is studied and presented in Figure 8.7. As suggested by the simulation results, higher A value does promote the water flux in both FO and PRO modes. However, this flux enhancement was not linear due to its adverse impact on enhancing the concentration polarization in osmotic process. The water flux variation in PRO

mode is more obvious than that in FO mode, considerably due to the higher water flux generated as well as the more significant draw dilution effect when the draw flows in the lumen in PRO mode. Overall, the results suggest an improvement of osmotic flux performance with a higher A value which would be beneficial for most FO processes.

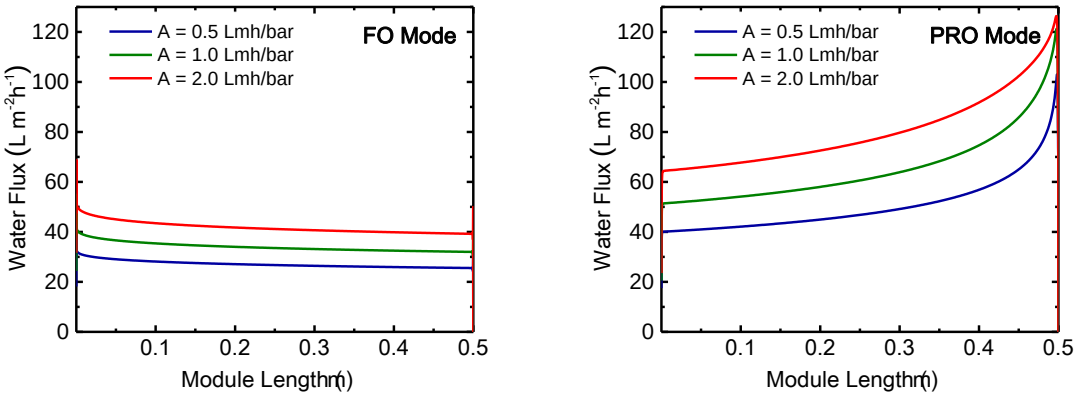

Figure 8.7. Modeling water flux variation along a 0.5 m membrane module with various pure water permeance (A) in counter-current flow pattern in FO and PRO modes.

8.4.2 Effect of support layer thickness

Figure 8.8 shows the 2D illustration of the NaCl concentration distribution in the three domains. Note that all the 2D illustrations were not drawn to scale, though the variation in the support layer thickness is demonstrated with increment in the axial scale in Figure 8.8. Clearly, a more significant concentration gradient in the supporting structure is observed with a thicker support layer thickness (persumbly 400 μm). This, with all other investigations of FO membrane design criteria, suggests that a thin supporting structure is beneficial for the FO process due to a reduced ICP effect [132, 231]. However, when we compared the linear water flux variation along the module as shown in Figure 8.9, it showed some interesting results.

The water flux along module did not show significant variation with the thick support layer

(400 μm), presumably due to the low water flux generated because of the severe ICP effect. Further reducing the support layer thickness, one observes the increase in the water flux, as well as the water flux variation, especially in PRO mode. The water flux decreased about 60% from the inlet to the outlet of the draw solution when t=100 μm, while that decrement was just about 30% when t=200 μm in the PRO mode. The overall water flux for the 100 μm membrane was about 62 LMH which is just marginally higher than that of 58 LMH of the 200 μm membrane module. Again, this is due to the initial higher water flux generated with the thinner support layer which greatly impaired the osmotic driving force across the membrane along the module [230]. This is an often overlooked effect because in lab scale testing we do not normally use a module as long as 0.5 m, and the water flux result reflects the overall J_w which could not give us insights to the variation of water flux along the module [230, 235, 236]. With the model, one would be able to visualize the substantial water flux variation along module. As the modeling result suggests here, reducing the support layer thickness by 50% only resulted in a 7% water flux enhancement when a moderate long (0.5 m) module was used. Such a result would induce some rational thoughts on whether it is worthwhile to delicately tailor the supporting structure to make it thinner though the difference would be negligible at a large scale. In addition, the modeling did not account for the possible mechanical concerns accompany with a thin supporting structure, though which should be kept in mind when designing a membrane for a particular osmotic process such as pressure retarded osmosis (PRO) [120, 122, 245].

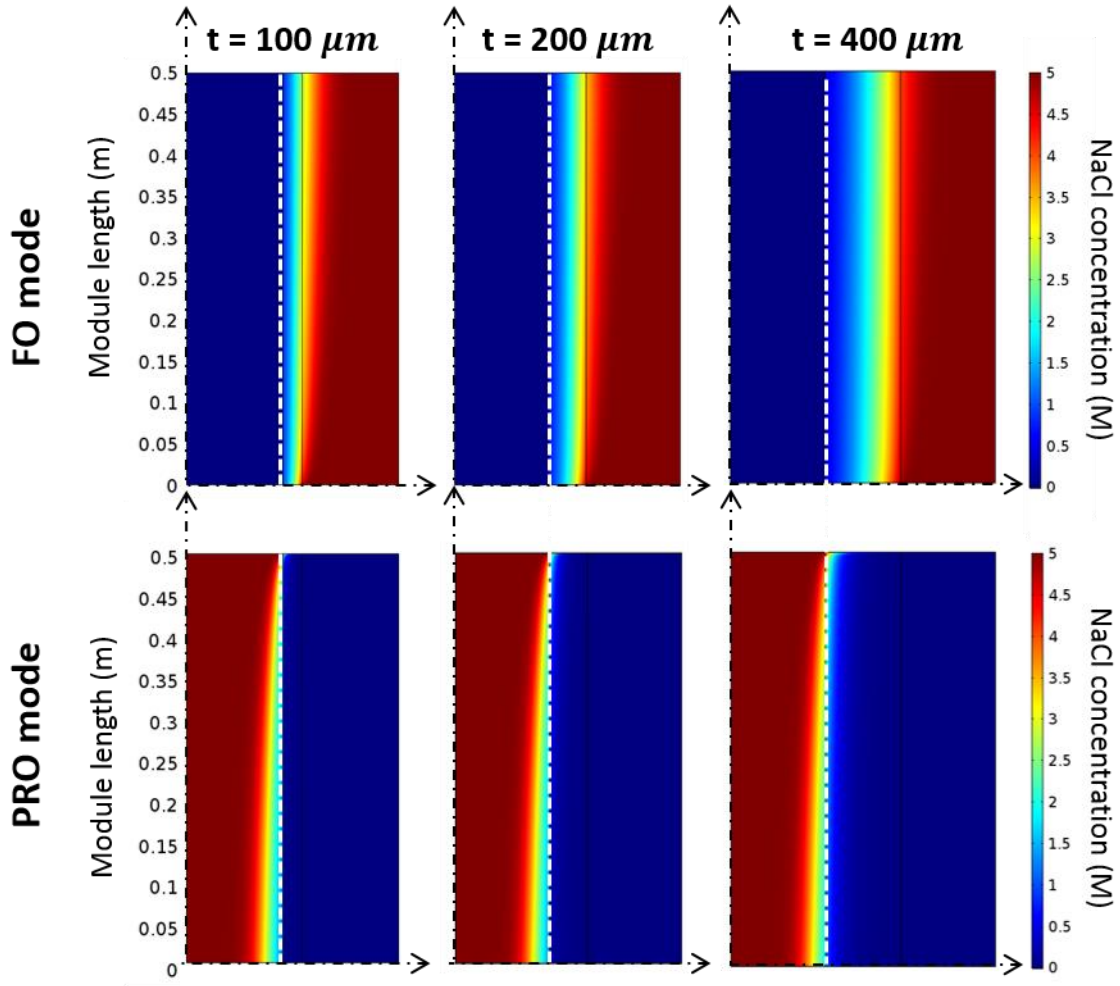

Figure 8.8. Two dimensional NaCl concentration distribution in 0.5 m long axisymmetric hollow fiber element with various t value in both FO and PRO modes. White dash line is indicative of selective layer, light black line is indicative of domain boundary and interfaces. Illustration figure is not drawn to scale.

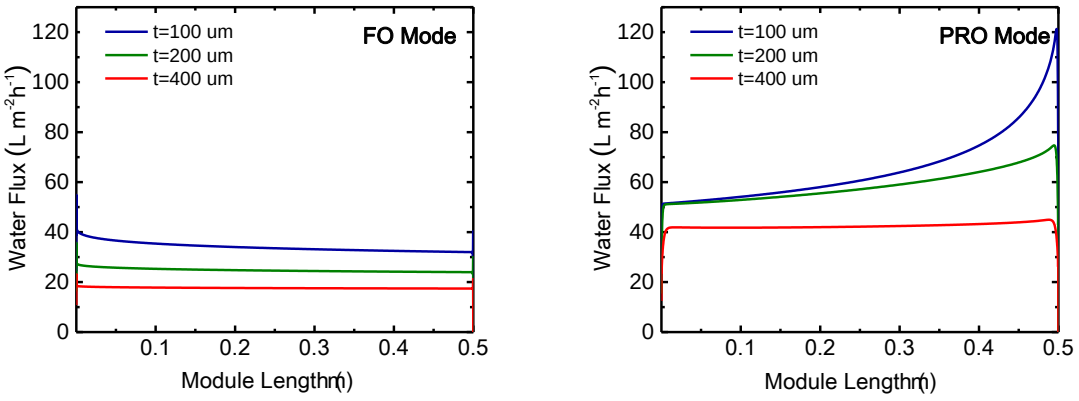

Figure 8.9. Modeling water flux variation along a 0.5 m membrane module with various support layer thickness (t) in counter-current flow pattern in FO and PRO modes.

8.4.3 Effect of module length

Along with studying the independent variables of membrane design, the model was also used to evaluate the impact of module design parameters, most notably, the module length (L). It has been believed that hollow fiber modules that designed for the mass/heat membrane contactor applications should be short instead of being long to reduce the driving force loss along the module and induce pressure drop along module [34]. In the model simulations, three different module lengths were studied ranging from 0.1 m, which is a typical lab scale, to 1 m, which is a typical industrial scale. The illustrative NaCl concentration distributions in the module at different lengths are shown in Figure 8.10. Again, the figures do not reflect the actual dimensions.

As shown in Figure 8.10, all cases demonstrated the ICP effect in the support layer, more obvious in FO mode. The boundary layers were formed most notably in the shell and lumen channel for FO and PRO mode, respectively. The water channel boundary layer was much thicker when longer module was used. This is due to the longer length which allowed the flow as well as the boundary layer to be well developed [243]. Again, such a boundary layer dramatically induced mass transfer resistance, especially in the longer module (1 m) thus inhibited the water flux.

Such module length effects on the water flux variation along the module is well presented in Figure 8.11. It is interesting to see that in these simulations, the module length effect on the water flux variation in FO mode was not very significant. This is presumably due to the low water flux (~ 30 LMH) that generated in the FO mode that would not cause significant driving force decline along module. But when in the PRO mode, the initial water flux at the draw

solution inlet could be as high as ~ 120 LMH under the modeling conditions. Such a high water flux would significantly induce severe CP effects, along with the loss of driving force and the draw solution dilution in the lumen with limited volume [230]. As a result, the water flux in the PRO mode showed significant variation along the module, especially in the long module (1 m), where the water flux decreased about 60% from the inlet to the outlet of the draw solution. Such results provide insights into how long the membrane module should be to maintain a reasonable high driving force across the membrane.

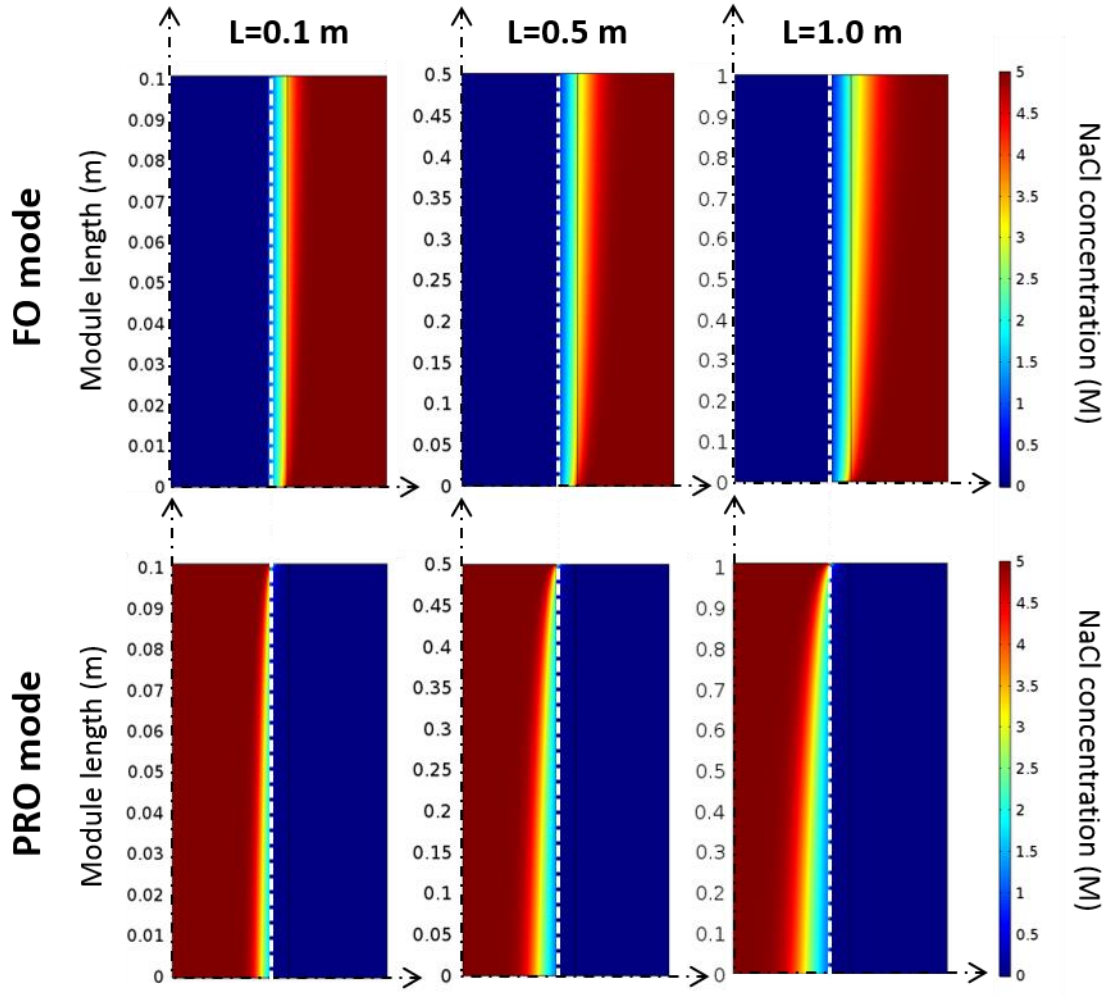

Figure 8.10. Two dimensional NaCl concentration distribution in axisymmetric hollow fiber element with various length (L) in both FO and PRO modes. White dash line is indicative of selective layer, light black line is indicative of domain boundary and interfaces. Illustration

figure is not drawn to scale.

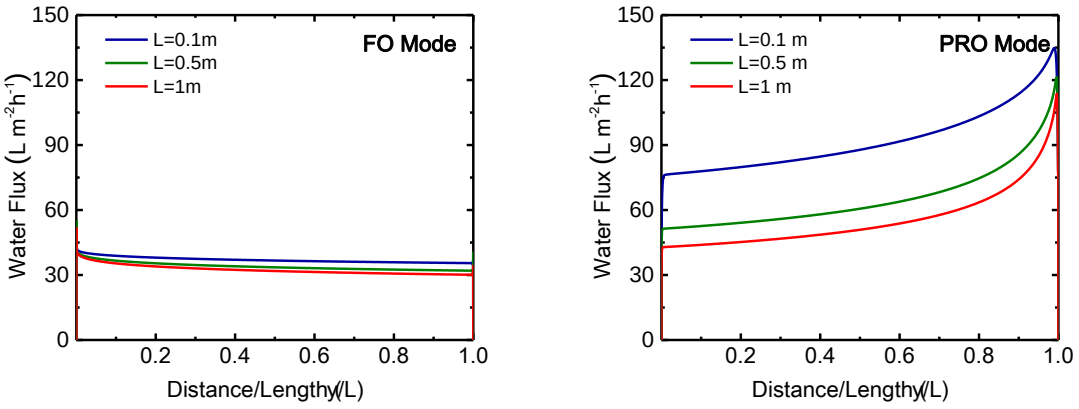

Figure 8.11. Modeling water flux variation along membrane modules with various length (L) in counter-current flow pattern in FO and PRO modes.

8.4.4 Effect of draw concentration

As an important operation parameter, the effect of the draw solution concentration (c_{draw}) was studied with ranging from 1 to 5 M NaCl solution. It is well understood that higher draw concentration would cause higher driving force thus higher water flux. However, as the draw solution recovery is challenging in the FO industry, it is still worthwhile to study such a parameter as to see whether a highly concentrated draw solution should be used to generate high osmotic performance despite the possible difficulties accompanied with the draw recovery.

As shown in Figure 8.12, the draw concentration distribution with various draw inlet concentrations were studied. Obviously, the concentration gradient is most notably along the membrane interface in support layer as ICP in FO mode and draw solution channel as ECP in PRO mode.

Figure 8.13 shows the water flux variation along membrane module that helps us to better interpret the performance. It seems that with increasing the draw concentration, the water flux

does increase due to the increase in driving force. But such effect was limited by the accompanied increment of mass transfer resistance. We do see that the water flux was almost doubled when we use tripled draw solution concentration from 1 M to 3 M. However, the water flux performance was just marginally improved when changing draw solution from 3 M NaCl to 5 M NaCl. Not to mention the significant water flux decline along with such a highly concentrated draw solution being used and the difficulties that one would encounter in the recovery of such highly concentrated draw solution.

This reminds us that a performance improvement by solely using high concentration draw solution may not be the key due to the fact that the osmotic process is always mass-transferly limited by the coupled effect of an increased water flux and a reduced osmotic driving force across membrane. On the other hand, this model simplified the problem by using NaCl as the draw solute, which is an ionic draw solute with high diffusivity and low solution viscosity. Draw solute like NaCl would allow readily diffusion and achieve better overall performance. Thus not to mention the other draw solutes that are polymer or larger molecule based, which would induce significant ECP effect and potential membrane fouling [232, 233].

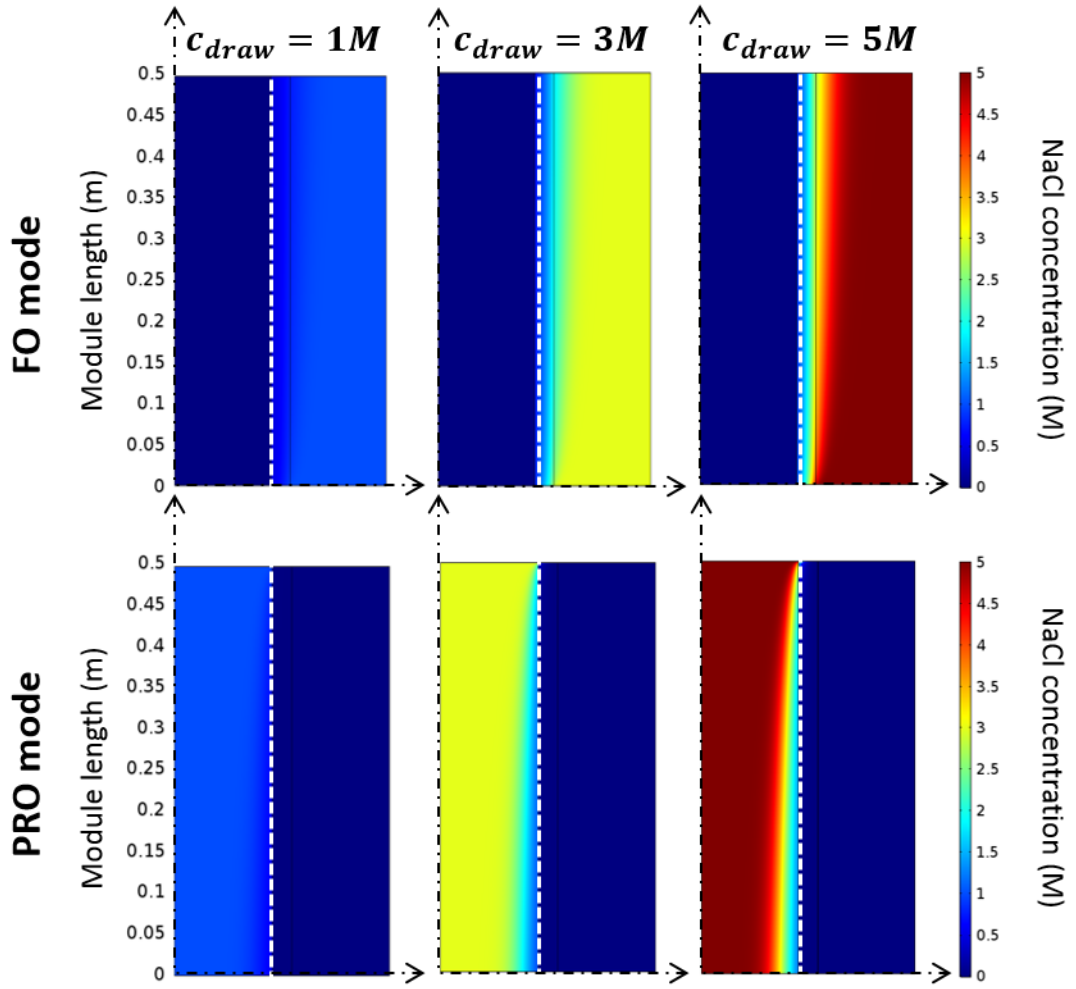

Figure 8.12. Two dimensional NaCl concentration distribution in 0.5 m long axisymmetric hollow fiber element with various draw solution concentrations in both FO and PRO modes. White dash line is indicative of selective layer, light black line is indicative of domain boundary and interfaces. Illustration figure is not drawn to scale.

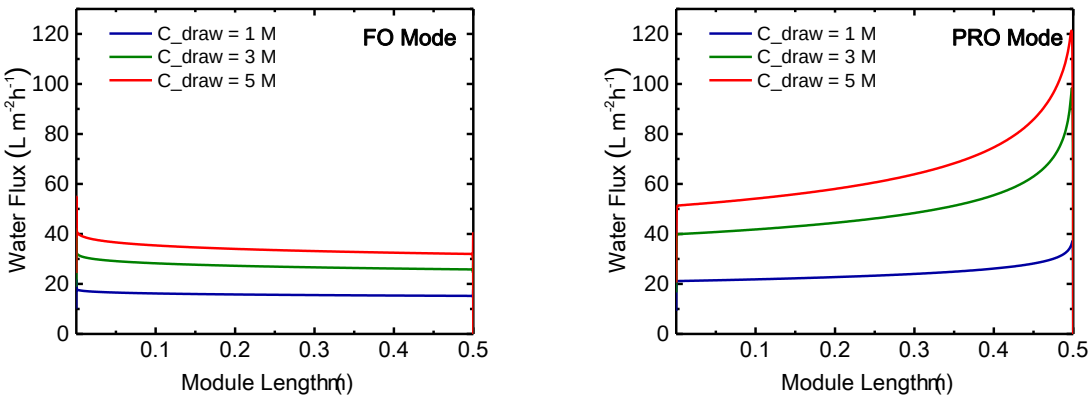

Figure 8.13. Modeling water flux variation along a 0.5 m membrane module with various NaCl draw solution concentrations (c_{draw}) in counter-current flow pattern in FO and PRO modes.

8.5 Model implementation and conclusion

As discussed in Section 8.4, the independent hollow fiber FO membrane and module design parameters were individually studied using the model. This provides an easy access to the FO community for the rational design of a hollow fiber membrane or module for a particular application. As there are numerous osmotic processes, conceiving every possible combination of membrane, module, and solution configuration is limited by the scope of this study. Thus, the model is built as a COMSOL application that attached in the supporting information. This application is built with the new 'application builder' feature that released with COMSOL Multiphysics 5.0 and can be directly used without rebuilding the model [242]. A series of membrane and module parameters are required to input while the model can be run and analyze osmotic flux performance of the membrane element.

In this study, we developed an experimentally verifiable modeling tool for predicting hollow fiber element performance which would enable prediction of element performance for a variety of osmotic processes (FO, PRO, dewatering). This model was rooted in mass transfer fundamentals and would help identify which independent parameters are most important when considering *both* membrane *and* element design. With such a tool, academics and industry alike would be able to design an element around their specific membrane technology, design a membrane around their required element specifications, or design both a membrane and element for a specific osmotic process. Such a tool has never before existed while it is also released for the first time as an open source application through the journal publication.

Chapter 9. Conclusions and recommendations

9.1 Concluding remarks

In this dissertation work, we firstly reported the performance of an early generation thin film composite (TFC) forward osmosis membrane from Hydration Technology Innovations (HTI). This membrane incorporated a selective barrier with a hydrophilic support structure with a low structural parameter, giving it improved performance over previous commercial membranes. This membrane represented the first TFC FO membrane manufactured on a 40-inch continuous production line and was shown to have superior performance when compared to the cellulose acetate (CA) membrane that has been often used in previous FO studies. This TFC membrane platform replaced the CA membrane as a benchmark for FO, further pushing the bar higher for improving FO membrane performance with new membrane designs.

With the commercial benchmark FO membranes guiding the design of novel TFC membranes, high performance flat sheet membranes were developed for FO process in this dissertation work. Hydrophilic sulfonated polymers and appropriate PET nonwovens were combined towards an optimized design of high performance thin film composite membrane for FO. The PET nonwoven fabrics enabled the use of delicate sulfonated polymers by reinforcing the mechanical properties for industrial conditions. Meanwhile, the sulfonated polymers enabled the use of hydrophobic PET fabric by integrating it into the support without enhancing mass transfer resistance. These results exhibited great promise of combining sulfonated polymers with appropriate PET nonwoven fabrics for future membrane designs for forward and pressure retarded osmosis.

Alongside the development of flat sheet membranes for FO, in this dissertation work, polyacrylonitrile supported TFC hollow fiber membranes were investigated for use in forward osmosis. The intrinsically hydrophillic PAN substrate material was used to mitigate ICP by ensuring wetting of the supporting structure. A simple way was described to adjust the structure of the fibers in order to elucidate the structure-performance relationships of TFC hollow fiber membranes during osmosis. While exhibiting good osmotic performance overall, the best performing membrane exhibited one of the lowest structural parameter of TFC hollow fiber membranes reported in the open literature. The thinnest membrane had a wall thickness of ~ 50 μm and was shown to have excellent performance when compared to the flat sheet counterparts and other shell-selective hollow fiber membranes reported in the literature.

To guide rational design of TFC hollow fiber membranes for osmotic processes, fundamental investigations were conducted to elucidate the structure-performance relationship of TFC membranes in FO processes. In this work, support layer surface pore size was identified has a significant impact on the formation of TFC membrane formation on the hollow fiber platform. We hypothesized a model that suggested that pore size and spacing are both critical in polyamide formation due to the direction amine diffuses into the organic phase during film formation. The resulting variability of roughness, in turn, impacts flux performance. This is especially noted in the PRO mode where the draw solution can contact a much greater surface area as noted by the increased surface area measured by AFM.

An exciting finding of this work was that a commercial ultrafiltration hollow fiber could serve as a support for a TFC membrane used in FO. While UF membranes are not designed with FO specifications in mind, these membranes not only performed well as supports for TFC membranes, they outperformed the only commercial TFC benchmark in the literature. These membranes may also serve as a platform for other fundamental transport work involving FO membranes and TFC fabrication. Such a finding may have ramifications across FO research

groups since now they have the ability to fabricate TFC hollow fiber membranes via a simple and facile interfacial polymerization process. The ability to fabricate membranes, especially those that can exhibit high packing density, is essential to applied research in osmotic processes given the challenges in finding stable and consistent supplies of commercial FO membranes.

As a continuation of using commercial ultrafiltration membranes as supports for making TFC hollow fiber FO membranes. In this work, commercial hollow fiber ultrafiltration *modules* were also used as a platform to make TFC hollow fiber FO membranes. Polyamide selective layers were formed *within the module* using a facile approach that employed conventional membrane chemistries. This approach, though having been done for lab-scale modules, had never been done at module scale. The results demonstrate that TFC hollow fiber FO membranes with reasonable performance can be produced at scale with relative ease using off-the-shelf UF modules. Further improvements could be realized if such a commercially produced module could incorporate fibers with a tailored support designed specifically for FO applications. Even without modifications, this study demonstrates that module-scale FO testing is possible in an academic laboratory without needing to resort to costly and difficult fiber spinning. Easy access to modules may enable continuation of the work on module- and volume- normalized performance metrics that may become more important to industry in the coming years as new FO applications emerge into the marketplace.

This dissertation also served as one of the first studies for optimizing the design parameters for hollow fiber membranes and modules for osmotic processes using computational fluid dynamics model. In this work, we developed an experimentally verifiable modeling tool for predicting hollow fiber element performance which would enable prediction of element performance for a variety of osmotic processes (FO, PRO, dewatering). The independent hollow fiber FO membrane and module design parameters were individually studied using the model. This model was rooted in mass transfer fundamentals and would help identify which

independent parameters are most important when considering *both* membrane *and* element design. With such a tool, academics and industry alike would be able to design an element around their specific membrane technology, design a membrane around their required element specifications, or design both a membrane and element for a specific osmotic process. Such a tool has never before existed while it will be released for the first time as an open source application to benefit the broader community.

9.2 Future directions and recommendations

Based on experimental results and findings obtained from current research, the following recommendations may provide further insight for future work related to the development of membranes and modules for osmotic processes.

9.2.1 Future work on the membrane development for osmotic processes

While many of the academically designed membranes for osmotic processes were based on novel materials or intricate fabrication methods, they would possibly encounter scaling up problem when transferring to the commercial sector. Costly materials and intricate fabrication methods would inhibit the commercialization of high performance FO membranes that developed in the academic labs. So it may be a worthwhile option to step back to the existing commercial platforms to make TFC membranes in a simple, accessible and facile way. This is especially applicable for the hollow fiber platform because the high packing density would be more tolerant to the possibly lowered water flux that may accompany with using the existing commercial platforms.

In this dissertation work, commercial ultrafiltration hollow fiber platform was used to develop TFC hollow fiber membranes mainly for applications in forward osmosis. However, with a good choice of pressure-tolerant commercial UF platform, TFC hollow fiber membranes can also be developed for pressure retarded osmosis (PRO) or nanofiltration (NF) applications. An option is to use braid-reinforced hollow fiber membrane to develop shell-selective membranes for PRO or NF applications. A number of companies such as GE (Zenon) and KMS have commercialized braid-reinforced hollow fiber membranes with a polyester braid obtained by braiding yarn [246, 247]. It is worthwhile to adopt these platforms to conduct facile interfacial polymerization to make TFC membranes. Though the mass transfer resistance within the supporting structure might be considerable due to the thick braid-reinforced structure in the application of PRO.

9.2.2 Future work on the module development for osmotic processes

Similarly, the development of a TFC membrane module for osmotic processes can also base on the existing commercial platforms. However, this would be difficult for flat-sheet configuration or shell-selective hollow fiber membranes due to the fact that these membranes were already potted in the module, which makes it difficult to conduct interfacial polymerization. Nevertheless, one can modify the hollow fiber modules to make lumen-selective TFC membranes for osmotic processes with a simple and facile method. Easy access to modules may enable continuation of the work that may become more important to industry in the coming years as new FO applications emerge into the marketplace.

The interdependency between the membrane and module development should not be overlooked. A high performance membrane may be limited by the inadequete design of module.

In return, a sophisticated design of module may not be necessary when the performance is limited by the low performance of membrane. This requires the academic researchers and industry entities to work closely with each other. Pilot scale revalidation of osmotic processes may be an option to allow examination of the feasibility.

Since the experimental would be costly and time-consuming, a good way to guide module development is via computational modeling. In this study, we developed a comprehensive and experimentally verified computational fluid dynamics model for hollow fiber membranes that established relationships between both membrane properties and module design and overall osmotic performance. Based on this basic model, a number of modifications can be made. Options of draw solutes, options of feed solutes, cross flow patterns, options of lumen- or shell-selective hollow fibers can all be modified to allow studying various osmotic processes (FO, PRO or dewatering). It worth to note that such a model could be modified for use in the flat sheet configuration when considering an open boundary instead of the symmetry boundary condition in the model setting.

9.2.3 Future work on the osmotic processes

Forward osmosis offers a unique solution to some of our most challenging water treatment processes such as water reuse, produced water treatment, brine dewatering, and zero liquid discharge systems. It is worthwhile to conduct fundamental researches to study the membrane fouling behavior in the FO processes. This would greatly enrich the current studies on the membrane developments and guide a rational design of membranes and modules to avoid fouling and enable the use of FO in treating challenging waters.

Integrating the osmotic processes with other processes would be a good use of current knowledge in this field. Hybrid FO-RO and hybrid FO-MD processes have been studied and showed promise in water treatment. A thermos-osmotic energy conversion process that is

capable of converting thermal energy gradients to electricity has also been proposed recently [248]. Developing efficient hybrid osmotic process for water treatment or power generation would be in the interest of broader membrane, chemical and environmental engineering community.

Appendix 1. Evaluating commercial biomimetic hollow fiber membrane for forward osmosis

To be published as

Ren, J., Andersen, M.F., McCutcheon, J.R., "A new commercial biomimetic hollow fiber membrane for forward osmosis".

A1. 1. Introduction

Forward osmosis (FO) is an emergent membrane technology that harnesses the natural osmotic pressure difference to drive water across a semipermeable membrane from a diluted feed solution to a concentrated draw solution while rejecting most solutes [10, 60]. FO requires no applied hydraulic pressure and is capable of treating waters with high salinity and fouling propensity [12-14]. Water reuse [16, 214], produced water treatment [65, 66], brine dewatering [19, 215], and zero liquid discharge systems [9, 213] are all enabled by FO technology.

The field of FO has been active for the past 10 years as research groups all around the world have been focused on developing high performance membranes [25, 27, 31, 91, 216]. Industry joined the effort and companies like Fluid Technology Solutions (FTS, formerly Hydration Technology Innovations, HTI) [32], Oasys Water [33, 94], Porifera [96], Toyobo [97] and Cheil Industry [73, 98] emerged with their own brand of membrane technology. These membranes, however, are largely focused on the platform of flat sheet membranes. HTI uses a spiral wound element with the same dimensions as today's RO elements but incorporates a cellulose acetate

membrane [135, 136, 224, 225]. Oasys Water uses spiral wound elements and Porifera uses plate-and-frame modules with their own brand of thin film composite (TFC) membranes, respectively [94-96, 223]. Only recently have Toyobo and Cheil Industry offered modules in hollow fiber platform at semi-pilot scale [98, 249].

Hollow fiber membranes have shown great promise for ultrafiltration, dialysis, and gas separation due to their high packing density, and self-supported structure [34]. These benefits are also well translated to FO as it requires no or low transmembrane pressure but large surface area. A number of high performance hollow fiber membranes have been developed in academic laboratories around the world. These membranes were mostly based on the thin film composite (TFC) platform where the selective and support layers can be tailored independently [29, 31, 101-103, 105, 112-114, 116, 122]. These membranes, while demonstrating high osmotic flux performance, also involved employing novel materials or intricate fabrication methods. A number of high performance TFC hollow fiber FO membranes were fabricated with novel materials in selective or support layers such as sulfonated polyphenylenesulfone (sPPSU) [112], cellulose acetate butyrate (CAB) [64], carbon nanotubes [107], polyhedral oligomeric silsesquioxane (POSS) [57], etc. Moreover, intricate fabrication methods such as layer-by-layer (LbL) formation of selective layer [108], shell-selective batch coating [101], polyelectrolyte post-treatment [103] and dual layer spinning [31, 105] were adopted. With the use of costly novel materials and intricate fabrication methods, most of the current hollow fiber membrane designs face the difficulty of scaling up. However, one exception, aquaporin-incorporated biomimetic membrane, is emerging and has drawn significant attentions from the FO community.

Aquaporin as a pore-forming protein that is ubiquitous in living cells [250]. It has been incorporated in membrane fabrications form “water channels” that excludes ionic species under right conditions. The idea of incorporating aquaporin in desalination membrane was firstly

reported by Kumar et al. [251]. After that, a number of aquaporin-based membranes have been developed in academic labs for the applications such as reverse osmosis, nanofiltration and forward osmosis [252-257]. The high performance and excellent stability that brought by this biomimetic nanotechnology has offered great promise for its real-world application. Aquaporin A/S has been the one company that strives to commercialize this technology, in both flat sheet and hollow fiber configurations.

This study is focused on introducing a new aquaporin-based biomimetic hollow fiber membrane that developed for FO applications. Miniature membrane modules were provided by Aquaporin A/S (Denmark) and tested under different conditions using bench scale systems. The results revealed an excellent performance which showed great promise in the full scale application of this aquaporin-based hollow fiber membrane.

A1.2. Experimental

A1.2.1 Materials

Aquaporin Inside ™ (AQP) hollow fiber membrane modules were received from Aquaporin A/S (Denmark) and shown in Figure A1.1. The modules are all transparent PVC modules in 210 mm length and 25.4 mm diameter. Each module accommodates 107 fibers with inner diameter of $300 \pm 40\ \mu m$ and effective membrane area of 116 cm^2. Aquaporin coating was on the inner surface (lumen side) of hollow fibers. For osmotic flux tests, sodium chloride (NaCl, crystalline, >99.0%) were purchased from Fisher Scientific (Pittsburgh, PA). Deionized water (DI) was obtained from a Milli-Q ultrapure water purification system (Millipore, Billerica, MA).

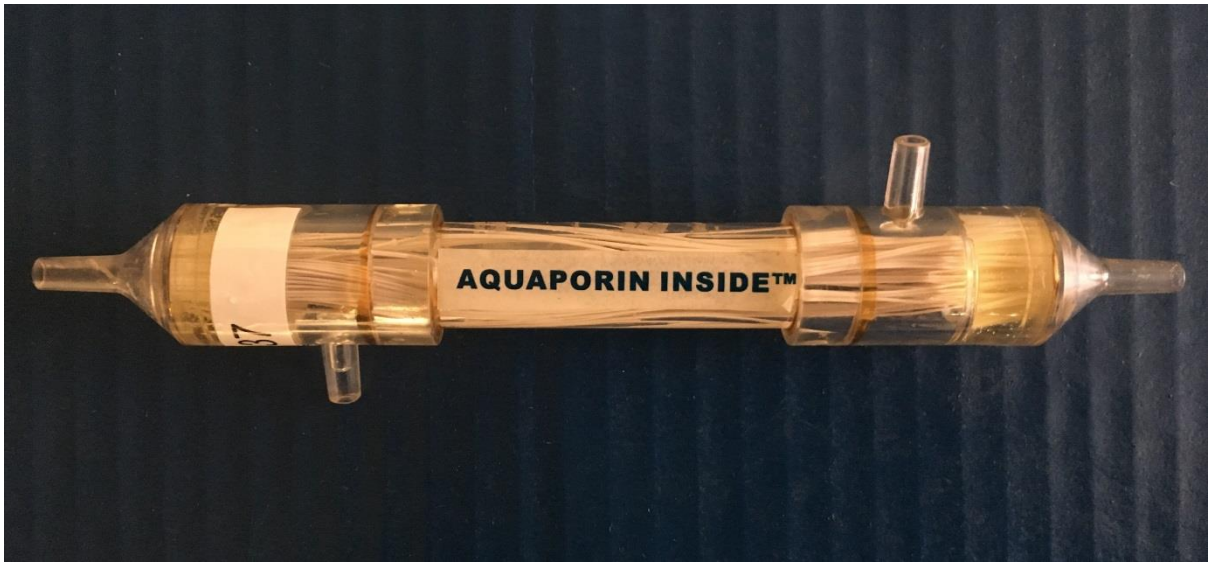

Figure A1.1. Photograph of Aquaporin Inside™ hollow fiber membrane module.

A1.2.2 Membrane characterization

The surface morphology and cross-sectional structure of the AQP hollow fiber membranes were imaged with a cold cathode field emission scanning electron microscope (FESEM, JSM-6335F, JEOL Ltd., Japan). To preserve the cross section pore structure, the samples were submerged in liquid nitrogen and then freeze fractured. Before imaging, the samples were sputter coated with gold.

A1.2.3 Osmotic flux performance of TFC membranes

Osmotic water flux and reverse salt flux through Aquaporin Inside ™ hollow fiber membranes were characterized using a custom lab-scale cross-flow forward osmosis. The similar experimental setup was described in earlier investigations [101]. Feed and draw solutions were delivered using gear pumps in counter-current flow arrangement. Osmotic flux tests were carried out with the membrane oriented in both FO mode (the membrane lumen

selective layer faces the feed solution) and PRO mode (the membrane lumen selective layer faces the draw solution). The osmotic water flux, J_w, was calculated by dividing the volumetric flux by the membrane area. By measuring the conductivity of the feed solutions at certain time points during the tests, the reverse salt flux, J_s, was calculated by dividing the NaCl mass flow rate by the membrane area. The specific salt flux is simply a ratio of salt flux to water flux, J_s/J_w. Two testing conditions – a lab-scale testing standard methodology and one suggested by Aquaporin A/S – were used.

A1.2.3.1 Standard method

To make reasonable comparisons with other hollow fiber membranes, a testing protocol that is similar to other studies was used [29, 98, 114]. In this method, water and salt fluxes were measured at $20 \pm 0.5℃$ using DI feed and NaCl draw solution with concentration ranging from 0.3M to 1.5M. The Reynolds number in the lumen and shell side of the hollow fiber module were set at the maximum within the capacity of the current apparatus as 170 and 280, respectively. Transmembrane pressure were set as 2 ± 0.5 psi on both lumen and shell sides.

A1.2.3.2 Aquaporin method

The testing methodology suggested by Aquaporin A/S is based on the production quality control process. In this method, the temperature was same with standard method at $20 \pm 0.5℃$. DI feed and 1M NaCl draw solution were used. Volumetric flow rate was set at 30 ml/min on both the lumen and shell sides with Reynolds number of 20 and 7, respectively. Transmembrane pressure, which is the average of inlet and outlet pressure, was maintained same at 2 ± 0.5 psi on lumen and shell sides.

A1.2.3.3 Determination of structural parameter

Osmotic water flux and reverse salt flux can be used to calculate the structural parameter (S), which is a support layer property for FO membranes. The S value is commonly defined as the product of the thickness (t) and tortuosity (τ), divided by the porosity (ε) in FO. It is an indicator of the severity of the mass transfer resistance within the supporting structure of the membrane (internal concentration polarization, ICP). The S value can be determined using Equation 1 and 2 using an Excel-based method developed by Tiraferri and released through his publication [177],

$$J_w = A\left\{\frac{\pi_D \exp\left(-\frac{J_w S}{D}\right) - \pi_F \exp\left(\frac{J_w}{k}\right)}{1+\frac{B}{J_w}\left[\exp\left(\frac{J_w}{k}\right) - \exp\left(-\frac{J_w S}{D}\right)\right]}\right\} \quad \text{(A1.1)}$$

$$J_s = B\left\{\frac{c_D \exp(-\frac{J_w S}{D}) - c_F \exp(\frac{J_w}{k})}{1+\frac{B}{J_w}\left[\exp(\frac{J_w}{k}) - \exp(-\frac{J_w S}{D})\right]}\right\} \quad \text{(A1.2)}$$

In these equations, the water flux (J_w) and the salt flux (J_s) are directly measured. The concentrations of the draw (c_D) and feed solutions (c_F) are known. The mass transfer coefficient (*k)* can be calculated from the Sherwood Number correlations for both sides of the membrane. Diffusivity (*D*) can be taken from the literature. Osmotic pressures of the feed (π_F) and draw (π_D) solutions can be calculated using the van't Hoff equation. This leaves the structural parameter (*S*), water permeance (*A*), and salt permeability (*B)* as the only unknowns. The method divides the FO experiment into a discrete number of stages, which requires four water and salt flux measurements to be carried out with four different draw solution concentrations (0.3M, 0.6M, 1M and 1.5M) with a DI water feed. Once all four data points are captured, the model allows the user to input the other known values, and then solves for the three unknown parameters to fit the data simultaneously.

A1.3. Results and discussion

A1.3.1 Morphology of membranes

The cross-sectional morphology of the AQP hollow fiber membranes are shown in Figure A1.2. As shown, the wall thickness was measured to be around 80 micron. The cross section shows spongy-like structure throughout the entire structure. The image at higher magnification (Figure A1.2b) reveals visible dense region close to the lumen and shell surfaces. Such structure would be beneficial in the real operation due to the mechanical property offered by the dense spongy-like structure, with the absence of macrovoids which create weak spots. Figure A1.2c shows the close look at the cross-sectional structure at the selective layer at high magnification. Interestingly, a dense structure with a thickness of about a couple microns was observed close to the inner surface, indicating a potential thick selective layer of the AQP membranes.

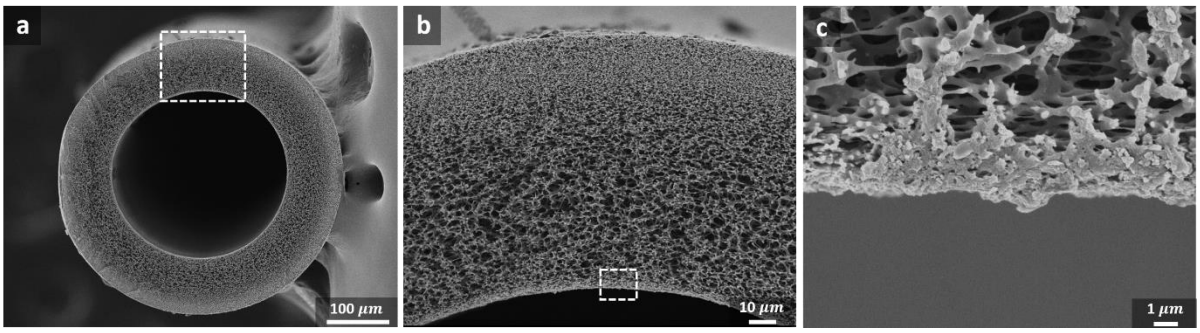

Figure A1.2. Cross-section FESEM images of Aquaporin Inside™ hollow fiber membrane at (a) 170×; (b) 800×; (c) 5000×.

The surface morphology of the hollow fiber membrane are shown in Figure A1.3. Figure A1.3a shows the morphology of supporting layer lumen surface before incorporating aquaporin protein. The support lumen surface showed porous structure with pores at the scale of microns.

Figure A1.3b shows the morphology of lumen selective layer of the membrane after incorporating aquaporin. The porous structure was mainly covered by the dense incorporation of aquaporin, though some visible pores can still be seen from the images. Thus, osmotic flux test were conducted to evaluate the FO performance and to characterize the separation properties in the following section.

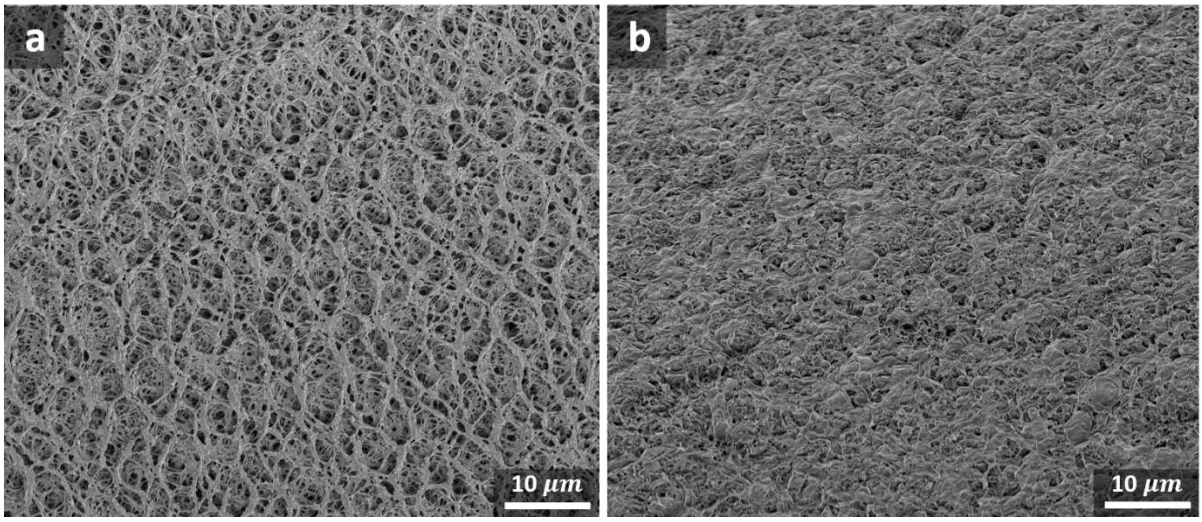

Figure A1.3. Inner surface FESEM images of Aquaporin Inside™ hollow fiber membrane at 5000×, (a) without aquaporin; (b) with aquaporin.

A1.3.2 Performance of TFC membranes

A1.3.2.1 Osmotic performance under standard method

The AQP hollow fiber membranes were evaluated under FO and PRO modes using DI water as the feed and NaCl as the draw solution. The osmotic water fluxes and reverse salt fluxes (J_w and J_s) tested using the standard method are presented in Figure A1.4. These results suggested a good performance of AQP hollow fiber membranes. The water and salt fluxes increased with ranging draw solution concentration from 0.3M to 1.5M due to increased

osmotic pressure driving force. At 1M NaCl draw solution as the standard testing protocol suggested [176], the AQP hollow fiber membranes exhibited reasonably high water flux of 13.2 and 21.0 LMH with moderately low reverse salt flux of 1.7 and 3.6 gMH in FO and PRO modes, respectively. These results surpassed the only commercial TFC hollow fiber membrane from Cheil Industry in the market, thus could be adopted as a new benchmark for the hollow fiber FO membrane development in academia and industry.

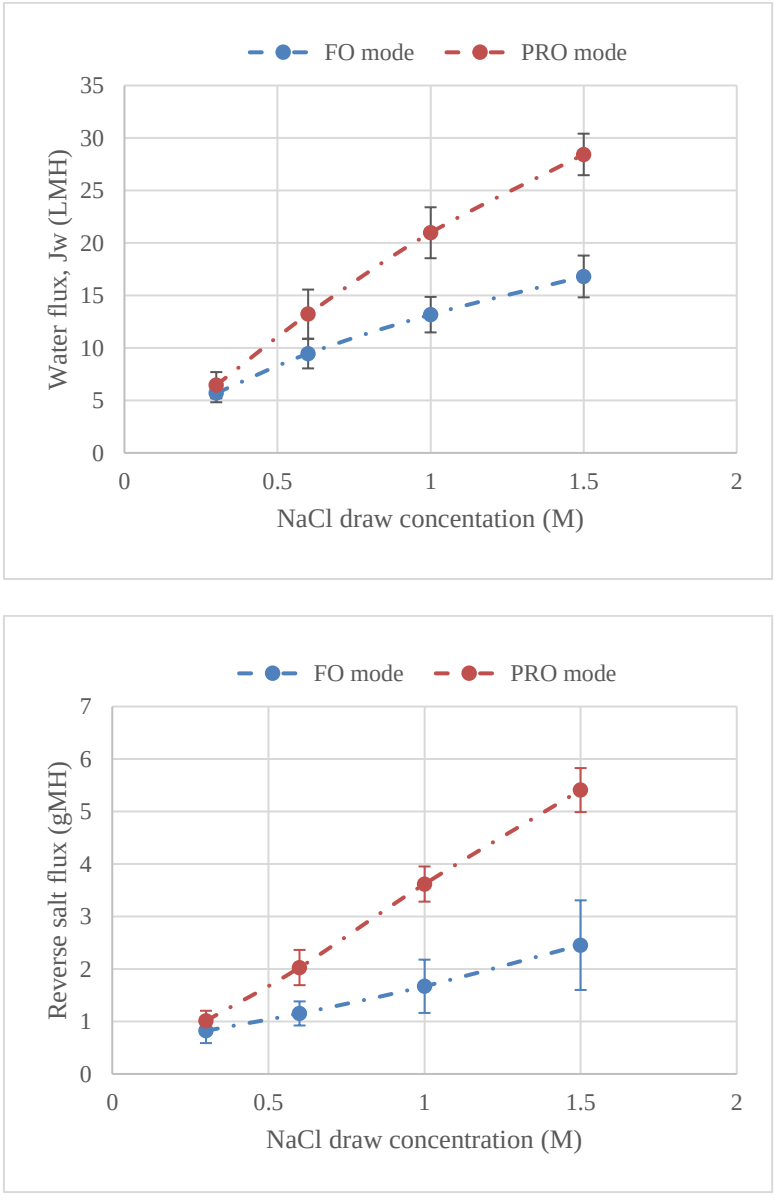

Figure A1.4. Water flux and reverse salt flux (J_w and J_s) of FO and PRO mode tests for

AQP membranes using standard method. Error bars indicate standard deviation of at least two individual modules. Operating conditions: NaCl draw solution, DI water feed, 20 ℃ feed and draw solution temperature, 170 and 280 lumen and shell side Reynolds number, no transmembrane hydraulic pressure.

A1.3.2.2 Osmotic performance under AQP method

The osmotic flux performance of AQP membranes using Aquaporin method was compared with the results from Standard tests at 1M NaCl as shown in Figure A1.5. The results using Aquaporin method showed lower water and reverse salt flux in both FO and PRO modes. We attribute this to the fact that the cross flow velocity used in the AQP method was considerably low (low Re of 20 and 7 on lumen and shell side, respectively). This resulted in an insufficient mass transfer on the membrane surface which exacerbated the mass transfer resistance within the channel (known as external concentration polarization, i.e. ECP) that impaired the water and reverse salt flux.

Comparing the osmotic flux results to the only available TFC hollow fiber membrane on the market from Cheil Industry [73, 98], the AQP membranes showed superior performance. It worth to note that the testing conditions for the three membranes were different. The Re of the tests in this study is generally lower than that in the literature and benchmark conditions due to the limit of the FO system. This suggests that even with a more profound ECP in the testing, the AQP membrane still surpassed the Cheil membrane in the osmotic performance.

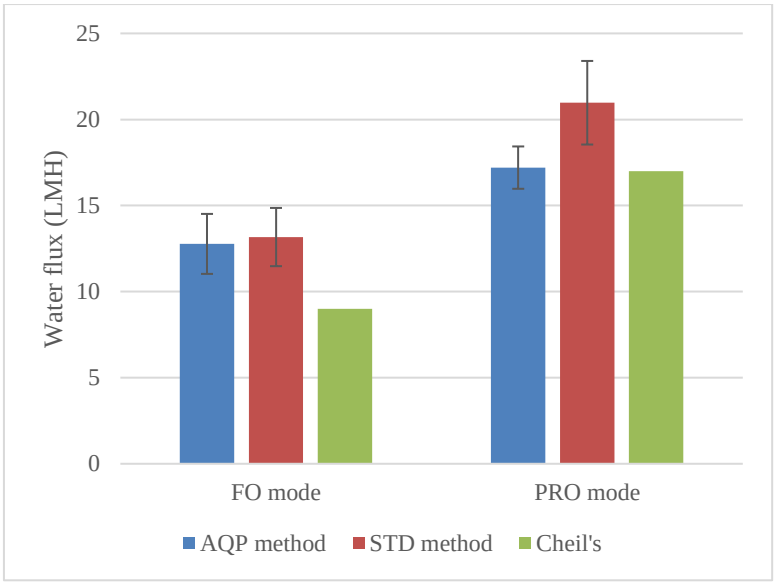

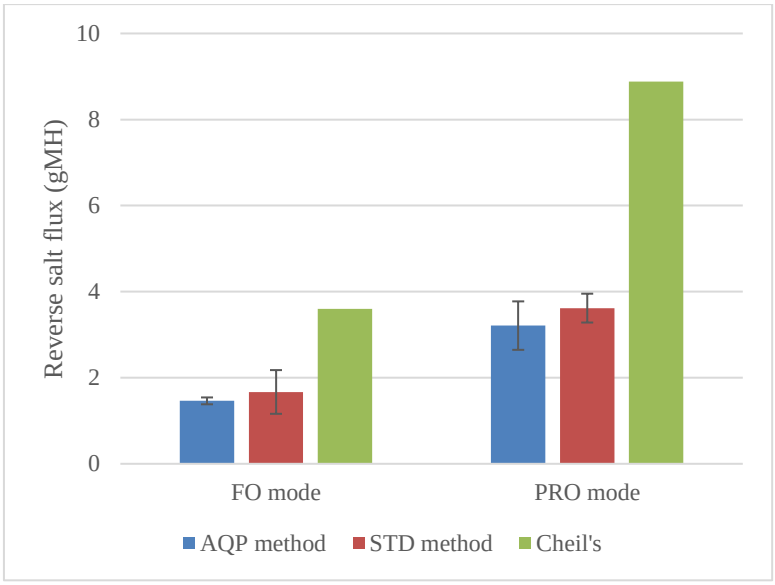

Figure A1.5. Water flux and reverse salt flux (J_w and J_s) of FO and PRO mode tests for AQP membranes using Aquaporin and Standard methods, and commercial benchmark membrane from Cheil's Industry [73, 98]. Error bars indicate standard deviation of at least two individual modules. Operating conditions: 1M NaCl draw solution, DI water feed, 20 ℃ feed and draw solution temperature. 20 and 7 lumen and shell side Reynolds number in Aquaporin method while 170 and 280 lumen and shell side Reynolds number in Standard method.

A1.3.2.3 Membrane properties

The membrane intrinsic properties, pure water permeance A, salt permeability B, and structural parameter S were evaluated using an empirical method that developed by Tiraferri et al. [177]. The AQP membrane showed A value of 0.43 $\pm$0.10 LMH/bar and B value of 0.050$\pm$ 0.007 LMH. The A value is in the lower range comparing with other commercial FO membranes in flat sheet configuration. Alongside the low A value, the B value is also significantly lower than other flat sheet counterparts [32, 33]. These results are consistent with the osmotic flux performance discussed in the previous section where the water and reverse salt flux were both relatively low compared with the commercial flat-sheet membranes.

The structural parameter gives insight to the extent of ICP, where a low S value correlates with less ICP. The S value of the AQP membrane were determined as 210.5$\pm$55.5 μm. This is by far one of the lowest S value for the TFC hollow fiber membranes. Apparently this is due to a thin supporting structure of ~ 80 μm and a high porosity that can be observed from the cross-sectional FESEM images.

A1.3.2.4 Performance comparisons

As a commercial membrane emerging, the performance is compared with existing benchmarks from both academia and industry. Table A1.1 and A1.2 show the performance comparison of AQP membranes with academic and commercial membranes, respectively.

In Table A1.1, the AQP hollow fiber membrane was firstly compared with an aquaporin-based hollow fiber membrane developed by Li et al [253]. It can be seen that the academic membrane largely surpassed the performance of the commercial AQP membrane in this work. This again proved that in this field, we do not lack good membranes, but good products. Most of the membranes perform well at lab-scale but the performance would be compromised when

operates in a pilot scale module. Thus the effort by Aquaporin A/S demonstrated significant meaning in which transferring the laboratory techniques to the full-scale applications. Again, compared with other academic hollow fiber FO membranes, the AQP membranes only showed average performance due to the fact that this membrane was manufactured at scale.

The AQP membranes, however, showed superb performance when compared with the commercial competitors such as Toyobo and Cheil Industry [98, 249]. Interestingly, these commercial hollow fiber FO membranes were both based on simplest platforms with ordinary materials: cellulose acetate based asymmetric membrane and polyethersulfone based TFC membrane. It demonstrated the commercial value of the membrane that designed with simplicity. Now that the aquaporin-based hollow fiber FO membranes can be made at scale, it would be promising to see the full-scale AQP hollow fiber modules in the near future.

Membranes	**Feed**	**Draw**	**Water flux ($L\ m^{-2}h^{-1}$)**		**Salt flux ($g\ m^{-2}h^{-1}$)**		**A (LMH/ bar)**	**B (LMH)**	**S (μm)**	**Ref**
			FO mode	**PRO mode**	**FO mode**	**PRO mode**				
Aquaporin	DI	0.6 M NaCl	9.46	13.22	1.15	2.03	0.43	0.05	210	This work
AHF (LPR 100)	DI	0.5 M NaCl	N/A	55.20	N/A	4.50	7.70	0.43	N/A	[253]
#B-FO HF	DI	0.5 M NaCl	14.00	32.20	1.75	3.54	2.22	0.20	595	[29]
#C-FO HF	DI	0.5 M NaCl	18.50	42.60	1.50	4.00	3.50	0.22	550	[30]
FO-PES$_{water}$	DI	0.5 M NaCl	22.50	25.60	2.80	3.20	1.18	0.14	219	[31]
1.5 mol % sPPSU	DI	0.5 M NaCl	22.51	49.39	5.49	11.00	1.99	0.04	163	[112]
LBL-21	DI	0.5 M $MgCl_2$	21.50	73.00	0.65	4.38	N/A	N/A	N/A	[98]

Table A1.1. Comparison of osmotic flux performance of AQP hollow fiber membrane with hollow fiber FO membranes reported in the literature.

Membranes	Feed	Draw	Water flux ($L\ m^{-2}h^{-1}$)		Salt flux ($g\ m^{-2}h^{-1}$)		A (LMH/ bar)	B (LMH)	S (μm)	Ref
			FO mode	PRO mode	FO mode	PRO mode				
Aquaporin	DI	1 M NaCl	13.20	21.00	1.70	3.60	0.43	0.05	210	This work
Toyobo HF-A	DI	1 M NaCl	4.00	8.00	0.70	N/A	0.27	0.08	1024	[249]
Toyobo HF-B	DI	1 M NaCl	5.00	9.00	0.35	N/A	0.29	0.02	724	[249]
Toyobo HF-C	DI	1 M NaCl	8.00	15.00	0.59	N/A	0.55	0.04	639	[249]
Cheil	DI	1 M NaCl	10.00	19.00	3.60	8.88	N/A	N/A	N/A	[98]

Table A1.2. Comparison of osmotic flux performance of AQP hollow fiber membrane with commercial benchmarks.

A1.4. Conclusion

In this study, we report the performance of a biomimetic hollow fiber FO membrane from Aquaporin. This membrane incorporates aquaporin 'water channel' in the selective layer which was formed on the lumen surface of a hollow fiber porous support. The osmotic flux tests revealed an excellent performance that surpassed the only commercial hollow fiber FO membranes on the market, thus could be adopted as a new benchmark for the hollow fiber FO membrane development in academia and industry. It also demonstrated the great effort from the industry in applying bio-inspired nanotechnology for real-world applications.

References

[1] P.H. Gleick, The human right to water, Water policy, 1 (1998) 487-503.

[2] F.R. Rijsberman, Water scarcity: fact or fiction?, Agricultural water management, 80 (2006) 5-22.

[3] P.H. Gleick, Water in crisis: a guide to the world's fresh water resources, Oxford University Press, Inc., 1993.

[4] H. Yang, X. Zhang, A.J. Zehnder, Water scarcity, pricing mechanism and institutional reform in northern China irrigated agriculture, Agricultural water management, 61 (2003) 143-161.

[5] Y. Jiang, China's water scarcity, Journal of Environmental Management, 90 (2009) 3185-3196.

[6] Global Risks Report 2017, World Economic Forum, (2017).

[7] M. Elimelech, W.A. Phillip, The future of seawater desalination: energy, technology, and the environment, Science, 333 (2011) 712-717.

[8] T. Asano, A.D. Levine, Wastewater reclamation, recycling and reuse: past, present, and future, Water science and technology, 33 (1996) 1-14.

[9] T. Tong, M. Elimelech, The Global Rise of Zero Liquid Discharge for Wastewater Management: Drivers, Technologies, and Future Directions, Environmental Science & Technology, (2016).

[10] T. Cath, A. Childress, M. Elimelech, Forward osmosis: Principles, applications, and recent developments, Journal of Membrane Science, 281 (2006) 70-87.

[11] L.A. Hoover, W.A. Phillip, A. Tiraferri, N.Y. Yip, M. Elimelech, Forward with Osmosis: Emerging Applications for Greater Sustainability, Environmental Science & Technology, 45 (2011) 9824-9830.

[12] T.-S. Chung, S. Zhang, K.Y. Wang, J. Su, M.M. Ling, Forward osmosis processes: Yesterday, today and tomorrow, Desalination, 287 (2012) 78-81.

[13] S. Zhao, L. Zou, C.Y. Tang, D. Mulcahy, Recent developments in forward osmosis: opportunities and challenges, Journal of Membrane Science, 396 (2012) 1-21.

[14] B. Mi, M. Elimelech, Organic fouling of forward osmosis membranes: fouling reversibility and cleaning without chemical reagents, Journal of Membrane Science, 348 (2010) 337-345.

[15] B.D. Coday, P. Xu, E.G. Beaudry, J. Herron, K. Lampi, N.T. Hancock, T.Y. Cath, The sweet spot of forward osmosis: Treatment of produced water, drilling wastewater, and other complex and difficult liquid streams, Desalination, 333 (2014) 23-35.

[16] K.L. Hickenbottom, N.T. Hancock, N.R. Hutchings, E.W. Appleton, E.G. Beaudry, P. Xu, T.Y. Cath, Forward osmosis treatment of drilling mud and fracturing wastewater from oil and gas operations, Desalination, 312 (2013) 60-66.

[17] J.R. McCutcheon, R.L. McGinnis, M. Elimelech, A novel ammonia—carbon dioxide forward (direct) osmosis desalination process, Desalination, 174 (2005) 1-11.

[18] R.L. McGinnis, N.T. Hancock, M.S. Nowosielski-Slepowron, G.D. McGurgan, Pilot demonstration of the NH 3/CO 2 forward osmosis desalination process on high salinity brines, Desalination, 312 (2013) 67-74.

[19] R.W. Holloway, A.E. Childress, K.E. Dennett, T.Y. Cath, Forward osmosis for concentration of anaerobic digester centrate, Water Research, 41 (2007) 4005-4014.

[20] E.M. Garcia-Castello, J.R. McCutcheon, M. Elimelech, Performance evaluation of sucrose concentration using forward osmosis, Journal of Membrane Science, 338 (2009) 61-66.

[21] S. Zhang, P. Wang, X. Fu, T.-S. Chung, Sustainable water recovery from oily wastewater via forward osmosis-membrane distillation (FO-MD), Water Research, 52 (2014)

112-121.

[22] C.R. Martinetti, A.E. Childress, T.Y. Cath, High recovery of concentrated RO brines using forward osmosis and membrane distillation, Journal of Membrane Science, 331 (2009) 31-39.

[23] M. Xie, L.D. Nghiem, W.E. Price, M. Elimelech, A forward osmosis–membrane distillation hybrid process for direct sewer mining: system performance and limitations, Environmental Science & Technology, 47 (2013) 13486-13493.

[24] F. Zaviska, Y. Chun, M. Heran, L. Zou, Using FO as pre-treatment of RO for high scaling potential brackish water: Energy and performance optimisation, Journal of Membrane Science, 492 (2015) 430-438.

[25] N.Y. Yip, A. Tiraferri, W.A. Phillip, J.D. Schiffman, M. Elimelech, High performance thin-film composite forward osmosis membrane, Environmental Science & Technology, 44 (2010) 3812-3818.

[26] N.-N. Bui, M.L. Lind, E.M.V. Hoek, J.R. McCutcheon, Electrospun nanofiber supported thin film composite membranes for engineered osmosis, Journal of Membrane Science, 385-386 (2011) 10-19.

[27] L. Huang, J.R. McCutcheon, Hydrophilic nylon 6,6 nanofibers supported thin film composite membranes for engineered osmosis, Journal of Membrane Science, 457 (2014) 162-169.

[28] J. Ren, B. O'Grady, G. de Jesus, J.R. McCutcheon, Sulfonated polysulfone supported high performance thin film composite membranes for forward osmosis, Polymer.

[29] R. Wang, L. Shi, C.Y. Tang, S. Chou, C. Qiu, A.G. Fane, Characterization of novel forward osmosis hollow fiber membranes, Journal of Membrane Science, 355 (2010) 158-167.

[30] S. Chou, L. Shi, R. Wang, C.Y. Tang, C. Qiu, A.G. Fane, Characteristics and potential applications of a novel forward osmosis hollow fiber membrane, Desalination, 261 (2010) 365-

372.

[31] P. Sukitpaneenit, T.-S. Chung, High Performance Thin-Film Composite Forward Osmosis Hollow Fiber Membranes with Macrovoid-Free and Highly Porous Structure for Sustainable Water Production, Environmental Science & Technology, 46 (2012) 7358-7365.

[32] J. Ren, J.R. McCutcheon, A new commercial thin film composite membrane for forward osmosis, Desalination, 343 (2014) 187-193.

[33] J.T. Arena, S.S. Manickam, K.K. Reimund, P. Brodskiy, J.R. McCutcheon, Characterization and Performance Relationships for a Commercial Thin Film Composite Membrane in Forward Osmosis Desalination and Pressure Retarded Osmosis, Industrial & Engineering Chemistry Research, 54 (2015) 11393-11403.

[34] R. Baker, Membrane technology and applications, John Wiley & Sons, 2012.

[35] M.-C. Yang, E.L. Cussler, Designing hollow-fiber contactors, AIChE Journal, 32 (1986) 1910-1916.

[36] T.S. Chung, S.K. Teoh, X. Hu, Formation of ultrathin high-performance polyethersulfone hollow-fiber membranes, Journal of Membrane Science, 133 (1997) 161-175.

[37] J.M. Henis, M.K. Tripodi, Composite hollow fiber membranes for gas separation: the resistance model approach, Journal of Membrane Science, 8 (1981) 233-246.

[38] T. LaTerra, Liquid purification using reverse osmosis hollow fibers, in, Google Patents, 1983.

[39] D.L. Shaffer, J.R. Werber, H. Jaramillo, S. Lin, M. Elimelech, Forward osmosis: Where are we now?, Desalination, 356 (2015) 271-284.

[40] R.L. Riley, H.K. Lonsdale, C.R. Lyons, Composite membranes for seawater desalination by reverse osmosis, Journal of applied polymer science, 15 (1971) 1267-1276.

[41] J.E. Cadotte, R.J. Petersen, R.E. Larson, E.E. Erickson, A new thin-film composite seawater reverse osmosis membrane, Desalination, 32 (1980) 25-31.

[42] A. Prakash Rao, N.V. Desai, R. Rangarajan, Interfacially synthesized thin film composite RO membranes for seawater desalination, Journal of Membrane Science, 124 (1997) 263-272.

[43] C.H. Tan, H.Y. Ng, Modified models to predict flux behavior in forward osmosis in consideration of external and internal concentration polarizations, Journal of Membrane Science, 324 (2008) 209-219.

[44] J.R. McCutcheon, M. Elimelech, Modeling water flux in forward osmosis: Implications for improved membrane design, AIChE Journal, 53 (2007) 1736-1744.

[45] S. Loeb, L. Titelman, E. Korngold, J. Freiman, Effect of porous support fabric on osmosis through a Loeb-Sourirajan type asymmetric membrane, Journal of Membrane Science, 129 (1997) 243-249.

[46] J.R. McCutcheon, M. Elimelech, Influence of concentrative and dilutive internal concentration polarization on flux behavior in forward osmosis, Journal of Membrane Science, 284 (2006) 237-247.

[47] M. Kurihara, Y. Fusaoka, T. Sasaki, R. Bairinji, T. Uemura, Development of crosslinked fully aromatic polyamide ultra-thin composite membranes for seawater desalination, Desalination, 96 (1994) 133-143.

[48] A. Prakash Rao, S.V. Joshi, J.J. Trivedi, C.V. Devmurari, V.J. Shah, Structure–performance correlation of polyamide thin film composite membranes: effect of coating conditions on film formation, Journal of Membrane Science, 211 (2003) 13-24.

[49] S. Veríssimo, K.V. Peinemann, J. Bordado, Thin-film composite hollow fiber membranes: An optimized manufacturing method, Journal of Membrane Science, 264 (2005) 48-55.

[50] A.K. Ghosh, B.-H. Jeong, X. Huang, E.M.V. Hoek, Impacts of reaction and curing conditions on polyamide composite reverse osmosis membrane properties, Journal of

Membrane Science, 311 (2008) 34-45.

[51] C.Y. Tang, Y.-N. Kwon, J.O. Leckie, Effect of membrane chemistry and coating layer on physiochemical properties of thin film composite polyamide RO and NF membranes: I. FTIR and XPS characterization of polyamide and coating layer chemistry, Desalination, 242 (2009) 149-167.

[52] N. Widjojo, T.-S. Chung, M. Weber, C. Maletzko, V. Warzelhan, A sulfonated polyphenylenesulfone (sPPSU) as the supporting substrate in thin film composite (TFC) membranes with enhanced performance for forward osmosis (FO), Chemical Engineering Journal, 220 (2013) 15-23.

[53] K.Y. Wang, T.-S. Chung, J.-J. Qin, Polybenzimidazole (PBI) nanofiltration hollow fiber membranes applied in forward osmosis process, Journal of Membrane Science, 300 (2007) 6-12.

[54] Q. Yang, K.Y. Wang, T.-S. Chung, Dual-layer hollow fibers with enhanced flux as novel forward osmosis membranes for water production, Environmental Science & Technology, 43 (2009) 2800-2805.

[55] D. Emadzadeh, W.J. Lau, T. Matsuura, M. Rahbari-Sisakht, A.F. Ismail, A novel thin film composite forward osmosis membrane prepared from PSf–TiO 2 nanocomposite substrate for water desalination, Chemical Engineering Journal, 237 (2014) 70-80.

[56] J.-Y. Lee, C.Y. Tang, F. Huo, Fabrication of Porous Matrix Membrane (PMM) Using Metal-Organic Framework as Green Template for Water Treatment, Scientific Reports, 4 (2014).

[57] F.-J. Fu, S. Zhang, S.-P. Sun, K.-Y. Wang, T.-S. Chung, POSS-containing delamination-free dual-layer hollow fiber membranes for forward osmosis and osmotic power generation, Journal of Membrane Science, 443 (2013) 144-155.

[58] The Water-Energy-Food Nexus: A new approach in support of food security and

sustainable agriculture, Food and Agriculture Organization of the United Nations, (2014) 28.

[59] M. Bazilian, H. Rogner, M. Howells, S. Hermann, D. Arent, D. Gielen, P. Steduto, A. Mueller, P. Komor, R.S. Tol, Considering the energy, water and food nexus: Towards an integrated modelling approach, Energy Policy, 39 (2011) 7896-7906.

[60] C. Klaysom, T.Y. Cath, T. Depuydt, I.F. Vankelecom, Forward and pressure retarded osmosis: potential solutions for global challenges in energy and water supply, Chemical Society Reviews, 42 (2013) 6959-6989.

[61] S. Zhao, L. Zou, D. Mulcahy, Brackish water desalination by a hybrid forward osmosis–nanofiltration system using divalent draw solute, Desalination, 284 (2012) 175-181.

[62] J.R. McCutcheon, R.L. McGinnis, M. Elimelech, Desalination by ammonia–carbon dioxide forward osmosis: influence of draw and feed solution concentrations on process performance, Journal of Membrane Science, 278 (2006) 114-123.

[63] D. Roy, M. Rahni, P. Pierre, V. Yargeau, Forward osmosis for the concentration and reuse of process saline wastewater, Chemical Engineering Journal, 287 (2016) 277-284.

[64] G. Han, J.S. de Wit, T.-S. Chung, Water reclamation from emulsified oily wastewater via effective forward osmosis hollow fiber membranes under the PRO mode, Water Research, 81 (2015) 54-63.

[65] B.D. Coday, T.Y. Cath, Forward osmosis: Novel desalination of produced water and fracturing flowback (PDF), Journal-American Water Works Association, 106 (2014) E55-E66.

[66] M.R. Chowdhury, J. Ren, K. Reimund, J.R. McCutcheon, A hybrid dead-end/cross-flow forward osmosis system for evaluating osmotic flux performance at high recovery of produced water, Desalination.

[67] E. Beaudry, K. Lampi, Membrane technology for direct-osmosis concentration of fruit juices, Food Technology, 44 (1990).

[68] K.B. Petrotos, H.N. Lazarides, Osmotic concentration of liquid foods, Journal of Food

Engineering, 49 (2001) 201-206.

[69] R. York, R. Thiel, E. Beaudry, Full-scale experience of direct osmosis concentration applied to leachate management, in: Proceedings of the Seventh International Waste Management and Landfill Symposium (Sardinia'99), S. Margherita di Pula, Cagliari, Sardinia, Italy, 1999.

[70] Q. Yang, K.Y. Wang, T.-S. Chung, A novel dual-layer forward osmosis membrane for protein enrichment and concentration, Separation and Purification Technology, 69 (2009) 269-274.

[71] http://www.htiwater.com/divisions/humanitarian/products.html.

[72] S. Phuntsho, H.K. Shon, S. Hong, S. Lee, S. Vigneswaran, A novel low energy fertilizer driven forward osmosis desalination for direct fertigation: evaluating the performance of fertilizer draw solutions, Journal of Membrane Science, 375 (2011) 172-181.

[73] F. Lotfi, S. Phuntsho, T. Majeed, K. Kim, D.S. Han, A. Abdel-Wahab, H.K. Shon, Thin film composite hollow fibre forward osmosis membrane module for the desalination of brackish groundwater for fertigation, Desalination, 364 (2015) 108-118.

[74] K. Lee, R. Baker, H. Lonsdale, Membranes for power generation by pressure-retarded osmosis, Journal of Membrane Science, 8 (1981) 141-171.

[75] S. Bhattacharjee, A.S. Kim, M. Elimelech, Concentration polarization of interacting solute particles in cross-flow membrane filtration, Journal of Colloid and Interface Science, 212 (1999) 81-99.

[76] M. Elimelech, S. Bhattacharjee, A novel approach for modeling concentration polarization in crossflow membrane filtration based on the equivalence of osmotic pressure model and filtration theory, Journal of Membrane Science, 145 (1998) 223-241.

[77] E.M.V. Hoek, M. Elimelech, Cake-enhanced concentration polarization: A new fouling mechanism for salt-rejecting membranes, Environmental Science & Technology, 37

(2003) 5581-5588.

[78] L.F. Song, M. Elimelech, Theory of Concentration Polarization in Cross-Flow Filtration, Journal of the Chemical Society-Faraday Transactions, 91 (1995) 3389-3398.

[79] R.B. Bird, W.E. Stewart, E.N. Lightfoot, Transport phenomena, Rev. 2nd ed., J. Wiley, New York, 2007.

[80] A. Tiraferri, N.Y. Yip, W.A. Phillip, J.D. Schiffman, M. Elimelech, Relating performance of thin-film composite forward osmosis membranes to support layer formation and structure, Journal of Membrane Science, 367 (2011) 340-352.

[81] J.R. McCutcheon, M. Elimelech, Influence of membrane support layer hydrophobicity on water flux in osmotically driven membrane processes, Journal of Membrane Science, 318 (2008) 458-466.

[82] L. Huang, Novel Hydrophilic Nylon 6,6 Supported Thin Film Composite Membranes for Osmotically Driven Processes, Doctoral Dissertations, 741 (2015).

[83] S. Stern, T. Sinclair, P. Gareis, N. Vahldieck, P. Mohr, Helium recovery by permeation, Industrial & Engineering Chemistry, 57 (1965) 49-60.

[84] R.E. Pattle, Production of Electric Power by mixing Fresh and Salt Water in the Hydroelectric Pile, Nature, 174 (1954) 660-660.

[85] http://www.htiwater.com/company/hti_history.html.

[86] S. Lin, Mass transfer in forward osmosis with hollow fiber membranes, Journal of Membrane Science, 514 (2016) 176-185.

[87] K.Y. Wang, Q. Yang, T.-S. Chung, R. Rajagopalan, Enhanced forward osmosis from chemically modified polybenzimidazole (PBI) nanofiltration hollow fiber membranes with a thin wall, Chemical Engineering Science, 64 (2009) 1577-1584.

[88] J. Su, Q. Yang, J.F. Teo, T.-S. Chung, Cellulose acetate nanofiltration hollow fiber membranes for forward osmosis processes, Journal of Membrane Science, 355 (2010) 36-44.

[89] N.Y. Yip, A. Tiraferri, W.A. Phillip, J.D. Schiffman, L.A. Hoover, Y.C. Kim, M. Elimelech, Thin-film composite pressure retarded osmosis membranes for sustainable power generation from salinity gradients, Environmental Science & Technology, 45 (2011) 4360-4369.

[90] S. Chou, R. Wang, L. Shi, Q. She, C. Tang, A.G. Fane, Thin-film composite hollow fiber membranes for pressure retarded osmosis (PRO) process with high power density, Journal of Membrane Science, 389 (2012) 25-33.

[91] N.-N. Bui, J.R. McCutcheon, Hydrophilic Nanofibers as New Supports for Thin Film Composite Membranes for Engineered Osmosis, Environmental Science & Technology, 47 (2013) 1761-1769.

[92] N. Widjojo, T.-S. Chung, M. Weber, C. Maletzko, V. Warzelhan, The role of sulphonated polymer and macrovoid-free structure in the support layer for thin-film composite (TFC) forward osmosis (FO) membranes, Journal of Membrane Science, 383 (2011) 214-223.

[93] J. Ren, B. O'Grady, G. deJesus, J.R. McCutcheon, Sulfonated polysulfone supported high performance thin film composite membranes for forward osmosis, Polymer, 103 (2016) 486-497.

[94] R. McGinnis, G. McGurgan, Forward osmosis membranes, U.S. Patent (2012) US 12/862,584.

[95] C.H. Kim, J.H. Lee, High-flux forward osmosis membrane assembly, and forward osmosis module containing same, W.O. Patent (2015) PCT/KR2014/007893.

[96] R. Revanur, I. Roh, J.E. Klare, A. Noy, O. Bakajin, Thin film composite membranes for forward osmosis, and their preparation methods, U.S. Patent (2014) US 13/200,780.

[97] K. Marui, K. Tokunaga, Y. Terashima, H. Suenaga, A. Kumano, Hollow-fiber membrane element and membrane module for forward osmosis, W.O. Patent (2015) PCT/JP2015/054204.

[98] T. Majeed, S. Phuntsho, S. Sahebi, J.E. Kim, J.K. Yoon, K. Kim, H.K. Shon, Influence

of the process parameters on hollow fiber-forward osmosis membrane performances, Desalination and Water Treatment, (2014) 1-12.

[99] S. Loeb, S. Sourirajan, Sea water demineralization by means of a semipermeable membrane, University of California, Department of Engineering, 1963.

[100] P.W. Morgan, S.L. Kwolek, Interfacial polycondensation. II. Fundamentals of polymer formation at liquid interfaces, Journal of Polymer Science Part A: Polymer Chemistry, 34 (1996) 531-559.

[101] J. Ren, J.R. McCutcheon, Polyacrylonitrile supported thin film composite hollow fiber membranes for forward osmosis, Desalination, 372 (2015) 67-74.

[102] S.-P. Sun, T.-S. Chung, Outer-Selective Pressure-Retarded Osmosis Hollow Fiber Membranes from Vacuum-Assisted Interfacial Polymerization for Osmotic Power Generation, Environmental Science & Technology, 47 (2013) 13167-13174.

[103] L. Setiawan, R. Wang, K. Li, A.G. Fane, Fabrication of novel poly (amide–imide) forward osmosis hollow fiber membranes with a positively charged nanofiltration-like selective layer, Journal of Membrane Science, 369 (2011) 196-205.

[104] L. Setiawan, R. Wang, K. Li, A.G. Fane, Fabrication and characterization of forward osmosis hollow fiber membranes with antifouling NF-like selective layer, Journal of Membrane Science, 394–395 (2012) 80-88.

[105] L. Setiawan, R. Wang, L. Shi, K. Li, A.G. Fane, Novel dual-layer hollow fiber membranes applied for forward osmosis process, Journal of Membrane Science, 421–422 (2012) 238-246.

[106] L. Setiawan, R. Wang, S. Tan, L. Shi, A.G. Fane, Fabrication of poly(amide-imide)-polyethersulfone dual layer hollow fiber membranes applied in forward osmosis by combined polyelectrolyte cross-linking and depositions, Desalination, 312 (2013) 99-106.

[107] K. Goh, L. Setiawan, L. Wei, W. Jiang, R. Wang, Y. Chen, Fabrication of novel

functionalized multi-walled carbon nanotube immobilized hollow fiber membranes for enhanced performance in forward osmosis process, Journal of Membrane Science, 446 (2013) 244-254.

[108] C. Liu, L. Shi, R. Wang, Enhanced hollow fiber membrane performance via semi-dynamic layer-by-layer polyelectrolyte inner surface deposition for nanofiltration and forward osmosis applications, Reactive and Functional Polymers, 86 (2015) 154-160.

[109] W. Fang, R. Wang, S. Chou, L. Setiawan, A.G. Fane, Composite forward osmosis hollow fiber membranes: Integration of RO- and NF-like selective layers to enhance membrane properties of anti-scaling and anti-internal concentration polarization, Journal of Membrane Science, 394-395 (2012) 140-150.

[110] W. Fang, C. Liu, L. Shi, R. Wang, Composite forward osmosis hollow fiber membranes: Integration of RO- and NF-like selective layers for enhanced organic fouling resistance, Journal of Membrane Science, 492 (2015) 147-155.

[111] J.R. McCutcheon, M. Elimelech, Influence of membrane support layer hydrophobicity on water flux in osmotically driven membrane processes, Journal of Membrane Science, 318 (2008) 458-466.

[112] P. Zhong, X. Fu, T.-S. Chung, M. Weber, C. Maletzko, Development of Thin-Film Composite forward osmosis hollow fiber membranes using direct sulfonated polyphenylenesulfone (sPPSU) as membrane substrates, Environmental Science & Technology, 47 (2013) 7430-7436.

[113] P. Li, S.S. Lim, J.G. Neo, R.C. Ong, M. Weber, C. Staudt, N. Widjojo, C. Maletzko, T.S. Chung, Short- and Long-Term Performance of the Thin-Film Composite Forward Osmosis (TFC-FO) Hollow Fiber Membranes for Oily Wastewater Purification, Industrial & Engineering Chemistry Research, 53 (2014) 14056-14064.

[114] L. Shi, S. Chou, R. Wang, W. Fang, C. Tang, A. Fane, Effect of substrate structure on

the performance of thin-film composite forward osmosis hollow fiber membranes, Journal of Membrane Science, 382 (2011) 116-123.

[115] N. Peng, N. Widjojo, P. Sukitpaneenit, M.M. Teoh, G.G. Lipscomb, T.S. Chung, J.Y. Lai, Evolution of polymeric hollow fibers as sustainable technologies: Past, present, and future, Prog Polym Sci, 37 (2012) 1401-1424.

[116] L. Luo, P. Wang, S. Zhang, G. Han, T.-S. Chung, Novel thin-film composite tri-bore hollow fiber membrane fabrication for forward osmosis, Journal of Membrane Science, 461 (2014) 28-38.

[117] X. Li, W.L. Ang, Y. Liu, T.S. Chung, Engineering design of outer‐selective tribore hollow fiber membranes for forward osmosis and oil‐water separation, AIChE Journal, 61 (2015) 4491-4501.

[118] F.-J. Fu, S.-P. Sun, S. Zhang, T.-S. Chung, Pressure retarded osmosis dual-layer hollow fiber membranes developed by co-casting method and ammonium persulfate (APS) treatment, Journal of Membrane Science, 469 (2014) 488-498.

[119] S. Chou, R. Wang, A.G. Fane, Robust and high performance hollow fiber membranes for energy harvesting from salinity gradients by pressure retarded osmosis, Journal of Membrane Science, 448 (2013) 44-54.

[120] S. Zhang, P. Sukitpaneenit, T.-S. Chung, Design of robust hollow fiber membranes with high power density for osmotic energy production, Chemical Engineering Journal, 241 (2014) 457-465.

[121] S. Zhang, T.-S. Chung, Minimizing the instant and accumulative effects of salt permeability to sustain ultrahigh osmotic power density, Environmental Science & Technology, 47 (2013) 10085-10092.

[122] G. Han, P. Wang, T.-S. Chung, Highly Robust Thin-Film Composite Pressure Retarded Osmosis (PRO) Hollow Fiber Membranes with High Power Densities for Renewable

Salinity-Gradient Energy Generation, Environmental Science & Technology, 47 (2013) 8070-8077.

[123] G. Han, S. Zhang, X. Li, T.-S. Chung, High performance thin film composite pressure retarded osmosis (PRO) membranes for renewable salinity-gradient energy generation, Journal of Membrane Science, 440 (2013) 108-121.

[124] G. Han, T.S. Chung, Robust and high performance pressure retarded osmosis hollow fiber membranes for osmotic power generation, AIChE Journal, 60 (2014) 1107-1119.

[125] X. Li, T.-S. Chung, Thin-film composite P84 co-polyimide hollow fiber membranes for osmotic power generation, Applied Energy, 114 (2014) 600-610.

[126] X. Li, T. Cai, T.-S. Chung, Anti-fouling behavior of hyperbranched polyglycerol-grafted poly (ether sulfone) hollow fiber membranes for osmotic power generation, Environmental Science & Technology, 48 (2014) 9898-9907.

[127] J.T. Arena, B. McCloskey, B.D. Freeman, J.R. McCutcheon, Surface modification of thin film composite membrane support layers with polydopamine: Enabling use of reverse osmosis membranes in pressure retarded osmosis, Journal of Membrane Science, 375 (2011) 55-62.

[128] P.G. Ingole, W. Choi, K.H. Kim, C.H. Park, W.K. Choi, H.K. Lee, Synthesis, characterization and surface modification of PES hollow fiber membrane support with polydopamine and thin film composite for energy generation, Chemical Engineering Journal, 243 (2014) 137-146.

[129] R.L. McGinnis, M. Elimelech, Global Challenges in Energy and Water Supply: The Promise of Engineered Osmosis, Environmental Science & Technology, 42 (2008) 8625-8629.

[130] R. Baker, Membrane technology and applications. 2004, Membrane Technology and Research Inc., Menlo Park, CA.

[131] K.D. Vos, Kinetic study of the hydrolysis of cellulose acetate in the pH range of 2–

10, Journal of applied polymer science, 10 (1966) 825-832.

[132] J.R. McCutcheon, M. Elimelech, Influence of concentrative and dilutive internal concentration polarization on flux behavior in forward osmosis, Journal of Membrane Science, 284 (2006) 237-247.

[133] T.Y. Cath, M. Elimelech, J.R. McCutcheon, R.L. McGinnis, A. Achilli, D. Anastasio, A.R. Brady, A.E. Childress, I.V. Farr, N.T. Hancock, J. Lampi, L.D. Nghiem, M. Xie, N.Y. Yip, Standard Methodology for Evaluating Membrane Performance in Osmotically Driven Membrane Processes, Desalination, 312 (2013) 31-38.

[134] M. Mulder, Basic principles of membrane technology, Springer, 1996.

[135] Y. Xu, X. Peng, C.Y. Tang, Q.S. Fu, S. Nie, Effect of draw solution concentration and operating conditions on forward osmosis and pressure retarded osmosis performance in a spiral wound module, Journal of Membrane Science, 348 (2010) 298-309.

[136] Y.C. Kim, S.-J. Park, Experimental Study of a 4040 Spiral-Wound Forward-Osmosis Membrane Module, Environmental Science & Technology, 45 (2011) 7737-7745.

[137] J. Wei, C. Qiu, C.Y. Tang, R. Wang, A.G. Fane, Synthesis and characterization of flat-sheet thin film composite forward osmosis membranes, Journal of Membrane Science, 372 (2011) 292-302.

[138] A. Kulkarni, D. Mukherjee, W.N. Gill, Flux enhancement by hydrophilization of thin film composite reverse osmosis membranes, J Membrane Sci, 114 (1996) 39-50.

[139] J. Kochan, T. Wintgens, R. Hochstrat, T. Melin, Impact of wetting agents on the filtration performance of polymeric ultrafiltration membranes, Desalination, 241 (2009) 34-42.

[140] S. Zhang, F. Fu, T.-S. Chung, Substrate modifications and alcohol treatment on thin film composite membranes for osmotic power, Chemical Engineering Science, 87 (2013) 40-50.

[141] V. Freger, Swelling and Morphology of the Skin Layer of Polyamide Composite

Membranes: An Atomic Force Microscopy Study, Environ Sci Technol, 38 (2004) 3168-3175.

[142] C. Klaysom, T.Y. Cath, T. Depuydt, I.F. Vankelecom, Forward and pressure retarded osmosis: potential solutions for global challenges in energy and water supply, Chem Soc Rev, 42 (2013) 6959-6989.

[143] J. McCutcheon, N.N. Bui, Forward Osmosis, Desalination: Water from Water, (2014) 255-285.

[144] T.Y. Cath, A.E. Childress, M. Elimelech, Forward osmosis: principles, applications, and recent developments, Journal of Membrane Science, 281 (2006) 70-87.

[145] T.-S. Chung, X. Li, R.C. Ong, Q. Ge, H. Wang, G. Han, Emerging forward osmosis (FO) technologies and challenges ahead for clean water and clean energy applications, Current Opinion in Chemical Engineering, 1 (2012) 246-257.

[146] A. Tiraferri, N.Y. Yip, W.A. Phillip, J.D. Schiffman, M. Elimelech, Relating performance of thin-film composite forward osmosis membranes to support layer formation and structure, Journal of Membrane Science, 367 (2011) 340-352.

[147] R.J. Petersen, Composite reverse osmosis and nanofiltration membranes, Journal of Membrane Science, 83 (1993) 81-150.

[148] N.-N. Bui, M.L. Lind, E. Hoek, J.R. McCutcheon, Electrospun nanofiber supported thin film composite membranes for engineered osmosis, Journal of Membrane Science, 385 (2011) 10-19.

[149] R.C. Ong, T.-S. Chung, J.S. de Wit, B.J. Helmer, Novel cellulose ester substrates for high performance flat-sheet thin-film composite (TFC) forward osmosis (FO) membranes, Journal of Membrane Science, 473 (2015) 63-71.

[150] D. Stillman, L. Krupp, Y.-H. La, Mesh-reinforced thin film composite membranes for forward osmosis applications: The structure–performance relationship, Journal of Membrane Science, 468 (2014) 308-316.

[151] J. Ren, J.R. McCutcheon, A new commercial thin film composite membrane for forward osmosis, Desalination, 343 (2014) 187-193.

[152] P. Xing, G.P. Robertson, M.D. Guiver, S.D. Mikhailenko, K. Wang, S. Kaliaguine, Synthesis and characterization of sulfonated poly(ether ether ketone) for proton exchange membranes, Journal of Membrane Science, 229 (2004) 95-106.

[153] S. Xue, G. Yin, Proton exchange membranes based on poly(vinylidene fluoride) and sulfonated poly(ether ether ketone), Polymer, 47 (2006) 5044-5049.

[154] H. Xu, K. Chen, X. Guo, J. Fang, J. Yin, Synthesis of novel sulfonated polybenzimidazole and preparation of cross-linked membranes for fuel cell application, Polymer, 48 (2007) 5556-5564.

[155] M. Ulbricht, Advanced functional polymer membranes, Polymer, 47 (2006) 2217-2262.

[156] M. Kumar, M. Ulbricht, Novel ultrafiltration membranes with adjustable charge density based on sulfonated poly(arylene ether sulfone) block copolymers and their tunable protein separation performance, Polymer, 55 (2014) 354-365.

[157] G.M. Geise, B.D. Freeman, D.R. Paul, Characterization of a sulfonated pentablock copolymer for desalination applications, Polymer, 51 (2010) 5815-5822.

[158] H.B. Park, B.D. Freeman, Z.-B. Zhang, M. Sankir, J.E. McGrath, Highly Chlorine-Tolerant Polymers for Desalination, Angewandte Chemie, 120 (2008) 6108-6113.

[159] M. Paul, H.B. Park, B.D. Freeman, A. Roy, J.E. McGrath, J.S. Riffle, Synthesis and crosslinking of partially disulfonated poly(arylene ether sulfone) random copolymers as candidates for chlorine resistant reverse osmosis membranes, Polymer, 49 (2008) 2243-2252.

[160] W. Xie, G.M. Geise, B.D. Freeman, C.H. Lee, J.E. McGrath, Influence of processing history on water and salt transport properties of disulfonated polysulfone random copolymers, Polymer, 53 (2012) 1581-1592.

[161] W. Xie, J. Cook, H.B. Park, B.D. Freeman, C.H. Lee, J.E. McGrath, Fundamental salt and water transport properties in directly copolymerized disulfonated poly(arylene ether sulfone) random copolymers, Polymer, 52 (2011) 2032-2043.

[162] G. Han, T.-S. Chung, M. Toriida, S. Tamai, Thin-film composite forward osmosis membranes with novel hydrophilic supports for desalination, Journal of Membrane Science, 423-424 (2012) 543-555.

[163] K.Y. Wang, T.-S. Chung, G. Amy, Developing thin-film-composite forward osmosis membranes on the PES/SPSf substrate through interfacial polymerization, AIChE Journal, 58 (2012) 770-781.

[164] C. Klaysom, B.P. Ladewig, G.Q.M. Lu, L. Wang, Preparation and characterization of sulfonated polyethersulfone for cation-exchange membranes, Journal of Membrane Science, 368 (2011) 48-53.

[165] L. Unnikrishnan, P. Madamana, S. Mohanty, S.K. Nayak, Polysulfone/C30B nanocomposite membranes for fuel cell applications: effect of various sulfonating agents, Polymer-Plastics Technology and Engineering, 51 (2012) 568-577.

[166] B.R. O'Grady, Sulfonated Polyethersulfone as a New Platform for Thin Film Composite Membranes, Master's Theses, 417 (2013).

[167] L. Huang, N.-N. Bui, M.T. Meyering, T.J. Hamlin, J.R. McCutcheon, Novel hydrophilic nylon 6,6 microfiltration membrane supported thin film composite membranes for engineered osmosis, Journal of Membrane Science, 437 (2013) 141-149.

[168] J.Y. Kim, H.K. Lee, K.J. Baik, S.C. Kim, Liquid‐liquid phase separation in polysulfone/solvent/water systems, Journal of applied polymer science, 65 (1997) 2643-2653.

[169] J.G. Wijmans, J. Kant, M.H.V. Mulder, C.A. Smolders, Phase separation phenomena in solutions of polysulfone in mixtures of a solvent and a nonsolvent: relationship with membrane formation, Polymer, 26 (1985) 1539-1545.

[170] L. Xu, F. Qiu, Simultaneous determination of three Flory–Huggins interaction parameters in polymer/solvent/nonsolvent systems by viscosity and cloud point measurements, Polymer, 55 (2014) 6795-6802.

[171] J.-F. Blanco, J. Sublet, Q.T. Nguyen, P. Schaetzel, Formation and morphology studies of different polysulfones-based membranes made by wet phase inversion process, Journal of Membrane Science, 283 (2006) 27-37.

[172] J.-F. Li, Z.-L. Xu, H. Yang, L.-Y. Yu, M. Liu, Effect of TiO2 nanoparticles on the surface morphology and performance of microporous PES membrane, Applied Surface Science, 255 (2009) 4725-4732.

[173] V. Vatanpour, S.S. Madaeni, R. Moradian, S. Zinadini, B. Astinchap, Novel antibifouling nanofiltration polyethersulfone membrane fabricated from embedding TiO2 coated multiwalled carbon nanotubes, Separation and Purification Technology, 90 (2012) 69-82.

[174] Y. Li, H. Jia, F. Pan, Z. Jiang, Q. Cheng, Enhanced anti-swelling property and dehumidification performance by sodium alginate–poly(vinyl alcohol)/polysulfone composite hollow fiber membranes, Journal of Membrane Science, 407–408 (2012) 211-220.

[175] J.T. Arena, B. McCloskey, B.D. Freeman, J.R. McCutcheon, Surface modification of thin film composite membrane support layers with polydopamine: enabling use of reverse osmosis membranes in pressure retarded osmosis, Journal of Membrane Science, 375 (2011) 55-62.

[176] T.Y. Cath, M. Elimelech, J.R. McCutcheon, R.L. McGinnis, A. Achilli, D. Anastasio, A.R. Brady, A.E. Childress, I.V. Farr, N.T. Hancock, Standard methodology for evaluating membrane performance in osmotically driven membrane processes, Desalination, 312 (2013) 31-38.

[177] A. Tiraferri, N.Y. Yip, A.P. Straub, S. Romero-Vargas Castrillon, M. Elimelech, A

method for the simultaneous determination of transport and structural parameters of forward osmosis membranes, Journal of Membrane Science, 444 (2013) 523-538.

[178] C. Smolders, A. Reuvers, R. Boom, I. Wienk, Microstructures in phase-inversion membranes. Part 1. Formation of macrovoids, Journal of Membrane Science, 73 (1992) 259-275.

[179] C. Klaysom, S. Hermans, A. Gahlaut, S. Van Craenenbroeck, I.F.J. Vankelecom, Polyamide/Polyacrylonitrile (PA/PAN) thin film composite osmosis membranes: Film optimization, characterization and performance evaluation, Journal of Membrane Science, 445 (2013) 25-33.

[180] W.A. Phillip, J.S. Yong, M. Elimelech, Reverse draw solute permeation in forward osmosis: modeling and experiments, Environmental science & technology, 44 (2010) 5170-5176.

[181] Z. Zhou, J.Y. Lee, T.-S. Chung, Thin film composite forward-osmosis membranes with enhanced internal osmotic pressure for internal concentration polarization reduction, Chemical Engineering Journal, 249 (2014) 236-245.

[182] M. Sairam, E. Sereewatthanawut, K. Li, A. Bismarck, A.G. Livingston, Method for the preparation of cellulose acetate flat sheet composite membranes for forward osmosis—Desalination using MgSO4 draw solution, Desalination, 273 (2011) 299-307.

[183] C. Qiu, L. Setiawan, R. Wang, C.Y. Tang, A.G. Fane, High performance flat sheet forward osmosis membrane with an NF-like selective layer on a woven fabric embedded substrate, Desalination, 287 (2012) 266-270.

[184] X. Liu, H.Y. Ng, Double-blade casting technique for optimizing substrate membrane in thin-film composite forward osmosis membrane fabrication, Journal of Membrane Science, 469 (2014) 112-126.

[185] J. Ren, W. Zhao, C. Cheng, M. Zhou, C. Zhao, Comparison of pH-sensitivity between

two copolymer modified polyethersulfone hollow fiber membranes, Desalination, 280 (2011) 152-159.

[186] C. Cheng, L. Ma, D. Wu, J. Ren, W. Zhao, J. Xue, S. Sun, C. Zhao, Remarkable pH-sensitivity and anti-fouling property of terpolymer blended polyethersulfone hollow fiber membranes, Journal of Membrane Science, 378 (2011) 369-381.

[187] B. Qian, J. Li, Q. Wei, P. Bai, B. Fang, C. Zhao, Preparation and characterization of pH-sensitive polyethersulfone hollow fiber membrane for flux control, Journal of Membrane Science, 344 (2009) 297-303.

[188] J. Zhao, B. Li, X. Li, Y. Qin, C. Li, S. Wang, Numerical simulation of novel polypropylene hollow fiber heat exchanger and analysis of its characteristics, Applied Thermal Engineering, 59 (2013) 134-141.

[189] Q. Saren, C.Q. Qiu, C.Y. Tang, Synthesis and Characterization of Novel Forward Osmosis Membranes based on Layer-by-Layer Assembly, Environmental Science & Technology, 45 (2011) 5201-5208.

[190] D.-G. Yu, W.-L. Chou, M.C. Yang, Effect of bore liquid temperature and dope concentration on mechanical properties and permeation performance of polyacrylonitrile hollow fibers, Separation and Purification Technology, 51 (2006) 1-9.

[191] C. Feng, B. Shi, G. Li, Y. Wu, Preparation and properties of microporous membrane from poly(vinylidene fluoride-co-tetrafluoroethylene) (F2.4) for membrane distillation, Journal of Membrane Science, 237 (2004) 15-24.

[192] D.S.P. Rao, Strength of materials : A practical approach, Universities Press (India), Hyderbad, 2011.

[193] Y.-S. Yoo, N.-S. Huh, S. Choi, T.-W. Kim, J.-I. Kim, Collapse pressure estimates and the application of a partial safety factor to cylinders subjected to external pressure, Nuclear Engineering and Technology, 42 (2010) 450-459.

[194] P.S. Singh, S.V. Joshi, J.J. Trivedi, C.V. Devmurari, A.P. Rao, P.K. Ghosh, Probing the structural variations of thin film composite RO membranes obtained by coating polyamide over polysulfone membranes of different pore dimensions, Journal of Membrane Science, 278 (2006) 19-25.

[195] A.K. Ghosh, E.M.V. Hoek, Impacts of support membrane structure and chemistry on polyamide–polysulfone interfacial composite membranes, Journal of Membrane Science, 336 (2009) 140-148.

[196] G.Z. Ramon, M.C.Y. Wong, E.M.V. Hoek, Transport through composite membrane, part 1: Is there an optimal support membrane?, Journal of Membrane Science, 415–416 (2012) 298-305.

[197] G.Z. Ramon, E.M.V. Hoek, Transport through composite membranes, part 2: Impacts of roughness on permeability and fouling, Journal of Membrane Science, 425–426 (2013) 141-148.

[198] L. Huang, J.R. McCutcheon, Impact of support layer pore size on performance of thin film composite membranes for forward osmosis, Journal of Membrane Science, 483 (2015) 25-33.

[199] L. Huang, J.T. Arena, J.R. McCutcheon, Surface modified PVDF nanofiber supported thin film composite membranes for forward osmosis, Journal of Membrane Science, 499 (2016) 352-360.

[200] L. Lin, C. Feng, R. Lopez, O. Coronell, Identifying facile and accurate methods to measure the thickness of the active layers of thin-film composite membranes – A comparison of seven characterization techniques, Journal of Membrane Science, 498 (2016) 167-179.

[201] L. Lin, R. Lopez, G.Z. Ramon, O. Coronell, Investigating the void structure of the polyamide active layers of thin-film composite membranes, Journal of Membrane Science, 497 (2016) 365-376.

[202] S.Y. Kwak, S.G. Jung, Y.S. Yoon, D.W. Ihm, Details of surface features in aromatic polyamide reverse osmosis membranes characterized by scanning electron and atomic force microscopy, Journal of Polymer Science Part B Polymer Physics, 37 (1999) 1429-1440.

[203] J. Ren, Z. Li, F.-S. Wong, A new method for the prediction of pore size distribution and MWCO of ultrafiltration membranes, Journal of Membrane Science, 279 (2006) 558-569.

[204] H. Yan, X. Miao, J. Xu, G. Pan, Y. Zhang, Y. Shi, M. Guo, Y. Liu, The porous structure of the fully-aromatic polyamide film in reverse osmosis membranes, Journal of Membrane Science, 475 (2015) 504-510.

[205] T. Tsuru, S. Sasaki, T. Kamada, T. Shintani, T. Ohara, H. Nagasawa, K. Nishida, M. Kanezashi, T. Yoshioka, Multilayered polyamide membranes by spray-assisted 2-step interfacial polymerization for increased performance of trimesoyl chloride (TMC)/m-phenylenediamine (MPD)-derived polyamide membranes, Journal of Membrane Science, 446 (2013) 504-512.

[206] J. Lee, A. Hill, S. Kentish, Formation of a thick aromatic polyamide membrane by interfacial polymerisation, Separation and Purification Technology, 104 (2013) 276-283.

[207] Y. Song, P. Sun, L. Henry, B. Sun, Mechanisms of structure and performance controlled thin film composite membrane formation via interfacial polymerization process, Journal of Membrane Science, 251 (2005) 67-79.

[208] F. Pacheco, R. Sougrat, M. Reinhard, J.O. Leckie, I. Pinnau, 3D visualization of the internal nanostructure of polyamide thin films in RO membranes, Journal of Membrane Science, 501 (2016) 33-44.

[209] S. Karan, Z. Jiang, A.G. Livingston, Sub–10 nm polyamide nanofilms with ultrafast solvent transport for molecular separation, Science, 348 (2015) 1347-1351.

[210] M. Hirose, H. Ito, Y. Kamiyama, Effect of skin layer surface structures on the flux behaviour of RO membranes, Journal of Membrane Science, 121 (1996) 209-215.

[211] V. Freger, Outperforming nature's membranes, Science, 348 (2015) 1317-1318.

[212] T. Fujioka, N. Oshima, R. Suzuki, W.E. Price, L.D. Nghiem, Probing the internal structure of reverse osmosis membranes by positron annihilation spectroscopy: Gaining more insight into the transport of water and small solutes, Journal of Membrane Science, 486 (2015) 106-118.

[213] L. Chekli, S. Phuntsho, J.E. Kim, J. Kim, J.Y. Choi, J.-S. Choi, S. Kim, J.H. Kim, S. Hong, J. Sohn, A comprehensive review of hybrid forward osmosis systems: performance, applications and future prospects, Journal of Membrane Science, 497 (2016) 430-449.

[214] A. Achilli, T.Y. Cath, E.A. Marchand, A.E. Childress, The forward osmosis membrane bioreactor: a low fouling alternative to MBR processes, Desalination, 239 (2009) 10-21.

[215] H. Zhu, L. Zhang, X. Wen, X. Huang, Feasibility of applying forward osmosis to the simultaneous thickening, digestion, and direct dewatering of waste activated sludge, Bioresource Technology, 113 (2012) 207-213.

[216] X. Li, K.Y. Wang, B. Helmer, T.-S. Chung, Thin-Film Composite Membranes and Formation Mechanism of Thin-Film Layers on Hydrophilic Cellulose Acetate Propionate Substrates for Forward Osmosis Processes, Industrial & Engineering Chemistry Research, 51 (2012) 10039-10050.

[217] Modern Water commissions Al Najdah FO plant, Membrane Technology, 2012 (2012) 4.

[218] A. Deshmukh, N.Y. Yip, S. Lin, M. Elimelech, Desalination by forward osmosis: Identifying performance limiting parameters through module-scale modeling, Journal of Membrane Science, 491 (2015) 159-167.

[219] T.Y. Cath, S. Gormly, E.G. Beaudry, M.T. Flynn, V.D. Adams, A.E. Childress, Membrane contactor processes for wastewater reclamation in space: Part I. Direct osmotic

concentration as pretreatment for reverse osmosis, Journal of Membrane Science, 257 (2005) 85-98.

[220] P. Xu, C. Bellona, J.E. Drewes, Fouling of nanofiltration and reverse osmosis membranes during municipal wastewater reclamation: membrane autopsy results from pilot-scale investigations, Journal of Membrane Science, 353 (2010) 111-121.

[221] B. Peñate, L. García-Rodríguez, Current trends and future prospects in the design of seawater reverse osmosis desalination technology, Desalination, 284 (2012) 1-8.

[222] J. Cadotte, R. Petersen, R. Larson, E. Erickson, A new thin-film composite seawater reverse osmosis membrane, Desalination, 32 (1980) 25-31.

[223] C. Benton, O. Bakajin, Separation systems, elements, and methods for separation utilizing stacked membranes and spacers, U.S. Patent (2014) US 14/137,903.

[224] N.T. Hancock, P. Xu, M.J. Roby, J.D. Gomez, T.Y. Cath, Towards direct potable reuse with forward osmosis: Technical assessment of long-term process performance at the pilot scale, Journal of Membrane Science, 445 (2013) 34-46.

[225] J.E. Kim, S. Phuntsho, F. Lotfi, H.K. Shon, Investigation of pilot-scale 8040 FO membrane module under different operating conditions for brackish water desalination, Desalination and Water Treatment, 53 (2014) 2782-2791.

[226] J. Vogel, J.S. Groth, K.H. Nielsen, O. Geschke, Hollow fiber module having tfc-aquaporin modified membranes, U.S. Patent (2015) US 14/610,504.

[227] J. Welty, C.E. Wicks, G.L. Rorrer, R.E. Wilson, Fundamentals of Momentum, Heat and Mass Transfer, Wiley, 2007.

[228] J.R. Werber, A. Deshmukh, M. Elimelech, The Critical Need for Increased Selectivity, Not Increased Water Permeability, for Desalination Membranes, Environmental Science & Technology Letters, 3 (2016) 112-120.

[229] D.H. Jung, J. Lee, D.Y. Kim, Y.G. Lee, M. Park, S. Lee, D.R. Yang, J.H. Kim,

Simulation of forward osmosis membrane process: Effect of membrane orientation and flow direction of feed and draw solutions, Desalination, 277 (2011) 83-91.

[230] S. Phuntsho, S. Hong, M. Elimelech, H.K. Shon, Osmotic equilibrium in the forward osmosis process: Modelling, experiments and implications for process performance, Journal of Membrane Science, 453 (2014) 240-252.

[231] N.-N. Bui, J.T. Arena, J.R. McCutcheon, Proper accounting of mass transfer resistances in forward osmosis: Improving the accuracy of model predictions of structural parameter, Journal of Membrane Science, 492 (2015) 289-302.

[232] P. Dey, E.L. Izake, Magnetic nanoparticles boosting the osmotic efficiency of a polymeric FO draw agent: Effect of polymer conformation, Desalination, 373 (2015) 79-85.

[233] C. Boo, Y.F. Khalil, M. Elimelech, Performance evaluation of trimethylamine–carbon dioxide thermolytic draw solution for engineered osmosis, Journal of Membrane Science, 473 (2015) 302-309.

[234] L. Chekli, S. Phuntsho, H.K. Shon, S. Vigneswaran, J. Kandasamy, A. Chanan, A review of draw solutes in forward osmosis process and their use in modern applications, Desalination and Water Treatment, 43 (2012) 167-184.

[235] D. Xiao, W. Li, S. Chou, R. Wang, C.Y. Tang, A modeling investigation on optimizing the design of forward osmosis hollow fiber modules, Journal of Membrane Science, 392-393 (2012) 76-87.

[236] A. Sagiv, R. Semiat, Finite element analysis of forward osmosis process using NaCl solutions, Journal of Membrane Science, 379 (2011) 86-96.

[237] A. Sagiv, P.D. Christofides, Y. Cohen, R. Semiat, On the analysis of FO mass transfer resistances via CFD analysis and film theory, Journal of Membrane Science, 495 (2015) 198-205.

[238] Y. Fang, L. Bian, X. Wang, Understanding membrane parameters of a forward

osmosis membrane based on nonequilibrium thermodynamics, Journal of Membrane Science, 437 (2013) 72-81.

[239] R.K. McGovern, On the potential of forward osmosis to energetically outperform reverse osmosis desalination, Journal of Membrane Science, 469 (2014) 245-250.

[240] V. Yangali-Quintanilla, Z. Li, R.V. Linares, G. Amy, Apparatus, System, and Method for Forward Osmosis in Water Reuse, U.S. Patent (2013) US 13/535,819.

[241] J. Ren, J.R. McCutcheon, Making Thin Film Composite Hollow Fiber Forward Osmosis Membranes at the Module Scale using Commercial Ultrafiltration Membranes, Industrial & Engineering Chemistry Research, in press (2017).

[242] COMSOL Multiphysics: Version 5.1, 2015.

[243] R.B. Bird, W.E. Stewart, E.N. Lightfoot, Transport Phenomena, Wiley, 2007.

[244] A. Sagiv, A. Zhu, P.D. Christofides, Y. Cohen, R. Semiat, Analysis of forward osmosis desalination via two-dimensional FEM model, Journal of Membrane Science, 464 (2014) 161-172.

[245] F.-J. Fu, S. Zhang, T.-S. Chung, Sandwich-structured hollow fiber membranes for osmotic power generation, Desalination, 376 (2015) 73-81.

[246] M. Mahendran, K.P. Goodboy, L. Fabbricino, Hollow fiber membrane and braided tubular support therefor, in, Google Patents, 2002.

[247] Koch Membrane Systems Inc., http://www.kochmembrane.com/PDFs/Brochures/puron-mbr-brochure.aspx, (2017).

[248] A.P. Straub, N.Y. Yip, S. Lin, J. Lee, M. Elimelech, Harvesting low-grade heat energy using thermo-osmotic vapour transport through nanoporous membranes, Nature Energy, 1 (2016) 16090.

[249] M. Shibuya, M. Yasukawa, T. Takahashi, T. Miyoshi, M. Higa, H. Matsuyama, Effect

of operating conditions on osmotic-driven membrane performances of cellulose triacetate forward osmosis hollow fiber membrane, Desalination, 362 (2015) 34-42.

[250] C.Y. Tang, Y. Zhao, R. Wang, C. Hélix-Nielsen, A.G. Fane, Desalination by biomimetic aquaporin membranes: Review of status and prospects, Desalination, 308 (2013) 34-40.

[251] M. Kumar, M. Grzelakowski, J. Zilles, M. Clark, W. Meier, Highly permeable polymeric membranes based on the incorporation of the functional water channel protein Aquaporin Z, Proceedings of the National Academy of Sciences, 104 (2007) 20719-20724.

[252] X. Li, R. Wang, F. Wicaksana, C. Tang, J. Torres, A.G. Fane, Preparation of high performance nanofiltration (NF) membranes incorporated with aquaporin Z, Journal of Membrane Science, 450 (2014) 181-188.

[253] X. Li, S. Chou, R. Wang, L. Shi, W. Fang, G. Chaitra, C.Y. Tang, J. Torres, X. Hu, A.G. Fane, Nature gives the best solution for desalination: Aquaporin-based hollow fiber composite membrane with superior performance, Journal of Membrane Science, 494 (2015) 68-77.

[254] H. Wang, T.-S. Chung, Y.W. Tong, K. Jeyaseelan, A. Armugam, Z. Chen, M. Hong, W. Meier, Highly Permeable and Selective Pore-Spanning Biomimetic Membrane Embedded with Aquaporin Z, Small, 8 (2012) 1185-1190.

[255] Y. Zhao, C. Qiu, X. Li, A. Vararattanavech, W. Shen, J. Torres, C. Hélix-Nielsen, R. Wang, X. Hu, A.G. Fane, C.Y. Tang, Synthesis of robust and high-performance aquaporin-based biomimetic membranes by interfacial polymerization-membrane preparation and RO performance characterization, Journal of Membrane Science, 423-424 (2012) 422-428.

[256] P.S. Zhong, T.-S. Chung, K. Jeyaseelan, A. Armugam, Aquaporin-embedded biomimetic membranes for nanofiltration, Journal of Membrane Science, 407-408 (2012) 27-33.

[257] W. Ding, J. Cai, Z. Yu, Q. Wang, Z. Xu, Z. Wang, C. Gao, Fabrication of an aquaporin-based forward osmosis membrane through covalent bonding of a lipid bilayer to a microporous support, Journal of Materials Chemistry A, 3 (2015) 20118-20126.